DEVELOPMENT OF IODONIUM-BASED GRAM-NEGATIVE ANTIBACTERIAL COMPOUNDS AND TARGET IDENTIFICATION USING A CHEMOPROTEOMICS APPROACH

A THESIS

submitted in partial fulfilment of the

requirements

of the degree of

Doctor of Philosophy

by

POOJA KUMARI

20153371

INDIAN INSTITUTE OF SCIENCE EDUCATION AND RESEARCH PUNE - 411 008

2022

Dedicated to…..

My brother
Late Pravesh Kumar (babu)

भारतीय विज्ञान शिक्षा एवं अनुसंधान संस्थान, पुणे
INDIAN INSTITUTE OF SCIENCE EDUCATION AND RESEARCH (IISER), PUNE
(An Autonomous Institution, Ministry of Human Resource Development, Govt. of India)
Dr. Homi Bhabha Road, Pashan, Pune – 411 008

Harinath Chakrapani, Ph.D.
Professor – Chemistry
www.iiserpune.ac.in/~harinath/

CERTIFICATE

Certified that, the work incorporated in the thesis entitled, "***Development Of Iodonium-Based Gram-Negative Antibacterial Compounds And Target Identification Using A Chemoproteomics Approach***" submitted by ***Pooja Kumari*** was carried out by the candidate, under my supervision. The work presented here or any part of it has not been included in any other thesis submitted previously for the award of any degree or diploma from any other University or institution.

C. Harinath

Date: 7th March 2022 **Harinath Chakrapani**

Pune (Maharashtra), India.

DECLARATION

I declare that this written submission represents my ideas in my own words, and where others' ideas have been included, I have adequately cited and referenced the original sources. I also declare that I have adhered to all principles of academic honesty and integrity and have not misrepresented or fabricated or falsified any idea/data/fact/source in my submission. I understand that violation of the above will be cause for disciplinary action by the Institute and can also evoke penal action from the sources which have thus not been properly cited or from whom proper permission has not been taken when needed.

Date: 7th March 2022 **Pooja Kumari**

Pune (Maharashtra), India. **20153371**

Table of Contents

General Remarks

- ^{1}H spectra were recorded on a JEOL ECX 400 MHz or a Bruker 400 MHz spectrometer unless otherwise specified using as an internal tetramethylsilane (δ_H = 0.00). Chemical shifts are expressed in ppm units downfield to TMS.
- ^{13}C spectra were recorded on a JEOL 100 MHz or a Bruker 100 MHz spectrometer unlessotherwise specified using as an internal tetramethylsilane (δ_C = 0.0).
- Chemical shifts (δ) are reported in ppm and coupling constants (*J*) in Hz.
- Mass spectra were obtained using HRMS-ESI-Q-Time of Flight LC-MS (Synapt G2, Waters)).
- FT-IR spectra were obtained using Bruker Alpha-FT-IR spectrometer and reported in cm^{-1}.
- All reactions were monitored by Thin-Layer Chromatography carried out on precoated Merck silica plates (F254, 0.25 mm thickness); compounds were visualized by UV light.
- All reactions were carried out under nitrogen atmosphere with dried solvents under anhydrous conditions and yields refer to chromatographically homogenous materials unlessotherwise stated.
- All evaporations were carried out under reduced pressure on Büchi and Heildoph rotary evaporator below 45 °C unless otherwise specified.
- Silica gel 60-120 and 100-200 mesh were used for column chromatography.
- Materials were obtained from commercial suppliers and were used without further purification.
- Preparative HPLC purification was performed using high performance liquid chromatography (HPLC) with C-18 preparative column (21.2 mm × 250 mm, 10 μm; Kromasil®C-18).
- HPLC analysis data was obtained using Agilent Technologies 1260 Infinity, C18 reversedphase column (4.6 mm × 250 mm, 5 μm).
- Spectrophotometric and fluorimetric measurements were performed using Thermo Scientific Varioscan microwell plate reader.
- All SDS-PAGE gels (activity based gels and coomassie gels) were imaged on a Syngene G-Box Chemi-XRQ gel documentation system

Abbreviations

A. baumannii	*Acinetobacter baumannii*
ABPP	Activity-based protein profiling
AMP	Antimicrobial peptides
AMR	Antimicrobial Resistance
aPDT	Antibacterial photodynamic therapy
ATCC	American Type Culture Collection
ATP	Adenosine triphosphate
BODIPY	Boron-dipyrrolemethene
bs	Broad singlet
BSA	Bovine serum albumin
CFU	Colony forming unit
CH_2Cl_2	Dichloromethane
$CHCl_3$	Chloroform
CuAAC	Copper-catalysed azide-alkyne cycloaddition
$CuSO_4$	Copper(II) sulfate
CV	Column volume
DIPEA	Diisopropyl ethyl amine
DMAP	N, N-Dimethylaminopyridine
DMF	N, N'-Dimethyl formamide
DMSO	Dimethylsulfoxide
DNA	Deoxyribonucleic acid
DPBS	Dulbecco's Phosphate-Buffered Saline
DPIC	Diphenyleneiodonium chloride
Dpn1	Type IIM restriction enzyme
dt	Doublet of triplet
E. spp.	*Enterococcus spp.*
EDC	N′-ethylcarbodiimide hydrochloride
EDTA	Ethylenediaminetetraacetic acid
EPR	Electron paramagnetic resonance
eq.	Equivalents
ESI	Electron spray ionization
Et_2O	Diethyl ether

Et_3N	Triethylamine
EtOAc	Ethyl acetate
EtOH	Ethanol
FAD	Flavin adenine dinucleotide
FMN	Flavin mononucleotide
FP	Fuorophosphonate
g	Gram
GAPDH	Glyceraldehyde 3-phosphate dehydrogenase
GBP	Green Bell pepper
GSH	Glutathione
h	Hours
H. pylori	*Helicobacter pylori*
H_2O	Water
H_2S	Hydrogen sulfide
HCl	Hydrochloric acid
HDAC	Human histone deacetylases
HPLC	High performance liquid chromatography
HRMS	High-resolution mass spectrometry
HWP	Hungarian wax pepper
Hz	Hertz
IAA	Iodoacetamide alkyne
IAM	Iodoacetamide
INDQE	Indole-based quinone epoxide
IPTG	Isopropyl-β-d-thiogalactopyranoside
IR	Infrared
J	Coupling constant
K. pneumoniae	*Klebsiella pneumoniae*
LB	Luria-Bertani
LC/MS-	Liquid chromatography–mass spectrometry
m	Multiplet
m/z	Mass to Charge ratio
*m*CPBA	*meta*-Chloroperoxybenzoic acid
MDR	Multi-drug-resistant

Me	Methyl
MeOH	Methanol
mg	Milligram
MHB	Mueller Hinton broth II
MHz	Megahertz
MIC	Minimum Inhibitory Concentration
Min.	Minutes
mL	Millilitre
mM	Millimolar
mmol	Millimoles
MOA	Monoamine oxidases
MRSA	Methicillin-resistant *Staphylococcus aureus*
MS	Mass spectrum
MSSA	Methicillin-sensitive *Staphylococcus aureus*
Mtb	*Mycobacterium tuberculosis*
MW	Molecular weight
MWCO	Molecular weight cut off
Na_2SO_4	Sodium sulphate
$NaBH_4$	Sodium borohydride
NADH	Nicotinamide adenine dinucleotide
NADPH	Nicotinamide adenine dinucleotide phosphate
NaH	Sodium hydride
NaI	Sodium iodide
NE	Neutrophil elastase
NMR	Nuclear magnetic resonances
NO	Nitric oxide
NOS	Nitric oxide synthase
NP	Nanoparticles
NTA	Nitrilotriacetic acid
NTR	Nitroreductase
NuOF	NADH-quinone oxidoreductase subunit F
NuOG	NADH-quinone oxidoreductase subunit G
OD	optical density

P. aeruginosa	*Pseudomonas aeruginosa*
PBS	Phosphate buffer saline
PCR	Polymerase Chain Reaction
PDB	Protein Data Bank
PDT	Photodynamic therapy
PE	petrolium ether
PEG	Polyethylene glycol
pH	Potential of hydrogen
PPArg2	Protoporphyrin diarginate
PPI	Proton pump inhibitor
ppm	Parts per million
PRSP	Penicillin-resistant *Streptococcus pneumoniae*
PS	Photosensitizer
ROS	Reactive oxygen species
RT	Room temperature
s	Singlet
S. aureus	*Staphylococcus aureus*
SAR	Structural activity relationship
sdhb	succinate dehydrogenase iron-sulfur subunit β
SDS-PAGE	Sodium dodecyl sulfate–polyacrylamide gel electrophoresis
SLIC	Sequence and ligation independent cloning
t	Triplet
TB	Tuberculosis
TBTA	Tris(benzyltriazolylmethyl)amine
^{t}BuOH	*tert*-Butyl alcohol
TCEP	Tris(2-carboxyethyl)phosphine hydrochloride
TEAB	Triethylammonium bicarbonate
TFA	Trifluoroacetic acid
THF	Tetrahydrofuran
TLC	Thin layer chromatography
TMS	Tetramethylsilane
TOP-ABPP	Tandem orthogonal proteolysis–activity-based protein profiling
UV	Ultraviolet

VRE	Vancomycin-resistant *E. faecium*
VRSA	Vancomycin-resistant *Staphylococcus aureus*
WHO	World Health Organisation
WT	Wild type
XDR	Extensively drug-resistant
λem	Emission wavelength
λex	Excitation wavelength
μg	Microgram
μL	Microliter
μM	Micromolar

Acknowledgments

Life is a journey, and now, a part of the journey is going to end soon. I always thank the almighty Shiva for each day I have lived, and I am grateful for his guidance and blessings throughout my Ph.D. journey.

It was not a normal or easy journey for me, especially when I decided to change my research field from organic synthesis to chemical biology in mid of my Ph.D. program. Here, I express my gratitude towards my thesis supervisor ***Prof. Harinath Chakrapani****, who has imparted his knowledge and constantly supported me with an understanding spirit during my Ph.D. All of us have been affected by COVID-pandemic in many ways, but he has endlessly motivated me not only in research but also in life as well. I have been benefited from his critical review throughout my work, which helped me to become a better version of myself*

Next, I sincerely thank ***Dr. Siddhesh Kamat****, Department of Biology at IISER Pune, without whom the DPIC project would not have been at stage of completion. Collaboration with Siddhesh for the DPIC project was the pivotal moment in my Ph.D. His suggestions on crucial times were indeed beneficial. I got an opportunity to work in his lab. His lab members, DR. Dhanashree and Abinaya, were so helpful in teaching me various biological techniques.*

I would like to thank our collaborator ***Dr. Siddharh Chopra****, CSIR-CDRI, Lucknow, who has enthusiastically contributed to the DPIC project and has provided us all the MIC and A. baumannii data required for the continuation of the project.*

Next, I would like to thank my RAC committee members, ***Dr. Anu Raghunathan****, NCL Pune, and* ***Dr. Pinaki Talukdar****, IISER Pune, for their suggestions and comments during my RAC meetings.*

I would like to thank Director of IISER Pune, Prof. Jayant. B. Udgoankar and chair of the chemistry department Prof. H.N. Gopi, for providing excellent research lab facilities.

I would like to thank CSIR for the fellowship as financial support.

Dr. Ritima Das, a friend-turned-sister, has been a source of encouragement for me during many of my difficult moments. I'd never known affection like that from a sister until I met her. She has lavished me with affection and attention. She has witnessed all of my difficult days, my vulnerable situations at times, as well as the bright and cheerful moments I had here at IISER. I am fortunate to have her at my side at all times.

I thank my friend Jagan for giving positivity and making me smile in my bad times. He taught me that issues aren't always as serious as we make them out to be by overthinking them.

I thank my friends Kiran and Praveen because, despite the fact that they are not physically present here with me, we have maintained our long-distance connection and never felt as if we were chatting after ages. Ishika, we've bonded so well in such a short amount of time that it doesn't seem like we've only met a few months ago. Thank you for these memories to cherish, be it talking about random topics, sharing life experiences, having a long tea time conversation over the weekend, and so on. With your sweet talks, you've made my final year of Ph.D. one to remember.

It was a pivotal point in my Ph.D. when I switched research fields and joined Hari's lab, and I'd want to thank all of my former lab colleagues, Dr. Kundan, Dr. Ravi, Dr. Ajay, Dr. Preeti, and Dr. Amogh, for keeping the lab environment positive and encouraging me to keep improving. Especially, Ajay and Amogh mentored me in synthesis, instrumental techniques, and biological assay. Amogh has always supported my self-esteem and been by my side at my worst moments. Discussions with Anand were always helpful to me. My current lab colleagues Dr. Kavita, Anand, Laxman, Prerona, Suman, Bharat, Utsav, Pooja, Simran, Minhaj, and Dr. Amol and also the graduate students of the lab, Farhan, Harshit, Gaurav, Swetha, Ashwin, Mrityunjay, Suraj, Amal, Manjima, and Jishnu, they all had made the working environment healthy and upbeat with their fun bunters and leg-pulling. I had an opportunity to mentor Suraj and Utsav. I thank each of them for making this ride more precious and memorable.

I would like to thank Rupali, Yamini, Yashwantj ji, for their helping me to understand many biological concepts and methods.

I also thank the administrative staff. Mayuresh, Mahesh, Yathish, Tushar, and Mrs. Sayalee for their administrative help throughout my doctoral study and instrument operators Sandip (HRMS), Deepali, Chinmay, and Nitin (NMR), Ganesh (IR).

A special thanks to MAA, PAPAji, and my brother Himanshu, who supported me to pursue my education at a time when girls' education was not prioritised in our region. Especially after Babu's demise, it was even more difficult for them to send me away for education. It's been 7 years since I've been away from my family due to my Ph.D., and it's not just been difficult for me, but also for them as well. I'm happy and grateful they're still here with me. I also thank my Bhabhi who has shown me so much love and positivity. I hope I made it worth. I am excited to be the first girl in my family to achieve such academic success.

Abstract

Antimicrobial resistance (AMR), especially among Gram-negative pathogens, is a major problem worldwide, and new classes of chemotherapeutics with novel mechanisms are urgently needed. Diphenyleneiodonium (DPIC) chloride is an antiseptic agent with excellent activity against Gram-positive bacteria and moderate inhibitory activity against Gram-negative bacteria. A number of new approaches towards developing therapeutics against Gram-negative pathogens are in urgent need. Although several mechanistic studies have been conducted, primarily in mammalian cells, the biological targets for DPIC remain to be elucidated in bacteria. In order to understand the mechanism of action, an iodonium probe containing an alkyne handle was next synthesized. This probe enables biorthogonal reactions and aids in identifying proteins that the probe and, by extension DPI has modified. Preliminary findings using activity-based protein profiling (ABPP) methods with bacterial lysate revealed that the iodonium compound modifies proteins with preliminary data suggesting that this modification was covalent and through a cysteine residue. Next, in order to find the biological targets of DPIC, LC-MS/MS-based competitive ABPP was carried out with *E. coli*. This analysis revealed that proteins with redox cofactors, as well as those involved in respiration were the most likely biological targets for DPIC. In order to validate these results, one of the target proteins, NuOF was cloned, purified, and was found to be covalently modified by the probe, likely through a cysteine residue. Having identified targets of DPI in bacteria, we next proceeded to perform a structure-activity relationship study with a goal of improving potency against *Acinetobacter baumannii* (*A. baumannii*), which is listed among the top priority pathogens for new drug development by the World Health Organization. Given the abundance of heterocyclic compounds in bioactive molecules, such as antibiotics, a series of heterocyclic iodonium analogs were synthesized to enhance the spectrum the antibacterial activity towards Gram-negative bacteria. Several compounds in this series were found to have excellent inhibitory activity against Gram-negative bacteria, including multi-drug resistant *A. baumannii*. The lead compound in this series was found to have bactericidal activity against *A. baumannii*, had a favourable selectivity index, and showed excellent activity in an animal model for infection. Using chemproteomics methods, the targets of the lead compound were identified. In summary, our study of the structure-activity relationship with iodonium salts led to the identification of a promising antibacterial candidate, while chemoproteomics with a

newly developed probe provided insights into the unique mechanism of action for this class of antibacterials.

In a separate approach to addressing AMR, we developed a strategy for the light-activated generation of fluoroquinolones. The use of optical control over the delivery of antibacterials, also known as antimicrobial photopharmacology, involves developing strategies for spatiotemporal control over the generation of a drug and minimizes environmental exposure to the drug. We designed and synthesized BODIPY-Levo, a caged derivative of levofloxacin. The prodrug does not generate the active antibiotic unless exposed to light (470 nm). The efficacy of this conjugate to inhibit bacterial growth in the presence of light is demonstrated. In summary, two independent small molecule-based approaches to address antimicrobial resistance were developed.

Chapter 1: Introduction

1.1.Bacteria, Antibiotics and Antimicrobial resistance

Bacteria is a unicellular living microorganism, which is difficult to visualize by the naked eye without using a microscope.[1] Bacteria lack a nucleus and other organelles and have a cell wall which is consisting of peptidoglycans. Based on the architecture of the cell wall, bacteria can be either Gram-positive or Gram-negative bacteria.[2] These different bacterial cells are generally being identified by the Gram staining technique, Gram-positive bacteria retain the crystal violet color and appear as purple color, and Gram-negative do not retain the crystal violet color and appear as pink color due to the presence of outer lipid membrane.[1] Many bacteria are essential for human survival. For example, in the digestive system, gut microbes help to break down complex sugar or nutrients into forms that the body can use. Lactic acid bacteria, such as *Lactobacillus* and *Lactococcus,* are often used in the fermentation process. Some of the fermented food items contain bacteria that offer health benefits like strengthening the gastrointestinal health and anti-inflammatory effect.[3] While pathogenic bacteria cause diseases in human and animal bodies such as pneumonia, typhoid, and tuberculosis (TB). Infectious diseases caused by bacteria are among the leading causes of mortality worldwide.

An antibiotic is a chemical substance produced by or derived by certain microorganisms either to inhibit bacterial growth or kill bacteria. Antibiotics are widely used now to prevent and cure infectious diseases. Depending upon the activity, antibiotics are classified into two different categories, bacteriostatic and bactericidal.[4] Bacteriostatic antibiotics only inhibit bacterial growth, whereas bactericidal antibiotics kill the bacterium. Based on the mechanism of action, antibiotics are classified into various categories. Aminoglycosides and tetracyclines inhibit the protein synthesis by binding to the 30S subunit of the ribosome, whereas macrolides bind to the 50S subunit of the ribosome. Fluoroquinolones bind to the DNA gyrase and inhibit DNA synthesis. β-lactams inhibit cell wall synthesis.[4] Among these antibiotics, those that are active against a limited group of bacteria are known as narrow-spectrum antibiotics. On the other hand, broad-spectrum antibiotics are active against both Gram-positive as well as Gram-negative bacteria. In 1913, at the Congress for Internal Medicine at Wiesbaden, the scientist Paul Ehrlich announced the development of the first antibiotic, Salvarsan[5], to cure Syphilis, a sexually transmitted bacterial infection caused by *Treponema pallidum*. The discovery of Penicillin as “the wonder drug” had saved numerous lives during World War and rescued patients from several bacterial.[6] This led to the mass production of Penicillin at that time.

However, in a span of a few years, this antibiotic was ineffective against certain infections. It was discovered that the microorganisms were able to develop resistance against the antibiotic and were no longer sensitive to the antibiotic. This phenomenon is referred to as antimicrobial resistance (AMR). There are many factors that contribute to antimicrobial resistance[7,8], such as

- Overuse of antibiotics
- An incomplete course of antibiotic treatment by patients
- Use of antibiotics in food farming practices
- Poor hygiene control and longer exposure to infections in hospitals have evoked the emergence of multidrug-resistant bacteria extensively drug-resistant (XDR) bacteria
- Lack of new classes of antibiotics

In 2014, the World Health Organisation (WHO) had published a global surveillance report and shown the impact of multi-drug-resistant bacteria in the world. The report revealed that 45% of deaths in both South-East Asia and Africa were attributed to multi-drug-resistant (MDR) bacteria. The term "ESKAPE" refers to a panel of six highly virulent multidrug-resistant bacteria *Enterococcus spp.*, *Staphylococcus aureus, Klebsiella pneumoniae*, *Acinetobacter baumannii*, *Pseudomonas aeruginosa,* and *Enterobacter spp.* (ESKAPE) that are responsible for the majority of nosocomial infections.[9] The ESKAPE pathogens are inclined to develop a high level of multi-drug resistance and increase mortality and morbidity, therefore limiting the options for therapeutics.[9,10,11] Various studies revealed that the clones of the resistant ESKAPE pathogens are transmitted in communities and hospitals in both developing and developed countries.[12,13] Due to this, the world is at the edge of the post-antibiotic era, and if this trend continues, even the routine bacterial infections might not be treatable. Also, the timeline of antibiotic discovery and antibiotic resistance indicates that there was almost a large antibiotic discovery void after 1990, and Teixobactin was the last antibiotic discovered in 2020 (Figure 1.1).[14,15] Considering this as an upcoming global health threat, in 2018, WHO has listed out the ESKAPE pathogens on priority multi antibiotic-resistant bacteria to urgently discover and development of new antibiotics.[16] In this priority list, three categories of pathogens were described according to the need for new antibiotics, named critical, high, and medium. The critical priority list of pathogens included extended-spectrum β-lactamase (ESBL) or carbapenem-resistant *K. pneumoniae* and *Enterobacter spp.* along with Carbapenem-resistant *A. baumannii* and *P. aeruginosa*. Whereas methicillin and Vancomycin-resistant *S. aureus* (MRSA and VRSA) and Vancomycin-resistant *E. faecium* (VRE) were listed in the high

priority group.[16] The ESKAPE pathogens develop multi-drug resistance (MDR) through several mechanisms as listed out below:[17]

- by inactivating the drug by an enzyme
- by modifying the active site where the antibiotic binds,
- or reduce drug accumulation due to decreased permeability
- by effluxing the drug out

Due to dwindling treatment options, Gram-negative ESKAPE pathogens (*K. pneumoniae*, *A. baumannii*, *P. aeruginosa*, and *Enterobacter spp.*) require more resources and attention.

Figure 1. 1 Timeline of discovery of antibiotic and developed antibiotic resistance

1.2. Strategies to Combat Antimicrobial Resistance:

In order to address this antimicrobial resistance (AMR), many therapeutic strategies that are in development are the use of antibiotics in combination or with adjuvants, photodynamic therapy, spatiotemporal control over the antibiotic generation, use of antimicrobial peptides, bacteriophage therapy, phytochemicals, and nanoparticles as antibacterial agents, antibacterial antibodies, enhancement in the spectrum of antibacterial activity and discovery of a new class of antibiotics (Figure 1.2).[17]

Figure 1. 2 Strategy developed to Combat Antimicrobial Resistance

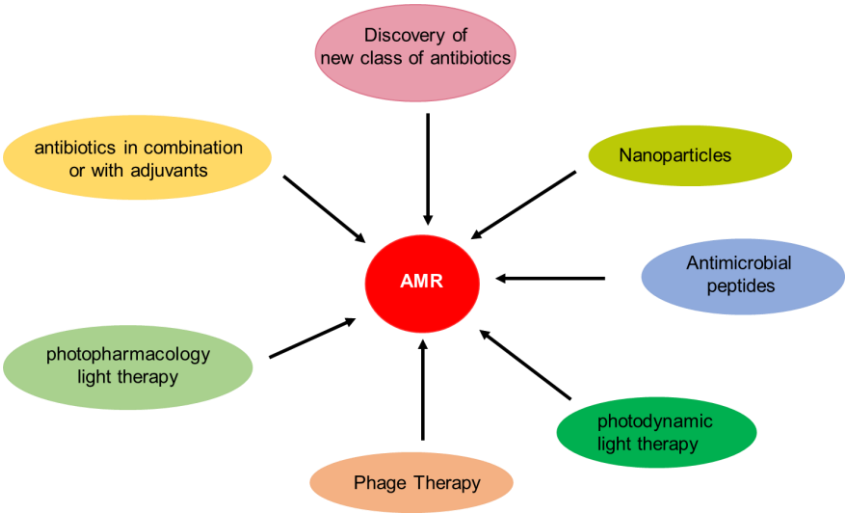

1.2.1. Antibiotics in combination or with adjuvants:

A multitude of studies revealed that antibiotic in combination is a good treatment method because the synergistic effect shown by both antibiotics in combination would be stronger than an individual antibiotic alone.[18,19,20] Also, the likelihood of the resistance developed by bacteria is low against a combination of two antibiotics than a single antibiotic. Antibiotics in combination also enhance the antibacterial spectrum of the heuristic therapy and is fruitful in severe infections caused by multiple pathogens.[21] For example, *in vitro* studies by Rybak and co-workers have shown that Fosfomycin is able to enhance the activity of Daptomycin, against vancomycin-resistant *Enterococcus faecium* and *E. faecalis* strains and shown synergistic bactericidal activity, when used in combination.[22] Adjuvants are compounds that by themselves have limited activity in inhibiting bacterial growth but are highly effective when used in combination with clinical drugs.[23] Adjuvants play a key role in fighting against bacterial resistance and can act by changing the morphology of the bacterial cells, by inactivating efflux pumps, or by increasing antibiotic uptake.[24,25] Vaborbactam is a popular adjuvant, which restored the activity of meropenem against *K. pneumoniae* carbapenemase and acts by inhibiting the β-lactamases.[26] At present, vaborbactam-meropenem combination is in clinical trial phase 3.[27] Along with this tazobactam, nacubactam, avibactam and metal chelators like deferoxamine, EDTA and deferasirox also inhibit *β*-lactamases.[28,29] Jan Michiels and co-workers have shown that 1-[(2,4-dichlorophenethyl)amino]-3-Phenoxypropan-2-ol in combination with different antibiotics kills all ESKAPE pathogens, making it a potential

adjuvant candidate.[30] However, most of the *in vitro* combination studies do not necessarily translate well in *in vivo* studies. Also, an antibiotic can cause a resistance mechanism to a second antibiotic when used together, resulting in antagonistic effects. In combination therapy, ESKAPE pathogens become resistant to either or both the antibiotics over time, due to the natural selection and horizontal transfer of antibiotic resistance gene.[31,32] Thus, combination therapy with antibiotics may not be always effective and alternative strategies are required to tackle antibiotic resistance.

1.2.2. Antimicrobial peptide:

Antimicrobial peptides (AMPs) are naturally occurring positively charged amphipathic molecules produced by multicellular organism as the first line of defense.[33] These proteins show broad-spectrum activity against bacteria, fungi, viruses, yeasts, and cancer cells. In general, AMPs interacts with bacterial cell membrane through electrostatic interactions and induce membrane disruption, resulting in cell lysis and death.[34] Unlike other antibiotics, the propensity for bacteria to develop resistance against AMP is low. AMPs enter inside cells without altering the membrane and bind to nucleic acid and proteins to inhibit the essential function of cells. In 1922, Lysozyme was the first human antimicrobial protein identified by Alexander Fleming from nasal mucus.[35] Gramicidin S, Tyrothric, Telavancin, and Vancomycin AMPs are used as therapeutics in the clinics.[36] *In vitro* studies done by Mira Edgerton and co-workers suggested that a histidine-rich human salivary peptide Histatin 5, exhibits potent anti-biofilm and bactericidal activity against ESKAPE pathogens.[37] Joakim Håkansson's group have shown that lactoferrin-derived AMP HLR1r displayed antibacterial activity against MRSA in an animal model.[38] *In vitro* studies suggested that HLR1r is non-toxic and anti-inflammatory and can be used as a topical agent. Owing to their broad-spectrum antibacterial activities, AMPs can be an alternative to conventional therapeutics. However, due to problems associated with the high cost of peptide as well as high cytotoxicity of some AMPs, translation into the clinic is challenging. Also, AMPS are susceptible cleavage by proteases and appropriate structural modifications need to be made to address this problem.

1.2.3. Nanotechnology:

In an alternative approach, nanotechnology, which utilizes antibacterial nanoparticles to treat infections caused by drug-resistant pathogens, is being used in clinics.[39] Being small in dimension, such particles can easily pass through the cell membrane and disturb the internal important cell functions.[40,41,42] Moreover, nanoparticles conjugated with antibiotics may

exhibit a synergistic effect against bacteria.[43] Vincent M Rotello's group has utilized the hydrophobically functionalized gold nanoparticles (Au-NPs) in combination with fluoroquinolone antibiotics against MDR *E. coli* infections and achieved an 8-16-fold reduction in antibiotic doses.[44] Similar synergistic effect was also shown by Hemeg's group with Au, Ag, and ZnO NPs and antibiotics against *E. faecium*, *S. aureus, A. baumannii*, *P. aeruginosa*, and *E. coli*.[39] Sivasubramanian co-workers employed two *Capsicum annuum's* food plants Green Bell pepper (GBP) and Hungarian wax pepper (HWP), with zero-valent silver nanoparticles and demonstrated their bactericidal effect against *S. aureus*. It was shown that HWP/GBP AgNPs potentially inhibit biofilm formation in an infected zebrafish model.[45] While these studies indicate the applicability of antibacterial NPs. Certain other parameters such as toxicity, pharmacokinetics, manufacturing of metal NPs at a large scale remain to be fully investigated.

1.2.4. Phage Therapy:

In another strategy, where phages (bacterial virus) are being used in the treatment of bacterial infections call bacteriophage therapy. Phages are known for selectively killing bacterial cells. Once the virus infects the host bacterial cell and reproduces itself within the cell, leading to the bacterial cell lysis or death, due to this selectivity towards host cells and rapid self-proliferation, bacteriophages can be an ideal therapeutic agent. Several *in vivo* and *in vitro* studies carried out using bacteriophages have shown promising effects against ESKAPE pathogens-mediated bacterial infections.[46,47,48] Phage therapy in combination with an antibiotic may show a synergistic effect. For example, in *in vitro* studies, Chan and co-workers have shown the synergistic effect of Phage PEV20 with ciprofloxacin against *P. aeruginosa*, a Gram-negative bacteria responsible for specific infections such as ventilator-associated pneumonia and sepsis.[49] However, due to the lack of understanding in mechanism responsible for synergistic effect, the fate of phage antibiotic combination therapy is yet in its infancy.

1.2.5. Antibacterial photodynamic therapy:

Another interesting strategy, known as antibacterial photodynamic therapy (aPDT) utilizes light as a source and a photosensitizer (PS) or photoactivatable dye to target bacterial infections. When a PS is exposed to the light of an appropriate wavelength, by intersystem crossing process, the PS transforms from singlet to triplet state and transfers energy or electron to surrounding species or oxygen to generate reactive oxygen species (ROS), which is toxic to cells.[50,51] Thus, it is very important for a PS to have greater selectivity towards bacterial cells, good permeability, and a higher absorption coefficient for a longer wavelength light source to

effectively penetrate through the infected tissues.[52,53,54] Chaoxing Li and co-workers have developed a boron-dipyrrolemethene (BODIPY)-enclosed glycosylated PS named as pGEMA-I and exemplified its antibacterial against *Pseudomonas aeruginosa* after exposing it to visible light (400-800 nm). Moreover, it is found to inhibit over 90% of biofilm caused by *P. aeruginosa*.[55] Bielawski's group has studied the bactericidal effects of Protoporphyrin diarginate (PPArg2) upon photoactivation at 624 nm wavelength on 40 clinical isolates of methicillin-sensitive *S. aureus* (MSSA) and methicillin-resistant *S. aureus* (MRSA), and their results revealed a significant reduction in the bacterial population.[56] Based on the literature reports available on PDT, the use of blue light 410 ±10 nm is recommended for the treatment of topical wound infections.[57,58,59] It was demonstrated that the photoexcitation of the intracellular porphyrins ring present in the bacterial cell membrane by blue light triggered the production of highly cytotoxic ROS, resulting in cell death. Oppenheim and co-workers studied the antibacterial activity of blue light (400 nm) on 34 clinical isolates of ESKAPE pathogens and found a significant reduction in bacterial viability after 15 to 30 min of blue light exposure.[60] The efficacy was improved when PDT was also being used in combination with antibiotics. For example, Grinholc and co-workers have shown the synergistic effect of blue light in combination with various antibiotics on resistant *P. aeruginosa* isolates and observed the reduction in several virulence factors.[61] Taken together, PDT seems to be an appropriate method for the treatment of certain infections caused by ESKAPE pathogens. However, more studies needed to be investigated for the toxicity or biocompatibility of combination methods with PDT in *in vivo* models to translate them into clinical therapeutics.

1.2.6. Antibacterial photopharmacology therapy:

The antibacterial molecule or antibiotic can also interact with targets present in mammalian cells as well.[62] For certain types of skin infections or chronic wound dressing, controlled release of antibiotics can be applied, which can be helpful to reduce the side effects. In order to achieve off-target activity and avoid the severe side of antibiotics, photopharmacology technique can be utilized, which offers light as an external handle to control the drug's action.[63,64] Several advantages are associated with light, which supports that light can be used as a trigger. For example, light is relatively noninterfering, biorthogonal, does not contaminate the samples.[65] In the antimicrobial photopharmocology field, an antibiotic is appended with either photocleavable group or optical switch, which upon activation releases the active form of antibiotic. An exemplary work by, Feringa and co-workers have shown that a model fluoroquinolone is attached with a diazo functional group which acts as an optical switch, and

upon activation with UV light, it goes through isomerization and generates the active antibiotic.[65] It was also revealed that once the antibiotic action is accomplished against *E. coli* and *S. aureus*, it can be inactivated with the use of another light source. In another study, Fuchter and co-workers have developed aminohydrolase-based photoswitchable bacterial HDAC (human histone deacetylases) homologs inhibitors with azobenzene and azopyrazole functionality and obtained good inhibitory activity.[66] It was also discovered that arylazopyrazole photoswitchable inhibitors had shown an increment in performance than azobenzene inhibitors. Along with photoswitches, various photocleavable protecting groups such as aryl carbonyl methyl groups, coumarins, and *o*-nitrobenzyl groups with a considerable difference in λ_{max} have been reported.[67,68,69] Forsythe and co-workers have shown a ciprofloxacin appended hydrogel with an *o*-nitroaryl cleavable group, which upon exposure to UV light releases ciprofloxacin.[70] Using Muller–Hinton agar plate method, the antimicrobial effect of released antibiotics was demonstrated against *S. aureus* bacterium. In another study, Gademann and co-workers have incorporated vancomycin and cephalosporin antibiotics with an *o*-nitroaryl cleavable group, which can be activated with UV light. The antimicrobial activity of liberated antibiotics was assessed using bacterial growth curve analysis against *B. subtilis*, *S. aureus*, MRSA, *E. coli*, and *P. aeruginosa*.[71] However, the use of UV light is undesirable because of its phototoxicity. Hence, a visible light-triggered photocleavable group with an antibiotic is highly advantageous. This will be further discussed in Chapter **4**, where visible light-activated release of fluoroquinolone was demonstrated.

1.2.7. Drug discovery:

All aforesaid developed methods have certainly helped in their own way to overcome antibiotic resistance. However, most of the remedial strategies do not directly "tackle resistance" but circumvent it. Also, looking at the timeline and rate of emerging antibiotic resistance, discovery and identification of new antibacterials with novel mechanisms are urgently needed. Two general approaches for the identification of new active molecules are target-based drug discovery and phenotype-based drug discovery.[72,73] The principle of targets-based drug discovery includes the selection of targets and followed by the screening of various molecules using biochemical assays to identify the active or lead molecule.[73] In bacteria, a drug targets cell wall machinery, enzymes involved in protein synthesis, energy production sites, regulatory and transcriptional factors.[74] For example, Johnsson and co-workers have identified a benzothiazinone BTZ043 as a potent inhibitor of DprE1 enzyme which is involved in cell wall synthesis of *M. tuberculosis*.[75] At present, this compound is in clinical trial phase 2. However,

the availability of limited validated targets and results of *in vitro* studies may not describe the accurate interaction of compounds in native systems limits the use of target-based drug discovery.[76] Whereas, in phenotype-based drug discovery, several molecules are screened using biochemical phenotype assays in cells, tissues, or organisms to identify the lead molecule, which can be utilized to identify the targets.[77] Although it is commonly accepted that one drug has one target, this is not the case.[78] It is more likely that the identified molecule may interact with multiple targets and can have a complex mechanism of action. Thus, the target identification method is most crucial and important step in phenotype-based drug discovery. Various technologies for target identification have been developed. However, proteomics and genomic approaches with advanced molecular biology are the principal tools.[79] In proteomic approaches, the entire pool of proteins known as proteome is used to study the possible targets for a drug or drug-like molecule. In order to study covalent interaction, activity-based profiling is used.[80]

1.3. Activity-based protein profiling (ABPP):

Activity-based protein profiling (ABPP) has been quite extensively used to study the complex proteomes (a pool of proteins expressed by an organism) of different biological systems like cancer and bacterial cells.[81] In therapeutics, it helps to study the important protein's functionality or reactivity or the amino residue involved in important biological processes. ABPP is a chemoproteomic approach that exploits an activity-based chemical probe to discover the functional state of proteins or enzymes of cells or organisms. A classic activity-based chemical probe consists of a reactive group that would react with protein residue, and this active group is attached to a reporter tag or analytic handle through a linker (Figure 1.3). The analytic handle can be an alkyne or azide or biotin tag, which can be utilized to obtain readouts. With the reporter tag, biorthogonal chemistry using copper-catalysed Huisgen's azide-alkyne cycloaddition (CuAAC) can be employed,[82] where activity-based probe with alkyne/azide handle can react with fluorescent or azide/alkyne using copper catalyzed click reaction to obtain the readouts.[83,84]

ABPP involves the treatment of an unlabelled proteome with an activity-based chemical probe, where the reactive group of the probe will react with a certain residue of protein depending upon its activity. This is followed by the click reaction with a fluorescent azide/alkyne. The readouts or identification of target proteins can be obtained using Sodium dodecyl-sulfate polyacrylamide gel electrophoresis (SDS-PAGE) analysis or LC-MS/MS (Figure 1.4).[85–89]

Figure 1. 3 Design of Activity Based Chemical Probe

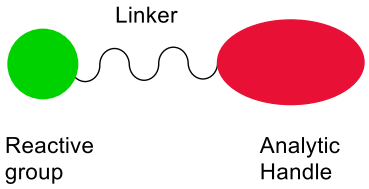

Due to indiscriminate reactions of the probe, certain off-target proteins may be identified during profiling. Hence, to filter out the off-targets, a competitive ABPP is designed (Figure 1.5).[86] In competitive ABPP, the proteome is first labelled with the active or lead molecule or inhibitor, which will react with certain protein residue and block them to react further with the probe in the next step. Another set of proteomes is reacted with DMSO, which will not interact with proteins, hence can be used as a control. Using SDS-PAGE, the readout can be visualized on a gel, where a lesser number of protein bands or bands with reduced intensity can be seen in the active molecule treated lane when compared to the DMSO treated lane. Further, LC-MS/MS, these protein targets can be identified and quantified.[90,91]

Figure 1. 4 Schematic of Activity-Based Protein Profiling

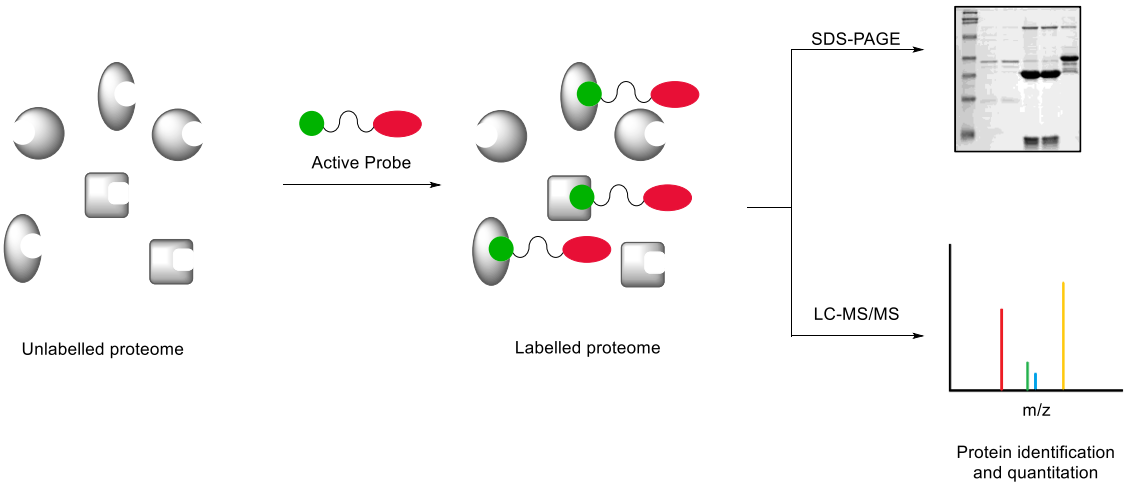

Chemoproteomic approaches have been extensively used in drug discovery on research platforms. A number of studies utilized the ABPP techniques to address antibiotic resistance. For example, Sieber and co-workers have designed and synthesized a library of *β*-Lactam probes[92] to utilize it *in vivo* labelling of enzymes responsible for antibiotic resistance, cell wall synthesizing enzyme, and virulence in resistant *Pseudomonas putida* and *Bacillus licheniformis*.[93] Using these β-Lactam probes, resistance and virulence-associated enzyme Caseinolytic protein protease (ClpP) were identified as drug targets along with penicillin-

binding proteins. In another study, these β-Lactam probes have been used to reduce the production of virulence factors by inhibiting the ClpP in *S. aureus*.[94] On the similar lines, the same group has shown the application of Showdomyocin antibiotic-based probe to *S. aureus* and identified MurA1 and MurA2 enzymes as antibiotic targets that play a crucial role in the process of cell wall synthesis and was previously identified as targets for Fosfomycin.[95]

Figure 1. 5 Schematic of Competitive Activity-Based Protein Profiling

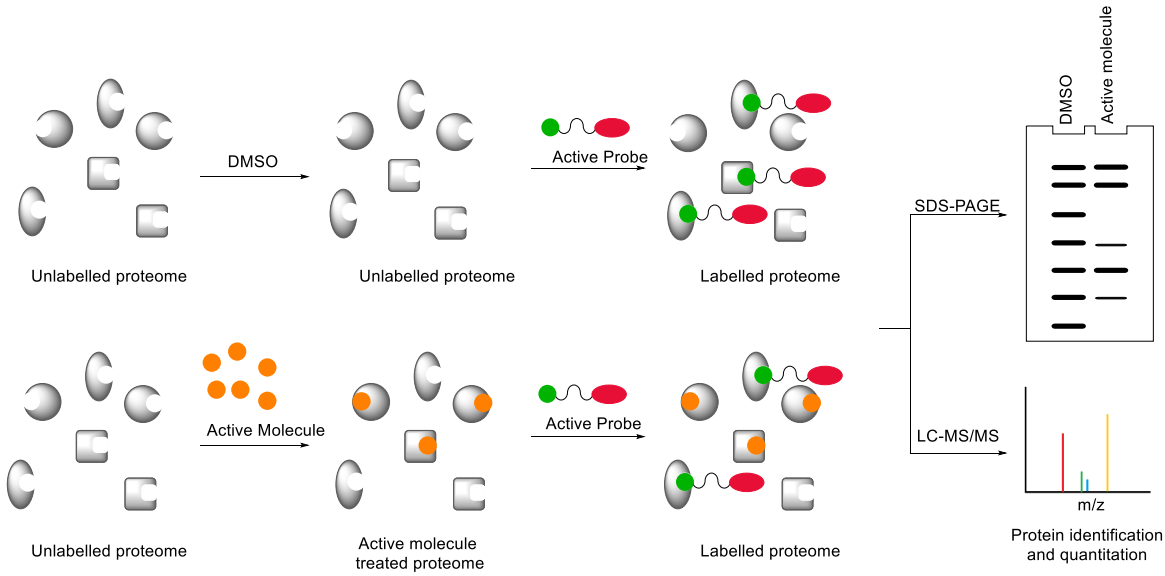

Natalie and co-workers have used a serine protease-based fluorophosphonate (FP) probe to characterize the active site of Rhomboid protease GlpG (Figure 1.6), an enzyme that irreversibly cleaves other polypeptides, which is important for cell regulation in *E. coli*.[96] Aaron and co-workers have developed a suite of *N*-halogenated glycosylamine, difluoro methyl phenyl aglycone, and 2- deoxy-2-fluoroglycoside probes for the labelling of cellulose-degrading enzymes and other glycoside hydrolases in *Clostridium thermocellum* bacterium.[97,98] To investigate the protein sensitivity under H_2O_2 stress conditions in *S. aureus* and *P. aeruginosa*, Cravatt and co-workers have profiled the functional cysteines with isotopic iodoacetamide probes using isotopic tandem orthogonal proteolysis–activity-based protein profiling (TOP-ABPP).[99] Using chemoproteomic approaches, reactive cysteine-based proteins, quorum sensing regulator LasR, acetaldehyde dehydrogenase (ExaC), arginine deiminase (ArcA), and glyceraldehyde 3-phosphate dehydrogenase (GAPDH) were identified as major targets. Using competitive ABPP, Cravatt and co-workers have designed an alkyne probe AspR1 based on metalloprotease inhibitors TAPI-0 and GM60001 and identified peptide deformylase as targets in *Chlamydia trachomatis*.[100]

Figure 1. 6 Reported examples Activity based probes

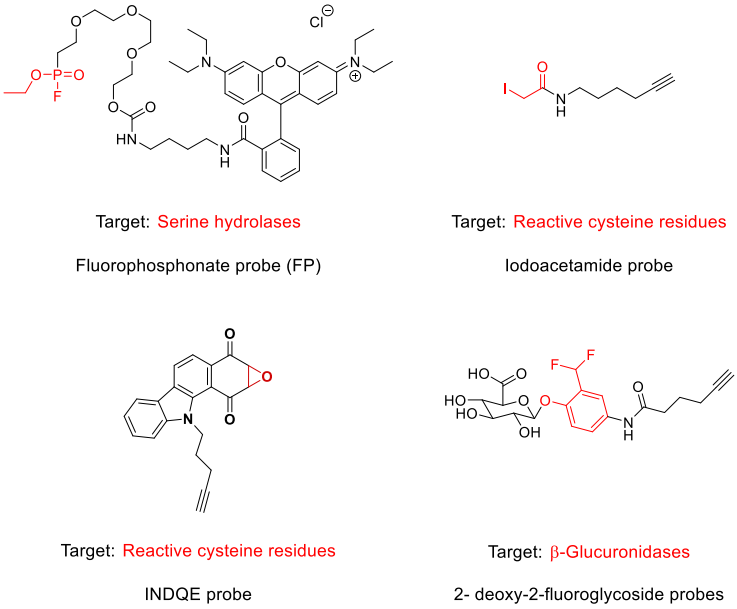

Chakrapani and co-workers have designed an indole-based quinone epoxide (INDQE) alkyne probe to profile the thiol proteome in *S. aureus* and identified transcriptional factors multiple antibiotic resistance regulons (marR) MarR_12840 and MarR_05815 as targets.[101] All these aforesaid reports revealed the utility of chemoproteomics approaches in drug discovery and target identification to address antibacterial resistance. In order to follow the phenotype-based drug discovery approach, screening of antibacterial molecules with a novel mechanism of action is required. Here, based on the available literature reports, the antibacterial iodonium class of molecules was selected as their mode of action is not explored yet in bacterial cells, and using chemoproteomic approaches, targets were identified in Gram-negative bacteria. This will be discussed in Chapters **2** and **4**.

1.4. Iodine and Iodonium compounds:

Iodine ([Kr] $4d^{10}$ $5s^2$ $5p^5$) was first discovered by a French chemist Bernard Courtois in 1811 and named by J. L. Gay Lussac in 1813.[102] Iodine is the largest in size, most polarizable, and least electronegative atom among halogens (Iχ = 2.66, Brχ = 2.96, Clχ = 3.16 and Fχ = 3.96). It can easily form polyvalent (valency up to 7) compounds. The common polyvalent iodine compounds are I (III) and I (V) species. First organic iodine I (III) compound $PhICl_2$ was synthesized by a German chemist C. H. C. Willgerodt in 1886.[103] The Martin–Arduengo nomenclature [N-X-L] is used for hypervalent iodonium compounds, where N is the no of a valence electron, X represents a central atom, and L indicates no of ligands.[104] Iodine- (III)

species have similar chemical properties to Hg(II), Tl(III), and Pb(IV) excluding the toxicity and environmental problems associated with these heavy metal congeners.

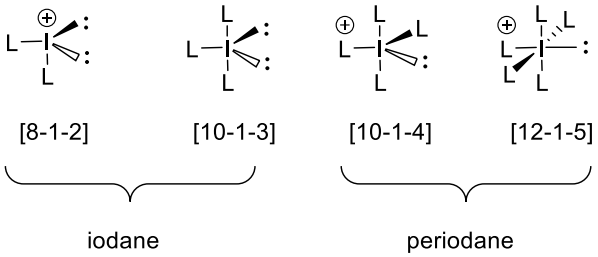

1.4.1. Chemistry of diaryliodonium compounds:

In Iodine- (III) species, diaryliodonium compounds have gained much attention as an arylating agent in synthetic organic chemistry with various substrates under polar, photochemical or catalytic conditions.

Figure 1. 7 Reaction of diaryliodonium compounds

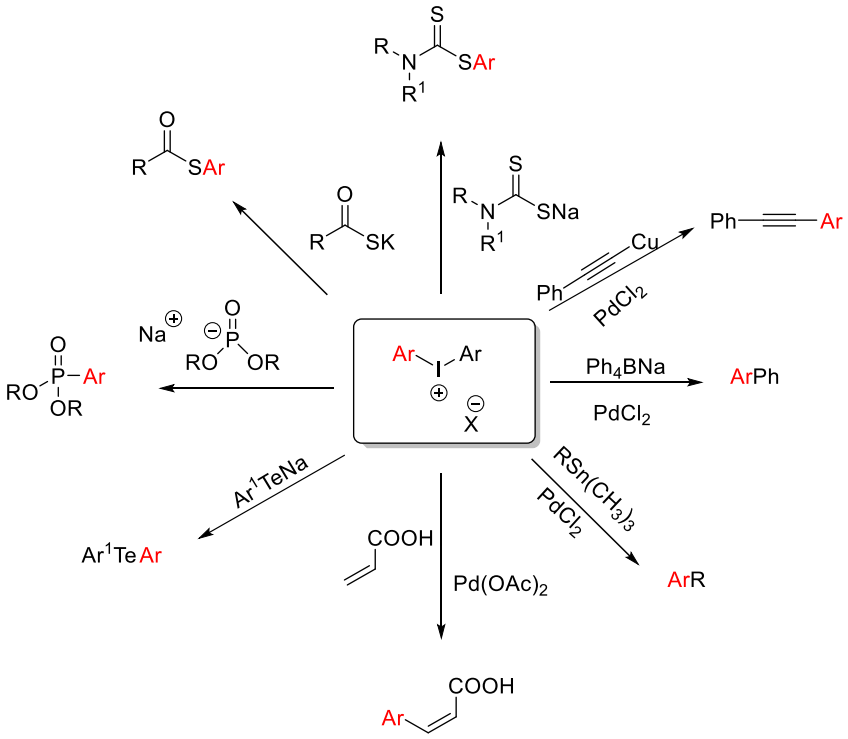

For example, under polar conditions, nucleophilic anion can react with diaryliodonium compounds and get arylated. This includes the arylation of thiocarboxylates,[105] thiocarbamates[106,107], and dialkyl phosphites[108] etc (Figure 1.7). Tolstaya and co-workers have proposed the mechanism of diaryliodonium compounds with nucleophiles under polar

conditions.[109,110,111] Diaryliodonium with nucleophile can form the [10-I-3 T-shape] hypervalent trigonal bipyramidal intermediate where the bulkier aryl moiety along and two lone pairs prefer to occupy the equatorial positions. For the non-rigid diaryliodonium compounds, the [10-I-3 T-shape] can undergo intramolecular rotation *via* [10-I-3 Y-shape] tetragonal pyramidal intermediate where the interaction of Ar-Nu is symmetry allowed, and nucleophile can bind at bulkier aryl moiety or most electron-deficient aryl moiety if the size of both aryl moiety is same. For the rigid diaryliodonium compounds, the transition from [10-I-3 T-shape] to [10-I-3 Y-shape] is not symmetry allowed. Thus, the [10-I-3 T-shape] undergoes homolysis and generates the aryl radical species [9-I-2], which can react with nucleophile radical along with available radical species and give multiple products (Figure 1.8).

Figure 1. 8 Proposed reaction mechanism of diaryliodonium compounds

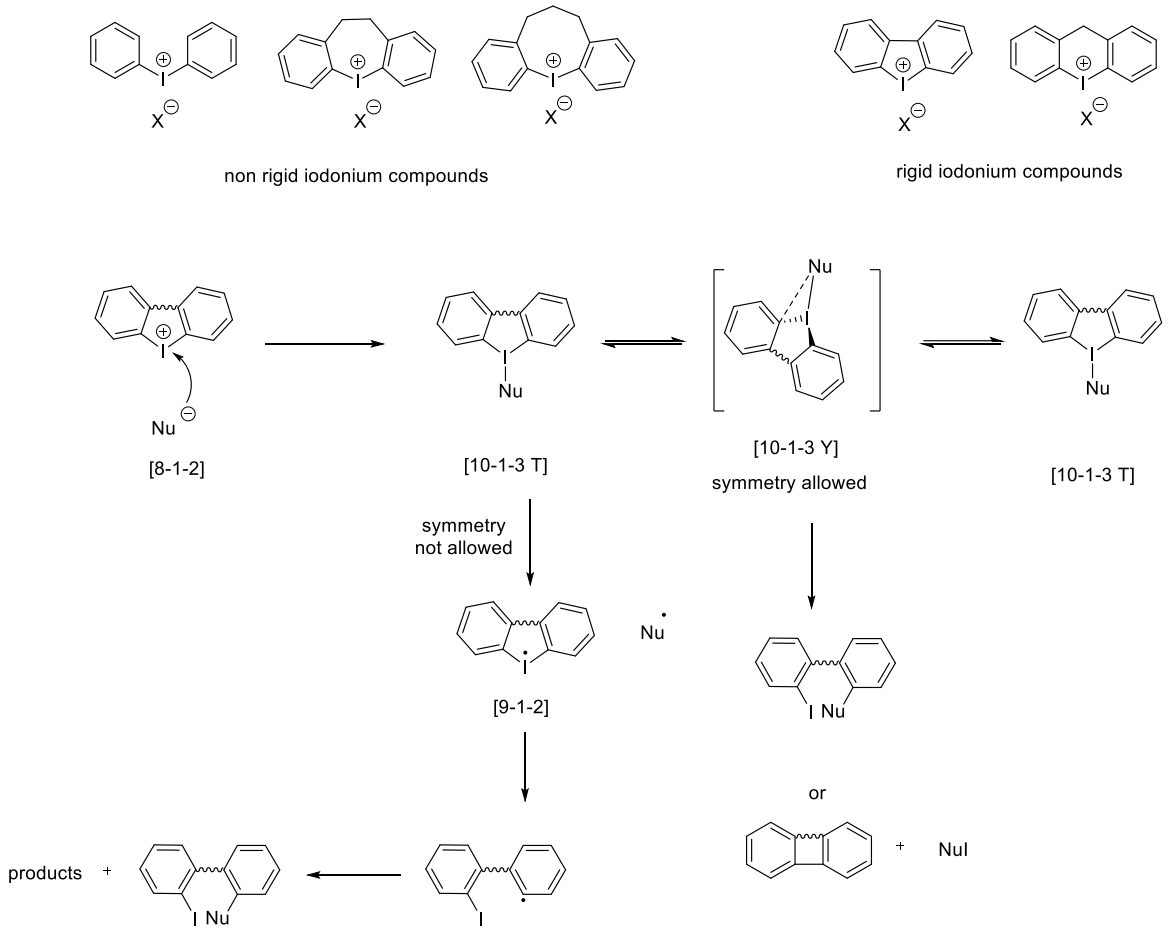

Arylation with diaryliodonium compounds also occurs through transition metal-catalyzed reactions. Palladium-catalyzed reaction with diaryliodonium compounds includes arylations of copper acetylide,[110] sodium tetraphenylborate,[112] organotin compounds[113], and acrylic acid[114]. The photochemical reaction with diaryliodonium compounds goes through the generation of

aryl radical or radical cation, and this can be applied as a photoinitiator in radical polymerization.[115]

1.4.2. Role of diaryliodonium compounds in biology:

Several literature reports mentioned the therapeutic role of the iodonium class of compounds in biological systems (Figure 1.9). For example, French and co-workers have reported that diphenyl iodonium chloride inhibits the virulent *Mycobacterium* and exhibits bacteriostatic effects against Gram-positive cocci and Gram-negative rods.[116] *In vivo* and animal studies suggested that diphenyl iodonium chloride significantly inhibited the growth of *tubercle bacilli* at a lower concentration. In another study, using the FDA agar plate technique, Witlin and co-workers have shown that derivatives of diphenyl iodonium chloride, for instance, bis-*p*-chlorophenyl iodonium sulphate, bis-*p*-bromophenyl iodonium iodide, bis-*p*-chlorophenyl iodonium iodide, bis-*p*-iodophenyl iodonium iodide, and diphenyl iodonium iodide, display the bacteriostatic effect.[117,118] In particular bis-*p*-chlorophenyl iodonium sulphate in saturated aqueous solution exhibited bactericidal activity against *Staphylococcus aureus*. In a similar vein, Worton and co-workers have reported that bis(3,4-dichlorophenyl) iodonium chloride displayed antiseptic, fungistatic properties and bacteriostatic effects against Gram-positive bacteria.[119] This compound has significantly reduced the transient and resident microflora of the skin shows, hence can be used as a dermatological agent. In another study, Jeong and co-workers have demonstrated diphenyleneiodonium chloride (DPIC) as a potent inhibitor of multi-drug resistant (MDR) *Helicobacter pylori* strains with <0.03 MIC (µg/mL).[120] *Helicobacter pylori* cause peptic ulcer disease and gastric cancer. The conventional treatment method of *Helicobacter pylori* infection is triple therapy, which is consisted of amoxicillin, clarithromycin, and proton pump inhibitor (PPI) for 7-14 days. However, due to the emergence of clarithromycin-resistant *Helicobacter pylori*, the effect of triple therapy has been reduced over time. Thus, DPIC, with its potent inhibitory activity against MDR *Helicobacter pylori* strains, can be a promising anti-*Helicobacter pylori* drug agent. Following up on this study, Pandey and co-workers have identified DPIC as a broad-spectrum antibacterial molecule that is significantly potent against multi-drug resistant *Staphylococcus aureus* (MIC; 1-2 µg/mL) and *Mycobacterium tuberculosis* (MIC; 0.03 µg/mL).[121] DPIC was also found to be highly effective against non-replicating *Mycobacterium tuberculosis* persisters. A synergism-based study demonstrated that DPIC interacts with front-line drug Rifampicin but not with Isoniazid. This suggests that DPIC can act as an adjuvant in combination therapy with Rifampicin and could significantly reduce the doses of Rifampicin. A subsequent study by Baell and co-

workers have demonstrated the structural activity relationship (SAR) of diphenyleneiodonium triflate series of compounds against multi-drug resistant ESKAP pathogens and *Mycobacterium tuberculosis* (*Mtb*).[122] The SAR studies demonstrated that the electron-donating group on DPI decreases its activity along with cytotoxicity and the electron-withdrawing group increases its activity as well as cytotoxicity. 5-chlorodiphenyleneiodonium triflate was found as lead candidate in this study, which was significantly potent against Gram-positive and Gram-negative bacteria, *Mycobacterium tuberculosis*, protozoan parasites and *Plasmodium spp*.

Figure 1. 9 Reported examples of iodonium salts as antibacterial

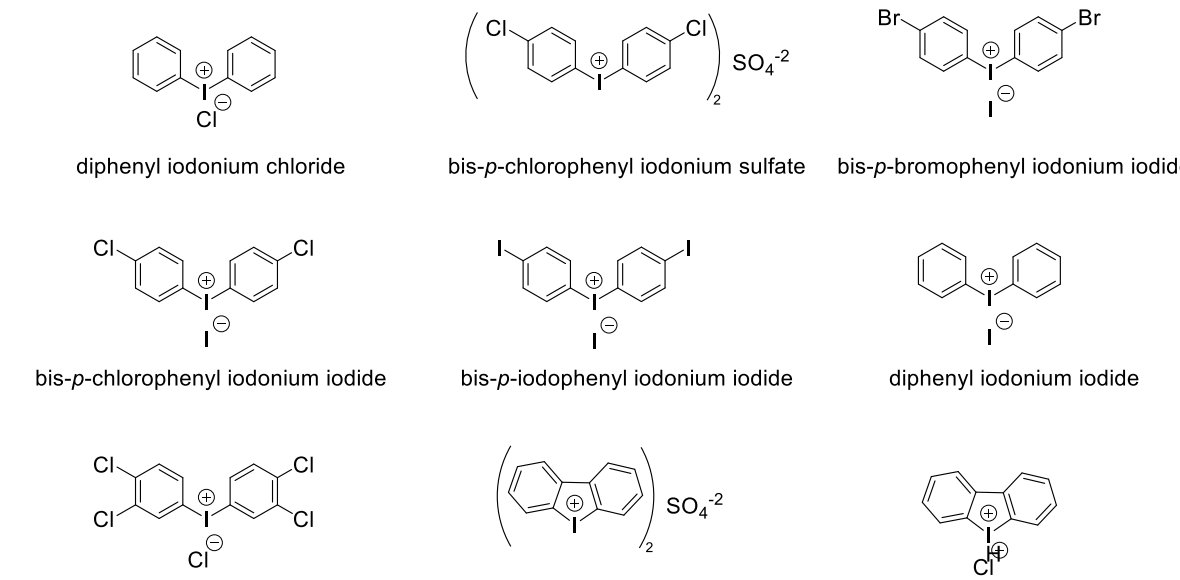

Diaryliodonium compounds are therefore promising therapeutic candidates. However, in bacterial cells, the mechanism of action or targets of the iodonium class of chemicals are remain to be identified.

Hence, we chose DPIC as a prototype of the iodonium class of compounds. Chemoproteomic methods can be used to identify the targets of DPIC in bacterial cells. Gram-negative bacteria *E. coli* was selected as a model organism for protein profiling. Using ABPP, the DPIC alkyne probe was synthesized, and the proteome of *E. coli* was profiled for target identification, as explained in Chapter **2**. The targets of DPIC in *E. coli* were identified using LC-MS/MS-based chemoproteomic methods. The promising target protein was cloned, purified, and validated using ABPP. Further to enhance the antibacterial activity spectrum of iodonium compounds,

heterocyclic iodonium compounds were designed, synthesized, and screened against ESKAPE pathogens. One of these, diheterocyclic iodonium, has been discovered as a lead chemical that is effective against Gram-negative multidrug-resistant bacteria *A. buamannii*. The proteome of *A. baumannii* was also profiled with the identified lead compound using ABPP methods, and targets were identified using an LC-MS/MS-based proteomics methodology, as discussed in Chapter **3**. Furthermore, a visible light-triggered release of a fluoroquinolone antibiotic was demonstrated utilizing one of the photopharmacology methods, as described in Chapter **4**.

1.5. Aims:

This thesis will discuss two different approaches to address antibiotic resistance.

1. **Identification of Targets for Iodonium Compounds and Structure-Activity Relationship Study to Enhance Activity against *A. baumannii*:**

Iodonium compounds were selected for their antibacterial activity in this strategy to develop a broad-spectrum antibacterial therapeutic agent with novel or drug-like targets.

a) Chemoproteomic approaches towards the probable target identification of DPIC in *E. coli*

ABPP approaches can be used to determine the targets of DPIC, a prototype of iodonium compound. For that, an activity-based probe based on DPIC scaffold can be synthesized to profile the Gram-negative bacterial proteome. Moreover, using chemoproteomic approaches, the activity-based probe can be employed to discover and validate the DPIC targets in bacterial cells.

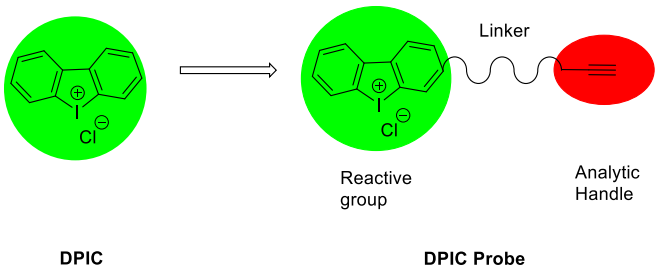

b) Enhancement in the antibacterial activity of iodonium compounds:

The ineffectiveness of reported DPIC analogs against Gram-negative bacteria like *A. baumannii*, remains a key concern. In order to address this, a Structure-activity relationship study could be used to find the lead compound of iodonium class of molecules against Gram-negative bacteria. Next, the lead compound targets can be discovered using chemoproteomic

techniques to fully understand the antibacterial effectiveness of the lead molecule against *A. baumannii*.

2. Visible-light controlled release of a fluoroquinolone antibiotic:

Antibacterial photopharmacology can be used to address antibiotic resistance as an alternative. A visible light-activated prodrug can be designed where a fluoroquinolone antibiotic is appended with a photocleavable fluorophore. Upon exposure to visible light, it should release the antibiotic and exhibit its antibacterial activity against Gram-positive and Gram-negative bacteria.

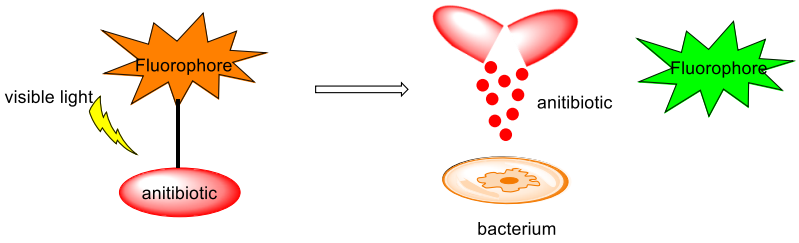

The obstacles and progress toward achieving all of these goals will be discussed in this thesis.

1.6. References:

(1) Bruslind, L. *General Microbiology*, 1st ed.; Oregon State University: Corvallis, 2019.

(2) Pelczar, J. M.; Krieg, N. R. *The World of Bacteria, Microbiology*, 5th ed.; Tata McGraw-Hill: New York, 2008.

(3) Medical News Today home page https://www.medicalnewstoday.com/.

(4) Lewis, K. Platforms for Antibiotic Discovery. *Nat. Rev. Drug Discov.* **2013**, *12*, 371–387. https://doi.org/10.1038/nrd3975.

(5) Ehrlich, P. Address in Pathology, On Chemiotherapy: Delivered before the Seventeenth International Congress of Medicine. *BMJ* **1913**, *2* (2746), 353–359. https://doi.org/10.1136/bmj.2.2746.353.

(6) Davies, J.; Davies, D. Origins and Evolution of Antibiotic Resistance. *Microbiol. Mol. Biol. Rev.* **2010**, *74* (3), 417–433. https://doi.org/10.1128/MMBR.00016-10.

(7) Prestinaci, F.; Pezzotti, P.; Pantosti, A. Antimicrobial Resistance: A Global Multifaceted Phenomenon. *Pathog. Glob. Health* **2015**, *109* (7), 309–318. https://doi.org/10.1179/2047773215Y.0000000030.

(8) Murray, C. J.; Ikuta, K. S.; Sharara, F.; Swetschinski, L.; Robles Aguilar, G.; Gray, A.; Han, C.; Bisignano, C.; Rao, P.; Wool, E.; Johnson, S. C.; Browne, A. J.; Chipeta, M. G.; Fell, F.; Hackett, S.; Haines-Woodhouse, G.; Kashef Hamadani, B. H.; Kumaran, E. A. P.; McManigal, B.; Agarwal, R.; Akech, S.; Albertson, S.; Amuasi, J.; Andrews, J.; Aravkin, A.; Ashley, E.; Bailey, F.; Baker, S.; Basnyat, B.; Bekker, A.; Bender, R.; Bethou, A.; Bielicki, J.; Boonkasidecha, S.; Bukosia, J.; Carvalheiro, C.; Castañeda-Orjuela, C.; Chansamouth, V.; Chaurasia, S.; Chiurchiù, S.; Chowdhury, F.; Cook, A. J.; Cooper, B.; Cressey, T. R.; Criollo-Mora, E.; Cunningham, M.; Darboe, S.; Day, N. P. J.; De Luca, M.; Dokova, K.; Dramowski, A.; Dunachie, S. J.; Eckmanns, T.; Eibach, D.; Emami, A.; Feasey, N.; Fisher-Pearson, N.; Forrest, K.; Garrett, D.; Gastmeier, P.; Giref, A. Z.; Greer, R. C.; Gupta, V.; Haller, S.; Haselbeck, A.; Hay, S. I.; Holm, M.; Hopkins, S.; Iregbu, K. C.; Jacobs, J.; Jarovsky, D.; Javanmardi, F.; Khorana, M.; Kissoon, N.; Kobeissi, E.; Kostyanev, T.; Krapp, F.; Krumkamp, R.; Kumar, A.; Kyu, H. H.; Lim, C.; Limmathurotsakul, D.; Loftus, M. J.; Lunn, M.; Ma, J.; Mturi, N.; Munera-Huertas, T.; Musicha, P.; Mussi-Pinhata, M. M.; Nakamura, T.; Nanavati, R.; Nangia, S.; Newton, P.; Ngoun, C.; Novotney, A.; Nwakanma, D.; Obiero, C. W.;

Olivas-Martinez, A.; Olliaro, P.; Ooko, E.; Ortiz-Brizuela, E.; Peleg, A. Y.; Perrone, C.; Plakkal, N.; Ponce-de-Leon, A.; Raad, M.; Ramdin, T.; Riddell, A.; Roberts, T.; Robotham, J. V.; Roca, A.; Rudd, K. E.; Russell, N.; Schnall, J.; Scott, J. A. G.; Shivamallappa, M.; Sifuentes-Osornio, J.; Steenkeste, N.; Stewardson, A. J.; Stoeva, T.; Tasak, N.; Thaiprakong, A.; Thwaites, G.; Turner, C.; Turner, P.; van Doorn, H. R.; Velaphi, S.; Vongpradith, A.; Vu, H.; Walsh, T.; Waner, S.; Wangrangsimakul, T.; Wozniak, T.; Zheng, P.; Sartorius, B.; Lopez, A. D.; Stergachis, A.; Moore, C.; Dolecek, C.; Naghavi, M. Global Burden of Bacterial Antimicrobial Resistance in 2019: A Systematic Analysis. *Lancet* **2022**, *399* (10325), 629–655. https://doi.org/10.1016/S0140-6736(21)02724-0.

(9) Rice, L. B. Federal Funding for the Study of Antimicrobial Resistance in Nosocomial Pathogens: No ESKAPE. *J. Infect. Dis.* **2008**, *197* (8), 1079–1081. https://doi.org/10.1086/533452.

(10) Pogue, J. M.; Kaye, K. S.; Cohen, D. A.; Marchaim, D. Appropriate Antimicrobial Therapy in the Era of Multidrug-Resistant Human Pathogens. *Clin. Microbiol. Infect.* **2015**, *21* (4), 302–312. https://doi.org/10.1016/j.cmi.2014.12.025.

(11) Boucher, H. W.; Talbot, G. H.; Bradley, J. S.; Edwards, J. E.; Gilbert, D.; Rice, L. B.; Scheld, M.; Spellberg, B.; Bartlett, J. Bad Bugs, No Drugs: No ESKAPE! An Update from the Infectious Diseases Society of America. *Clin. Infect. Dis.* **2009**, *48* (1), 1–12. https://doi.org/10.1086/595011.

(12) Årdal, C.; Outterson, K.; Hoffman, S. J.; Ghafur, A.; Sharland, M.; Ranganathan, N.; Smith, R.; Zorzet, A.; Cohn, J.; Pittet, D.; Daulaire, N.; Morel, C.; Rizvi, Z.; Balasegaram, M.; Dar, O. A.; Heymann, D. L.; Holmes, A. H.; Moore, L. S. P.; Laxminarayan, R.; Mendelson, M.; Røttingen, J.-A. International Cooperation to Improve Access to and Sustain Effectiveness of Antimicrobials. *Lancet* **2016**, *387* (10015), 296–307. https://doi.org/10.1016/S0140-6736(15)00470-5.

(13) Founou, L. L.; Founou, R. C.; Essack, S. Y. Antibiotic Resistance in the Food Chain: A Developing Country-Perspective. *Front. Microbiol.* **2016**, *7*. https://doi.org/10.3389/fmicb.2016.01881.

(14) Dahal, R. H.; Chaudhary, D. K. Microbial Infections and Antimicrobial Resistance in Nepal: Current Trends and Recommendations. *Open Microbiol. J.* **2018**, *12* (1), 230–

242. https://doi.org/10.2174/1874285801812010230.

(15) Gunjal, V. B.; Thakare, R.; Chopra, S.; Reddy, D. S. Teixobactin: A Paving Stone toward a New Class of Antibiotics? *J. Med. Chem.* **2020**, *63* (21), 12171–12195. https://doi.org/10.1021/acs.jmedchem.0c00173.

(16) Tacconelli, E.; Carrara, E.; Savoldi, A.; Harbarth, S.; Mendelson, M.; Monnet, D. L.; Pulcini, C.; Kahlmeter, G.; Kluytmans, J.; Carmeli, Y.; Ouellette, M.; Outterson, K.; Patel, J.; Cavaleri, M.; Cox, E. M.; Houchens, C. R.; Grayson, M. L.; Hansen, P.; Singh, N.; Theuretzbacher, U.; Magrini, N.; Aboderin, A. O.; Al-Abri, S. S.; Awang Jalil, N.; Benzonana, N.; Bhattacharya, S.; Brink, A. J.; Burkert, F. R.; Cars, O.; Cornaglia, G.; Dyar, O. J.; Friedrich, A. W.; Gales, A. C.; Gandra, S.; Giske, C. G.; Goff, D. A.; Goossens, H.; Gottlieb, T.; Guzman Blanco, M.; Hryniewicz, W.; Kattula, D.; Jinks, T.; Kanj, S. S.; Kerr, L.; Kieny, M.-P.; Kim, Y. S.; Kozlov, R. S.; Labarca, J.; Laxminarayan, R.; Leder, K.; Leibovici, L.; Levy-Hara, G.; Littman, J.; Malhotra-Kumar, S.; Manchanda, V.; Moja, L.; Ndoye, B.; Pan, A.; Paterson, D. L.; Paul, M.; Qiu, H.; Ramon-Pardo, P.; Rodríguez-Baño, J.; Sanguinetti, M.; Sengupta, S.; Sharland, M.; Si-Mehand, M.; Silver, L. L.; Song, W.; Steinbakk, M.; Thomsen, J.; Thwaites, G. E.; van der Meer, J. W.; Van Kinh, N.; Vega, S.; Villegas, M. V.; Wechsler-Fördös, A.; Wertheim, H. F. L.; Wesangula, E.; Woodford, N.; Yilmaz, F. O.; Zorzet, A. Discovery, Research, and Development of New Antibiotics: The WHO Priority List of Antibiotic-Resistant Bacteria and Tuberculosis. *Lancet Infect. Dis.* **2018**, *18* (3), 318–327. https://doi.org/10.1016/S1473-3099(17)30753-3.

(17) Santajit, S.; Indrawattana, N. Mechanisms of Antimicrobial Resistance in ESKAPE Pathogens. *Biomed Res. Int.* **2016**, *2016*, 1–8. https://doi.org/10.1155/2016/2475067.

(18) Lee, N.-Y.; Lee, C.-C.; Li, C.-W.; Li, M.-C.; Chen, P.-L.; Chang, C.-M.; Ko, W.-C. Cefepime Therapy for Monomicrobial Enterobacter Cloacae Bacteremia: Unfavorable Outcomes in Patients Infected by Cefepime-Susceptible Dose-Dependent Isolates. *Antimicrob. Agents Chemother.* **2015**, *59* (12), 7558–7563. https://doi.org/10.1128/AAC.01477-15.

(19) Babouee Flury, B.; Ellington, M. J.; Hopkins, K. L.; Turton, J. F.; Doumith, M.; Loy, R.; Staves, P.; Hinic, V.; Frei, R.; Woodford, N. Association of Novel Nonsynonymous Single Nucleotide Polymorphisms in AmpD with Cephalosporin Resistance and Phylogenetic Variations in AmpC , AmpR , OmpF , and OmpC in Enterobacter Cloacae

Isolates That Are Highly Resistant to Carbapenems. *Antimicrob. Agents Chemother.* **2016**, *60* (4), 2383–2390. https://doi.org/10.1128/AAC.02835-15.

(20) Kulengowski, B.; Rutter, W. C.; Campion, J. J.; Lee, G. C.; Feola, D. J.; Burgess, D. S. Effect of Increasing Meropenem MIC on the Killing Activity of Meropenem in Combination with Amikacin or Polymyxin B against MBL- and KPC-Producing Enterobacter Cloacae. *Diagn. Microbiol. Infect. Dis.* **2018**, *92* (3), 262–266. https://doi.org/10.1016/j.diagmicrobio.2018.06.013.

(21) Baronia, A.; Ahmed, A. Current Concepts in Combination Antibiotic Therapy for Critically Ill Patients. *Indian J. Crit. Care Med.* **2014**, *18* (5), 310–314. https://doi.org/10.4103/0972-5229.132495.

(22) Hall Snyder, A. D.; Werth, B. J.; Nonejuie, P.; McRoberts, J. P.; Pogliano, J.; Sakoulas, G.; Yim, J.; Singh, N.; Rybak, M. J. Fosfomycin Enhances the Activity of Daptomycin against Vancomycin-Resistant Enterococci in an In Vitro Pharmacokinetic-Pharmacodynamic Model. *Antimicrob. Agents Chemother.* **2016**, *60* (10), 5716–5723. https://doi.org/10.1128/AAC.00687-16.

(23) González-Bello, C. Antibiotic Adjuvants – A Strategy to Unlock Bacterial Resistance to Antibiotics. *Bioorg. Med. Chem. Lett.* **2017**, *27* (18), 4221–4228. https://doi.org/10.1016/j.bmcl.2017.08.027.

(24) Kalan, L.; Wright, G. D. Antibiotic Adjuvants: Multicomponent Anti-Infective Strategies. *Expert Rev. Mol. Med.* **2011**, *13*, e5. https://doi.org/10.1017/S1462399410001766.

(25) Bernal, P.; Molina-Santiago, C.; Daddaoua, A.; Llamas, M. A. Antibiotic Adjuvants: Identification and Clinical Use. *Microb. Biotechnol.* **2013**, *6* (5), 445–449. https://doi.org/10.1111/1751-7915.12044.

(26) Jorgensen, S. C. J.; Rybak, M. J. Meropenem and Vaborbactam: Stepping up the Battle against Carbapenem-Resistant Enterobacteriaceae. *Pharmacother. J. Hum. Pharmacol. Drug Ther.* **2018**, *38* (4), 444–461. https://doi.org/10.1002/phar.2092.

(27) Rubino, C. M.; Bhavnani, S. M.; Loutit, J. S.; Lohse, B.; Dudley, M. N.; Griffith, D. C. Single-Dose Pharmacokinetics and Safety of Meropenem-Vaborbactam in Subjects with Chronic Renal Impairment. *Antimicrob. Agents Chemother.* **2018**, *62* (3).

https://doi.org/10.1128/AAC.02103-17.

(28) Monogue, M. L.; Giovagnoli, S.; Bissantz, C.; Zampaloni, C.; Nicolau, D. P. In Vivo Efficacy of Meropenem with a Novel Non-β-Lactam–β-Lactamase Inhibitor, Nacubactam, against Gram-Negative Organisms Exhibiting Various Resistance Mechanisms in a Murine Complicated Urinary Tract Infection Model. *Antimicrob. Agents Chemother*. **2018**, *62* (9). https://doi.org/10.1128/AAC.02596-17.

(29) Yoshizumi, A.; Ishii, Y.; Kimura, S.; Saga, T.; Harada, S.; Yamaguchi, K.; Tateda, K.; Livermore, D. M.; Woodford, N.; Livermore, D. M. Efficacies of Calcium–EDTA in Combination with Imipenem in a Murine Model of Sepsis Caused by Escherichia Coli with NDM-1 β-Lactamase. *J. Infect. Chemother.* **2013**, *19* (5), 992–995. https://doi.org/10.1007/s10156-012-0528-y.

(30) Defraine, V.; Verstraete, L.; Van Bambeke, F.; Anantharajah, A.; Townsend, E. M.; Ramage, G.; Corbau, R.; Marchand, A.; Chaltin, P.; Fauvart, M.; Michiels, J. Antibacterial Activity of 1-[(2,4-Dichlorophenethyl)Amino]-3-Phenoxypropan-2-Ol against Antibiotic-Resistant Strains of Diverse Bacterial Pathogens, Biofilms and in Pre-Clinical Infection Models. *Front. Microbiol.* **2017**, *8*. https://doi.org/10.3389/fmicb.2017.02585.

(31) Bonomo, R. A.; Szabo, D. Mechanisms of Multidrug Resistance in Acinetobacter Species and Pseudomonas Aeruginosa. *Clin. Infect. Dis.* **2006**, *43* (Supplement_2), S49–S56. https://doi.org/10.1086/504477.

(32) Livermore, D. M.; Hope, R.; Brick, G.; Lillie, M.; Reynolds, R. Non-Susceptibility Trends among Enterobacteriaceae from Bacteraemias in the UK and Ireland, 2001-06. *J. Antimicrob. Chemother.* **2008**, *62* (Supplement 2), ii41–ii54. https://doi.org/10.1093/jac/dkn351.

(33) Wang, G. S.; Li, X.; Zasloff, M. A Database View of Naturally Occurring Antimicrobial Peptides: Nomenclature, Classification and Amino Acid Sequence Analysis. In *Antimicrobial peptides: discovery, design and novel therapeutic strategies*; CABI: Wallingford, 2010; pp 1–21. https://doi.org/10.1079/9781845936570.0001.

(34) Berglund, N. A.; Piggot, T. J.; Jefferies, D.; Sessions, R. B.; Bond, P. J.; Khalid, S. Interaction of the Antimicrobial Peptide Polymyxin B1 with Both Membranes of E. Coli: A Molecular Dynamics Study. *PLOS Comput. Biol.* **2015**, *11* (4), e1004180.

https://doi.org/10.1371/journal.pcbi.1004180.

(35) Fleming Alexander. On a Remarkable Bacteriolytic Element Found in Tissues and Secretions. *Proc. R. Soc. London. Ser. B, Contain. Pap. a Biol. Character* **1922**, *93* (653), 306–317. https://doi.org/10.1098/rspb.1922.0023.

(36) Gomes, B.; Augusto, M. T.; Felício, M. R.; Hollmann, A.; Franco, O. L.; Gonçalves, S.; Santos, N. C. Designing Improved Active Peptides for Therapeutic Approaches against Infectious Diseases. *Biotechnol. Adv.* **2018**, *36* (2), 415–429. https://doi.org/10.1016/j.biotechadv.2018.01.004.

(37) Du, H.; Puri, S.; McCall, A.; Norris, H. L.; Russo, T.; Edgerton, M. Human Salivary Protein Histatin 5 Has Potent Bactericidal Activity against ESKAPE Pathogens. *Front. Cell. Infect. Microbiol.* **2017**, *7*. https://doi.org/10.3389/fcimb.2017.00041.

(38) Björn, C.; Mahlapuu, M.; Mattsby-Baltzer, I.; Håkansson, J. Anti-Infective Efficacy of the Lactoferrin-Derived Antimicrobial Peptide HLR1r. *Peptides* **2016**, *81*, 21–28. https://doi.org/10.1016/j.peptides.2016.04.005.

(39) Hemeg, H. Nanomaterials for Alternative Antibacterial Therapy. *Int. J. Nanomedicine* **2017**, *Volume 12*, 8211–8225. https://doi.org/10.2147/IJN.S132163.

(40) Rai, M. K.; Deshmukh, S. D.; Ingle, A. P.; Gade, A. K. Silver Nanoparticles: The Powerful Nanoweapon against Multidrug-Resistant Bacteria. *J. Appl. Microbiol.* **2012**, *112* (5), 841–852. https://doi.org/10.1111/j.1365-2672.2012.05253.x.

(41) Dakal, T. C.; Kumar, A.; Majumdar, R. S.; Yadav, V. Mechanistic Basis of Antimicrobial Actions of Silver Nanoparticles. *Front. Microbiol.* **2016**, *7*. https://doi.org/10.3389/fmicb.2016.01831.

(42) Durán, N.; Durán, M.; de Jesus, M. B.; Seabra, A. B.; Fávaro, W. J.; Nakazato, G. Silver Nanoparticles: A New View on Mechanistic Aspects on Antimicrobial Activity. *Nanomedicine Nanotechnology, Biol. Med.* **2016**, *12* (3), 789–799. https://doi.org/10.1016/j.nano.2015.11.016.

(43) Saha, B.; Bhattacharya, J.; Mukherjee, A.; Ghosh, A.; Santra, C.; Dasgupta, A. K.; Karmakar, P. In Vitro Structural and Functional Evaluation of Gold Nanoparticles Conjugated Antibiotics. *Nanoscale Res. Lett.* **2007**, *2* (12), 614. https://doi.org/10.1007/s11671-007-9104-2.

(44) Gupta, A.; Saleh, N. M.; Das, R.; Landis, R. F.; Bigdeli, A.; Motamedchaboki, K.; Rosa Campos, A.; Pomeroy, K.; Mahmoudi, M.; Rotello, V. M. Synergistic Antimicrobial Therapy Using Nanoparticles and Antibiotics for the Treatment of Multidrug-Resistant Bacterial Infection. *Nano Futur.* **2017**, *1* (1), 015004. https://doi.org/10.1088/2399-1984/aa69fb.

(45) Lotha, R.; Shamprasad, B. R.; Sundaramoorthy, N. S.; Ganapathy, R.; Nagarajan, S.; Sivasubramanian, A. Zero Valent Silver Nanoparticles Capped with Capsaicinoids Containing Capsicum Annuum Extract, Exert Potent Anti-Biofilm Effect on Food Borne Pathogen Staphylococcus Aureus and Curtail Planktonic Growth on a Zebrafish Infection Model. *Microb. Pathog.* **2018**, *124*, 291–300. https://doi.org/10.1016/j.micpath.2018.08.053.

(46) Pallavali, R. R.; Degati, V. L.; Lomada, D.; Reddy, M. C.; Durbaka, V. R. P. Isolation and in Vitro Evaluation of Bacteriophages against MDR-Bacterial Isolates from Septic Wound Infections. *PLoS One* **2017**, *12* (7), e0179245. https://doi.org/10.1371/journal.pone.0179245.

(47) Dvořáčková, M.; Růžička, F.; Benešík, M.; Pantůček, R.; Dvořáková-Heroldová, M. Antimicrobial Effect of Commercial Phage Preparation Stafal® on Biofilm and Planktonic Forms of Methicillin-Resistant Staphylococcus Aureus. *Folia Microbiol. (Praha).* **2019**, *64* (1), 121–126. https://doi.org/10.1007/s12223-018-0622-3.

(48) Jamal, M.; Andleeb, S.; Jalil, F.; Imran, M.; Nawaz, M. A.; Hussain, T.; Ali, M.; ur Rahman, S.; Das, C. R. Isolation, Characterization and Efficacy of Phage MJ2 against Biofilm Forming Multi-Drug Resistant Enterobacter Cloacae. *Folia Microbiol. (Praha).* **2019**, *64* (1), 101–111. https://doi.org/10.1007/s12223-018-0636-x.

(49) Lin, Y.; Chang, R. Y. K.; Britton, W. J.; Morales, S.; Kutter, E.; Chan, H.-K. Synergy of Nebulized Phage PEV20 and Ciprofloxacin Combination against Pseudomonas Aeruginosa. *Int. J. Pharm.* **2018**, *551* (1–2), 158–165. https://doi.org/10.1016/j.ijpharm.2018.09.024.

(50) Mai, B.; Gao, Y.; Li, M.; Wang, X.; Zhang, K.; Liu, Q.; Xu, C.; Wang, P. Photodynamic Antimicrobial Chemotherapy for Staphylococcus Aureus and Multidrug-Resistant Bacterial Burn Infection in Vitro and in Vivo. *Int. J. Nanomedicine* **2017**, *Volume 12*, 5915–5931. https://doi.org/10.2147/IJN.S138185.

(51) Yang, M.-Y.; Chang, K.-C.; Chen, L.-Y.; Wang, P.-C.; Chou, C.-C.; Wu, Z.-B.; Hu, A. Blue Light Irradiation Triggers the Antimicrobial Potential of ZnO Nanoparticles on Drug-Resistant Acinetobacter Baumannii. *J. Photochem. Photobiol. B Biol.* **2018**, *180*, 235–242. https://doi.org/10.1016/j.jphotobiol.2018.02.003.

(52) Hu, X.; Huang, Y.-Y.; Wang, Y.; Wang, X.; Hamblin, M. R. Antimicrobial Photodynamic Therapy to Control Clinically Relevant Biofilm Infections. *Front. Microbiol.* **2018**, *9*. https://doi.org/10.3389/fmicb.2018.01299.

(53) Cieplik, F.; Deng, D.; Crielaard, W.; Buchalla, W.; Hellwig, E.; Al-Ahmad, A.; Maisch, T. Antimicrobial Photodynamic Therapy – What We Know and What We Don't. *Crit. Rev. Microbiol.* **2018**, *44* (5), 571–589. https://doi.org/10.1080/1040841X.2018.1467876.

(54) Wozniak, A.; Grinholc, M. Combined Antimicrobial Activity of Photodynamic Inactivation and Antimicrobials–State of the Art. *Front. Microbiol.* **2018**, *9*. https://doi.org/10.3389/fmicb.2018.00930.

(55) Zhao, Y.; Lu, Z.; Dai, X.; Wei, X.; Yu, Y.; Chen, X.; Zhang, X.; Li, C. Glycomimetic-Conjugated Photosensitizer for Specific Pseudomonas Aeruginosa Recognition and Targeted Photodynamic Therapy. *Bioconjug. Chem.* **2018**, *29* (9), 3222–3230. https://doi.org/10.1021/acs.bioconjchem.8b00600.

(56) Grinholc, M.; Szramka, B.; Kurlenda, J.; Graczyk, A.; Bielawski, K. P. Bactericidal Effect of Photodynamic Inactivation against Methicillin-Resistant and Methicillin-Susceptible Staphylococcus Aureus Is Strain-Dependent. *J. Photochem. Photobiol. B Biol.* **2008**, *90* (1), 57–63. https://doi.org/10.1016/j.jphotobiol.2007.11.002.

(57) Amin, R. M.; Bhayana, B.; Hamblin, M. R.; Dai, T. Antimicrobial Blue Light Inactivation of Pseudomonas Aeruginosa by Photo-Excitation of Endogenous Porphyrins: In Vitro and in Vivo Studies. *Lasers Surg. Med.* **2016**, *48* (5), 562–568. https://doi.org/10.1002/lsm.22474.

(58) Katayama, B.; Ozawa, T.; Morimoto, K.; Awazu, K.; Ito, N.; Honda, N.; Oiso, N.; Tsuruta, D. Enhanced Sterilization and Healing of Cutaneous Pseudomonas Infection Using 5-Aminolevulinic Acid as a Photosensitizer with 410-Nm LED Light. *J. Dermatol. Sci.* **2018**, *90* (3), 323–331. https://doi.org/10.1016/j.jdermsci.2018.03.001.

(59) Wang, Y.; Harrington, O. D.; Wang, Y.; Murray, C. K.; Hamblin, M. R.; Dai, T. In Vivo Investigation of Antimicrobial Blue Light Therapy for Multidrug-Resistant Acinetobacter Baumannii Burn Infections Using Bioluminescence Imaging. *J. Vis. Exp.* **2017**, No. 122. https://doi.org/10.3791/54997.

(60) Halstead, F. D.; Thwaite, J. E.; Burt, R.; Laws, T. R.; Raguse, M.; Moeller, R.; Webber, M. A.; Oppenheim, B. A. Antibacterial Activity of Blue Light against Nosocomial Wound Pathogens Growing Planktonically and as Mature Biofilms. *Appl. Environ. Microbiol.* **2016**, *82* (13), 4006–4016. https://doi.org/10.1128/AEM.00756-16.

(61) Fila, G.; Kawiak, A.; Grinholc, M. S. Blue Light Treatment of Pseudomonas Aeruginosa : Strong Bactericidal Activity, Synergism with Antibiotics and Inactivation of Virulence Factors. *Virulence* **2017**, *8* (6), 938–958. https://doi.org/10.1080/21505594.2016.1250995.

(62) Ritter, J.; Flower, R.; Henderson, G.; Loke, Y. K.; MacEwan, D.; Rang, H. *Rang & Dale's Pharmacology*, 8th ed.; Elsevier, Churchill Livingstone: London, 2015.

(63) Velema, W. A.; Szymanski, W.; Feringa, B. L. Photopharmacology: Beyond Proof of Principle. *J. Am. Chem. Soc.* **2014**, *136* (6), 2178–2191. https://doi.org/10.1021/ja413063e.

(64) Broichhagen, J.; Frank, J. A.; Trauner, D. A Roadmap to Success in Photopharmacology. *Acc. Chem. Res.* **2015**, *48* (7), 1947–1960. https://doi.org/10.1021/acs.accounts.5b00129.

(65) Velema, W. A.; van der Berg, J. P.; Szymanski, W.; Driessen, A. J. M.; Feringa, B. L. Orthogonal Control of Antibacterial Activity with Light. *ACS Chem. Biol.* **2014**, *9* (9), 1969–1974. https://doi.org/10.1021/cb500313f.

(66) Weston, C. E.; Krämer, A.; Colin, F.; Yildiz, Ö.; Baud, M. G. J.; Meyer-Almes, F.-J.; Fuchter, M. J. Toward Photopharmacological Antimicrobial Chemotherapy Using Photoswitchable Amidohydrolase Inhibitors. *ACS Infect. Dis.* **2017**, *3* (2), 152–161. https://doi.org/10.1021/acsinfecdis.6b00148.

(67) Klán, P.; Šolomek, T.; Bochet, C. G.; Blanc, A.; Givens, R.; Rubina, M.; Popik, V.; Kostikov, A.; Wirz, J. Photoremovable Protecting Groups in Chemistry and Biology: Reaction Mechanisms and Efficacy. *Chem. Rev.* **2013**, *113* (1), 119–191.

https://doi.org/10.1021/cr300177k.

(68) Deiters, A. Principles and Applications of the Photochemical Control of Cellular Processes. *ChemBioChem* **2009**, *11* (1), 47–53. https://doi.org/10.1002/cbic.200900529.

(69) Brieke, C.; Rohrbach, F.; Gottschalk, A.; Mayer, G.; Heckel, A. Light-Controlled Tools. *Angew. Chemie Int. Ed.* **2012**, *51* (34), 8446–8476. https://doi.org/10.1002/anie.201202134.

(70) Shi, Y.; Truong, V. X.; Kulkarni, K.; Qu, Y.; Simon, G. P.; Boyd, R. L.; Perlmutter, P.; Lithgow, T.; Forsythe, J. S. Light-Triggered Release of Ciprofloxacin from an in Situ Forming Click Hydrogel for Antibacterial Wound Dressings. *J. Mater. Chem. B* **2015**, *3* (45), 8771–8774. https://doi.org/10.1039/C5TB01820J.

(71) Shchelik, I. S.; Tomio, A.; Gademann, K. Design, Synthesis, and Biological Evaluation of Light-Activated Antibiotics. *ACS Infect. Dis.* **2021**, *7* (3), 681–692. https://doi.org/10.1021/acsinfecdis.1c00015.

(72) Swinney, D. C.; Anthony, J. How Were New Medicines Discovered? *Nat. Rev. Drug Discov.* **2011**, *10* (7), 507–519. https://doi.org/10.1038/nrd3480.

(73) SAMSDODD, F. Target-Based Drug Discovery: Is Something Wrong? *Drug Discov. Today* **2005**, *10* (2), 139–147. https://doi.org/10.1016/S1359-6446(04)03316-1.

(74) Pushkaran, A. C.; Biswas, R.; Mohan, C. G. Impact of Target-Based Drug Design in Anti-Bacterial Drug Discovery for the Treatment of Tuberculosis; 2019; pp 307–346. https://doi.org/10.1007/978-3-030-05282-9_10.

(75) Trefzer, C.; Škovierová, H.; Buroni, S.; Bobovská, A.; Nenci, S.; Molteni, E.; Pojer, F.; Pasca, M. R.; Makarov, V.; Cole, S. T.; Riccardi, G.; Mikušová, K.; Johnsson, K. Benzothiazinones Are Suicide Inhibitors of Mycobacterial Decaprenylphosphoryl-β-<scp>d</Scp> -Ribofuranose 2′-Oxidase DprE1. *J. Am. Chem. Soc.* **2012**, *134* (2), 912–915. https://doi.org/10.1021/ja211042r.

(76) Santos, R.; Ursu, O.; Gaulton, A.; Bento, A. P.; Donadi, R. S.; Bologa, C. G.; Karlsson, A.; Al-Lazikani, B.; Hersey, A.; Oprea, T. I.; Overington, J. P. A Comprehensive Map of Molecular Drug Targets. *Nat. Rev. Drug Discov.* **2017**, *16* (1), 19–34. https://doi.org/10.1038/nrd.2016.230.

(77) Szabo, M.; Svensson Akusjärvi, S.; Saxena, A.; Liu, J.; Chandrasekar Janebjer, G.;

Kitambi, S. S. Cell and Small Animal Models for Phenotypic Drug Discovery. *Drug Des. Devel. Ther.* **2017**, *Volume 11*, 1957–1967. https://doi.org/10.2147/DDDT.S129447.

(78) Terstappen, G. C.; Schlüpen, C.; Raggiaschi, R.; Gaviraghi, G. Target Deconvolution Strategies in Drug Discovery. *Nat. Rev. Drug Discov.* **2007**, *6* (11), 891–903. https://doi.org/10.1038/nrd2410.

(79) Yue, R.; Shan, L.; Yang, X.; Zhang, W. Approaches to Target Profiling of Natural Products. *Curr. Med. Chem.* **2012**, *19* (22), 3841–3855. https://doi.org/10.2174/092986712801661068.

(80) Backus, K. M.; Correia, B. E.; Lum, K. M.; Forli, S.; Horning, B. D.; González-Páez, G. E.; Chatterjee, S.; Lanning, B. R.; Teijaro, J. R.; Olson, A. J.; Wolan, D. W.; Cravatt, B. F. Proteome-Wide Covalent Ligand Discovery in Native Biological Systems. *Nature* **2016**, *534* (7608), 570–574. https://doi.org/10.1038/nature18002.

(81) Cravatt, B. F.; Wright, A. T.; Kozarich, J. W. Activity-Based Protein Profiling: From Enzyme Chemistry to Proteomic Chemistry. *Annu. Rev. Biochem.* **2008**, *77* (1), 383–414. https://doi.org/10.1146/annurev.biochem.75.101304.124125.

(82) Kolb, H. C.; Sharpless, K. B. The Growing Impact of Click Chemistry on Drug Discovery. *Drug Discov. Today* **2003**, *8* (24), 1128–1137. https://doi.org/10.1016/S1359-6446(03)02933-7.

(83) Speers, A. E.; Adam, G. C.; Cravatt, B. F. Activity-Based Protein Profiling in Vivo Using a Copper(I)-Catalyzed Azide-Alkyne [3 + 2] Cycloaddition. *J. Am. Chem. Soc.* **2003**, *125* (16), 4686–4687. https://doi.org/10.1021/ja034490h.

(84) Speers, A. E.; Cravatt, B. F. Profiling Enzyme Activities In Vivo Using Click Chemistry Methods. *Chem. Biol.* **2004**, *11* (4), 535–546. https://doi.org/10.1016/j.chembiol.2004.03.012.

(85) Liu, Y.; Patricelli, M. P.; Cravatt, B. F. Activity-Based Protein Profiling: The Serine Hydrolases. *Proc. Natl. Acad. Sci.* **1999**, *96* (26), 14694–14699. https://doi.org/10.1073/pnas.96.26.14694.

(86) Kidd, D.; Liu, Y.; Cravatt, B. F. Profiling Serine Hydrolase Activities in Complex Proteomes. *Biochemistry* **2001**, *40* (13), 4005–4015. https://doi.org/10.1021/bi002579j.

(87) Patricelli, M. P.; Giang, D. K.; Stamp, L. M.; Burbaum, J. J. Direct Visualization of Serine Hydrolase Activities in Complex Proteomes Using Fluorescent Active Site-Directed Probes. *Proteomics* **2001**, *1* (8), 1067–1071. https://doi.org/10.1002/1615-9861(200109)1:9<1067::AID-PROT1067>3.0.CO;2-4.

(88) Greenbaum, D.; Baruch, A.; Hayrapetian, L.; Darula, Z.; Burlingame, A.; Medzihradszky, K. F.; Bogyo, M. Chemical Approaches for Functionally Probing the Proteome. *Mol. Cell. Proteomics* **2002**, *1* (1), 60–68. https://doi.org/10.1074/mcp.T100003-MCP200.

(89) Jessani, N.; Niessen, S.; Wei, B. Q.; Nicolau, M.; Humphrey, M.; Ji, Y.; Han, W.; Noh, D.-Y.; Yates, J. R.; Jeffrey, S. S.; Cravatt, B. F. A Streamlined Platform for High-Content Functional Proteomics of Primary Human Specimens. *Nat. Methods* **2005**, *2* (9), 691–697. https://doi.org/10.1038/nmeth778.

(90) Greenbaum, D. C.; Arnold, W. D.; Lu, F.; Hayrapetian, L.; Baruch, A.; Krumrine, J.; Toba, S.; Chehade, K.; Brömme, D.; Kuntz, I. D.; Bogyo, M. Small Molecule Affinity Fingerprinting. *Chem. Biol.* **2002**, *9* (10), 1085–1094. https://doi.org/10.1016/S1074-5521(02)00238-7.

(91) Leung, D.; Hardouin, C.; Boger, D. L.; Cravatt, B. F. Discovering Potent and Selective Reversible Inhibitors of Enzymes in Complex Proteomes. *Nat. Biotechnol.* **2003**, *21* (6), 687–691. https://doi.org/10.1038/nbt826.

(92) Gersch, M.; Kreuzer, J.; Sieber, S. A. Electrophilic Natural Products and Their Biological Targets. *Nat. Prod. Rep.* **2012**, *29* (6), 659. https://doi.org/10.1039/c2np20012k.

(93) Staub, I.; Sieber, S. A. β-Lactams as Selective Chemical Probes for the in Vivo Labeling of Bacterial Enzymes Involved in Cell Wall Biosynthesis, Antibiotic Resistance, and Virulence. *J. Am. Chem. Soc.* **2008**, *130* (40), 13400–13409. https://doi.org/10.1021/ja803349j.

(94) Böttcher, T.; Sieber, S. A. β-Lactones as Specific Inhibitors of ClpP Attenuate the Production of Extracellular Virulence Factors of Staphylococcus Aureus. *J. Am. Chem. Soc.* **2008**, *130* (44), 14400–14401. https://doi.org/10.1021/ja8051365.

(95) Böttcher, T.; Sieber, S. A. Showdomycin as a Versatile Chemical Tool for the Detection

of Pathogenesis-Associated Enzymes in Bacteria. *J. Am. Chem. Soc.* **2010**, *132* (20), 6964–6972. https://doi.org/10.1021/ja909150y.

(96) Sherratt, A. R.; Blais, D. R.; Ghasriani, H.; Pezacki, J. P.; Goto, N. K. Activity-Based Protein Profiling of the Escherichia Coli GlpG Rhomboid Protein Delineates the Catalytic Core. *Biochemistry* **2012**, *51* (39), 7794–7803. https://doi.org/10.1021/bi301087c.

(97) Chauvigné-Hines, L. M.; Anderson, L. N.; Weaver, H. M.; Brown, J. N.; Koech, P. K.; Nicora, C. D.; Hofstad, B. A.; Smith, R. D.; Wilkins, M. J.; Callister, S. J.; Wright, A. T. Suite of Activity-Based Probes for Cellulose-Degrading Enzymes. *J. Am. Chem. Soc.* **2012**, *134* (50), 20521–20532. https://doi.org/10.1021/ja309790w.

(98) Anderson, L. N.; Culley, D. E.; Hofstad, B. A.; Chauvigné-Hines, L. M.; Zink, E. M.; Purvine, S. O.; Smith, R. D.; Callister, S. J.; Magnuson, J. M.; Wright, A. T. Activity-Based Protein Profiling of Secreted Cellulolytic Enzyme Activity Dynamics in Trichoderma Reesei QM6a, NG14, and RUT-C30. *Mol. Biosyst.* **2013**, *9* (12), 2992. https://doi.org/10.1039/c3mb70333a.

(99) Deng, X.; Weerapana, E.; Ulanovskaya, O.; Sun, F.; Liang, H.; Ji, Q.; Ye, Y.; Fu, Y.; Zhou, L.; Li, J.; Zhang, H.; Wang, C.; Alvarez, S.; Hicks, L. M.; Lan, L.; Wu, M.; Cravatt, B. F.; He, C. Proteome-Wide Quantification and Characterization of Oxidation-Sensitive Cysteines in Pathogenic Bacteria. *Cell Host Microbe* **2013**, *13* (3), 358–370. https://doi.org/10.1016/j.chom.2013.02.004.

(100) Balakrishnan, A.; Patel, B.; Sieber, S. A.; Chen, D.; Pachikara, N.; Zhong, G.; Cravatt, B. F.; Fan, H. Metalloprotease Inhibitors GM6001 and TAPI-0 Inhibit the Obligate Intracellular Human Pathogen Chlamydia Trachomatis by Targeting Peptide Deformylase of the Bacterium. *J. Biol. Chem.* **2006**, *281* (24), 16691–16699. https://doi.org/10.1074/jbc.M513648200.

(101) Kulkarni, A.; Soni, I.; Kelkar, D. S.; Dharmaraja, A. T.; Sankar, R. K.; Beniwal, G.; Rajendran, A.; Tamhankar, S.; Chopra, S.; Kamat, S. S.; Chakrapani, H. Chemoproteomics of an Indole-Based Quinone Epoxide Identifies Druggable Vulnerabilities in Vancomycin-Resistant Staphylococcus Aureus. *J. Med. Chem.* **2019**, *62* (14), 6785–6795. https://doi.org/10.1021/acs.jmedchem.9b00774.

(102) Greenwood, N. N.; Earnshaw, A. *Chemistry of the Elements*, 2nd ed.; Elsevier

Butterworth-Heinemann: London, 1997.

(103) Willgerodt, C. Ueber Einige Aromatische Jodidchloride. *J. f*[illegible]*r Prakt. Chemie* **1885**, *33* (1), 154–160. https://doi.org/10.1002/prac.18860330117.

(104) Perkins, C. W.; Martin, J. C.; Arduengo, A. J.; Lau, W.; Alegria, A.; Kochi, J. K. An Electrically Neutral .Sigma.-Sulfuranyl Radical from the Homolysis of a Perester with Neighboring Sulfenyl Sulfur: 9-S-3 Species. *J. Am. Chem. Soc.* **1980**, *102* (26), 7753–7759. https://doi.org/10.1021/ja00546a019.

(105) You, J.-Z.; Chen, Z.-C. Hypervalent Iodine in Synthesis; 5. 1 The Reaction Between Diaryliodonium Salts and Thiocarboxylic Acid Salts: A Convenient Method for the Synthesis of S -Aryl Thiocarboxylates. *Synthesis (Stuttg).* **1992**, *1992* (06), 521–522. https://doi.org/10.1055/s-1992-26150.

(106) Chen, Z.; Jin, Y.; Stang, P. J. Polyvalent Iodine in Synthesis. 2. A New Method for the Preparation of Aryl Esters of Dithiocarbamic Acids. *J. Org. Chem.* **1987**, *52* (18), 4117–4118. https://doi.org/10.1021/jo00227a032.

(107) Chen, D. W.; Zhang, Y. Da; Chen, Z. C. Hypervalent Iodine in Synthesis. *Synth. Commun.* **1995**, *25* (11), 1627–1631. https://doi.org/10.1080/00397919508015847.

(108) Liu, Z.-D.; Chen, Z.-C. Synthesis of Arylphosphonates by Arylation of Phosphite Anions Using Diaryliodonium Salts. *Synthesis (Stuttg).* **1993**, *1993* (04), 373–374. https://doi.org/10.1055/s-1993-25865.

(109) Grushin, V. V. Carboranylhalonium Ions: From Striking Reactivity to a Unified Mechanistic Analysis of Polar Reactions of Diarylhalonium Compounds. *Acc. Chem. Res.* **1992**, *25* (11), 529–536. https://doi.org/10.1021/ar00023a007.

(110) Grushin, V. V.; Demkina, I. I.; Tolstaya, T. P. Unified Mechanistic Analysis of Polar Reactions of Diaryliodonium Salts. *J. Chem. Soc. Perkin Trans. 2* **1992**, No. 4, 505. https://doi.org/10.1039/p29920000505.

(111) Pinto de Magalhães, H.; Lüthi, H. P.; Togni, A. Breaking Down the Reactivity of λ^3-Iodanes: The Impact of Structure and Bonding on Competing Reaction Mechanisms. *J. Org. Chem.* **2014**, *79* (17), 8374–8382. https://doi.org/10.1021/jo501714f.

(112) Bumagin, N. A.; Luzikova, E. V.; Sukhomlinova, L. I.; Tolstoya, T. P.; Beletskaya, I. P. Palladium Catalyzed Cross-Coupling of Symmetrical Diaryliodonium Salts with

Sodium Tetraphenylborate in Water. *Russ. Chem. Bull.* **1995**, *44* (2), 385–386. https://doi.org/10.1007/BF00702162.

(113) Bumagin, N. A.; Sukhomlinova, L. I.; Igushkina, S. O.; Banchikov, A. N.; Tolstaya, T. P.; Beletskaya, I. P. Palladium-Catalyzed Cross-Coupling of Diaryliodonium Salts with Organotin Compounds. *Bull. Russ. Acad. Sci. Div. Chem. Sci.* **1992**, *41* (11), 2128–2129. https://doi.org/10.1007/BF00863388.

(114) Bumagin, N. A.; Sukhomlinova, L. I.; Banchikov, A. N.; Tolstaya, T. P.; Beletskaya, I. P. Palladium-Catalyzed Arylation of Acrylic Acid by Diaryliodonium Salts in Water. *Bull. Russ. Acad. Sci. Div. Chem. Sci.* **1992**, *41* (11), 2130–2130. https://doi.org/10.1007/BF00863389.

(115) A., V. *Organic Chemistry of Polycoordinated Iodine*; VCH Publishers, Inc.: New York, 1992.

(116) Freedlander, B. L.; French, F. Chemotherapy of Certain Iodonium and Sulfonium Compounds. *Exp. Biol. Med.* **1946**, *63* (2), 319–322. https://doi.org/10.3181/00379727-63-15587.

(117) Gershenfeld, L.; Witlin, B. The Bacteriostatic Efficiency of Iodonium Compounds; Toxicity Studies of Certain Members of This Group. *Am. J. Pharm. Sci. Support. Public Health* **1948**, *120* (5), 170–175.

(118) Gershenfeld, L.; Witlin, B. Iodonium Compounds and Their Antibacterial Activity. *Am. J. Pharm. Sci. Support. Public Health* **1948**, *120* (5), 158–169.

(119) Engelhard, W. E.; Worton, A. G. Evaluation of an Iodonium Compound as an Antiseptic Agent. *J. Am. Pharm. Assoc. (Scientific ed.)* **1956**, *45* (6), 402–404. https://doi.org/10.1002/jps.3030450616.

(120) Chung, J.-W.; Kim, S. Y.; Park, H. J.; Chung, C. S.; Lee, H. W.; Lee, S. M.; Kim, I.; Pak, J. H.; Lee, G. H.; Jeong, J.-Y. *In Vitro* Activity of Diphenyleneiodonium toward Multidrug-Resistant *Helicobacter Pylori* Strains. *Gut Liver* **2017**, *11* (5), 648–654. https://doi.org/10.5009/gnl16503.

(121) Pandey, M.; Singh, A. K.; Thakare, R.; Talwar, S.; Karaulia, P.; Dasgupta, A.; Chopra, S.; Pandey, A. K. Diphenyleneiodonium Chloride (DPIC) Displays Broad-Spectrum Bactericidal Activity. *Sci. Rep.* **2017**, *7* (1), 11521–11528.

https://doi.org/10.1038/s41598-017-11575-5.

(122) Nguyen, N.; Wilson, D. W.; Nagalingam, G.; Triccas, J. A.; Schneider, E. K.; Li, J.; Velkov, T.; Baell, J. Broad Activity of Diphenyleneiodonium Analogues against Mycobacterium Tuberculosis, Malaria Parasites and Bacterial Pathogens. *Eur. J. Med. Chem.* **2018**, *148*, 507–518. https://doi.org/10.1016/j.ejmech.2017.10.010.

Chapter 2: Chemoproteomic Approaches Towards the Probable Target Identification of DPIC in *E. coli*

2.1. Introduction:

In Chapter 1, the antibacterial properties of iodonium compounds were discussed.[1,2] In the context of antibiotic resistance, diphenylene iodonium chloride (DPIC) is reported to be active against MDR *Helicobacter pylori*, *Staphylococcus aureus*, and *Mycobacterium tuberculosis*.[3,4] In another SAR-based study on the DPI triflate series of compounds, Baell and co-workers have identified 5-chlorodiphenyleneiodonium triflate as a potent inhibitor of MDR ESKAPE pathogens. However, the lead compound was found to be quite toxic to mammalian cells.[5] Hence, structural modifications carried out thus far that appear to increase potency also enhance toxicity. Furthermore, the mechanism of action or specific targets of the iodonium class of molecules in bacterial cells are not completely characterized. Efforts towards target identification, primarily in mammalian model systems, are listed below. DPIC has been considered as an inhibitor of NADH/ NADPH oxidase. Jones and co-workers have shown that diphenyleneiodonium (DPI) inhibits the NADPH-dependent superoxide production and cytochrome b-245 of neutrophile.[6] Autoradiography labelling study with polypeptides of flavoprotein by DPI [^{125}I] in the presence of NADPH suggested that NADPH competes with DPI at the binding site of the enzyme or in the presence of NADPH , the enzyme does not bind DPI, likely due to a conformational change.. Later, O'Donnell and co-workers observed an interaction of DPI with free flavin and identified DPI-FAD adduct using HPLC based studies.[7] In this study, it was shown that DPI treatment in the presence of NADPH oxidase has significantly reduced the recoverable FAD during turnover, and this inhibition of NADPH oxidase by DPI is found to be dependent on NADPH concentration. On the contrary to a previous report,[6] it was suggested that NADPH and DPI do not compete for the same binding site of the enzyme and discovered flavins as the binding site for DPI. Collectively, it was hypothesized that DPI inhibits NADPH oxidase through a radical-mediated mechanism where DPI accepts the electron during turnover and generates an aryl radical, which is now available to react with the nearby prosthetic group or on proteins to form the DPI adducts. In another study, Wikstriirn and co-workers have shown that DPI inhibits the activity of NADH-ubiquinone oxidoreductase of complex I in mitochondria and *E. coli*.[8] Using spectroscopy and EPR-based studies on purified complex I, it was demonstrated that DPI binds to FMN, which further blocks the oxidation of FMN and the reduction of iron-sulphur cluster. Later, Nathan and co-workers have shown that DPI and its analogues inhibit nitric oxide synthase (NOS) of

macrophages and endothelial cells.[9] The irreversible inhibition of NOS is discovered to be dependent on time and temperature but not on enzyme catalysis. However, inhibition of NOS by DPI was found to be blocked by NADPH and FAD. This finding suggested that NOS inhibition by DPI is dependent on NADPH utilizing flavoproteins. In contrast to this claim, Ghigo and colleagues found that DPI inhibits both the tricarboxylic acid cycle and the pentose phosphate pathway in N11 glial cells in a dose-dependent manner and is not necessarily a flavoprotein inhibitor.[10] Next, using high-throughput drug-screening in a cancer stem cell model, Ozsvari and colleagues discovered DPIC as a non-toxic inhibitor of mitochondrial respiration complex I and II.[11] It was found that DPI inhibits the flavoenzymes which led to the significant reduction in ATP levels and eventually inhibited proliferation of cancer stem cells. In another study, with the help of enzyme kinetic assays and spectroscopic methods, Mattevi and co-workers have demonstrated that DPI reversibly inhibits the human MAO (monoamine oxidases) A and B.[12] With the help of an elucidated crystal structure of MAO B, it was shown that DPI strongly binds with active site and flavin through multiple hydrophobic interactions.

All these aforementioned studies carried out in mammalian cells indicate that DPIC is not a specific inhibitor of NADPH oxidase and may interact with other proteins and enzymes. However, despite the known inhibitory effects of this compound, the interaction of DPIC with proteins is yet to be investigated in bacterial cells. Considering this, we decided to investigate the possible targets of this potent antibacterial agent utilizing activity-based protein profiling (ABPP) as one of the chemoproteomic approaches. ABPP is a technique where a proteome of an organism is treated with the molecule of interest with a pre-installed analytic handle such as an alkyne. The treated proteome is then reacted with a fluorescent azide using click chemistry. The protein samples are then run on an SDS-PAGE platform. By this process, only covalently modified proteins are visualized by fluorescence scanning. The modified proteins, which could be the probable targets of the molecule of interest, can then be identified by performing LC/MS-MS based proteomics.[13–17] Since most of the well-known targets of antibiotics are common across both Gram-positive and Gram-negative bacteria, *E. coli* was chosen as a model organism for this study.

2.2. Results and Discussion:

2.2.1. Synthesis of DPIC alkyne probe:

In order to perform ABPP, it would be necessary to have analytical handle such as an alkyne appended to DPIC. Hence, the DPIC is a hydrophobic molecule, adding an alkyne *via* a PEG (polyethylene glycol) chain would make the probe less hydrophobic and more suitable for biological studies. Hence, the retrosynthesis of the PEG chain based DPIC alkyne probe was designed scheme 2.1.

Scheme 2. 1 Retrosynthesis scheme for DPIC-PEG-alkyne probe

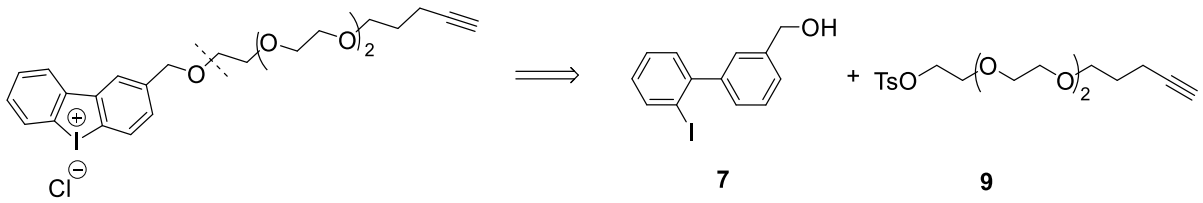

In order to synthesize an alkyne containing DPIC probe, it was envisaged that compound 6, which has a carboxylic acid could first be prepared. The carboxylic acid 6 or compound 7, which is the alcohol derived from reduction of 6 could then be subsequently functionalized with an alkyne containing side chain. Here, 2-bromo aniline was coupled with aryl boronic acid using Suzuki coupling reaction conditions. Next, the bi-aryl amine **4** was reacted with sodium nitrite and potassium iodide (diazotization conditions) to get bi aryl iodide **5**. Further, compound **5** was hydrolyzed to biphenyl iodo carboxylic acid **6**. This compound was reacted with borane dimethylsulfide to afford the alcohol **7**. During purification, the formation of the de-halogenated compound was also observed. This observation suggests that aryl iodide compounds are light-sensitive and unstable, and iodine or iodide may have fallen off during workup. Hence, the crude was taken to the next step without further purification.

Scheme 2. 2 Synthesis scheme for compound 7

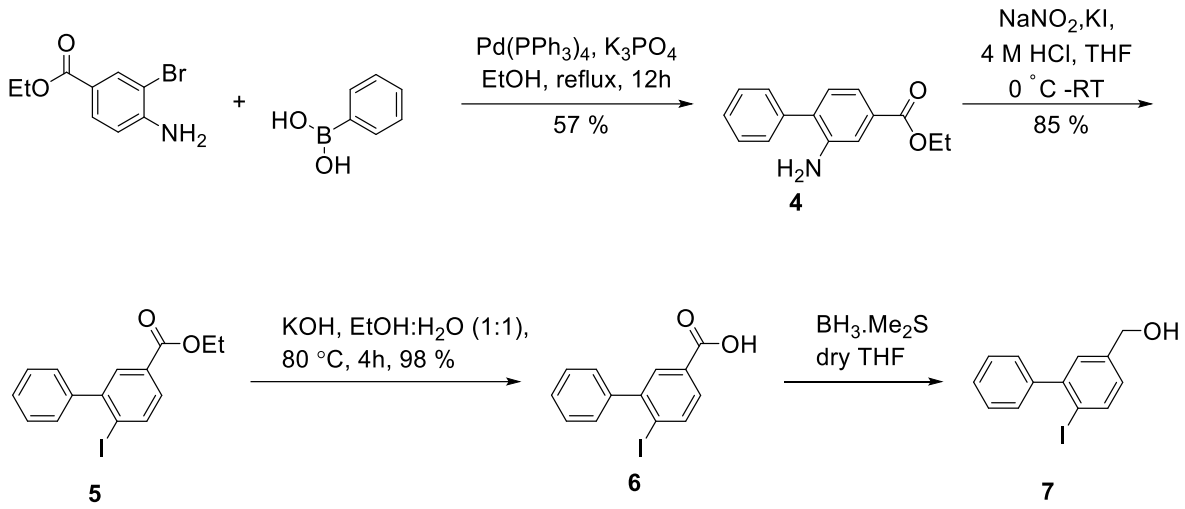

Compound **8** was synthesized from 5-chloropentyne and tetra ethylene glycol in the presence of NaI (iodide displaces chloride to produce a better electrophile). Next, the tosylate **9** was prepared by the reaction of the primary alcohol with tosyl chloride. Next, the tosylate **9** was treated with **7** methanol to produce the iodide **10**. The general method for the synthesis of DPI involves the oxidation of the bi-aryliodide with *m*CPBA. The likely mechanism is the formation of the iodonium ion, which then reacts with the neighbouring aryl ring the afford DPI. When **10** was reacted with *m*CPBA, despite several attempts, an inseparable mixture of products resulted.

Scheme 2. 3 Synthesis scheme for DPIC-peg-alkyne probe

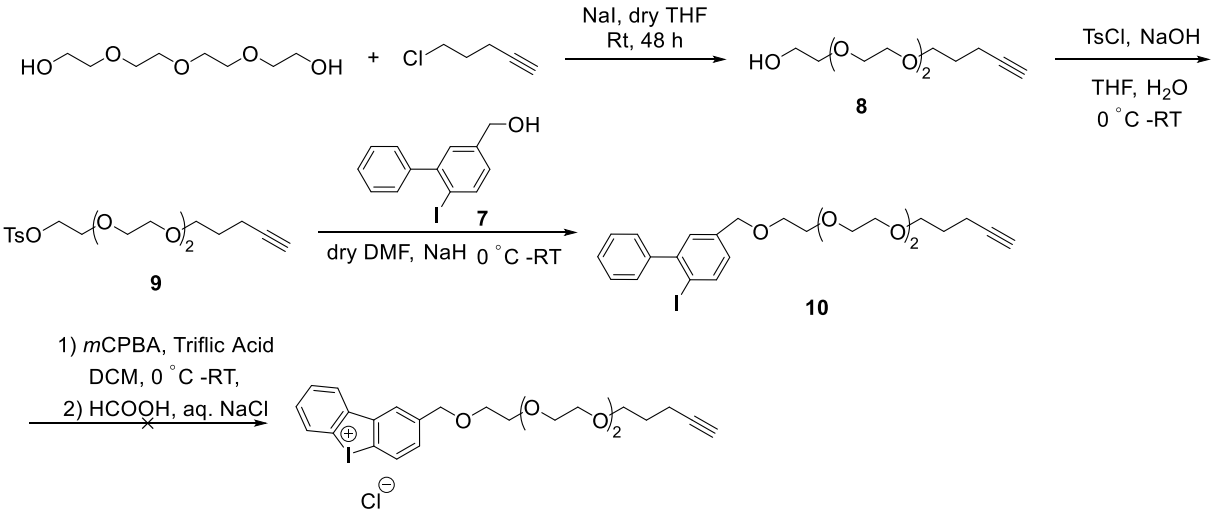

Hence, the synthetic scheme was redesigned to append the shorter length alkyne to **6** through an ester or an amide bond. Due to the propensity of carboxylic acid-based esters to undergo hydrolysis by esterases, the amide was considered. Amide bonds are normally more resistant to hydrolysis under cell lysate conditions. Following Scheme 2.4., first propargyl amine was coupled with previously synthesized iodo biphenyl carboxylic acid, using EDC-DMAP coupling reaction. This resulting alkyne intermediate was oxidized to afford the DPIC alkyne probe **P1** in a 32% yield.

Scheme 2. 4 Synthesis scheme for DPIC-alkyne probe P1

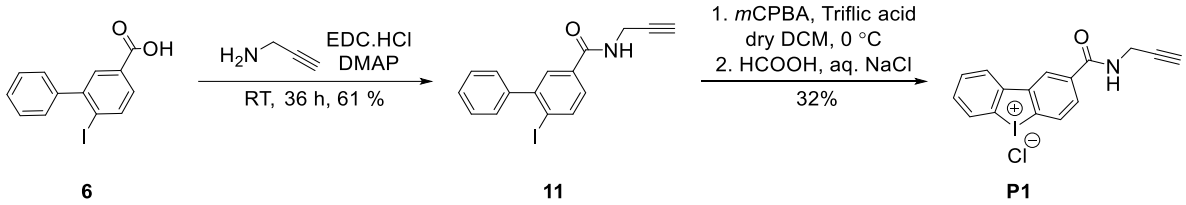

The alkyne probe **P1** was assessed for its antibacterial activity against Gram-negative pathogen *E. coli*. The *E. coli* cells were treated with DPI, the alkyne probe at different concentrations, and Levofloxacin as a positive control. The growth of cells was monitored over time. Growth curve analysis showed that **P1** inhibited the growth of bacteria in a dose-dependent manner supporting the use of this compound to elucidate the targets of DPI (Figure 2.1).

Figure 2. 1 Growth curve of E. coli ATCC 25922 treated with 1a and Probe P1

Ctrl indicates bacterial cells; Levo indicates Levofloxacin; (Data provided by: Dr. Sidharth Chopra lab, CSIR-CDRI Lucknow)

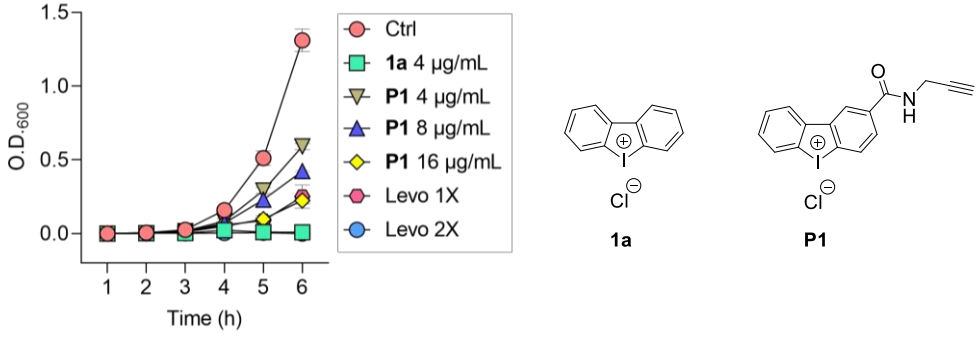

2.2.2 Activity-based protein profiling (ABPP) with DPIC alkyne probe P1 in *E. coli*:

Next, protein profiling by probe **P1** was investigated using ABPP. *E. coli* cells were grown overnight and lysed in 1X PBS, fractionated and separated the membrane and soluble fraction using an ultracentrifuge. Using BSA protein standards, the protein concentration was determined by the Bradford assay and adjusted to 1 mg/mL with 1X PBS for both the proteome membrane and soluble. The proteome was treated with DPIC alkyne probe **P1** with different concentrations (0-100 µM), and as a control, one set of the proteome was treated with DMSO alone. All the aforementioned reaction mixtures were incubated for 1 h. Only proteins that are modified by **P1** would have the alkyne appended on them, which would be available for the copper-catalyzed alkyne-azide cycloaddition (CuAAC) "Click" reaction with a reporter azide such as the fluorescent rhodamine azide, Alexa fluor 488.

Then, the proteome was visualized by sodium dodecyl sulphate polyacrylamide gel electrophoresis (SDS-PAGE) using standard gel-based ABPP protocols.[18] A dose-dependent protein labelling by probe **P1** was observed in soluble fraction than membrane fraction. This indicated that probe **P1** preferentially reacts with cytosolic proteins over membrane proteins (Figure 2.2 and 2.3). Thus, the soluble proteome was selected for further ABPP based studies.

Figure 2. 2 Dose-dependent profiling in soluble fraction of E. coli with DPIC alkyne probe P1

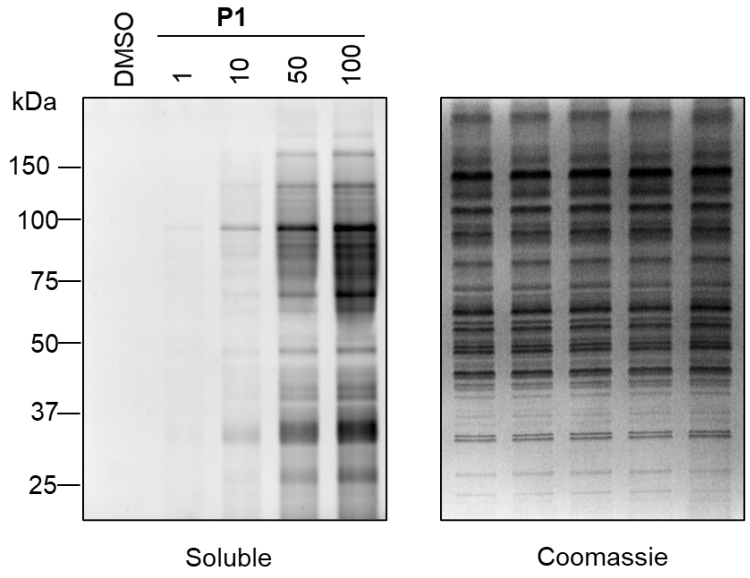

Figure 2. 3 Dose-dependent profiling in membrane fraction of E. coli with DPIC alkyne probe P1

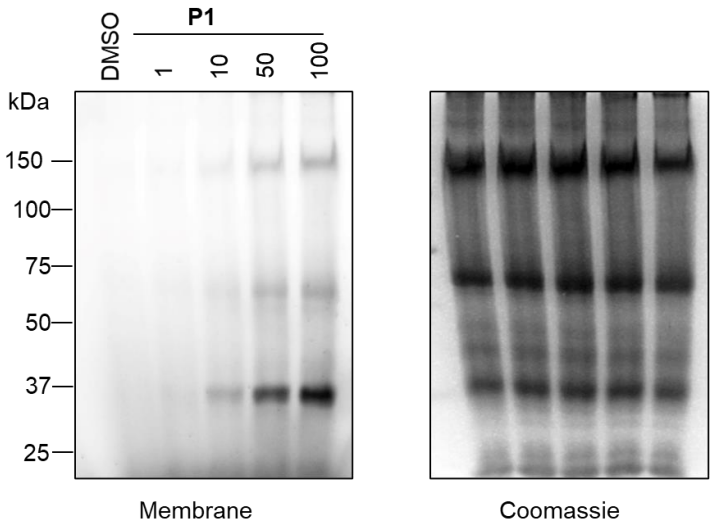

Being positively charged, DPIC is expected to behave like an electrophile.Nucleophilic amino residue of protein would react with probe **P1** and get themselves modified. Among amino residues, the relative order of the nucleophilicity of the functional group is $RS^- > RNH_2 > RCOO^- = ROH$. Thus, thiol-based proteins are normally more nucleophilic and are likely to react with electrophiles such as **P1**. In order to investigate the selectivity of the probe **P1** towards thiol, a competitive-ABPP based experiment was conducted. The competitive-ABPP is based on the hypothesis that the target proteins of the probe and a known inhibitor or covalent modifying agent are the same. Here, since cysteine residues are being considered, **IAM**, a thiol blocking agent[19], which covalently modifies cysteine residues was used. By blocking cysteine residues, **IAM** inhibits or prevents the reaction of cysteine-containing proteins with **P1** or **DPI**. The *E. coli* proteome was treated with **IAM** (10 mM)followed by treatment with **P1** (100 µM)or with **P1** alone. After the click reaction with rhodamine azide and SDS-PAGE, if **P1** modified cysteine residues in the proteome, a diminution in signal in the **IAM**-pretreated sample when compared with **P1** alone is expected (Figure 2.4).

Figure 2. 4 Chase experiment - In vitro modification of proteins in soluble fraction of E. coli with P1

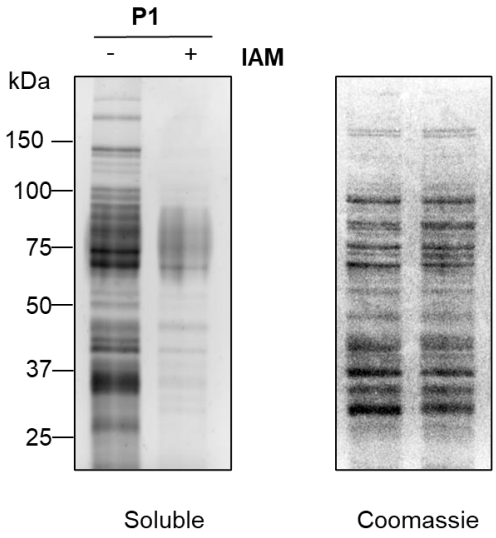

Having established that the probe **P1** preferentially reacts with the cysteine residue of thiol-based proteins, a competitive ABPP based experiment was conducted with DPIC as a competitor. In this experiment, the proteome was first treated with DPIC in a dose-dependent manner, followed by probe **P1** (100 µM). A reduction in intensity of several protein bands (marked as *) with increasing concentration of DPIC was observed indicating that DPIC covalently modifies certain proteins in the soluble proteome (Figure 2.5).

Figure 2. 5 Chase experiment - In vitro modification of proteins in soluble fraction of E. coli with DPIC 1a chased with P1

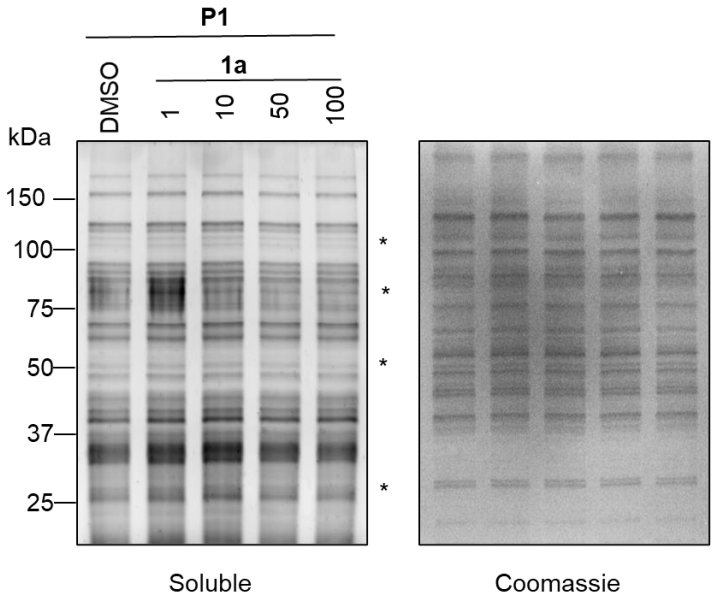

Next, the reactivity of DPIC towards thiol-based proteins was also assessed. In this experiment, the proteome was pre-treated with DPIC (250 µM), followed by the iodoacetamide alkyne (**IAA**) probe (100 µM). The iodoacetamide alkyne probe is used to profile the thiol-based proteins[19]. A significant reduction in the intensity of certain protein bands in the DPIC pre-treated proteome (marked as *) when compared with the proteome treated with only **IAA** was observed (Figure 2.6). This finding is consistent with our earlier result with **IAM** and **P1**, and together these results suggest that DPIC reacted with cysteine residues of the proteins.

Figure 2. 6 Chase experiment - In vitro modification of proteins in soluble fraction of E. coli with DPIC 1a and chased with iodoacetamide alkyne (IAA)

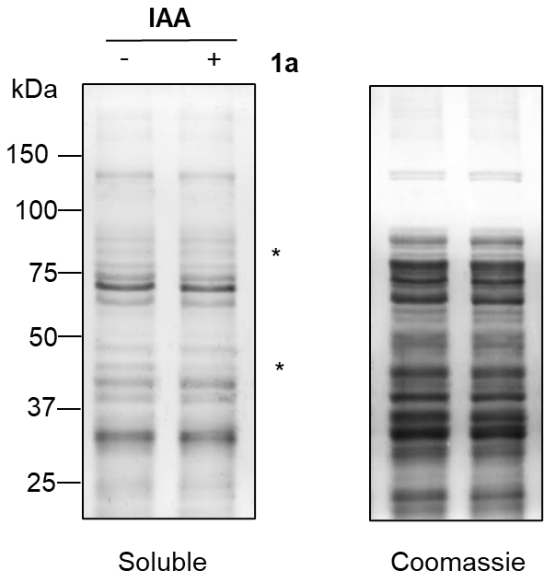

2.2.3. Target Identification of DPIC using competitive LC-MS/MS-based ABPP experiment with probe P1 in *E. coli*:

Using **P1** as a chemoproteomics probe, a competitive LC-MS/MS-based ABPP experiment was next conducted to identify the targets of DPIC. Here, the soluble proteome of *E. coli* was first treated with DPIC (250 µM) for 1 h, followed by DPIC alkyne probe **P1** (100 µM) for 1 h. Then a click reaction was performed with biotin azide. Due to the strong binding between biotin and streptavidin, these functional groups have been widely employed in conjunction with LC/MS-MS techniques to ascertain targets.[19] Thus, in this study, the proteins appended with DPIC alkyne probe **P1** are expected to be biotinylated and therefore can be identified using standard techniques after enrichment by avidin-agarose beads. This was followed by 14 hours

of trypsin digestion, wherein proteins are cleaved into small peptides, which were detected using LC-MS/MS analysis (Figure 2.7). A filter criterion was followed to list out the probable targets of DPIC, where a highly significant (lower p-value) relative ratio [Fold Change (FC) = DMSO/DPIC] of DMSO and DPIC treated proteins was considered to be ≥1.5 in each replicate. Based on these filtering criteria, three proteins named NADH-quinone oxidoreductase subunit F (NuOF), succinate dehydrogenase iron-sulfur subunit *β* (sdhb), and NADH-quinone oxidoreductase subunit G (NuOG) were listed as the probable targets of DPIC out of 125 proteins identified by LC-MS/MS.

Figure 2. 7 Schematic for proteomics using probe P1

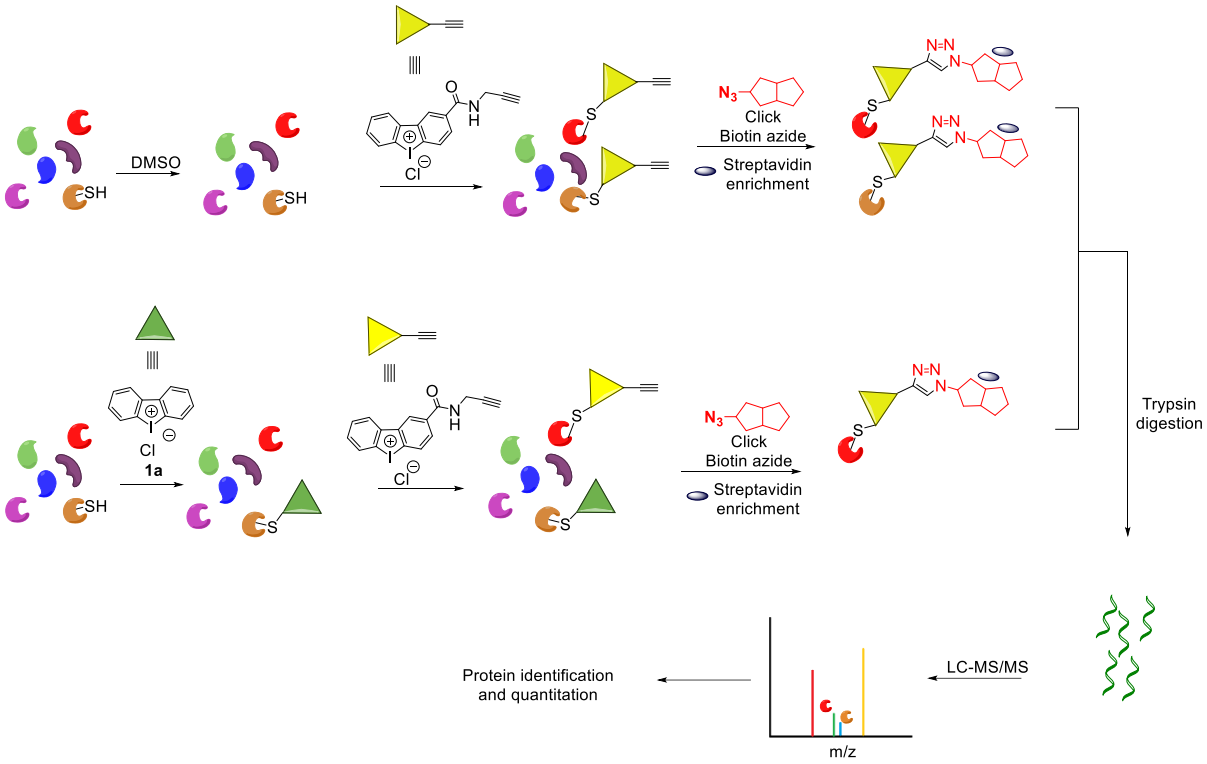

All three targets are redox proteins that are involved in the bacterial respiratory system (Table 2.1). Inhibition of these proteins may inhibit the process of bacterial respiration and the survival of bacteria. One of these three potential targets, NuOF, was chosen for further studies since it was the most inhibited by DPIC.

Table 2. 1 List of identified probable targets of 1a from the soluble fraction of E. coli using chemoproteomic experiment

Entry	Accession no	Protein Name	DMSO/DPIC	Mol. Wt (Da)
1.	WP_000789500.1	NADH-quinone oxidoreductase subunit F (NuOF)	2.963930506	49,292 Da
2.	WP_001235254.1	Succinate dehydrogenase iron-sulfur subunit (sdhb)	2.038832141	26,770 Da
3.	WP_000190939.1	NADH-quinone oxidoreductase subunit G (NuOG)	1.853371519	100,299 Da

2.2.4. Bioinformatics of target protein NuOF:

NuOF and NuOG are proton pumping complex I subunits, while sdhb is a non-proton pumping complex II subunit.[20] The iron-sulfur clusters found in all three target proteins direct electron flow during respiration.[21] NuOF is involved in the initiation of the respiration process. NuOF subunit consists of one FMN binding site and one [4Fe-4S] iron-sulfur cluster. When the respiration process begins, NADH releases NAD+ and an electron near the FMN binding site, which is then captured by FMN. The electrons are translocated to complex II through the iron-sulfur cluster present in these subunits of complex I. *E. coli* NuOF has nine cysteine residues of which, a bioinformatics analysis across various bacterial species revealed that five of these are highly conserved.[22] One of the conserved cysteine residues is involved in the FMN binding site, whereas the other four are engaged in iron-sulfur cluster coordination ([4Fe-4S]) (Table 2.2).

Table 2. 2 Bioinformatics assay for NuOF

Entry	Redox protein	Cysteine residues	Conserved cysteine residues
1.	NADH-quinone oxidoreductase subunit F (NuOF)	C89, C180, C215, C223, C351, C354, C357, C388, C398	FMN: C180 N3, 4Fe-4S: C351, C354, C357, C398

Gene cloning, protein expression, and purification were next carried out for NuOF, using *E. coli* as a model organism for validating the target.

Figure 2. 8 Schematic representation for the process of cloning, overexpression and protein purification

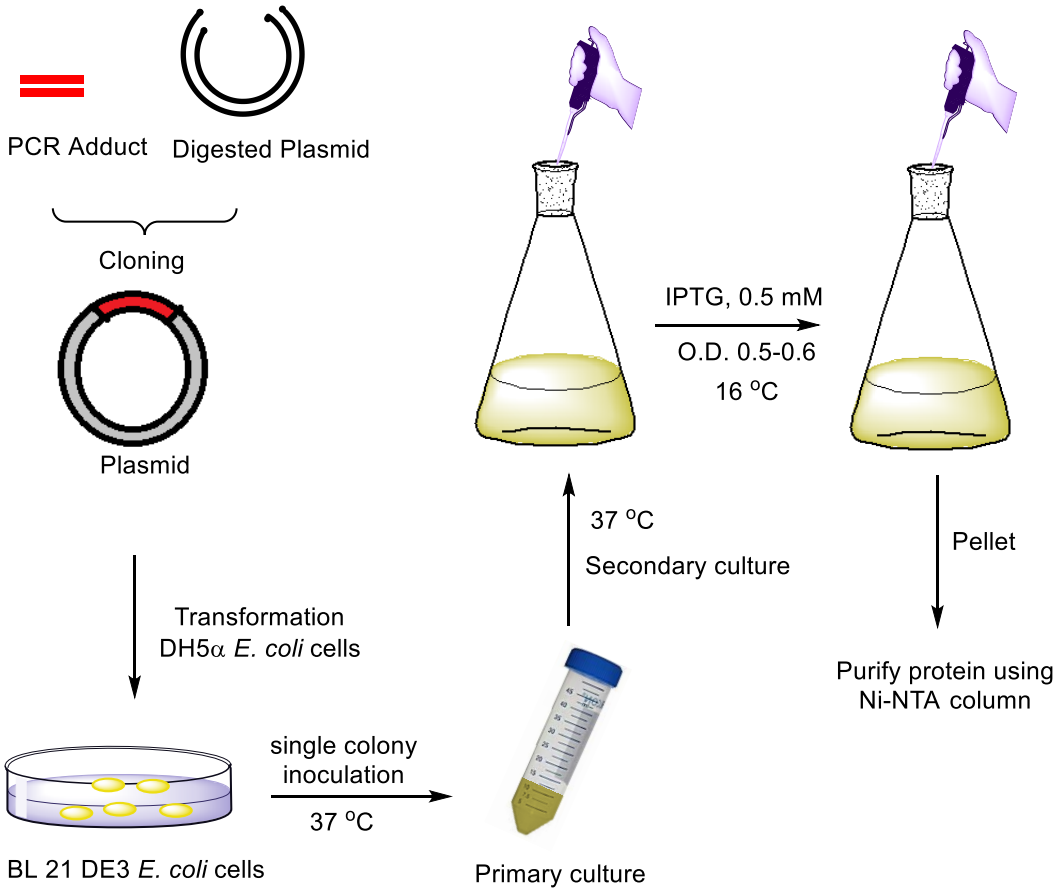

2.2.5. Polymerase Chain Reaction (PCR):

Plasmid pET-22b(+) was utilized for gene cloning. The forward and reverse primers of NuOF were designed with their restriction sites (Table 2.3). Standard PCR procedures were used to amplify the NuOF gene. On an agarose gel, an aliquot of the PCR mixture was examined for the expected amplicon size. The PCR adduct was purified using the Hi-media PCR purification kit, and the extracted amplicon's purity was validated using an agarose gel.

Table 2. 3 Primers and restriction sites

S. No.	Primer Name	length	% GC	Tm	Restriction Site	Primer Sequence (5′ → 3′)
1	pET-22b (+) NuOF_Fwd	36	31	56	NdeI	GAAGGAGATATACATAATG AAAAACATTAT CCGTAC
2	pET-22b (+) NuOF_Rev	31	55	66	BamHI	AGCTCGAATTCGGATCCCA GCGCTCTTTCAG

Figure 2. 9 A) PCR amplification of NuOF; B) Restriction digestion of plasmid pET-22b (+) using restriction enzyme

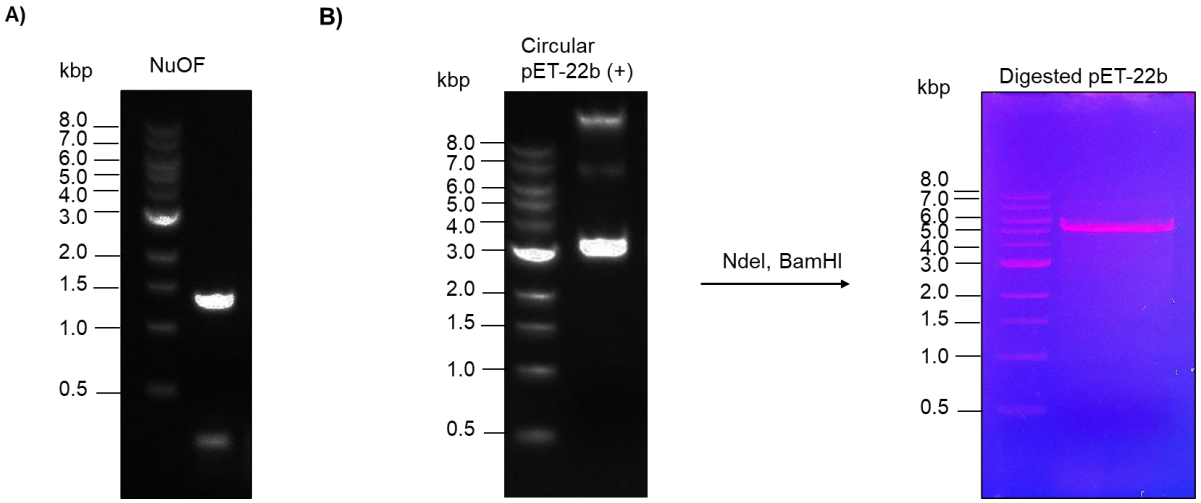

2.2.6. Restriction Digestion and Cloning:

Plasmid pET-22b(+) was digested at restriction sites NdeI and BamHI with restriction enzymes. The digested plasmid was isolated using Qiagen gel extraction kit. By keeping the 6X His tag at the C terminal, the gene was cloned in pET-22b(+) using the Sequence and ligation independent cloning (SLIC) method and then transformed into *E. coli* PPY cells.

2.2.7. Sequencing:

Isolated colonies were obtained after cloning. A total of 6 isolated colonies were identified and grown in LB media with 1X ampicillin, and plasmids were extracted using a regular Mini-prep kit. Before submitting the samples for sequencing analysis, aliquots of isolated plasmid

samples were run on agarose gel, and gene insertion was observed for sample C3 (Figure 2.10). This was further confirmed by sequencing analysis.

Figure 2. 10 Cloning of plasmid pET-22b (+) with NuOF PCR adduct

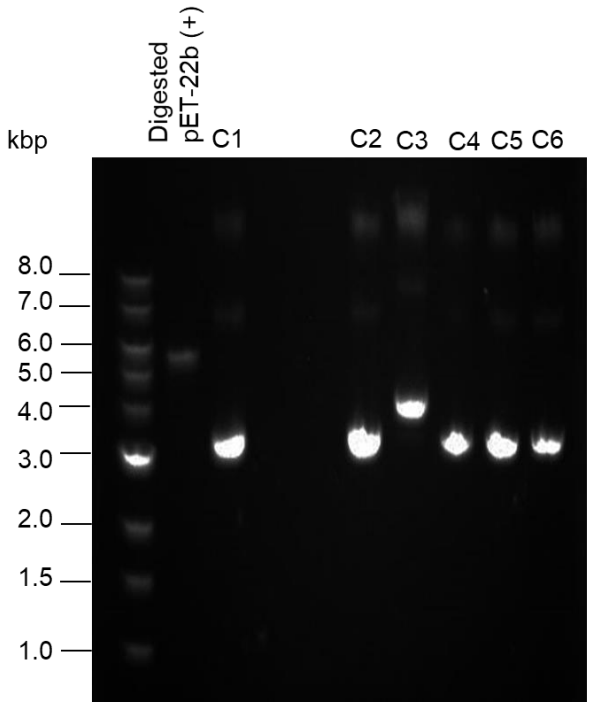

2.2.8. Transformation into *E. coli* DH5α cells:

E. coli DH5α cells are competent cells that are extensively used in molecular biology to insert the plasmid. Due to the lack of endonucleases, these cells help to make multiple copies of the plasmid. The plasmid is generally transformed into the cells using a Heat Shock method (42 °C for 90 sec). The cells were grown in LB media for 1 h at 37 °C, and then plated on an ampicillin pre-coated Nutrient Agar plate to avoid contamination. Plasmid carries the ampicillin antibiotic-resistant gene.

2.2.9. Overexpression in *E. coli* BL21(DE3) cells:

After confirming the sequence, the plasmid was transformed into *E. coli* BL21(DE3) cells. BL21 (DE3) cells are competent cells that lack proteases and are extensively used in molecular biology to overexpress the protein of interest using IPTG. IPTG is a chemical mimic of allolactose, which is a lactose metabolite known to trigger the *lac* operon for overexpression of gene. Protein was expressed using 0.5 mM of IPTG at 16 °C for 16 h (Figure 2.11).

Figure 2. 11 Overexpression observed in A) SDS-PAGE-Coomassie; B) Western blot developed using primary His antibody

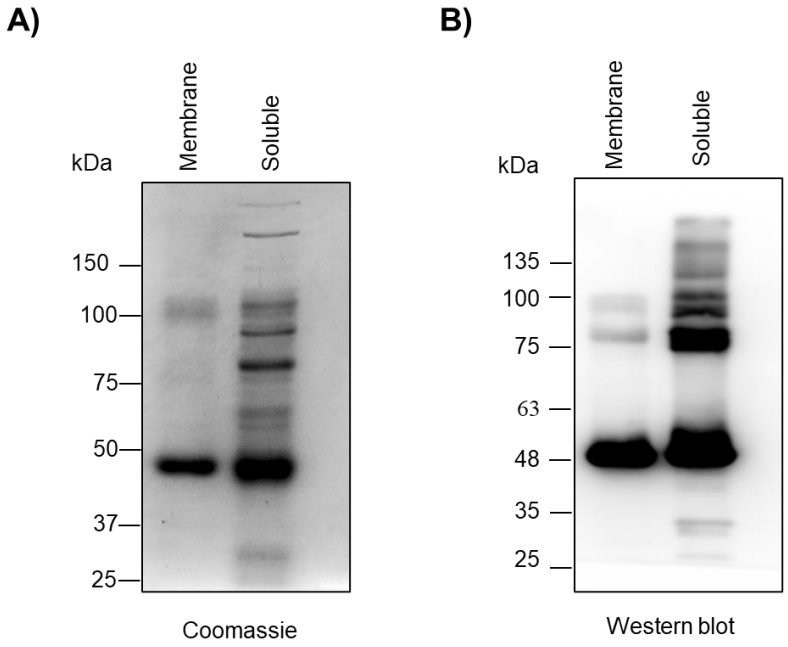

2.2.10. Protein Purification:

E. coli cells with overexpressed protein were harvested and fractionated. Both membrane and soluble fractions were visualized for overexpression after SDS-PAGE. Overexpression of protein was observed in the soluble fraction, which was confirmed by developing a western blot using an anti-His-primary antibody. Next, the His-tagged protein was purified using Ni-NTA affinity column chromatography. where, the His-tagged protein binds to the Ni^{+2} and forms the Ni-His complex. In the elution buffer, imidazole is utilized to elute the protein. Imidazole strongly binds to Ni and replaces the His-tagged protein. SDS-PAGE was used to evaluate the purity of the eluted protein, that was collected in fractions (Figure 1.12). The protein-containing fractions were combined together and desalted in dialysis buffer using a dialysis membrane. The protein concentration was estimated using Bradford assay. The aliquots were flash-frozen using liquid nitrogen and stored at -80 °C till further use.

Figure 2. 12 SDS-PAGE-Coomassie: protein purification of NuOF

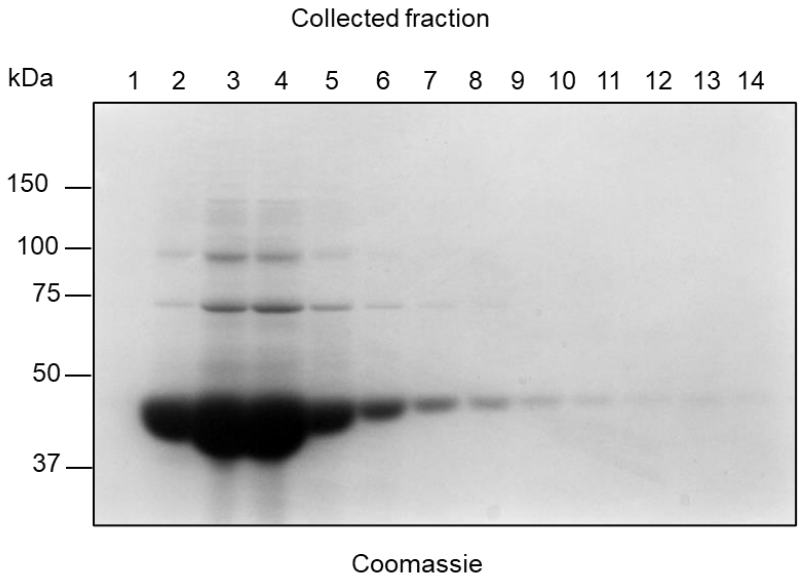

2.2.11. Labelling of target protein:

In order to validate the target protein, NuOF (0-20 µM) was treated with probe **P1** (100 µM) and visualized using in-gel fluorescence as described previously. Labelling by probe **P1** was observed with increasing protein concentration, and signal saturation was observed beyond 5 µM of protein (Figure 2.13. A). Hence, 5 µM concentration of protein was selected for further studies.

Figure 2. 13 A) Labelling of wild-type NuOF target protein with DPIC probe P1 (100 µM); B) gel filtration experiment with probe P1 (25 µM)

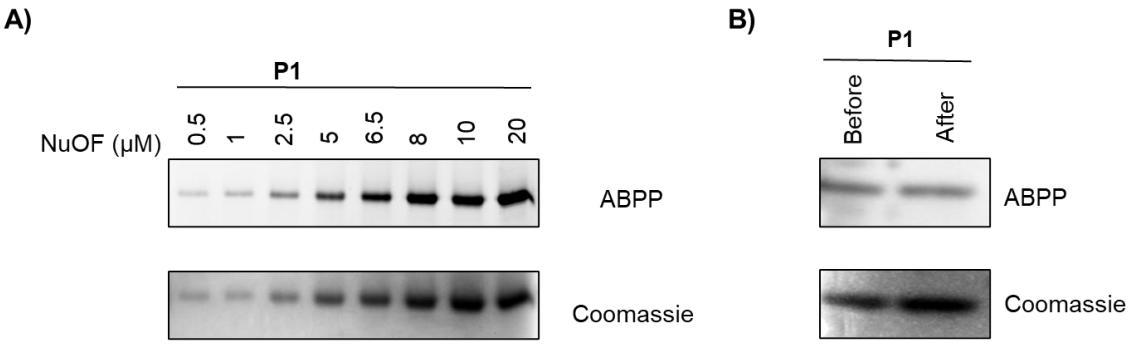

In order to understand if **P1** modified NuOF through a covalent bond, NuOF (5 µM) was treated with probe **P1** (25 µM). Dialysis was next performed using a dialysis membrane with a

molecular weight cut off (MWCO) of 6-8 kDa in dialysis buffer. All small molecules with a molecular weight less than 6 kDa that are not bound to protein would be removed using this method. The DPIC alkyne probe has a molecular weight of 396 Da, and if the interaction between probe **P1** and protein is non-covalent, the probe will leach out during dialysis. When a click reaction is performed with the protein using a reporter azide and visualized after SDS-PAGE, a signal would indicate a covalent bond between the protein and **P1**. The probe **P1** (100 µM) was treated with a fixed concentration of protein, and half of this reaction mixture was kept aside prior to dialysis. After dialysis, a click reaction was performed with both dialyzed and non-dialyzed protein and visualized after SDS-PAGE. A signal for probe **P1** labelling was observed in both dialyzed and non-dialyzed conditions confirming that probe **P1** covalently modifies NuOF (Figure 2.13. B).

Having established that **P1** covalently modified NuOF, the ability of DPIC to modify NuOF was studied through a competition experiment. A fixed concentration of the protein pre-treated with DPIC (250 µM, 1 h) was treated with the probe **P1** (100 µM, 1 h). Standard ABPP and SDS-PAGE protocols were followed, and for the protein pre-treated with DPI, a significant reduction in the intensity of the signal attributable to modification of the protein by **P1** was observed. Hence, modification of NuOF by **P1** is reduced by DPIC, suggesting a similar mode of interaction of these iodonium salts with proteins (Figure 2.14 A).

Figure 2. 14 ABPP chase experiments with NuOF

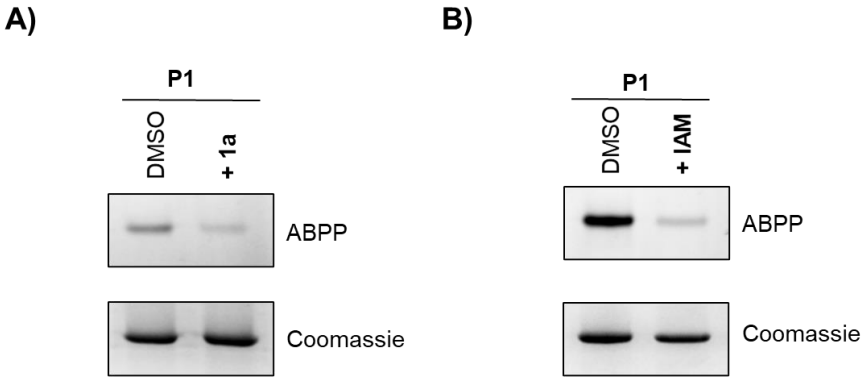

As discussed before, probe **P1** reacts with cysteine residues in proteins. So, a similar competitive ABPP based experiment was conducted with iodoacetamide as a competitor. The iodoacetamide pre-treated NuOF protein aliquots were treated with probe **P1**. A significant reduction in signal in the iodoacetamide-treated protein when compared with untreated was

observed (Figure 2.14 B). This strongly suggested that the probe modifies cysteine residues of the protein. A cysteine to alanine point mutant of this protein to validate the target protein was next carried out to ascertain if any of the conserved cysteine residues were involved in modification by **P1**/DPI.

2.2.12. Site-directed mutagenesis:

In NuOF, C180 is part of the FMN binding site while C351, C354, C357 and C398 is involved in coordination with Fe^{+2} of [4Fe-4S] iron-sulfur cluster. Cysteine to alanine point mutations for C180, C351, C354 were considered. Forward primers were designed for these cysteine point mutations, and T7 terminator was used as a reverse primer (Table 2.4).

Table 2. 4 Primers for cysteine mutants of NuOF

Entry	Primer name	length	% GC	Tm	Primer Sequence (5′ → 3′)
1	C180A Fwd	35	69	73	GAAGGAGATATACATAATGA AAAACATTAT CCGTAC
2	C354A Fwd	38	66	74	AGCTCGAATTCGGATCCCAGC GCTCTTTCAG
3	C354A Fwd	37	76	77	GGGCAGGGCGCTACATCGCCG GGGAAGAAA CAGCG
5	T7 Terminator Rev	37	76	77	GTGAGTCCTGCGGCTGGGCTA CGCCGTGCCGCGACG G

Megaprimer using standard PCR from mutant forward primer and T7 terminator with pET-22b(+)_NuOF as template DNA was prepared (Figure 2.15). Then, the whole plasmid PCR amplification method was utilized to amplify the gene for respective cysteine mutants. Dpn1 enzyme was used for selectively having the amplified mutant plasmid as Dpn1 enzyme would chop up the template plasmid used in PCR at the methylated adenine site. Aliquots from the reaction were run on an agarose gel and an intense band for circular plasmid was observed in the reaction performed with G_{xL} polymerase enzyme for each mutant (Figure 2.16). This was followed by the transformation in *E. coli* DH5α cells, and colonies were observed only from G_{xL} enzyme-mediated reaction. Plasmids were extracted from the isolated colonies for each mutant, and samples were sequenced.

Figure 2. 15 PCR amplification for megaprimer of cysteine point mutants of NuOF

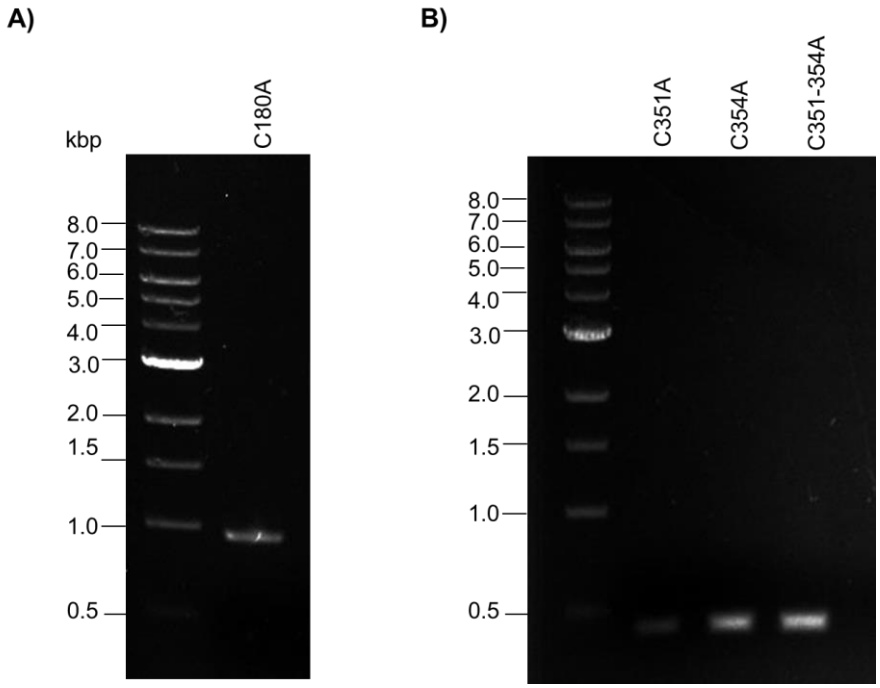

Figure 2. 16Agarose gel after whole plasmid PCR amplification and Dpn1degestion for cysteine point mutants of NuOF

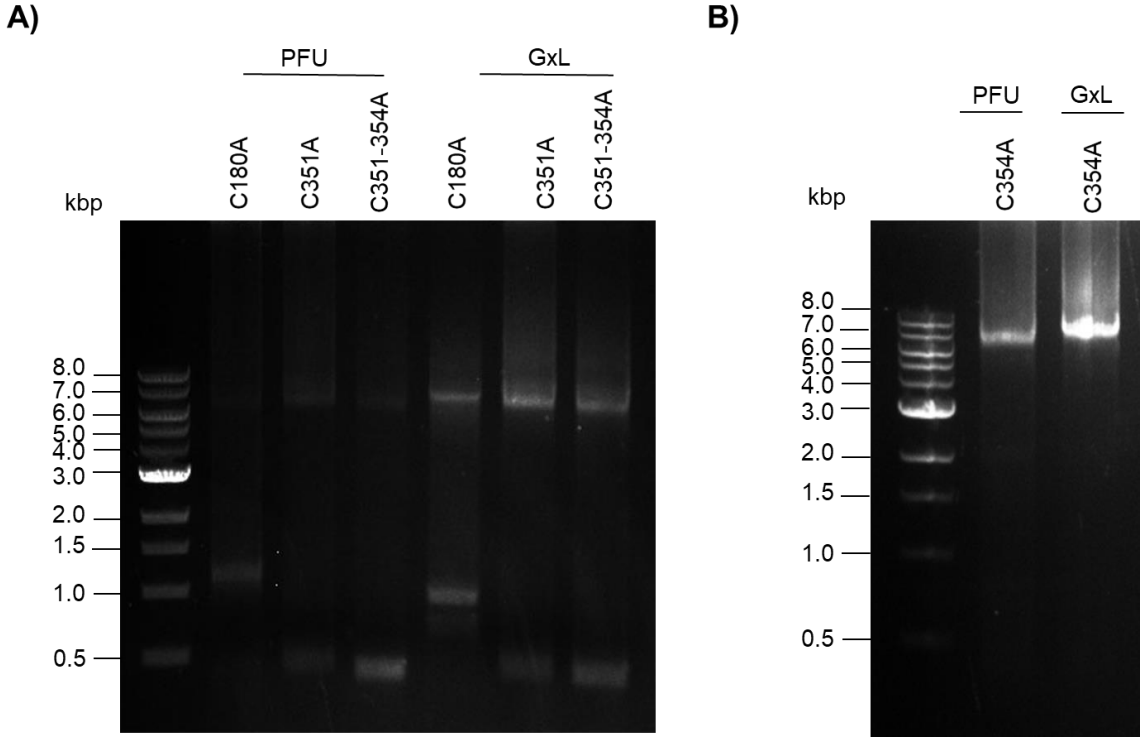

2.2.13. Overexpression and protein purification:

After confirming the cysteine to alanine point mutation through sequence analysis, overexpression of each mutant was done using the same protocol as used for wild type NuOF. The expression of each cysteine mutant was observed in the membrane fraction and was diminished in the soluble fraction. The proteins were purified from the protein expressed in the soluble fraction using the same condition used for wild type NuOF. Thus, each purified mutant protein's yield was lower than wild type protein.

Figure 2. 17 SDS-PAGE: overexpression observed for the mutant protein

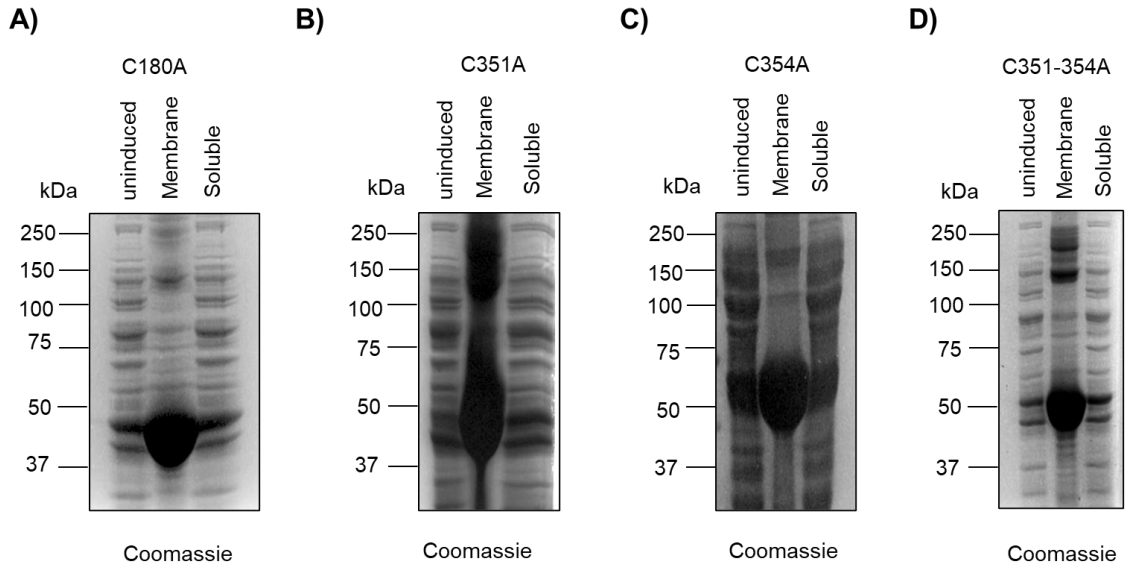

Figure 2. 18 SDS-PAGE: protein purification for cysteine mutants of NuOF

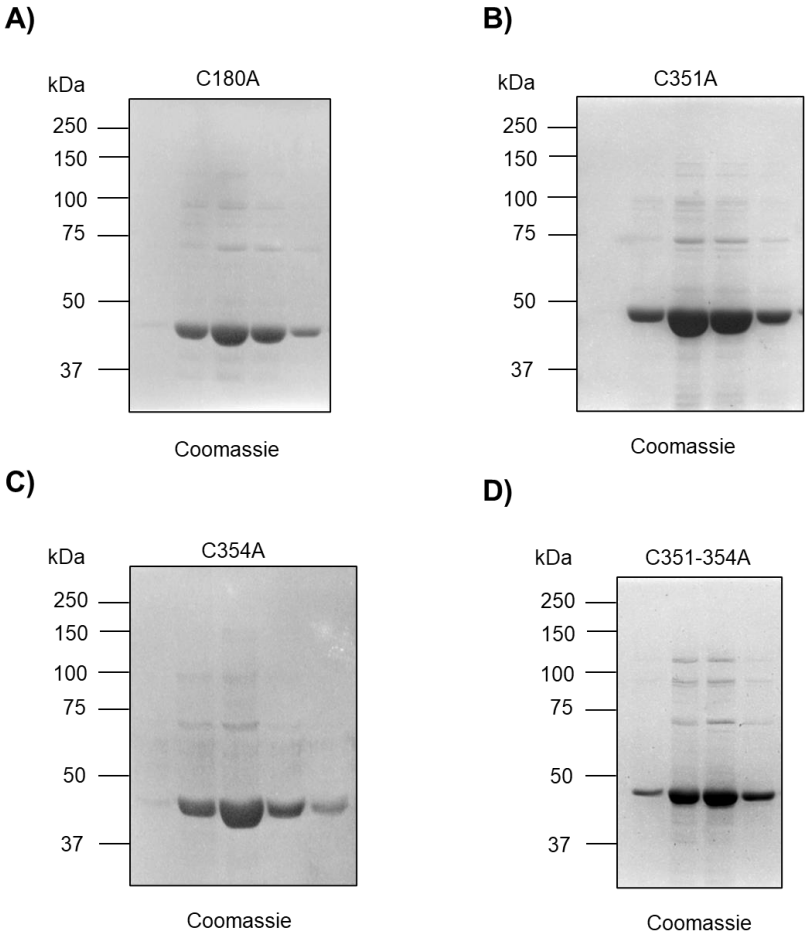

2.2.14. Labelling of mutant proteins with probe P1:

A fixed concentration (5 µM) of each mutant and wild-type protein was treated probe **P1** (0-100 µM). A click reaction was performed on this alkyne appended protein with Rhodamine azide and visualized after SDS-PAGE. If a cysteine to alanine mutant continues to be labelled by **P1**, it is likely that the labelling is happening through other cysteine residues in the protein, suggesting that the cysteine that has been mutated is not an important residue for labelling by **P1**. Labelling with C180A suggested that C180 is not the target site of the probe **P1** (Figure 2.19. A). Previous studies show that this residue is near the FMN binding site.[22] A similar labelling profile was observed with C351A and C354A mutant proteins (Figure 2.19. B, C). Hence, we decided to make a double alanine mutant for Cys351 and Cys354 residues. When tested using standard labelling techniques, a significant reduction in the intensity of the signal for the double mutant C351-354A when compared with WT was observed (Figure 2.19. D).

Taken together, these results show that among the cysteine residues in NuOF, C351 and C354 were targets for modification by **P1**/DPI.

Figure 2. 19 ABPP for validation of wild-type NuOF using cysteine point mutants

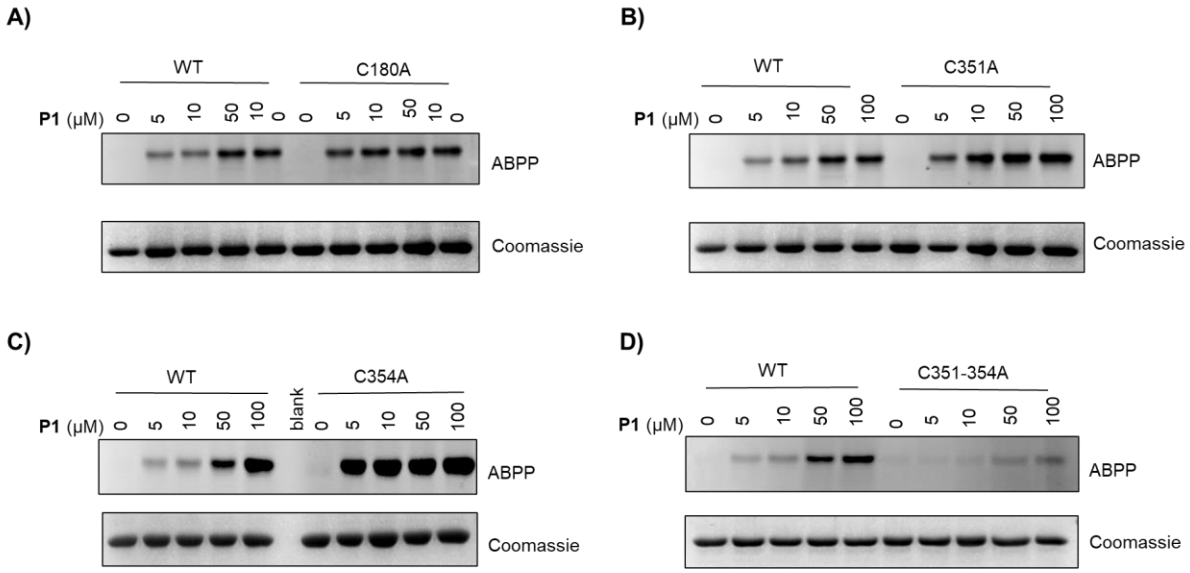

2.2.15. *In silico* docking analysis:

Unfortunately, the structure of *E. coli* NuOF is not available in the PDB, but a high-resolution three-dimensional structure of NuOF from *A. aeolicus* (PDB: 6Q9K) that shares 43% sequence identity with *E. coli* NuOF is available.[23] More importantly, all the aforementioned conserved cysteine residues are a part of this reported structure. A molecular docking study was performed on possible binding sites of DPIC in NuOF from *A. aeolicus* and identified four putative binding sites.

Figure 2. 20 In silico docking analysis into the catalytic site (pocket 4) of NuOF from A. aeolicus (PDB:6Q9K) with DPIC

(Data provided by Anand Kumar, T., Ph.D, Prof. Harinath Chakrapani Lab, IISER Pune)

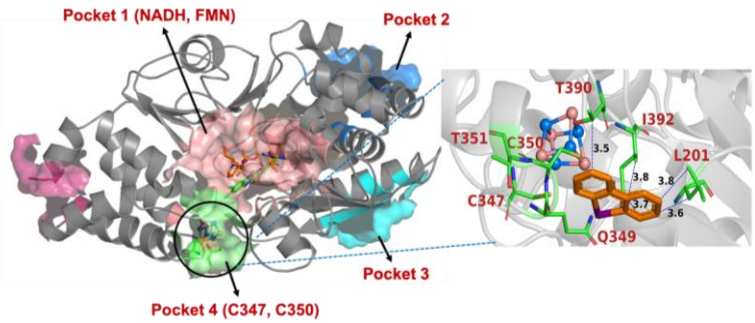

The binding pocket (pocket ID 4) with the active cysteine residues (C347 and C350) that is located in the proximity of the [4Fe-4S] cluster was chosen for molecular docking with DPIC. Notably, and in sync with our experimental studies, it was found that the lowest energy conformation (Affinity -4.1 kcal/mol) was in closest proximity to two cysteine residues, Cys347 and Cys350, which correspond to Cys351 and Cys354 in *E. coli* NuOF. DPIC exhibited a favourable binding affinity and showed optimal binding at the docking site near C350 and showed common hydrophobic interactions with several amino-acid residues (T390, I392, L201).

2.2.16. Plausible mechanism of NuOF protein labelling by DPIC:

As discussed in Chapter **1**, in polar reaction conditions, when a nucleophile reacts with a rigid iodonium compound like DPIC, it forms the [10-I-3 T-shape] hypervalent trigonal bipyramidal intermediate.[24–27] It undergoes homolysis and generates biaryl radical and nucleophile radical. Then, this nucleophile radical reacts with the biaryl radical and forms a biaryl nucleophile adduct (Figure 2. 21).

Figure 2. 21 Proposed reaction mechanism of DPIC with nucleophile under polar reaction condition

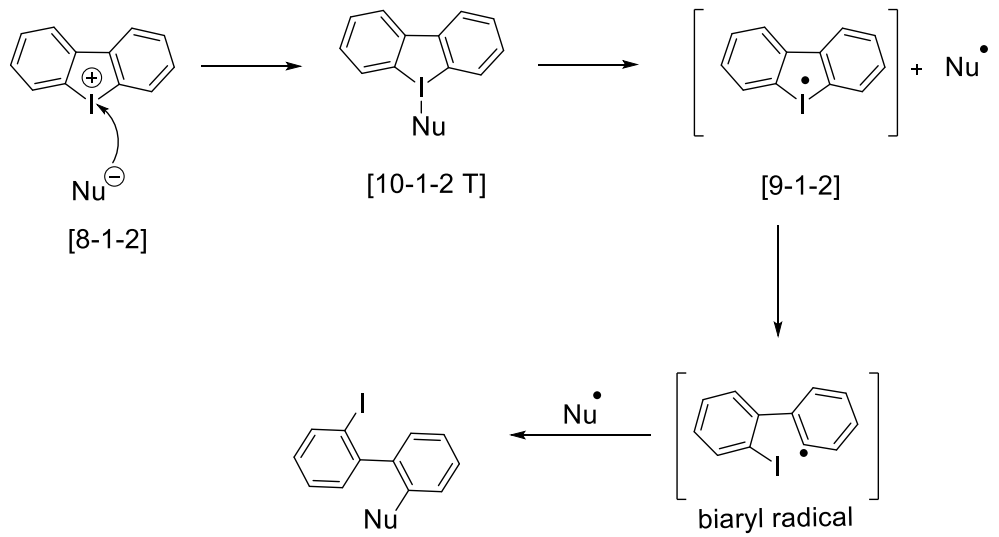

Our labelling studies showed that DPIC covalently modifies NuOF protein through a cysteine residue. Hence, the cysteine residue of NuOF protein can probably react with the iodonium center of DPIC. Following the polar reaction-based mechanism, it can form a covalent biaryl protein adduct through cysteine residue.

2.3. Summary:

Antibacterial molecule DPIC (**1a**) was selected as a prototype of the iodonium class of compounds. In this Chapter, activity-based protein profiling (ABPP) of the proteome of *E. coli* was undertaken to identify the probable targets of DPIC. ABPP requires an analytical handle on the active drug or drug-like molecule, and hence, DPIC alkyne probe **P1** was synthesized. Probe **P1**'s antibacterial activity was tested, and it was active against *E. coli*, suggesting that probe **P1** can be used for target identification using ABPP methods. Next, using ABPP, the *E. coli* proteome was profiled with Probe **P1**, and profiling of cytosolic proteins was considerable than membrane proteins. Following that, a competitive ABPP experiment using iodoacetamide (**IAM**) revealed that probe **P1** predominantly reacts with cysteine residues of thiol-based proteins. DPIC similarly reacts with cysteine residues of proteins when chased with iodoacetamide alkyne (**IAA**). Together these two experiments strongly suggested that DPIC and DPIC alkyne probe have common targets, which are cysteine residues of thiol-based proteins. Next, a competitive ABPP based LC-MS/MS chemoproteomics experiment was performed to identify the probable targets of DPIC. Following the fulfilment of filtering criteria, three target proteins were listed among identified target proteins. These proteins are found to be redox proteins and are a part of the bacterial respiratory system. Among these, NuOF was selected for validation studies. NuOF protein was cloned, overexpressed and purified using standard protocols. ABPP-based labelling studies with NuOF disclosed that probe **P1** covalently modifies NuOF. Next, a competitive ABPP based labelling with DPIC showed that DPIC covalently reacts with NuOF. A similar study with **IAM** revealed that probe **P1** modifies cysteine residues of NuOF. In order to validate this, cysteine to alanine point mutants for certain conserved cysteine residues C180, C351, and C354 of NuOF were generated. ABPP-based labelling studies with these mutants showed that probe **P1** modifies these mutant proteins, indicating that probe **P1** reacts with other available cysteine residues of the mutant protein. Hence, a cysteine to alanine double mutant for C351-C354 was created. Labelling studies with the double mutant C351-C354A of NuOF displayed a significant reduction in labelling by probe **P1**, suggesting that C351 and C354 are the sites for modification by probe **P1**. These cysteine residues C351 and C354 of NuOF are coordinated to Fe^{+2} ion of the [4Fe-4S] iron-sulfur cluster, which is involved in electron translocation during respiration and inhibiting this protein is likely to have an effect on cell viability.

2.4. Experimental and characterization Data:

2.4.1. Procedure for synthesis of ethyl 2-amino-[1,1'-biphenyl]-4-carboxylate (4)[28]:

To a stirred solution of ethyl 4-amino-3-bromobenzoate (3.0 g, 17.43 mmol) in EtOH (15 mL) were added aryllboronic acid (4.0 g, 20.92 mmol), K_3PO_4 (9.2 g, 43.57 mmol) and $Pd(PPh_3)_4$ (1.0 g, 0.871 mmol). The reaction was refluxed for 12 h under argon atmosphere. After completion of the reaction as monitored by TLC, the reaction mixture was cooled down to RT. EtOH was removed by rotary evaporation. The residue was dissolved in EtOAc and filtered through celite. The mixture was extracted with EtOAc, and the combined organic layers were washed with H_2O and brine, filtered through anhydrous Na_2SO_4, concentrated by rotary evaporation. The crude product was purified by column chromatography on a silica gel (PE/EtOAc = 20/1) to afford **4** (2.4 g, 69% yield) as a yellow liquid.

2.4.2. Procedure for synthesis ethyl 2-amino-[1,1'-biphenyl]-4-carboxylate (5)[28]:

To a stirred solution of **4** (2.3 g, 9.78 mmol) in THF (10 mL) was added 4 M aqueous HCl (11.1 mL), and the solution was cooled with an ice bath. $NaNO_2$ (1.0 g, 14.67 mmol) dissolved in H_2O (5 mL) was added dropwise. KI (4.87 g, 29.34 mmol) dissolved in H_2O (5 mL) was added after 20 min. The reaction mixture was stirred for 10 min with the ice bath, then slowly warmed up to RT and stirred for 1 h. The mixture was extracted with EtOAc, and the combined organic layers were washed with H_2O and brine, filtered through anhydrous Na_2SO_4, concentrated by rotary evaporation. The crude product was purified by column chromatography on silica gel (PE) to afford **5** (2.9 g, 85% yield) as a dark brown liquid.

2.4.3. Procedure for synthesis 6-iodo-[1,1'-biphenyl]-3-carboxylic acid (6):

To a stirred solution of compound **5** (500 mg, 1.42 mmol) in EtOH: H_2O [1:1] (5 mL), were added KOH (199 mg 3.55 mmol) at RT, and the reaction was stirred for 4 h at 80 $^{\circ}$C. After completion of the reaction as monitored by TLC, the reaction mixture was cooled down from RT to 0 $^{\circ}$C. The reaction mixture was quenched with 4 M HCl until pH became acidic. Then EtOAc was added to the reaction mixture. The organic components were extracted with EtOAc (3 X 15 mL). The collected organic phases were filtered through anhydrous Na_2SO_4, concentrated under vacuum to obtain pure product **6** (453 mg, 98%) as a grey yellow solid.

2.4. 4. Procedure for synthesis of (6-iodo-[1,1'-biphenyl]-3-yl)methanol (7)[29]:

To a solution of **6** (500 mg, 1.54 mmol) in dry THF (7 mL), was added borane dimethyl sulfide (293 mg, 3.09 mmol) in portions under nitrogen atmosphere with stirring, which was continued for 12 h. The reaction mixture was diluted with 2 M HCl (2 mL). The aqueous layer was extracted with multiple fractions of dichloromethane (3 × 10 mL_ The collected organic phases were filtered through anhydrous Na_2SO_4, concentrated under vacuum to obtain the crude product. The residue was taken ahead in the next step without purification.

2.4.5. Procedure for synthesis of 2-(2-((2-(pent-4-yn-1-yloxy)ethyl)peroxy)ethoxy)ethan-1-ol (8):

To a solution of NaI (4.2 g, 28.34 mmol) in dry DMF (30 mL), was added 5-chloropent-1-yne (1 g, 1 eq.) in portions, and the solution was stirred for 30 min at RT under nitrogen atmosphere. The tetra ethylene glycol (17 mL, 94.38 mmol) and NaH (60% dispersion in mineral oil, 870 mg, 22.65 mmol) was then added with stirring, which was continued for 48 h. The reaction mixture was diluted with ice-cold water (20 mL). The aqueous layer was extracted with multiple fractions of ethyl acetate (3 × 10 mL) The collected organic phases were filtered through anhydrous Na_2SO_4, concentrated under vacuum to obtain the crude product. The residue was taken ahead in next step without purification.

2.4.6. Procedure for synthesis of 2-(2-((2-(pent-4-yn-1-yloxy)ethyl)peroxy)ethoxy)ethyl 4 methylbenzenesulfonate (9)[29]:

To an ice-cold solution of **8** (3.3g, 12.9 mol) in THF (25 mL), was added a solution of NaOH (1.55 g, 38.8 mol) in water (10 mL), and the solution was stirred for 30 min at RT. A solution of 4-toluenesulfonyl chloride (4.94 g, 52910 mmol) in THF (15 mL) was added in portions with stirring which was continued for 3 h at 0 $^{\circ}$C. The reaction mixture was diluted with ice-cold water (20 mL). The aqueous layer was extracted with multiple fractions of dichloromethane (3 × 10 mL) The collected organic phases were filtered through anhydrous Na_2SO_4, concentrated under vacuum to obtain the crude product. The residue was purified using prep HPLC to obtain compound **9**.

2.4.7. Procedure for synthesis of 1-(6-iodo-[1,1'-biphenyl]-3-yl)-2,5,8,9,12-pentaoxaheptadec-16-yne (10)[30]:

To an ice-cold solution of NaH (60% dispersion in mineral oil, 174 mg, 0.725 mmol) in dry DMF (5 mL), was added a solution of **7** (150 mg, 0.483 mmol) in portions under nitrogen atmosphere with stirring, which was continued for 2h at 0 $^{\circ}$C. A solution of **9** (200 mg, 0.532

mmol) in dry DMF (2 mL) was added with stirring which was continued for 15h. The reaction mixture was diluted with ice-cold water (20 mL). The aqueous layer was extracted with multiple fractions of dichloromethane (3 × 10 mL) The collected organic phases were filtered through anhydrous Na_2SO_4, concentrated under vacuum to obtain the crude product. The residue was purified by column chromatography on a silica gel (0-8 % EtOAc/Hexane) to afford the white solid **10** with a 19 % yield

2.4.8. Procedure for synthesis of 6-iodo-N-(prop-2-yn-1-yl)-[1,1'-biphenyl]-3-carboxamide (11):

To a stirred solution of compound **6** (300 mg, 0.9256 mmol) in dry DCM: THF (9:1, 10 mL) were added EDC.HCl (195 mg, 1.018 mmol), DMAP (28 mg, 0.2314 mmol) and propargyl amine (65 µL, 1.018 mmol) and stirred for 12 h at RT. Then water was added to the reaction mixture. The organic components were extracted with DCM, filtered through Na_2SO_4 and concentrated. The residue was purified by column chromatography on a silica gel (0-17 % EtOAc/Hexane) to afford the white solid **11** with a 61 % yield.

2.4.9. Procedure for synthesis of 2-(prop-2-yn-1-ylcarbamoyl) dibenzo[b,d]iodol-5-ium chloride P1:

To a stirred solution of **11** (310 mg, 0.85 mmol) in anhydrous CH_2Cl_2 (5 mL) was added *m*-CPBA (151 mg, 0.87 mmol), TfOH (228 µL, 2.57 mmol). The solution was stirred for 1 h at RT before CH_2Cl_2 was removed by rotary evaporation. To the residue mixture dissolved in HCOOH (0.5 mL) was added saturated aq. NaCl (2 mL), and the mixture was stirred for 20 min and filtered. The collected solid was washed with ice-cold H_2O and Et_2O three times dried in a vacuum to afford the solid white **P1** with 32 % yield.

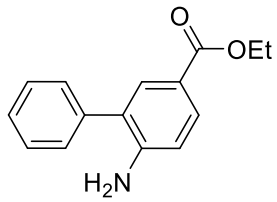

4

ethyl 6-amino-[1,1'-biphenyl]-3-carboxylate (4):

^{1}H NMR (400 MHz, $CDCl_3$) δ: 8.14-8.11 (m, 2H), 7.57-7.54 (m, 2H), 7.21-7.12 (m, 2H), 6.84 (dt, *J* = 7.5, 1.1 Hz, 1H), 6.77 (dd, *J* = 8.0, 1.0 Hz, 1H), 3.77 (s, 2H), 4.41 (q, *J* = 7.1 Hz, 2H),

1.42 (t, *J* = 7.1 Hz, 3H); ^{13}C NMR (100 MHz, $CDCl_3$) δ: 166.6, 144.4, 143.5, 130.4, 130.2, 129.4, 129.2, 129.2, 126.5, 118.9, 116.0, 115.2, 61.2, 14.5.

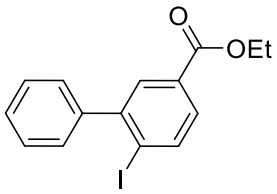

5

ethyl 6-iodo-[1,1'-biphenyl]-3-carboxylate (5):

^{1}H NMR (400 MHz, $CDCl_3$) δ: 8.11 (d, *J* = 7.9 Hz, 2H), 7.97 (d, *J* = 7.8 Hz, 1H), 7.43-7.39 (m, 3H), 7.29 (d, *J* = 7.6 Hz, 1H), 7.06 (t, *J* = 7.4 Hz, 1H), 4.1 (q, *J* = 7.0 Hz, 2H), 1.41 (t, *J* = 7.0 Hz, 3H); ^{13}C NMR (100 MHz, $CDCl_3$) δ: 166.5, 148.6, 145.8, 139.8, 130.0, 129.8, 129.5, 129.4, 128.4, 98.0, 61.2, 14.5.

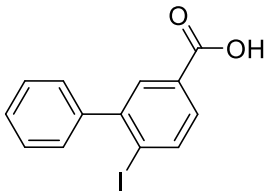

6

6-iodo-[1,1'-biphenyl]-3-carboxylic acid (6):

^{1}H NMR (400 MHz, DMSO-*d6*) δ:13.0 (s, 1H), 8.02-7.99 (m, 3H), 7.49 (dt, *J* = 7.5, 1.1 Hz, 1H), 7.45(d, *J* = 8.4 Hz, 2H), 7.36 (dd, *J* = 7.6, 1.5 Hz, 1H), 7.16 (dt, *J* = 7.6, 1.6 Hz, 1H), ^{13}C NMR (100 MHz, DMSO-*d6*) δ: 167.1, 147.9, 145.1, 139.4, 130.0, 129.4, 129.1, 128.6, 98.2.

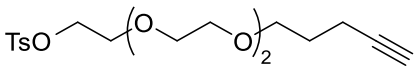

2-(2-((2-(pent-4-yn-1-yloxy)ethyl)peroxy)ethoxy)ethyl 4-methylbenzenesulfonate (9):

^{1}H NMR (400 MHz, $CDCl_3$) δ: 7.80-7.77 (m, 2H), 7.33 (d, *J* = 8.0 Hz, 2H), 4.16-4.13 (m, 2H), 3.69-3.59 (m, 8H), 3.55-3.52 (m, 4H), 2.44 (s, 3H), 2.27 (dt, *J* = 7.1, 2.7 Hz, 1H), 1.93-1.90 (m, 3H), 1.82-1.74 (m, 1H); ^{13}C NMR (100 MHz, $CDCl_3$) δ: 144.9, 133.1, 130.0, 130.0, 128.1, 128.1, 84.1, 70.8, 70.8, 70.7, 70.7, 70.6, 70.6, 70.3, 69.7, 69.4, 68.8, 28.6, 21.8, 15.3.

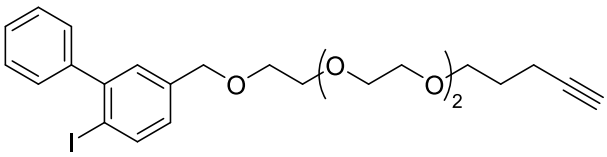

1-(6-iodo-[1,1'-biphenyl]-3-yl)-2,5,8,9,12-pentaoxaheptadec-16-yne (10):

^{1}H NMR (400 MHz, $CDCl_3$) δ: 7.91 (d, *J* = 8.0 Hz, 1H), 7.43-7.37 (m, 3H), 7.34-7.31 (m, 2H), 7.27 (d, *J* = 2.2 Hz, 1H), 4.53 (s, 2H), 3.68-3.56 (m, 16H), 3.54 7.33 (t, *J* = 6.3 Hz, 2H), 2.27 (td, *J* = 7.1, 2.6 Hz, 2H), 1.93 (t, *J* = 2.6 Hz, 1H), 1.81-1.75 (m, 2H); ^{13}C NMR (100 MHz, $CDCl_3$) δ: 146.6, 144.4, 139.6, 138.7, 129.4, 129.3, 128.2, 128.0, 127.7, 97.3, 84.1, 72.5, 70.7, 70.7, 70.7, 70.6, 70.6, 70.3, 69.8, 69.6, 69.6, 28.6,15.3.

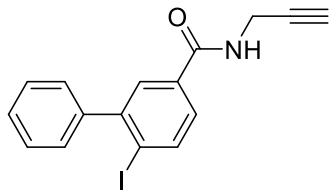

11

6-iodo-N-(prop-2-yn-1-yl)-[1,1'-biphenyl]-3-carboxamide (11):

^{1}H NMR (400 MHz, $CDCl_3$) δ: 7.96 (dd, *J* = 7.9, 1.0 Hz, 1H), 7.86-7.84 (m, 2H), 7.43-7.41 (m, 2H), 7.39 (dd, *J* = 7.5, 1.1 Hz, 1H), 7.28 (dd, *J* = 7.6, 2.0 Hz, 1H), 7.06 (dt, *J* = 7.7, 1.7 Hz, 1H), 6.38 (s, 1H), 4.29 (dd, *J* = 6.0, 2.6 Hz, 2H), 2.30 (t, *J* = 2.6 Hz, 1H); ^{13}C NMR (100 MHz, $CDCl_3$) δ: 166.9, 147.7, 145.6, 139.8, 133.0, 130.1 129.8, 129.4, 128.4, 126.9, 98.1, 79.5, 72.2, 30.0.

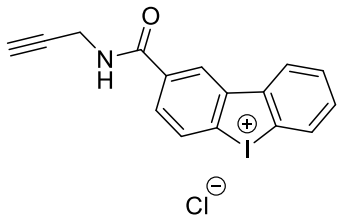

P1

2-(prop-2-yn-1-ylcarbamoyl) dibenzo[b,d]iodol-5-ium chloride (P1):

^{1}H NMR (400 MHz, MeOD) δ 8.69 (d, *J* = 1.5 Hz, 1H), 8.48-8.44 (m, 2H), 8.30 (d, *J* = 7.6 Hz, 1H), 8.25 (dd, *J* = 8.2, 1.5 Hz, 1H), 7.89 (dd, *J* = 11.2, 4.1 Hz, 1H), 7.78-7.73 (m, 1H), 4.22 (d, *J* = 2.5 Hz, 2H), 2.67 (t, *J* = 2.6 Hz, 1H); ^{13}C NMR (100 MHz, DMSO-*d6*) δ 164.8, 143.8, 140.6, 130.8, 130.5, 130.4, 128.4, 127.0, 126.0, 125.3, 124.6, 81.1, 73.2, 28.8; FT-IR (υ_{max}, cm^{-1}) 3374, 3201, 1602, 1318, 1077, 610; HRMS Calcd for $C_{16}H_{11}INO^{+}$ $[M]^{+}$: 359.9880 found $[M]^{+}$: 359.9890.

2.4.10 Time-kill kinetics of P1 against *E. coli*:

Briefly, *E. coli* (ATCC 25922) cultures were inoculated in Luria Bertani Broth medium and optical density (OD) of the cultures was measured at the 600 nm wavelength, followed by dilution to achieve ~10^5 CFU/mL. The probe **P1** were tested ranging from 2-16 mg/L in two-fold serial diluted fashion with 2.5 µL of each concentration added to each well of a 96-well round bottom microtiter plate. Later, 97.5 µL of bacterial suspension was added to each well containing the test compound along with appropriate controls. The plates were incubated at 37 ˚C for 18-24 h following which the growth was enumerated and MIC was identified. The MIC is defined as the lowest compound concentration where there is no visible growth. For each compound, MIC determinations were carried independently 3 times using duplicate samples.

2.4.11. Protocols for ABPP experiments:

2.4.11.1. Preparation of proteomic fractions:

E. coli (ATCC 25922) was cultured in Luria Bertani Broth medium at 37 °C overnight. The cultured bacteria were re-suspended in 1X PBS, lysed using a probe sonicator, followed by centrifugation at 100,000 g, at 4 °C for 1 hour to separate soluble and membrane protein fractions.[31] Soluble fractions were then separated from the membrane pellets. The membrane pellets were washed, followed by re-suspension in 1X PBS. The protein concentration was measured by conducting either Bradford assay (Biorad) using BSA as a standard and lysates were finally diluted to 1mg/mL protein concentration with 1X PBS, which was used for all further work.

2.4.11.2. Chase experiment:

100 µL of 1mg/mL protein for both membrane and soluble fraction was taken in a 1.5 mL microcentrifuge tube. 1 µL of a 100X stock solution of the compound **1a** in DMSO was added and incubated for 60 min at 37 °C at 700 rpm. To the above solution, IAA or **P1** probe (1 µL of a 100X stock solution of the in DMSO) was added and incubated for 60 min at 37 °C at 700 rpm. A 'click' mixture (11 µL) consisting of a 6 µL TBTA (1.7 mM in 4:1 DMSO-^{t}BuOH), 2 µL $CuSO_4.5H_2O$ (50 mM in water), 2 µL TCEP (50 mM in DPBS - Dulbecco's PBS 1X), 1 µL Rhodamine azide (Alexa Fluor 488, 10 mM in DMSO), was added to every tube and incubated for 60 min at 25 °C at 700 rpm. The loading dye (4x, 40 µL) was added to every tube prior to loading the samples onto the gel.[18]

2.4.11.3. Mass spectrometry based chemoproteomics[32,33]:

E. coli cells were lysed in 1X PBS by sonication and fractionated into membrane and soluble fractions by ultracentrifugation (100,000 g, 4 ^{o}C ,1 hour). The soluble fraction (1 mL) was incubated with **1a** or vehicle (DMSO) at 250 μM final concentration for 1 hour at 37 ^{o}C at 700 rpm. Each group contained three biological replicates. The compound or vehicle treated soluble proteomes were chased with **P1** (100 μM, 1 hour at 37 ^{o}C, 700 rpm). The click reaction was done with biotin-azide. Post-biotinylation, the proteomes were denatured and precipitated using methanol: chloroform (4:1) at 4 ^{o}C, and re-suspended in urea (0.5 mL 6 M in DPBS) by sonication. Reduction and alkylation were carried out with TCEP (10 mM) for 30 mins at 37 ^{o}C with constant shaking, and **IAM** (50 mM) for 30 mins at room temperature (25^{o}C) in the dark, respectively. The biotinylated proteins were enriched using avidin-agarose beads (100 μL, Sigma-Aldrich) by shaking at room temperature for 1.5 hours in DPBS containing 0.2% (w/v) SDS in a final volume of 6 mL. The beads were pelleted by centrifugation (1000 g, 25 ^{o}C, 5 min), and sequentially washed using 10 mL of 0.2% (w/v) SDS in DPBS (3X), 10 mL of DPBS (3X) and 10 mL of deionized water (3X). The beads were transferred to a Protein LoBind 1.5 mL microcentrifuge tube. On-bead protein digestion was performed using sequence grade trypsin (1.5 μg, Promega) in 200 μL of urea (2 M in 100 mM TEAB buffer) at 37 ^{o}C for 14 hours at 180 rpm. Reaction was quenched by adding TFA to final concentration of 1% (v/v). Peptides were cleaned on C18 Stage tips and subjected to LC-MS/MS analysis on Agilent 6540 Accurate-Mass Q-ToF mass spectrometer coupled with Agilent HPLC-Chip Cube system. Peptides were separated on Agilent HPLC-Chip consisting of C18 enrichment and analytical column (75 μm, 10 cm) system. The LC run was a 6 hours long linear acetonitrile gradient (5% to 50%). Mass spectrometry data was collected in an information-dependent acquisition (IDA) mode over a mass range of 300 – 2000 m/z, and each full MS survey scan was followed by 10 fragment scans. Dynamic exclusion was enabled for all experiments (repeat count 1, exclusion duration 30 s). Protein identification and quantitation was carried out using Protein Piolet software 5.0.2. Spectral data were searched against *E. coli* K-12 MG1655 protein databases downloaded from the NCBI FTP server. Precursor mass tolerance of 0.01 Da and fragment mass tolerance of 40 p.p.m. was allowed. The peptides and proteins were filtered at 1 % false discovery rate. Label free quantitation was performed using LFQ option in the Protein Piolet software 5.0.2. Protein LFQ intensity value was accepted only when two or more quantifiable peptides were identified in more than 2 replicates per experimental group. Quantitation was

performed by taking a ratio of the average intensity with respect to control sample (DMSO treated).

2.4.12. Cloning:

Oligonucleotide primers were purchased from Eurofins, and DNA sequencing was also performed by Eurofins and 1st base (Table 2.5). Amplification of PCR was performed with Hi-Proof DNA Polymerase (Hi-media) using colony PCR for *E. coli* K-12 MG1655. The *NuOF* open reading frames was amplified by PCR. The standard PCR mixture (10 µl) contains 100 ng of template DNA and 100 to 250 ng of each forward and reverse primer of gene. The gradient PCR cycling conditions were as follows: 95 °C (5 min); 35 cycles of 95 °C (45 sec), 56.7 °C (30 sec), 72 °C (3 min) and 72 °C (5 min). The PCR products were cloned into NdeI/BamHI site of pET-22b(+) Vector using SLIC (sequence- and ligation-independent cloning) method with a C-terminal 6X-His tag and (Novagen) to yield plasmid pET22b-NuOF, for protein expressions in *E coli* strain BL21 (DE3).[34]

For creating the NuOF C180A, C351A, C354A and C351-354A mutant, a forward primer containing the altered sequence was used along with the T7 reverse primer to amplify the mutated part of the gene from pET-22b(+) containing the WT NuOF in PCR. DpnI enzyme was added to PCR reaction tube and incubated for 1 h at 37 °C and transformed into *E. coli* DH5-α cells.

The standard PCR mixture for megaprimer (10 µl) contains 100 ng of template DNA and 100 to 250 ng of each mutagenic forward primer and T7 reverse primer for mutants. The gradient PCR cycling conditions were as follows: 95°C (3 min); 35 cycles of 95 °C (45 sec), {56.8 °C for C180A, 55.2 °C for C351A, 58.7 °C for C354A and 59 °C for C351-354A (30 sec), and 72 °C (3 min) and 72 °C (5 min). The PCR products were isolated using Hi-media PCR purification kit. Next, amplification of these megaprimers was done with pET22b-NuOF. The standard PCR mixture (25 µl) contains 100 ng of template DNA and 100 to 250 ng of each mutagenic forward primer and T7 reverse primer for mutants. The gradient PCR cycling conditions were as follows: 95 °C (2 min); 35 cycles of 95 °C (45 sec), 68 °C (10 min), 68 °C (1 min), and 68 °C (15 min). After the PCRs, DpnI (10 U) was added, and the mixture was incubated at 37 °C for 1 h. The PCR mixtures were transformed into *E. coli* competent DH5α cells and plated on LB medium supplemented with 1X ampicillin. All mutations were verified by sequencing.

Table 2. 5 Primers for wild type and cysteine mutants of NuOF

Entry	Primer name	Plasmid constructed	Primer Sequence (5′ → 3′)
1	NuOF_Fwd	WT NuOF	GAAGGAGATATACATAATGAAA AACATTAT CCGTAC
2	NuOF_Rev	WT NuOF	AGCTCGAATTCGGATCCCAGCG CTCTTTCAG
3	C180A Fwd	NuOF_C180A	GGGCAGGGCGCTACATCGCCGG GGAAGAAA CAGCG
4	C351A Fwd	NuOF_C351A	TTT TTC GCC CGT GAG TCC GCC GGC TGG TGT ACG CCG TG
5	C354A Fwd	NuOF_C354A	GTGAGTCCTGCGGCTGGGCTAC GCCGTGCCGCGACG G
6	C351-C354A Fwd	NuOF_C351-C354A	GTTTTTCGCCCGTGAGTCCGCCG GCTGGGCTACGCCGTG CCGCGACGGTC
7	T7 Terminator Rev	T7 Terminator	GCTAGTTATTGCTCAGCGG

2.4.13. Expression and purification:

Plasmids pET-22b(+)-NuOF was transformed into *E coli* BL21 (DE3). The cells were maintained in LB broth supplemented with 100 μg/mL of ampicillin at 37 °C. For protein expression, 1 M of IPTG was added to the culture to a final concentration of 0.5 mM IPTG to induce protein expression when the cells grow to the log phase (OD_{600}≈0.6). The cells were further incubated for 16 h at 16 °C for protein expression.

After expression of proteins, cells were harvested by centrifugation (6000 rpm, 4 °C, 20 min) and binding buffer (50 mM Tris, pH 8 at RT and 20 mM imidazole) was added to the pellet in a 1:100 ratio. The cell suspension was sonicated by a tip probe sonicator on ice. The soluble and insoluble protein fractions were separated by centrifugation (18000 g, 4 °C, 20 min) and the supernatant was collected for protein purification. The soluble fraction was passed through a pre-packed Ni-NTA column (5 mL, GE Life Sciences) pre-washed with 10 column volumes

(CV) of binding buffer. The column was then washed with 10 CV of wash buffer comprising 50 mM Tris pH 8 at RT 20 mM imidazole. The protein was eluted with buffer comprising 50 mM Tris pH 8 at RT, and 500 mM imidazole and dialyzed against 50 mM Tris pH 8 at RT. Aliquots of the purified proteins were flash frozen in liquid nitrogen and stored at -80 $^{\circ}$C until further use. The cysteine residues at positions Cys-180, Cys 351, Cys 354 and Cys-351-354 (of NuOF), were mutated to alanine by standard DpnI dependent site-directed mutagenesis. The mutant proteins were purified and stored as described above.

2.4.14 Gene and Protein sequences:

Table 2. 6 Target protein NuOF gene and protein sequences

Protein	NuOF 1337 bp, 445 aa
Gene Sequence	ATGAAAAACATTATCCGTACTCCCGAAACGCATCCGCT GACCTGGCGTCTGCGCGATGACAAACAGCCAGTGTGGC TGGACGAATACCGCAGCAAAAACGGTTACGAAGGCGC GCGTAAGGCGCTGACCGGGCTGTCTCCGGACGAAATC GTTAATCAGGTAAAAGACGCTGGTCTGAAAGGGCGCG GCGGCGCGGGCTTCTCGACTGGCCTGAAATGGAGCCT GATGCCGAAAGACGAATCCATGAACATCCGTTACCTG CTGTGTAATGCCGATGAAATGGAGCCGGGCACCTATA AAGACCGCCTGTTGATGGAGCAACTGCCGCACCTGCT GGTGGAAGGTATGCTCATCTCCGCGTTTGCGCTGAAA GCTTACCGTGGCTACATCTTCCTGCGTGGCGAATATAT CGAAGCGGCAGTTAATCTGCGCCGTGCCATTGCCGAAG CCACCGAAGCGGGTCTGCTTGGCAAAAACATTATGGGA ACAGGTTTCGATTTCGAACTGTTCGTCCATACCGGGGCA GGGCGCTACATCTGCGGGGAAGAAACAGCGTTAATCAA CTCCCTGGAAGGACGTCGTGCTAACCCACGCTCGAAGCC ACCCTTCCCGGCAACCTCCGGCGCATGGGGTAAACCGAC CTGTGTCAACAACGTCGAAACCCTGTGTAACGTTCCGGC GATCCTCGCTAACGGCGTGGAGTGGTATCAGAACATCTC GAAAAGTAAAGATGCTGGCACCAAGCTGATGGGCTTCTC CGGTCGGGTGAAAAATCCGGGACTGTGGGAACTGCCGTT CGGCACCACCGCACGCGAGATCCTCGAAGATTACGCCGG

	TGGTATGCGTGATGGTCTGAAATTTAAAGCCTGGCAGCCA GGCGGCGCGGGGACTGACTTCCTGACCGAAGCGCACCTTG ATCTGCCGATGGAATTCGAAAGTATCGGTAAAGCGGGCAG CCGTCTGGGTACGGCGCTGGCGATGGCGGTTGACCATGAG ATCAACATGGTGTCGCTGGTGCGTAACCTGGAAGAGTTTTT CGCCCGTGAGTCCTGCGGCTGGTGTACGCCGTGCCGCGACG GTCTGCCGTGGAGCGTGAAAATTCTGCGTGCGCTGGAGCGT GGTGAAGGTCAGCCGGGCGATATCGAAACACTTGAGCAACT GTGTCGATTCTTAGGCCCGGGTAAAACTTTCTGTGCCCACGC ACCTGGTGCAGTGGAGCCGTTACAGAGCGCCATCAAATATTT CCGCGAAGAATTTGAGGCGGGAATCAAACAGCCGTTCAGCA ATACCCATTTGATTAATGGGATTCAGCCGAACCTGCTGAAAG AGCGCTGGTAA
Protein Sequence	MKNIIRTPETHPLTWRLRDDKQPVWLDEYRSKNGYEGARKAL TGLSPDEIVNQVKDSGLKGRGGAGFSTGLKWSLMPKDESMNIR YLLCNADEMEPGTYKDRLLMEQLPHLLVEGMLISAFALKAYRG YIFLRGEYIEAAVNLRRAIAEATEAGLLGKNIMGTGFDFELFVHT GAGRYICGEETALINSLEGRRANPRSKPPFPATSGAWGKPTCVN NVETLCNVPAILANGVEWYQNISKSKDAGTKLMGFSGRVKNPG LWELPFGTTAREILEDYAGGMRDGLKFKAWQPGGAGTDFLTEA HLDLPMEFESIGKAGSRLGTALAMAVDHEINMVSLVRNLEEFFA RESCGWCTPCRDGLPWSVKILRALERGEGQPGDIETLEQLCRFL GPGKTFCAHAPGAVEPLQSAIKYFREEFEAGIKQPFSNTHLINGI QPNLLKERW • Cysteine residues are marked in red color

2.4.15. Target validation using ABPP:

The protein concentrations for both wild-type and mutant proteins were estimated using a standard protein estimation (Bradford) assay 100 µL aliquots of 5 µM NuOF, were further used for all the assays.

2.4.16. ABPP based labelling:

These aliquots were treated with varying concentrations of **P1** (0 – 100 μM) at 37 °C for 1 hour. Following which the click reaction was performed as described earlier, and the reactions were quenched by adding 40 μL of 4X loading dye. The samples were resolved and activity was visualized using a 10% SDS-PAGE gel using established protocols.

2.4.17. Competitive ABPP based labelling:

These aliquots were treated with varying concentrations of DPIC (**1a**, 0 – 250 μM) or **IAM** (0-1mM) at 37 °C for 1 hour and then treated with DPIC alkyne (100 μM) at 37 °C for 1 hour. Following which the click reaction was performed, and the reactions were quenched by adding 40 μL of 4X loading dye. The samples were resolved and activity was visualized using a 10% SDS-PAGE gel using established protocols.

2.4.18. Sequence alignment:

The sequences of NuOE (*A.aeolicus*; UniProtKB ID: O66842 and *E.coli*; UniProtKB ID: P0AFD1) and NuOF (*A.aeolicus*; UniProtKB ID: O66841 and *E.coli*; UniProtKB ID: P31979) were obtained from Uniprot database. The unweighted sequence alignments between NuOE and NuOF from *A.aeolicus* and *E.coli* were performed using T-coffee at the European Bioinformatics Institute website (https://www.ebi.ac.uk) using the default settings and displayed using Jalview. The sequence name indicates the Uniprot code, the organism of origin, and the numbers indicate the amino acid residues displayed. The consensus symbols: '*', ':' and "." under the amino acids indicate identical, conserved and semi-conserved residues respectively.

2.4.19. Prediction of putative ligand-binding pockets in NuOF protein

The Computed Atlas of Surface Topography of proteins (CASTp 3.0) web server was used to predict the putative ligand-binding pockets and elucidate the amino acids lining each pocket in the protein. The protein structure of NuOF from *A.aeolicus* (PDB ID: 6Q9K) was submitted in a standard PDB format on the server and a probe radius of 2.8 Å was used. The CASTp server uses the weighted Delaunay triangulation and the alpha complex method to measure the area and volume of each predicted pockets or voids utilizing both the solvent accessible surface model and molecular surface model. The scoring results of CASTp were provided in Table 1.

Table 2. 7 CASTp based scoring of the identified pockets in NuoF

Entry	Pocket ID	Area (SA)	Volume (SA)	Volume color	Representation style
A	1	563.314	522.663	Salmon red	Cartoon
B	2	98.003	56.840	Marine blue	
C	3	49.050	23.079	Cyan	
D	4	54.962	15.739	Green	
E	5	46.156	14.152	Yellow	
F	6	27.315	10.843	Warm-pink	
G	7	17.831	7.053	Not shown	
H	8	18.387	5.883	Not shown	
I	9	16.695	5.878	Not shown	
J	10	17.429	4.831	Not shown	

2.4.20. *In silico* molecular docking studies:

The energies of the systems were optimized theoretically by using the Gaussian 09 software.[35,36] These energies were computed by DFT methods by employing the B3LYP functional. Energy calculations were performed using the basis set Lanl2dz for heavier atoms (I, Cl or S) in conjunction with the 6-31G basis set (for all other atoms). The X-ray crystal structure of NuOF with a resolution of 1.99 Å was retrieved from PDB (PDB ID: 6Q9K). The protein and ligand PDBQT files were prepared using AutoDock Tools 1.5.6 (ADT) following the standard protocol. A grid box (15 x 15 x 15 $Å^3$) defined for pocket ID 4 (Table 2.7, entry D) in NuOF centered at the coordinates (x = 21.872, y = 10.022, z = -77.327) was used for focussed docking of flexible ligand dpIC into the active site containing active cysteines (C347 and C350). The docking parameters were set to default except for the following: exhaustiveness = 64, energy range = 3 kcal/mol and number of modes = 20. The best-scored docking pose with the lowest binding energy was selected for analysis and figures were visualized using PyMOL (The PyMOL Molecular Graphics System, Version 2.0 Schrödinger, LLC). LigPLOT+ was used to depict the 2D interactions of ligand and protein.

2.5. NMR Spectra:

^{1}H NMR of **4**

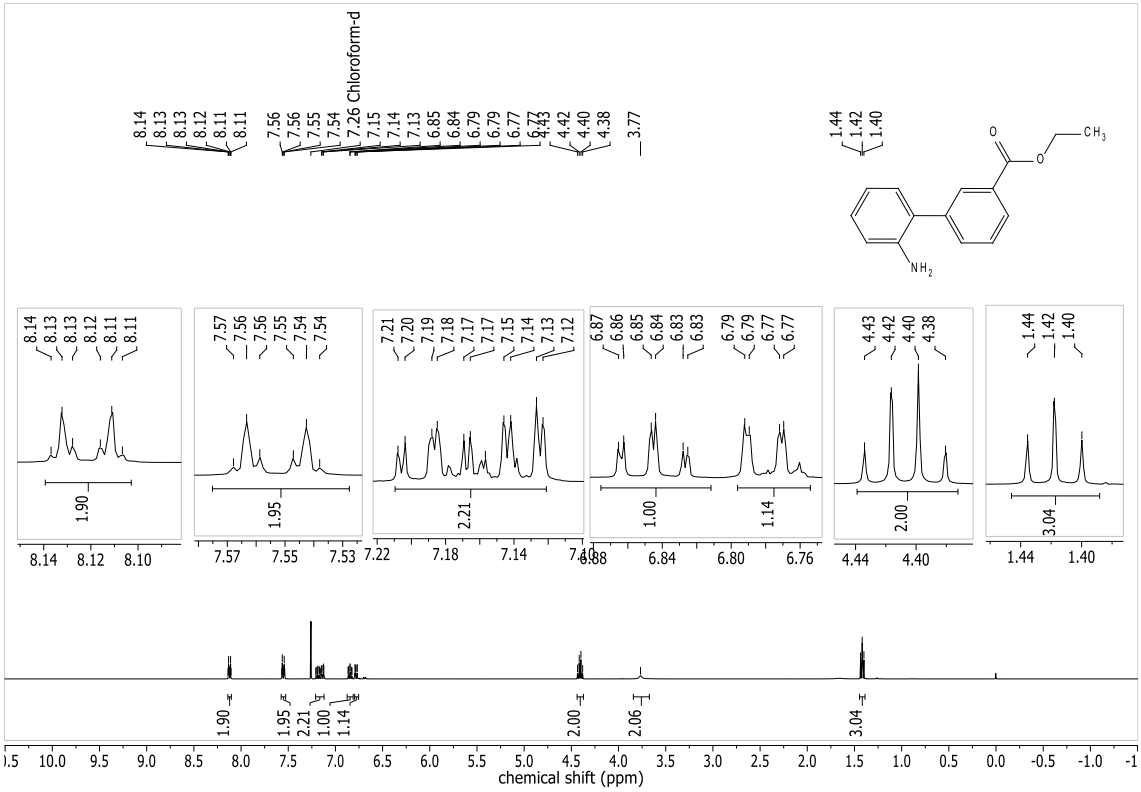

^{13}C NMR of **4**

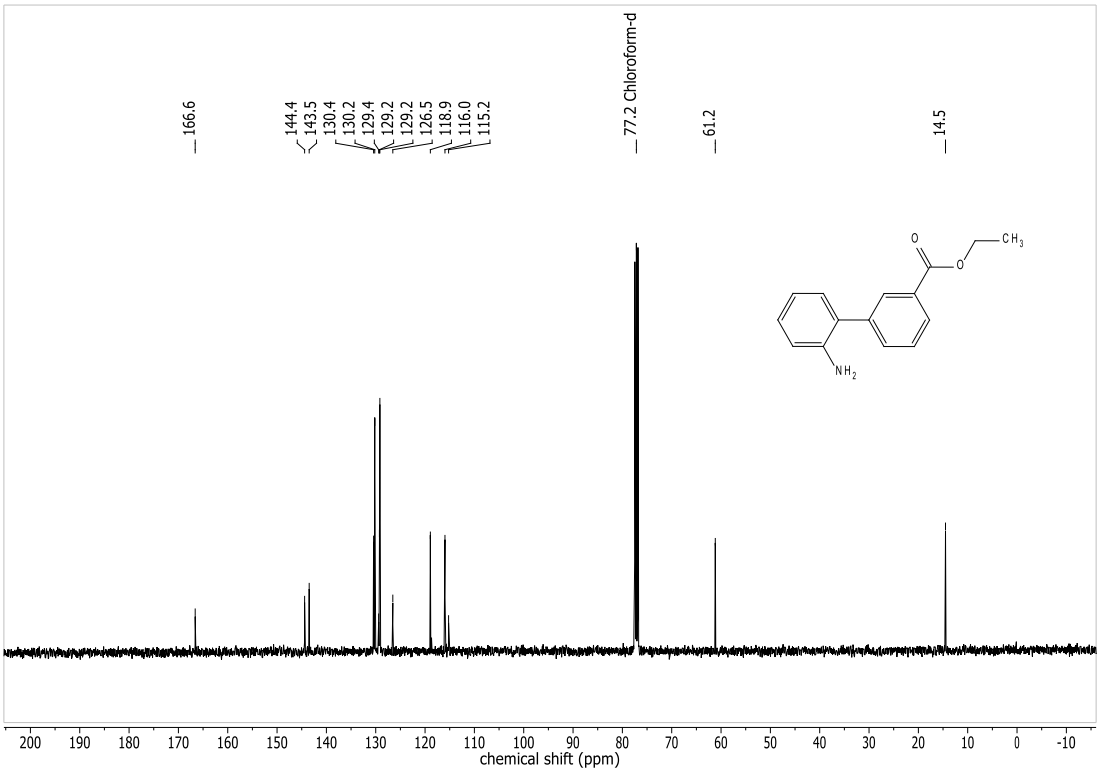

^{1}H NMR of **5**

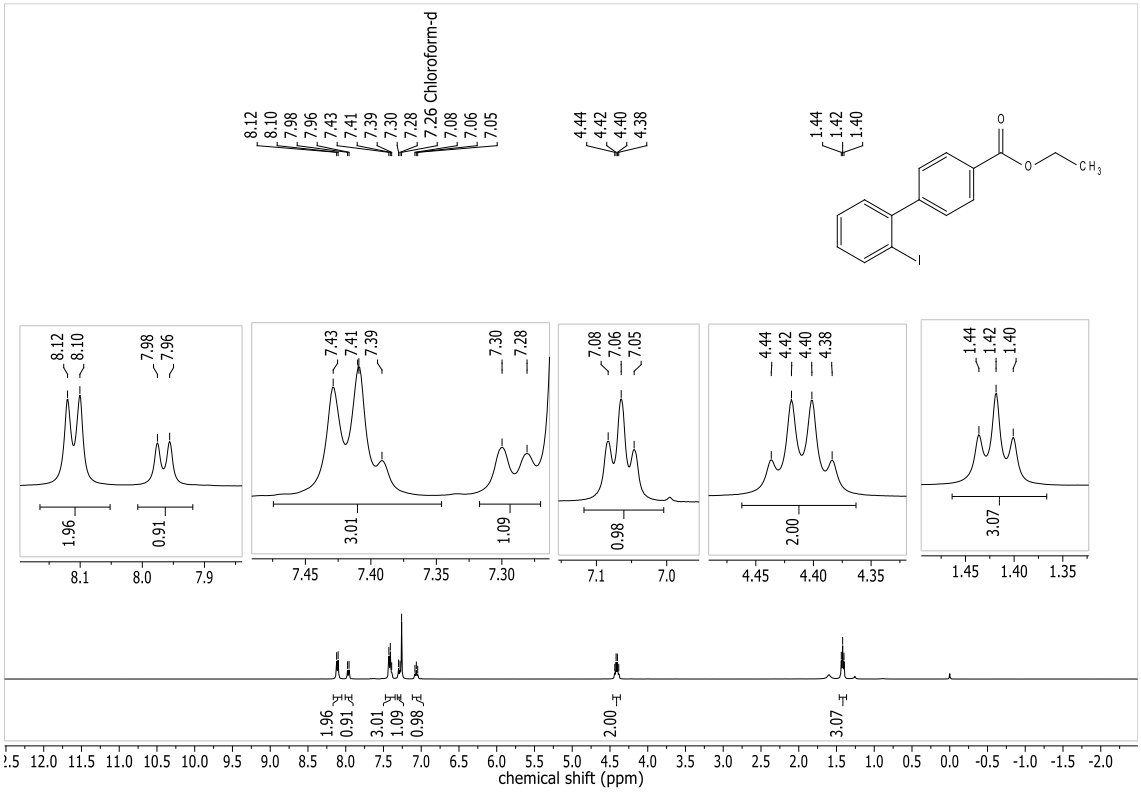

^{13}C NMR of **5**

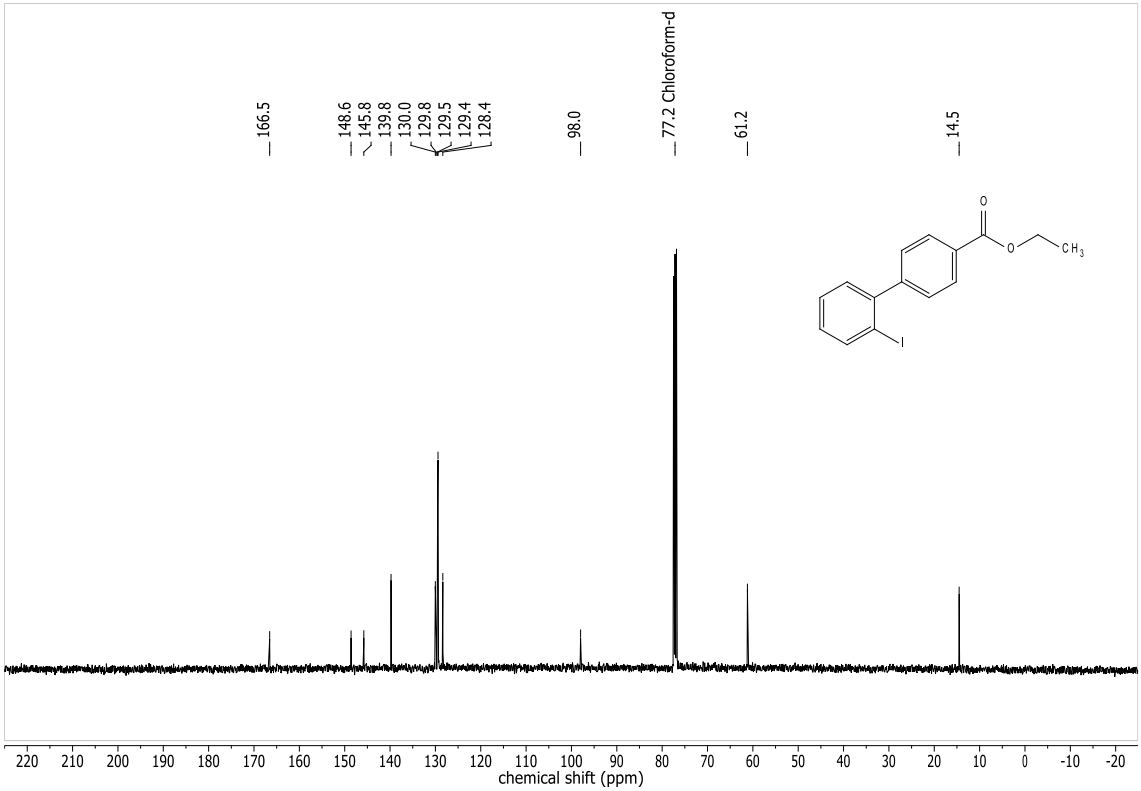

^{1}H NMR of **6**

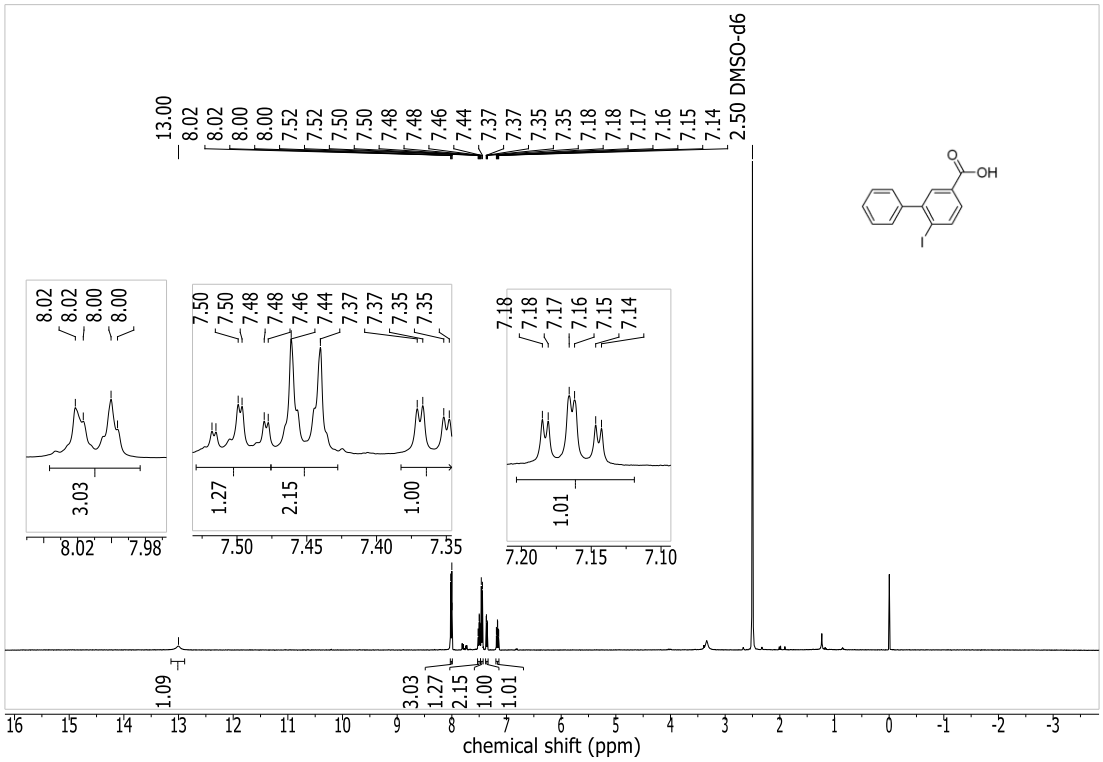

^{13}C NMR of **6**

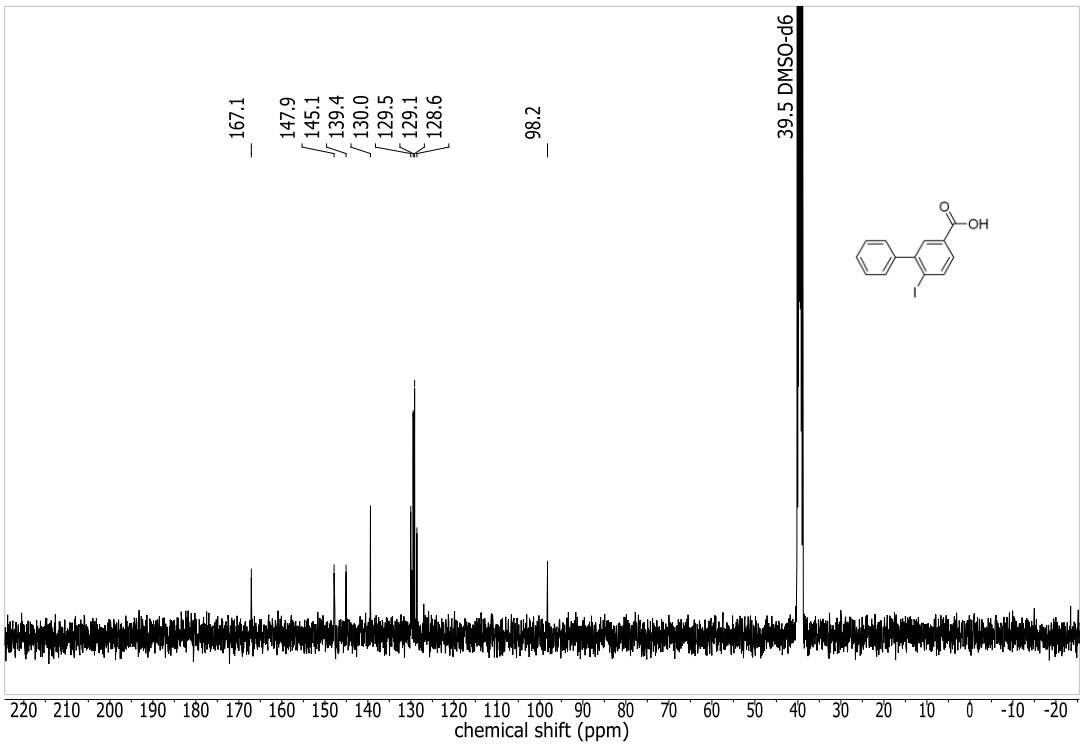

^{1}H NMR of **7**

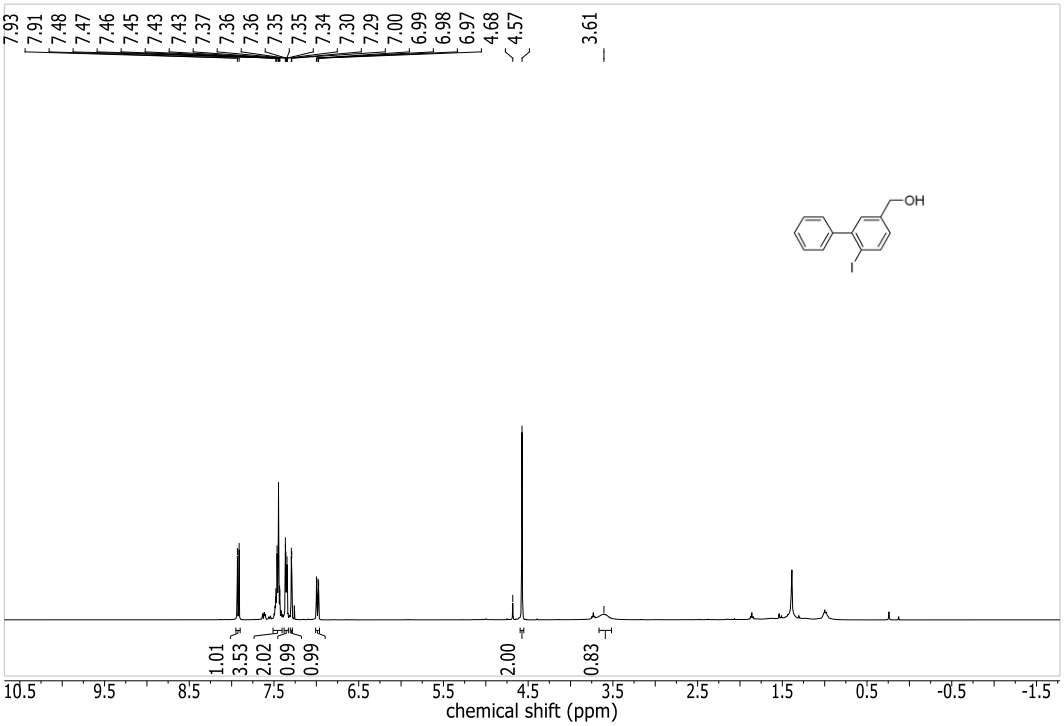

^{1}H NMR of **9**

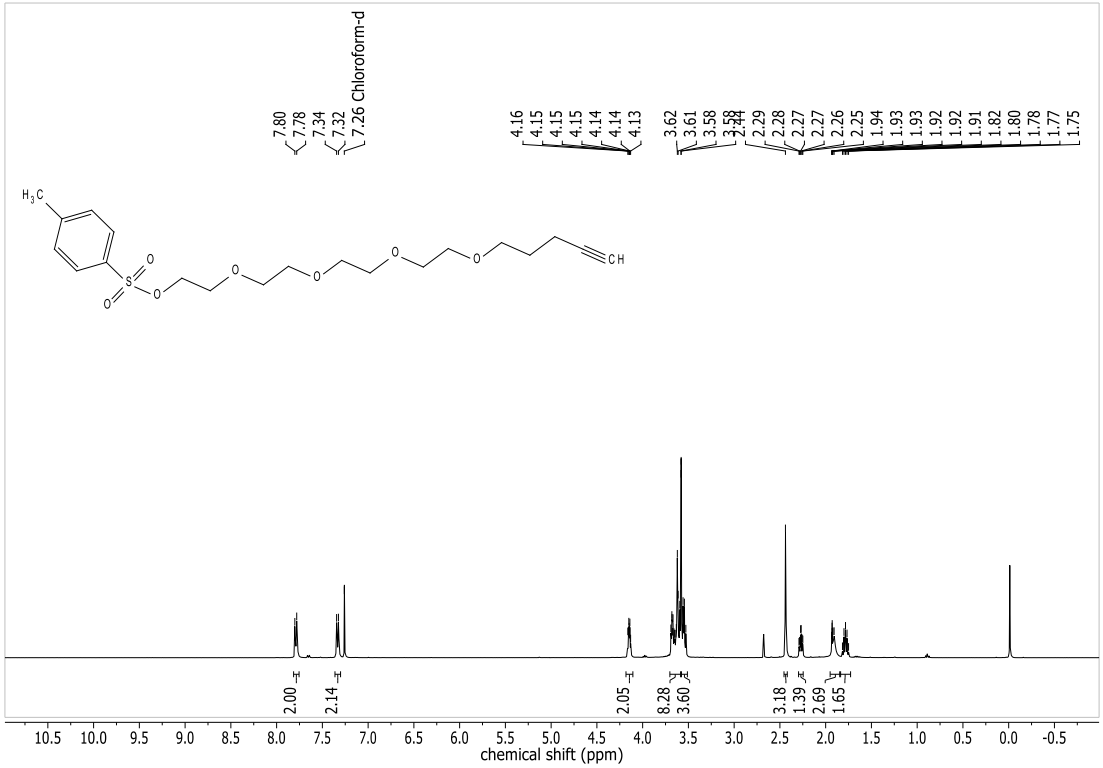

^{13}C NMR of **9**

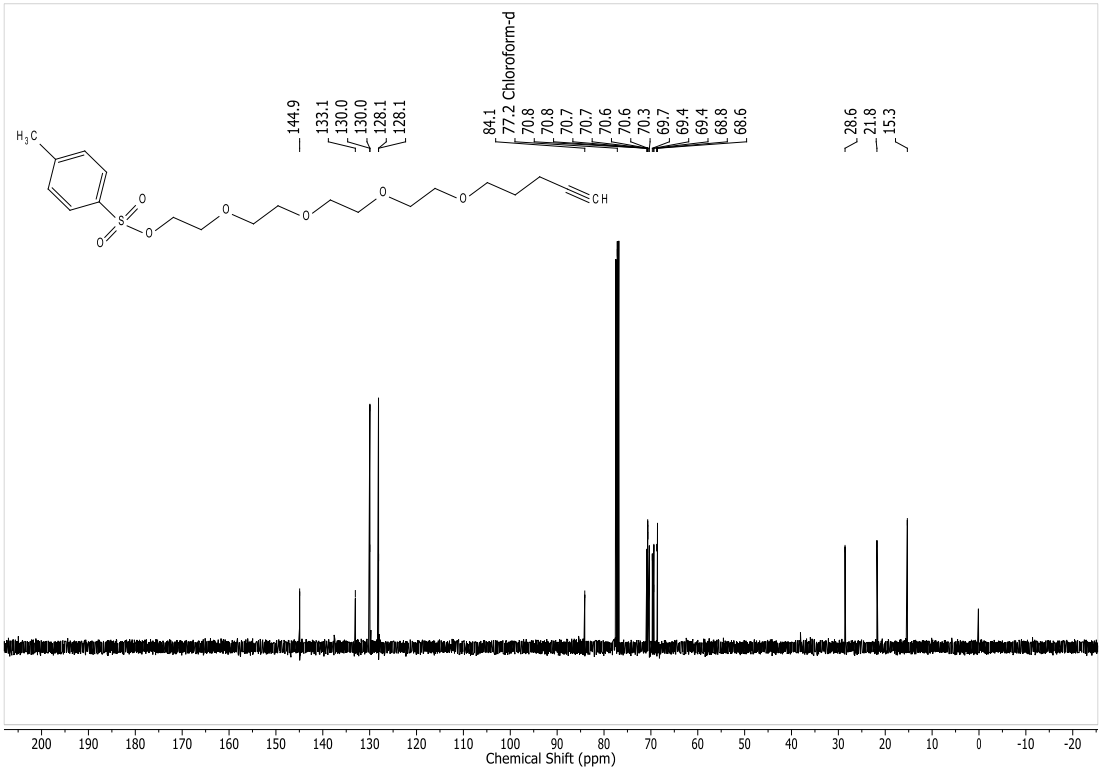

^{1}H NMR of **10**

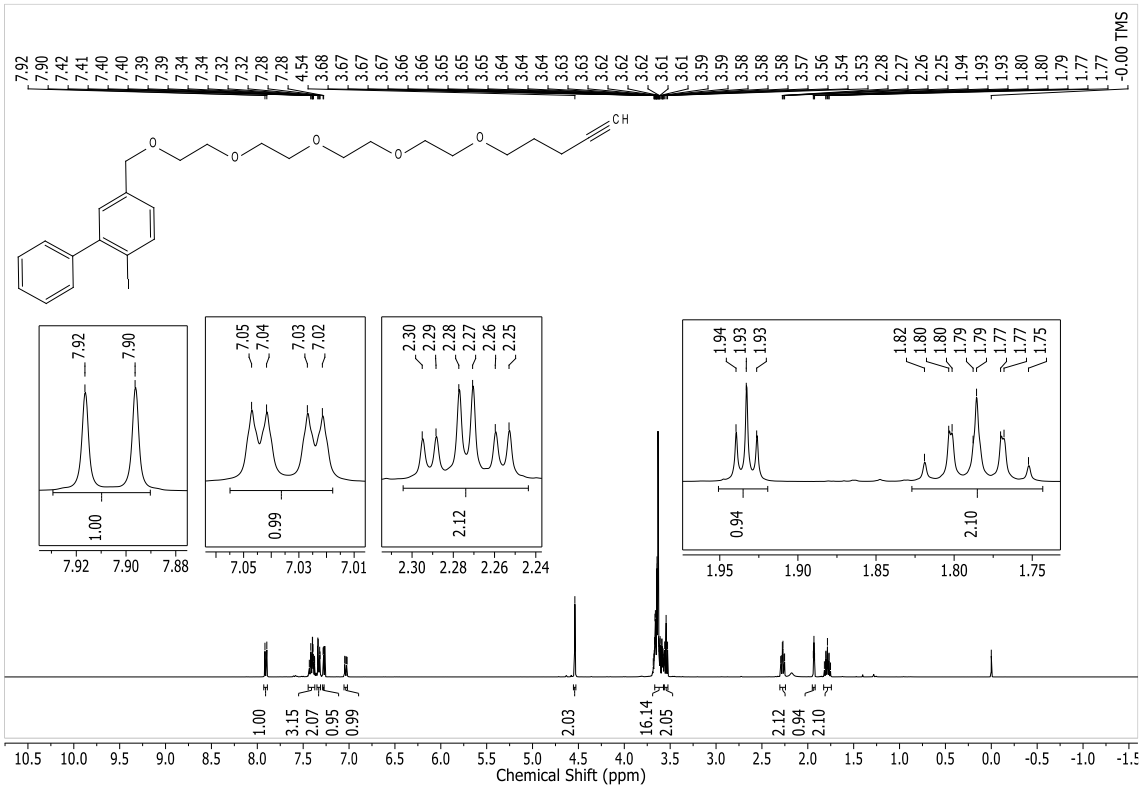

^{13}C NMR of **10**

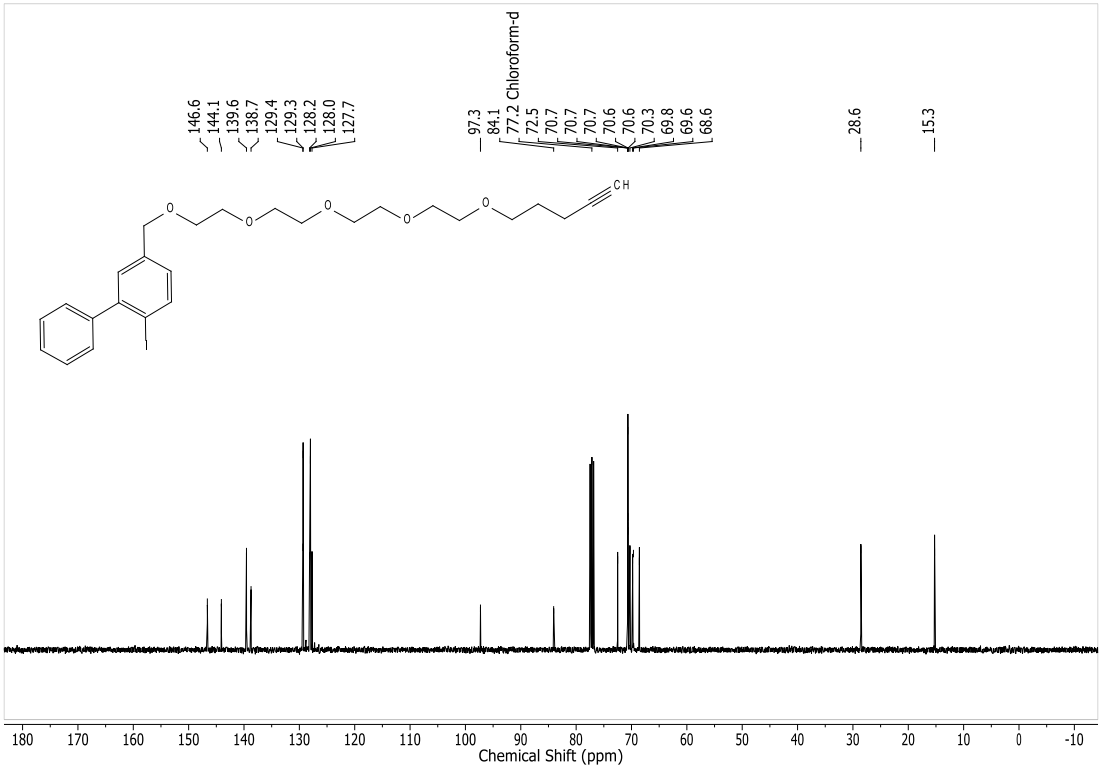

^{1}H NMR of **11**

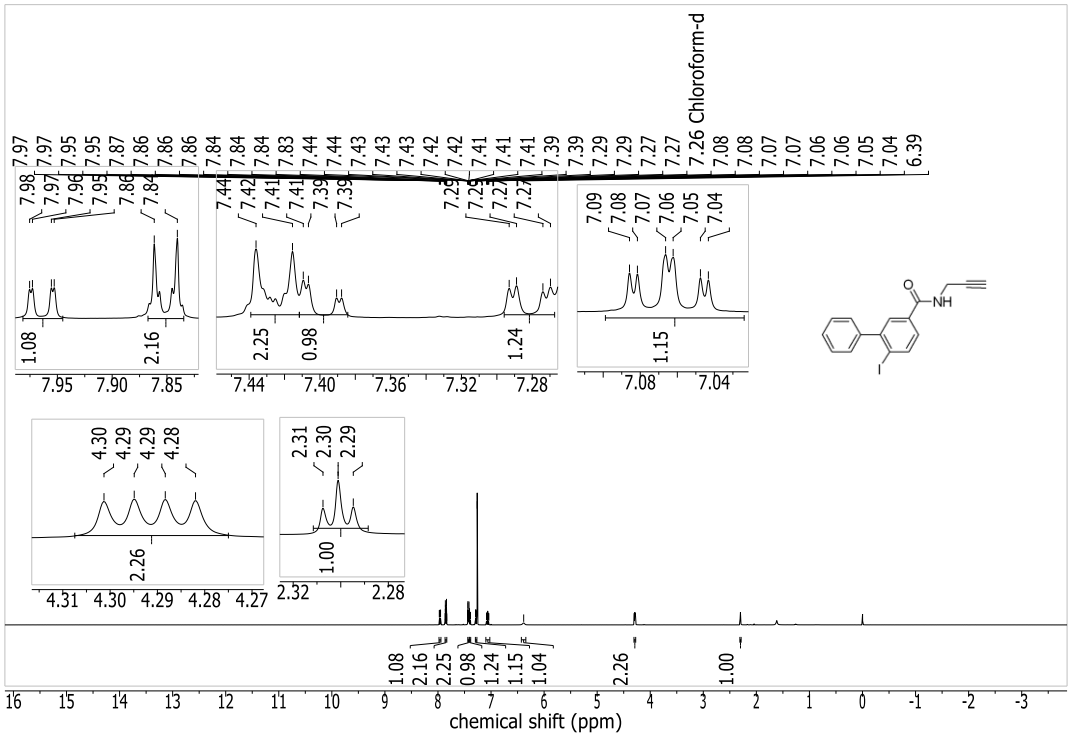

^{13}C NMR of **11**

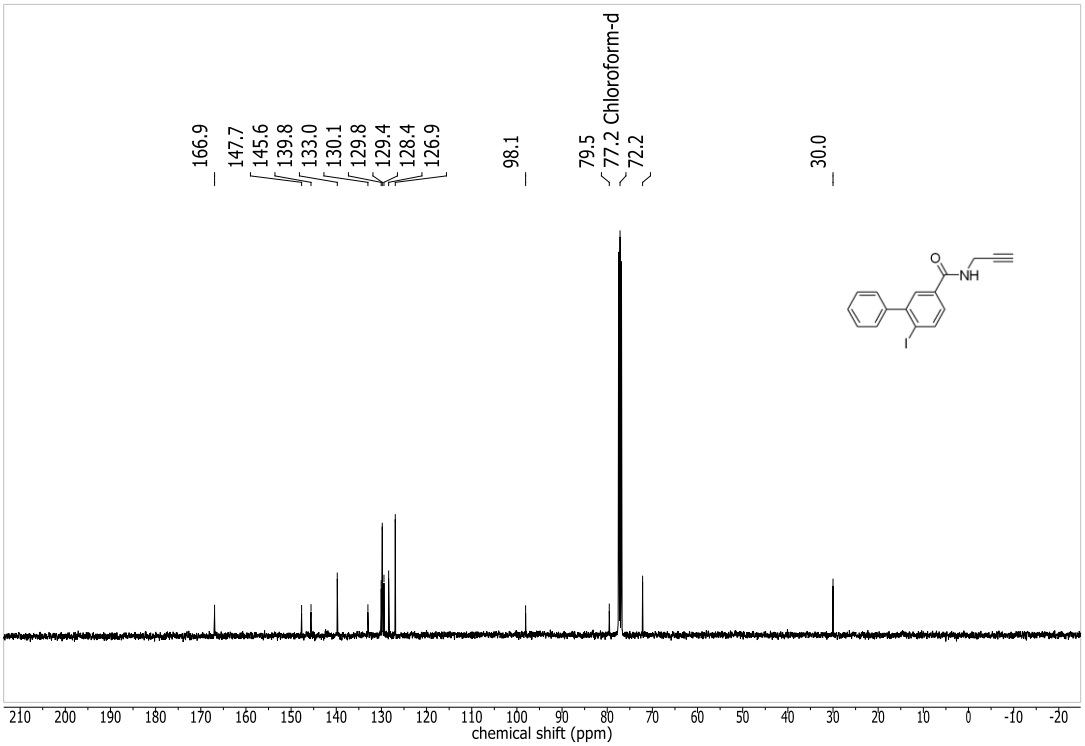

^{1}H NMR of **P1**

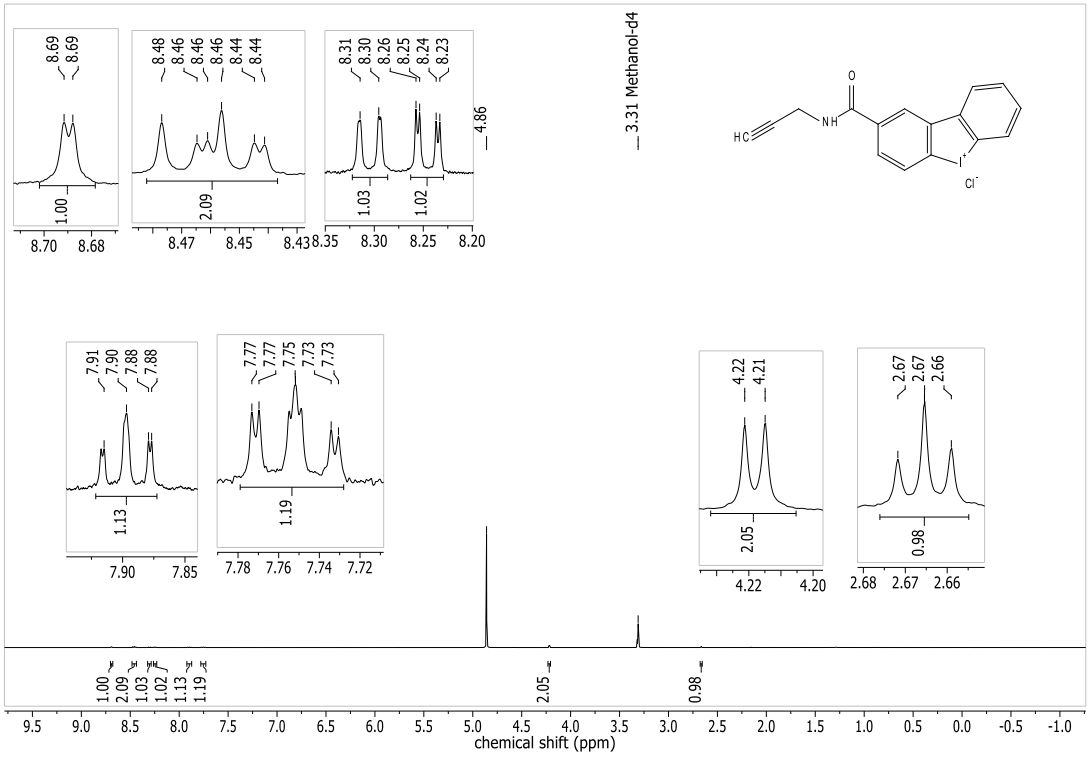

^{13}C NMR of **P1**

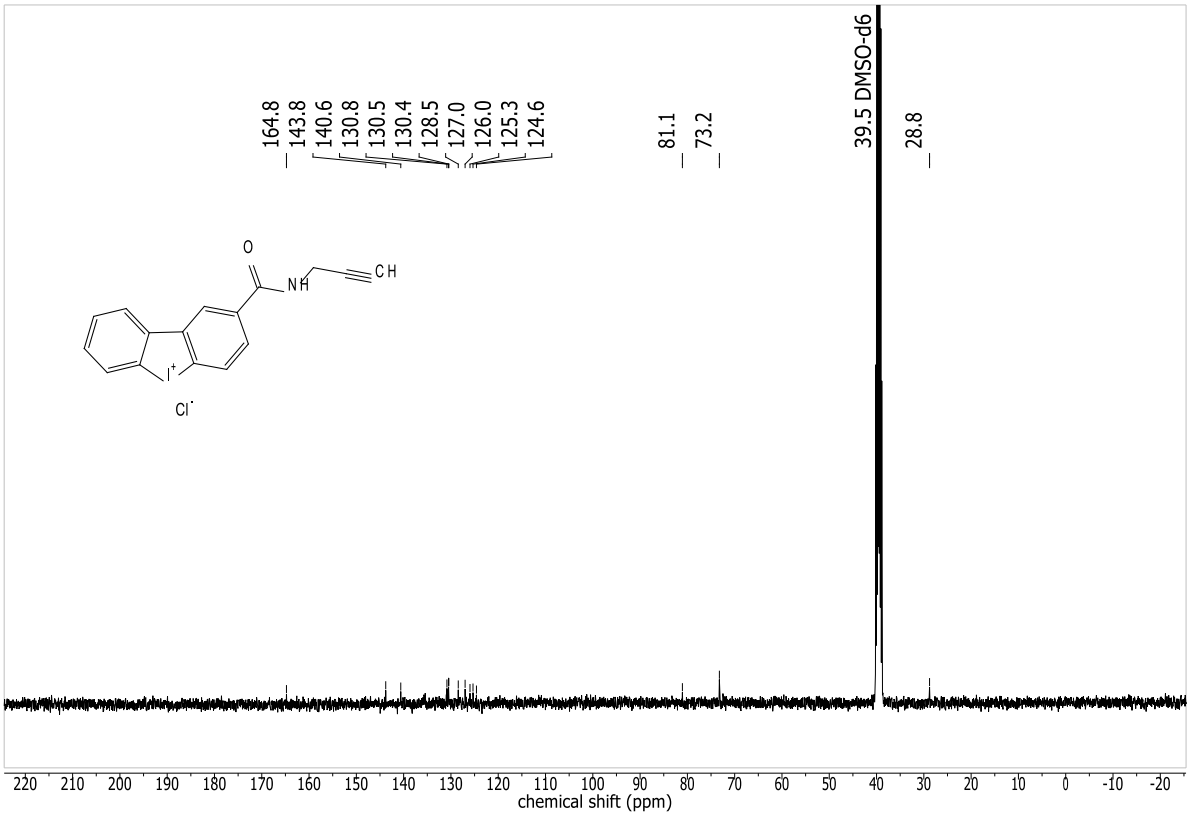
164.8
143.8
140.6
130.8
130.5
130.4
128.5
127.0
126.0
125.3
124.6
81.1
73.2
39.5 DMSO-d6
28.8
O
NH
CH
Cl
220 210 200 190 180 170 160 150 140 130 120 110 100 90 80 70 60 50 40 30 20 10 0 -10 -20
chemical shift (ppm)

2.6. References:

(1) Freedlander, B. L.; French, F. Chemotherapy of Certain Iodonium and Sulfonium Compounds. *Exp. Biol. Med.* **1946**, *63* (2), 319–322. https://doi.org/10.3181/00379727-63-15587.

(2) Engelhard, W. E.; Worton, A. G. Evaluation of an Iodonium Compound as an Antiseptic Agent. *J. Am. Pharm. Assoc. (Scientific ed.)* **1956**, *45* (6), 402–404. https://doi.org/10.1002/jps.3030450616.

(3) Chung, J.-W.; Kim, S. Y.; Park, H. J.; Chung, C. S.; Lee, H. W.; Lee, S. M.; Kim, I.; Pak, J. H.; Lee, G. H.; Jeong, J.-Y. *In Vitro* Activity of Diphenyleneiodonium toward Multidrug-Resistant *Helicobacter Pylori* Strains. *Gut Liver* **2017**, *11* (5), 648–654. https://doi.org/10.5009/gnl16503.

(4) Pandey, M.; Singh, A. K.; Thakare, R.; Talwar, S.; Karaulia, P.; Dasgupta, A.; Chopra, S.; Pandey, A. K. Diphenyleneiodonium Chloride (DPIC) Displays Broad-Spectrum Bactericidal Activity. *Sci. Rep.* **2017**, *7* (1), 11521–11528. https://doi.org/10.1038/s41598-017-11575-5.

(5) Nguyen, N.; Wilson, D. W.; Nagalingam, G.; Triccas, J. A.; Schneider, E. K.; Li, J.; Velkov, T.; Baell, J. Broad Activity of Diphenyleneiodonium Analogues against Mycobacterium Tuberculosis, Malaria Parasites and Bacterial Pathogens. *Eur. J. Med. Chem.* **2018**, *148*, 507–518. https://doi.org/10.1016/j.ejmech.2017.10.010.

(6) Cross, A. R.; Jones, O. T. G. The Effect of the Inhibitor Diphenylene Iodonium on the Superoxide-Generating System of Neutrophils. Specific Labelling of a Component Polypeptide of the Oxidase. *Biochem. J.* **1986**, *237* (1), 111–116. https://doi.org/10.1042/bj2370111.

(7) O'Donnell, V. B.; Tew, D. G.; Jones, O. T. G.; England, P. J. Studies on the Inhibitory Mechanism of Iodonium Compounds with Special Reference to Neutrophil NADPH Oxidase. *Biochem. J.* **1993**, *290* (1), 41–49. https://doi.org/10.1042/bj2900041.

(8) Majander, A.; Finel, M.; Wikström, M. Diphenyleneiodonium Inhibits Reduction of Iron-Sulfur Clusters in the Mitochondrial NADH-Ubiquinone Oxidoreductase (Complex I). *J. Biol. Chem.* **1994**, *269* (33), 21037–21042. https://doi.org/10.1016/S0021-9258(17)31926-9.

(9) Stuehr, D. J.; Fasehun, O. A.; Kwon, N. S.; Gross, S. S.; Gonzalez, J. A.; Levi, R.;

Nathan, C. F. Inhibition of Macrophage and Endothelial Cell Nitric Oxide Synthase by Diphenyleneiodonium and Its Analogs [1]. *FASEB J.* **1991**, *5* (1), 98–103. https://doi.org/10.1096/fasebj.5.1.1703974.

(10) Riganti, C.; Gazzano, E.; Polimeni, M.; Costamagna, C.; Bosia, A.; Ghigo, D. Diphenyleneiodonium Inhibits the Cell Redox Metabolism and Induces Oxidative Stress. *J. Biol. Chem.* **2004**, *279* (46), 47726–47731. https://doi.org/10.1074/jbc.M406314200.

(11) Ozsvari, B.; Bonuccelli, G.; Sanchez-Alvarez, R.; Foster, R.; Sotgia, F.; Lisanti, M. P. Targeting Flavin-Containing Enzymes Eliminates Cancer Stem Cells (CSCs), by Inhibiting Mitochondrial Respiration: Vitamin B2 (Riboflavin) in Cancer Therapy. *Aging (Albany. NY).* **2017**, *9* (12), 2610–2628. https://doi.org/10.18632/aging.101351.

(12) Iacovino, L. G.; Reis, J.; Mai, A.; Binda, C.; Mattevi, A. Diphenylene Iodonium Is a Noncovalent MAO Inhibitor: A Biochemical and Structural Analysis. *ChemMedChem* **2020**, *15* (15), 1394–1397. https://doi.org/10.1002/cmdc.202000264.

(13) Liu, Y.; Patricelli, M. P.; Cravatt, B. F. Activity-Based Protein Profiling: The Serine Hydrolases. *Proc. Natl. Acad. Sci.* **1999**, *96* (26), 14694–14699. https://doi.org/10.1073/pnas.96.26.14694.

(14) Kidd, D.; Liu, Y.; Cravatt, B. F. Profiling Serine Hydrolase Activities in Complex Proteomes. *Biochemistry* **2001**, *40* (13), 4005–4015. https://doi.org/10.1021/bi002579j.

(15) Patricelli, M. P.; Giang, D. K.; Stamp, L. M.; Burbaum, J. J. Direct Visualization of Serine Hydrolase Activities in Complex Proteomes Using Fluorescent Active Site-Directed Probes. *Proteomics* **2001**, *1* (8), 1067–1071. https://doi.org/10.1002/1615-9861(200109)1:9<1067::AID-PROT1067>3.0.CO;2-4.

(16) Greenbaum, D.; Baruch, A.; Hayrapetian, L.; Darula, Z.; Burlingame, A.; Medzihradszky, K. F.; Bogyo, M. Chemical Approaches for Functionally Probing the Proteome. *Mol. Cell. Proteomics* **2002**, *1* (1), 60–68. https://doi.org/10.1074/mcp.T100003-MCP200.

(17) Jessani, N.; Niessen, S.; Wei, B. Q.; Nicolau, M.; Humphrey, M.; Ji, Y.; Han, W.; Noh, D.-Y.; Yates, J. R.; Jeffrey, S. S.; Cravatt, B. F. A Streamlined Platform for High-Content Functional Proteomics of Primary Human Specimens. *Nat. Methods* **2005**, *2* (9), 691–697. https://doi.org/10.1038/nmeth778.

(18) Speers, A. E.; Adam, G. C.; Cravatt, B. F. Activity-Based Protein Profiling in Vivo Using a Copper(I)-Catalyzed Azide-Alkyne [3 + 2] Cycloaddition. *J. Am. Chem. Soc.* **2003**, *125* (16), 4686–4687. https://doi.org/10.1021/ja034490h.

(19) Weerapana, E.; Wang, C.; Simon, G. M.; Richter, F.; Khare, S.; Dillon, M. B. D.; Bachovchin, D. A.; Mowen, K.; Baker, D.; Cravatt, B. F. Quantitative Reactivity Profiling Predicts Functional Cysteines in Proteomes. *Nature* **2010**, *468* (7325), 790–795. https://doi.org/10.1038/nature09472.

(20) Friedrich, T.; Scheide, D. The Respiratory Complex I of Bacteria, Archaea and Eukarya and Its Module Common with Membrane-Bound Multisubunit Hydrogenases. *FEBS Lett.* **2000**, *479* (1–2), 1–5. https://doi.org/10.1016/S0014-5793(00)01867-6.

(21) Cheng, V. W. T.; Ma, E.; Zhao, Z.; Rothery, R. A.; Weiner, J. H. The Iron-Sulfur Clusters in Escherichia Coli Succinate Dehydrogenase Direct Electron Flow. *J. Biol. Chem.* **2006**, *281* (37), 27662–27668. https://doi.org/10.1074/jbc.M604900200.

(22) Velazquez, I.; Nakamaru-Ogiso, E.; Yano, T.; Ohnishi, T.; Yagi, T. Amino Acid Residues Associated with Cluster N3 in the NuoF Subunit of the Proton-Translocating NADH-Quinone Oxidoreductase from Escherichia Coli. *FEBS Lett.* **2005**, *579* (14), 3164–3168. https://doi.org/10.1016/j.febslet.2005.05.005.

(23) Schulte, M.; Frick, K.; Gnandt, E.; Jurkovic, S.; Burschel, S.; Labatzke, R.; Aierstock, K.; Fiegen, D.; Wohlwend, D.; Gerhardt, S.; Einsle, O.; Friedrich, T. A Mechanism to Prevent Production of Reactive Oxygen Species by Escherichia Coli Respiratory Complex I. *Nat. Commun.* **2019**, *10* (1), 2551. https://doi.org/10.1038/s41467-019-10429-0.

(24) Grushin, V. V.; Demkina, I. I.; Tolstaya, T. P. Unified Mechanistic Analysis of Polar Reactions of Diaryliodonium Salts. *J. Chem. Soc. Perkin Trans. 2* **1992**, No. 4, 505. https://doi.org/10.1039/p29920000505.

(25) Grushin, V. V. Carboranylhalonium Ions: From Striking Reactivity to a Unified Mechanistic Analysis of Polar Reactions of Diarylhalonium Compounds. *Acc. Chem. Res.* **1992**, *25* (11), 529–536. https://doi.org/10.1021/ar00023a007.

(26) Grushin, V. V. Cyclic Diaryliodonium Ions: Old Mysteries Solved and New Applications Envisaged. *Chem. Soc. Rev.* **2000**, *29* (5), 315–324. https://doi.org/10.1039/a909041j.

(27) Pinto de Magalhães, H.; Lüthi, H. P.; Togni, A. Breaking Down the Reactivity of λ ^{3} -Iodanes: The Impact of Structure and Bonding on Competing Reaction Mechanisms. *J. Org. Chem.* **2014**, *79* (17), 8374–8382. https://doi.org/10.1021/jo501714f.

(28) Liu, Z.; Zhu, D.; Luo, B.; Zhang, N.; Liu, Q.; Hu, Y.; Pi, R.; Huang, P.; Wen, S. Mild Cu(I)-Catalyzed Cascade Reaction of Cyclic Diaryliodoniums, Sodium Azide, and Alkynes: Efficient Synthesis of Triazolophenanthridines. *Org. Lett.* **2014**, *16* (21), 5600–5603. https://doi.org/10.1021/ol502654a.

(29) Tran-Van, A.-F.; Götz, S.; Neuburger, M.; Wegner, H. A. A Strain Induced Change of Mechanism from a [2 + 2 + 2] to a [2 + 1 + 2 + 1] Cycloaddition Reaction. *Org. Lett.* **2014**, *16* (9), 2410–2413. https://doi.org/10.1021/ol5007604.

(30) Zhou, M.; Zhang, X.; Bai, M.; Shen, D.; Xu, B.; Kao, J.; Ge, X.; Achilefu, S. Click Reaction-Mediated Functionalization of near-Infrared Pyrrolopyrrole Cyanine Dyes for Biological Imaging Applications. *RSC Adv.* **2013**, *3* (19), 6756. https://doi.org/10.1039/c3ra40441b.

(31) Kelkar, D. S.; Ravikumar, G.; Mehendale, N.; Singh, S.; Joshi, A.; Sharma, A. K.; Mhetre, A.; Rajendran, A.; Chakrapani, H.; Kamat, S. S. A Chemical–Genetic Screen Identifies ABHD12 as an Oxidized-Phosphatidylserine Lipase. *Nat. Chem. Biol.* **2019**, *15* (2), 169–178. https://doi.org/10.1038/s41589-018-0195-0.

(32) Kulkarni, A.; Soni, I.; Kelkar, D. S.; Dharmaraja, A. T.; Sankar, R. K.; Beniwal, G.; Rajendran, A.; Tamhankar, S.; Chopra, S.; Kamat, S. S.; Chakrapani, H. Chemoproteomics of an Indole-Based Quinone Epoxide Identifies Druggable Vulnerabilities in Vancomycin-Resistant Staphylococcus Aureus. *J. Med. Chem.* **2019**, *62* (14), 6785–6795. https://doi.org/10.1021/acs.jmedchem.9b00774.

(33) Kumar, K.; Mhetre, A.; Ratnaparkhi, G. S.; Kamat, S. S. A Superfamily-Wide Activity Atlas of Serine Hydrolases in Drosophila Melanogaster. *Biochemistry* **2021**, *60* (16), 1312–1324. https://doi.org/10.1021/acs.biochem.1c00171.

(34) Li, M. Z.; Elledge, S. J. SLIC: A Method for Sequence- and Ligation-Independent Cloning; 2012; pp 51–59. https://doi.org/10.1007/978-1-61779-564-0_5.

(35) Grimme, S. Semiempirical GGA-Type Density Functional Constructed with a Long-Range Dispersion Correction. *J. Comput. Chem.* **2006**, *27* (15), 1787–1799. https://doi.org/10.1002/jcc.20495.

(36) Frisch, M. J.; Trucks, G. W.; Schlegel, H. B.; Scuseria, G. E.; Robb, M. A.; Cheeseman, J. R.; Scalmani, G.; Barone, V.; Petersson, G. A.; Nakatsuji, H.; Li, X.; Caricato, M.; Marenich, A. V.; Bloino, J.; Janesko, B. G.; Gomperts, R.; Mennucci, B.; Hratchian, H. P.; Ortiz, J. V.; Izmaylov, A. F.; Sonnenberg, J. L.; Williams; Ding, F.; Lipparini, F.; Egidi, F.; Goings, J.; Peng, B.; Petrone, A.; Henderson, T.; Ranasinghe, D.; Zakrzewski, V. G.; Gao, J.; Rega, N.; Zheng, G.; Liang, W.; Hada, M.; Ehara, M.; Toyota, K.; Fukuda, R.; Hasegawa, J.; Ishida, M.; Nakajima, T.; Honda, Y.; Kitao, O.; Nakai, H.; Vreven, T.; Throssell, K.; Montgomery Jr., J. A.; Peralta, J. E.; Ogliaro, F.; Bearpark, M. J.; Heyd, J. J.; Brothers, E. N.; Kudin, K. N.; Staroverov, V. N.; Keith, T. A.; Kobayashi, R.; Normand, J.; Raghavachari, K.; Rendell, A. P.; Burant, J. C.; Iyengar, S. S.; Tomasi, J.; Cossi, M.; Millam, J. M.; Klene, M.; Adamo, C.; Cammi, R.; Ochterski, J. W.; Martin, R. L.; Morokuma, K.; Farkas, O.; Foresman, J. B.; Fox, D. J. Gaussian 16 Rev. C.01. Wallingford, CT 2016.

Chapter 3: Synthesis of DPIC Analogues and Evaluation of Their Antibacterial Activity against Gram-Negative Bacteria

3.1. Introduction:

In Chapter **1**, the antibacterial properties of iodonium compounds were discussed. In Chapter **2**, protein targets of DPIC in *E. coli* proteome were identified and validated using ABPP. Although DPIC displayed good antibacterial activity against Gram-negative bacteria[1–4], but the potency against MDR *A. baumannii*, an opportunistic Gram-negative pathogen was diminished. Baell and colleagues discovered 5-chlorodiphenyleneiodonium triflate as a potent inhibitor of MDR ESAKAPE pathogens by using a SAR study of DPI.[5] This compound was not only ineffective against *A. baumannii*, but it was also toxic to mammalian cells. *A. baumannii* is a troublesome pathogen responsible for various nosocomial and community-acquired infections such as skin and soft tissue, bloodstream, urinary tract infections, meningitis, and pneumonia.[6–8] Infections caused by *A. baumannii* are most common in immunocompromised people or those in hospitals with high-risk underlying illnesses.[9] This pathogen has acquired several genetic alterations over time and is now resistant to practically all antibiotics..[10] According to a report released by the WHO, carbapenem-resistant *A. baumannii* is on top of the critical priority list, highlighting the urgent need for novel therapies.[11] Three primary antibiotic resistance mechanisms in *A. baumannii* are

- **Inactivation of antibiotics:** *β*-lactamases that hydrolyze the penicillins or carbapenems. Carbapenem-resistant *A. baumannii* was noticed due to the presence of numerous such enzymes which inactivate the antibiotic.[12]
- **Reduced access to the target site:** The presence of porins in *A. baumannii* has led to the diminished accessibility of antibiotics to the target site. Similarly, efflux pumps also contributed to antibiotic resistance by throwing out the antibiotics from the target site.[13]
- **Modification of drug target:** *A. baumannii* generates changes within itself that alter the target site in response to broad-spectrum antibiotics, such as a mutation in topoisomerase genes, which is created in response to quinolones.[14]

To boost the effectiveness of iodonium compounds against *A. baumannii*, we aimed to synthesize a focused library of DPI analogs. Targets in *A. baumannii* will be identified utilizing chemoproteomic methods after one such analog is identified.

3.2. Results and Discussion:

3.2.1. Synthesis and SAR of iodonium compounds:

In order to address issues such as solubility and safety profile, as well as to broaden the antibacterial activity spectrum, using DPIC as a starting point, a structure-activity study was proposed. For the synthesis of DPI derivatives, general Scheme 3.1 was followed.

Scheme 3. 1 General Synthetic scheme for diphenyleneiodonium compounds

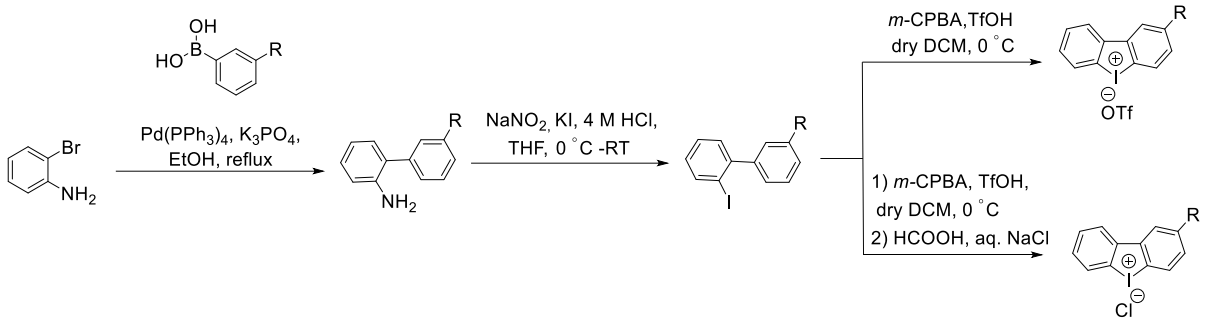

The Pd-catalyzed Suzuki coupling reaction of 2-bromo aniline with aryl boronic acid yielded biaryl amine intermediate, which upon diazotization using sodium nitrite and potassium iodide under acidic media resulted in biaryl iodide intermediate. Further, oxidation of biaryl iodide with *m*-chloroperbenzoic acid in the presence of triflic acid was performed to obtain diphenylene iodonium triflate. To prepare diphenylene iodonium chloride, the triflate anion was exchanged for the chloride anion using aqueous sodium chloride in formic acid. The introduction of any polar functional group over the benzene ring was thought to promote aqueous solubility. Hence, following Scheme 3.1, a few biaryl iodide compounds **12-14** were synthesized. However, the oxidation of biaryl iodide to iodonium salt was unsuccessful in each case.

Scheme 3. 2 Synthesis scheme for polar diphenyleneiodonium compound

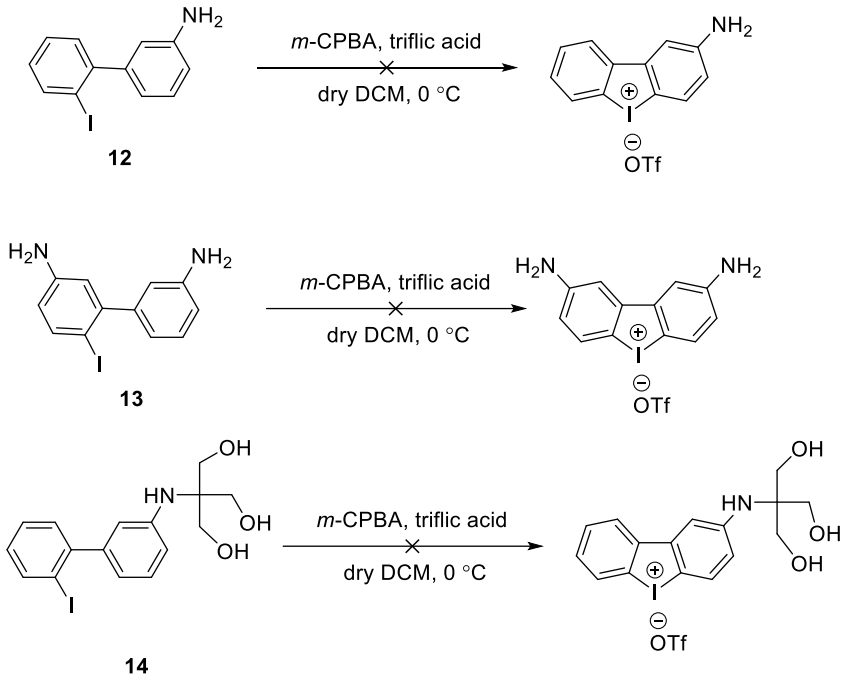

Next, carboxylic acid and ester derivatives of DPI were synthesized (Scheme 3.1), and it was discovered that these compounds have lower solubility in organic solvents than DPIC. Furthermore, when tested against ESKAP pathogens, these compounds have poor antibacterial efficacy. No significant difference was observed between the activity of triflate and chloride derivates of iodonium compounds.

Figure 3. 1 Structure of diphenyleneiodonium derivatives

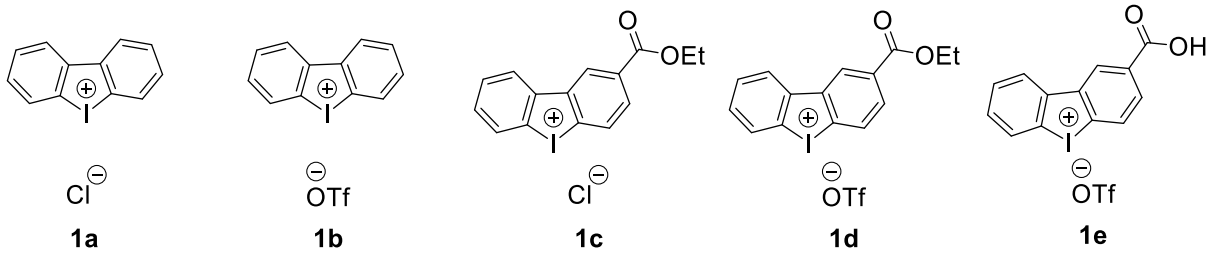

Table 3. 1 Antibacterial activity of the iodonium compounds against ESKAP pathogens

		MIC[a] (µg/mL)				
Entry	Cpd.	*E. coli*	*S. aureus*	*K. pneumoniae*	*A. baumannii*	*P. aeruginosa*
1	**1a**	4	1	16	4	4
2	**1b**	2	2	16	2	2
3	**1c**	8	2	>64	16	16
4	**1d**	4	1	64	8	8
5	**1e**	>64	>64	>64	>64	>64
6	Levofloxacin	0.0156	0.125	64	4	0.5

[a]MIC against ESKAP (*E. coli* ATCC25922, *S. aureus* ATCC 29213, *K. pneumoniae* BAA1705, *A. baumannii* BAA1605, *P. aeruginosa* ATCC 27853) pathogens. (Data provided by: Dr. Sidharth Chopra lab, CSIR-CDRI Lucknow)

Next, the synthesis of heterocyclic iodonium compounds was planned to improve the antibacterial activity. The heterocyclic ring such as pyridine or thiophene was considered instead of benzene. Pyridine is often used in medicinal chemistry due to several unique properties such as good hydrogen-bond forming ability, small molecular size, and increased water solubility[15]. Pyridine is a bioisostere of the benzene ring in several drugs.

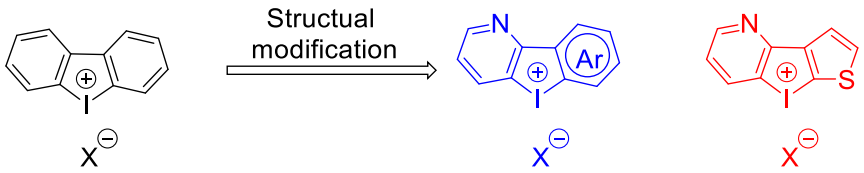

Another heterocycle that was considered was thiophene. This heterocycle is a well-known in medicine and is a constituent of a number of compounds with antibacterial, antihypertensive, and anticancer properties.[16]. The general synthetic approach was revised to synthesize the heterocyclic iodonium compounds. (Scheme 3.3).

Scheme 3. 3 Synthesis scheme for heterocyclic iodonium compound

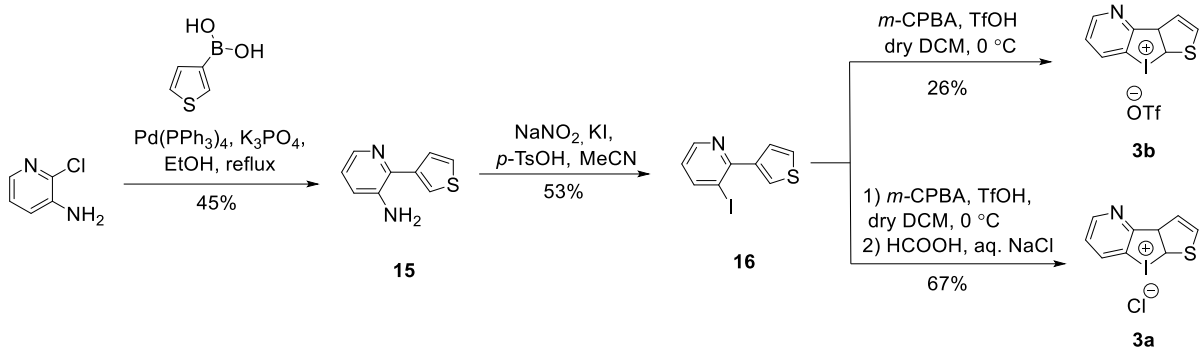

Following Scheme 3.3, a series of heterocyclic iodonium compounds were synthesized. (Compound **2a-2g** were synthesized by Mr. Suraj Sharma (BS-MS graduate) under my guidance using Scheme 3.3 with some modifications)

Figure 3. 2 Structure of heterocyclic iodonium derivatives

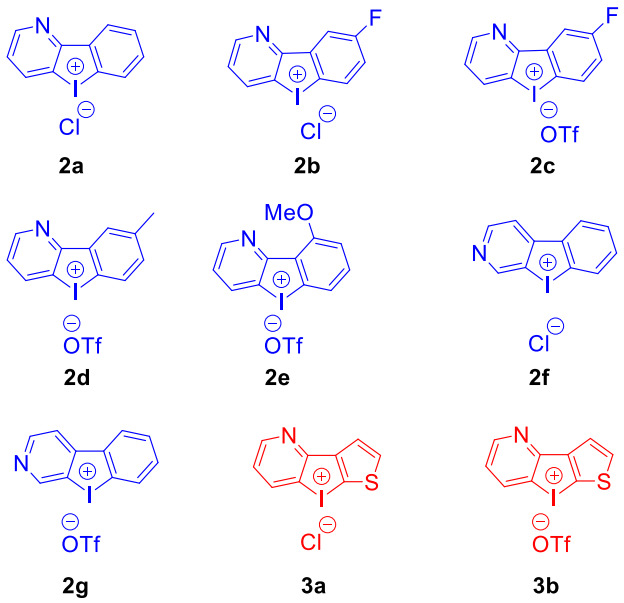

The antibacterial activity of these compounds was investigated against ESKAP pathogens (Table 3.2). Substitution of one benzene ring to pyridine has substantially improved the activity, notably in Gram-negative bacteria, i.e., *E. coli*, *K. pneumoniae*, *A. baumannii*, *P. aeruginosa*. Structural activity relationship (SAR) study also suggested that the compound with an electron-donating group such as methoxy functional group **2e** exhibits moderate activity against Gram-negative bacteria. Interestingly, the substitution of benzene rings with pyridine and thiophene **3a** and **3b** led to a significant increment in the activity against *A. baumannii*.

Table 3. 2 Antibacterial activity of the heterocyclic iodonium compounds against ESKAP pathogens

		MIC[a] (µg/mL)				
Entry	Cpd.	*E. coli*	*S. aureus*	*K. pneumoniae*	*A. baumannii*	*P. Aeruginosa*
1	**1a**	4	1	16	4	4
2	**2a**	0.25	0.5	2	0.125	0.25
3	**2b**	0.25	1	1	0.25	1
4	**2c**	0.125	0.25	2	0.125	0.5
5	**2d**	0.25	0.5	8	0.25	1
6	**2e**	0.5	1	2	8	4
7	**2f**	0.5	0.5	4	2	2
8	**2g**	0.5	0.5	2	2	2
9	**3a**	1	1	2	0.0625	1
10	**3b**	0.5	0.5	1	0.0625	0.5
11	Levofloxacin	0.0156	0.125	64	4	0.5

[a]MIC against ESKAP (*E. coli* ATCC25922, *S. aureus* ATCC 29213, *K. pneumoniae* BAA1705, *A. baumannii* BAA1605, *P. aeruginosa* ATCC 27853) pathogens. (Data provided by: Dr. Sidharth Chopra lab, CSIR-CDRI Lucknow)

As discussed earlier, the major challenge in discovering small molecules to develop into new antibiotics against Gram-negative pathogens has often been associated with the inability of the molecule to traverse the outer membrane barrier and poor accumulation within bacteria. To address the problems associated with antibiotic permeability, Hergenrother and co-workers examined the physicochemical properties of the diverse compounds that favor accumulation inside *E. coli*, a Gram-negative bacterium.[17] The compounds with a molecular wight of less than 600 Da, having an ionizable nitrogen, certain degree of hydrophobicity, low globularity, and lower number of rotatable bonds[18], were found to have increased accumulation in *E. coli*. These properties, together known as 'eNTRy rules' are useful guidelines while considering permeability in *E. coli*.

Hence, to investigate the ability of these iodonium compounds to fulfil the criteria of 'eNTRy rules,' in this study, their molecular properties were compared with FDA-approved antibiotics.

Molecular weight and clogP were obtained from ChemDraw 19.1 (Table 3.3). As anticipated, most of the tested FDA-approved antibiotics were highly polar (clogP < 0). On the other hand, phenyl-based iodonium compounds were more hydrophobic (clogP = 2.3 – 3.6) and less potent, while pyridine-based iodonium compounds were moderately hydrophobic (clogP = 1.1 – 1.52) and highly potent against *E. coli*. In a similar vein, the other physicochemical descriptors such as globularity and plane of best fit were calculated from an online server (www.entry-way.org) (Table 3.3). While the tested FDA-approved antibiotics exhibited high globularity and plane of best fit, they were moderately active (MIC range = 1-8 μg/mL). On the contrary, all the iodonium compounds except **1a**-**1e**, **2d**, **2e**, and **2g** showed low globularity and plane of best fit. However, they displayed moderate to high potency (MIC range = 0.125-16 μg/mL) against *A. baumannii*. Iodonium compounds such as **2a**, **2b**, **3a,** and **3b** with moderate hydrophobicity, lower globularity, and the plane of best fit displayed significant potency compared with the efficacy of traditionally antibiotics against *A. baumannii*.

Table 3. 3 Physicochemical descriptors calculated for iodonium compounds and antibiotics

Compounds	Mol. Wt. (Da)	clogP	PBF	Globularity	MIC (μg/mL) against *A. baumannii*
1a	314.55	2.65	0.011	0.0001	4
1b	428.16	2.65	0.181	0.0332	2
1c	385.61	3.15	0.309	0.0203	16
1d	500.23	3.15	0.398	0.0342	8
1e	472.17	2.39	0.239	0.0299	64
2a	315.54	1.36	0.00003	$0.2x10^{-9}$	0.125
2b	333.53	1.52	0.00002	$0.9\ x10^{-10}$	0.25
2c	447.14	1.52	0.204	$0.3\ x10^{-8}$	0.125
2d	443.18	1.86	0.251	0.036	0.25
2e	459.18	1.38	0.229	0.039	8
2f	315.54	1.15	0.00001	$0.06\ x10^{-10}$	2
2g	429.15	1.15	0.220	$0.4\ x10^{-8}$	2
3a	321.56	1.26	0.00003	$0.2\ x10^{-9}$	0.125
3b	435.17	1.26	0.223	0.041	0.125
LVX	361.37	-0.50	0.696	0.058	4
MXF	401.43	-0.08	0.887	0.093	8
CAZ	546.58	-7.97	0.891	0.047	128
CTX	455.47	-1.28	1.564	0.215	128
GEN	477.59	-1.79	1.369	0.181	64
TOB	467.51	-4.71	1.106	0.106	1
MIN	457.47	-0.42	1.30	0.187	2
MEM	383.46	-3.27	0.852	0.065	8
KAN	484.49	-5.17	1.05	0.09	128
VAN	1,449.3	-1.14	2.17	0.28	8
CIP	331.34	-1.12	0.69	0.07	32

LVX: Levofloxacin, MXF: Moxifloxacin, CAZ: Ceftazidime, CTX: Cefotaxime, GEN: Gentamicin, TOB: Tobramycin, MIN: Minocycline, MEM: Meropenem, KAN: Kanamycin,

VAN: Vancomycin, and CIP: Ciprofloxacin. (Data provided by: Anand Kumar T., Prof. Harinath Chakrapani Lab, IISER Pune)

Table 3. 4 Cytotoxicity profile of heterocyclic iodonium compounds against A. baumannii BAA 1605

Entry	Cpd.	*A. baumannii* BAA 1605	Selectivity index (SI)[a]
1	**2a**	0.125	<1
2	**2c**	0.125	<10
3	**2d**	0.25	<10
4	**3a**	0.0625	20
5	**3b**	0.0625	20

[a]SI= selectivity index relative to Vero cells and was calculated by CC_{50}/MIC_{90}; (MIC in µg/mL). (Data provided by: Dr. Sidharth Chopra lab, CSIR-CDRI Lucknow)

The cytotoxicity profile of selected compounds was then examined in Vero cells (Table 3.4). Compounds **3a** and **3b** were identified as lead compounds based on their safety profiles. Since chloride is a pharmaceutically acceptable anion of salt-based compounds[19], compound **3a** was selected for further studies.

Subsequently, **3a** was screened against a panel of patient-derived clinical isolates of multi-drug resistant (MDR) *A. baumannii* (Table 3.5), which are only susceptible to Polymyxin B. Remarkably, **3a** was found to be as effective against all of these clinical isolates as the routinely used Polymyxin B antibiotic against all of these clinical isolates.

Table 3. 5 MIC values of the 3a against MDR clinical isolates of A. baumannii

Entry	Bacterium	Strain	MIC[a] of **3a**	MIC[a] of Polymyxin B
1	*A. baumannii*	NR-9667	0.5	0.25
2	*A. baumannii*	NR-13376	0.25	0.5
3	*A. baumannii*	NR-13377	0.25	0.25
4	*A. baumannii*	NR-13381	0.25	0.5
5	*A. baumannii*	NR-13382	0.5	0.125
6	*A. baumannii*	NR-13384	0.25	0.5
7	*A. baumannii*	NR-17785	0.25	0.5
8	*A. baumannii*	NR-19298	0.25	0.5

[a]MIC in μg/mL (Data provided by: Dr. Sidharth Chopra lab, CSIR-CDRI Lucknow)

Next, a time-kill analysis study revealed that compound **3a** exhibits bactericidal activity against *A. baumannii* at 10x MIC (MIC: 0.0625 μg/mL), clearly suggesting the therapeutic efficacy of compound **3a**. In addition, the antibacterial potency of compound **3a** (1 mg/kg) and Polymyxin B (5 mg/kg) as a positive control were tested in a murine neutropenic thigh infection model. Compound **3a** was found to have excellent efficacy in this assay and significantly reduced *A. baumannii*-induced bacterial load. Together these results demonstrated that **3a** was bactericidal and worked well against *A. baumannii* in an animal model for infection

Figure 3. 3 A) Time-kill curves for A. baumannii BAA 1605 treated with 1X and 10X MIC of 3a and Polymyxin B; B) In vivo efficacy of 3a in murine neutropenic thigh infection model.

A) Ctrl indicates untreated cells; Cell survival was plotted at the 24-h time point as log-change in colony-forming units per mL (log10 CFU/mL), and the curves show mean + SD of three independent experiments; **B)** Mice (24 mice/group) were rendered neutropenic, and the thigh muscle was intramuscularly infected with *A. baumannii* BAA 1605 at 1 x 10^8 CFU. The infected mice were treated with intraperitoneal doses of **3a** (1 mg/kg) and Polymyxin B (5 mg/kg) at 3 h and 6 h post-infection. Polymyxin B was used as a reference antibiotic. Ctrl is untreated mice. Statistical significance is calculated with respect to Ctrl (****p < 0.0001). (Data provided by: Dr. Sidharth Chopra lab, CSIR-CDRI Lucknow)

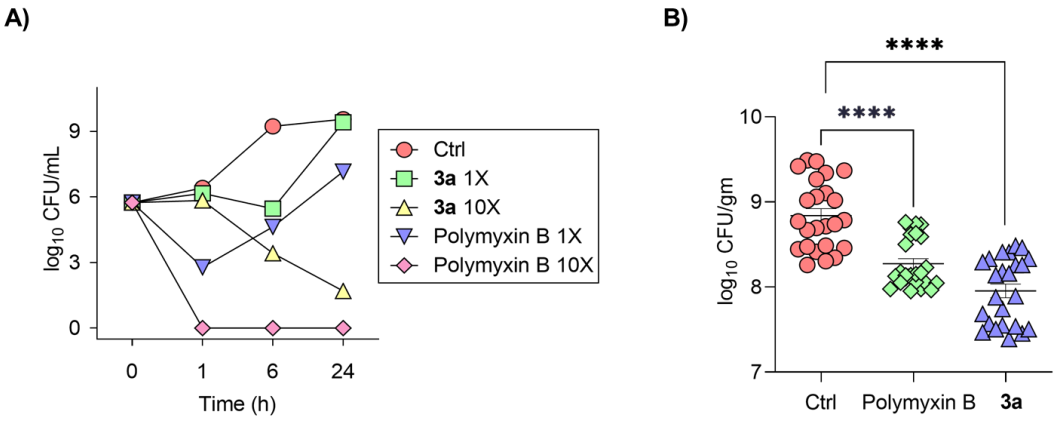

Having identified **3a** as the lead compound against *A. baumannii*, identification of protein targets for **3a** in *A. baumannii* was next carried out. The targets of the lead compound **3a** may differ from those discovered in *E. coli* with DPIC in Chapter.**2**.

3.2.2. Activity-based protein profiling (ABPP) with DPIC alkyne probe P1 in *A. baumannii*:

The whole-cell lysate of *A. baumannii* was centrifuged and fractionated into membrane and soluble fractions using an ultracentrifuge. Protein concentrations of these fractions were estimated using BSA protein standards with Bradford assay and adjusted to 1 mg/mL with 1X PBS. The proteomes were profiled with probe **P1** using previously described ABPP protocols. Probe **P1** caused dose-dependent covalent modification of various proteins was observed in both soluble and membrane proteomes (Figure 3.4, 3.5).

Figure 3. 4 Dose-dependent profiling of soluble fraction of A. baumannii with DPIC alkyne probe P1

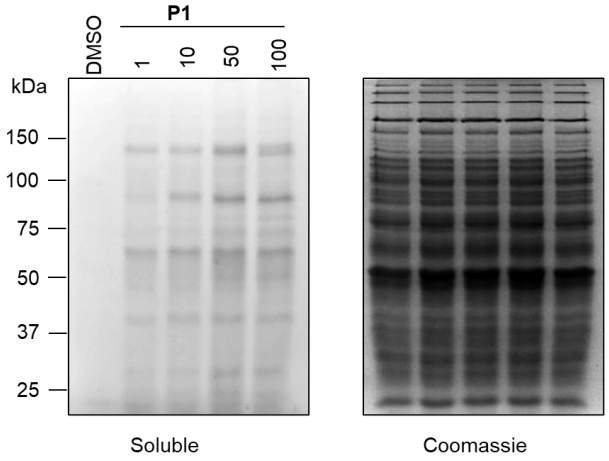

Figure 3. 5 Dose-dependent profiling in membrane fraction of A. baumannii with DPIC alkyne probe P1

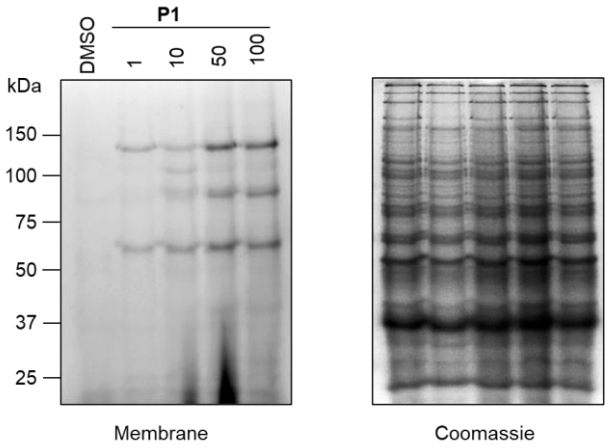

Next, a competitive ABPP based experiment was carried out using **3a** as a competitor. The membrane and soluble proteome were first independently treated with **3a** (1-250 µM, 1 h), followed by the treatment of probe **P1**(100 µM, 1 h). Click reaction was performed with this labelled proteome using fluorescent rhodamine azide and visualized after SDS-PAGE. In comparison to the only probe **P1** treated lane, compound **3a** treated lanes showed a significant reduction in the intensity of labeled proteins (Figure 3.6, 3.7 suggesting that **3a** covalently modifies certain proteins in the *A. buamannii* proteome.

Figure 3. 6 Chase experiment - In vitro modification of proteins in soluble fraction of A. buamannii with 3a chased with P1

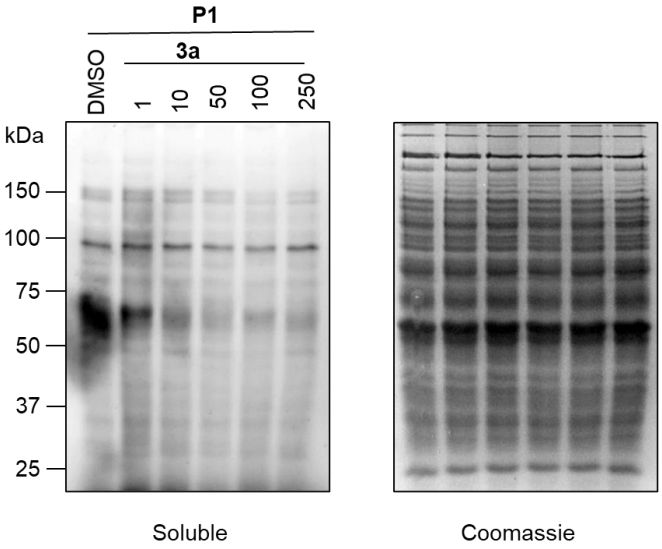

Figure 3. 7 Chase experiment - In vitro modification of proteins in membrane fraction of A. buamannii with 3a chased with P1

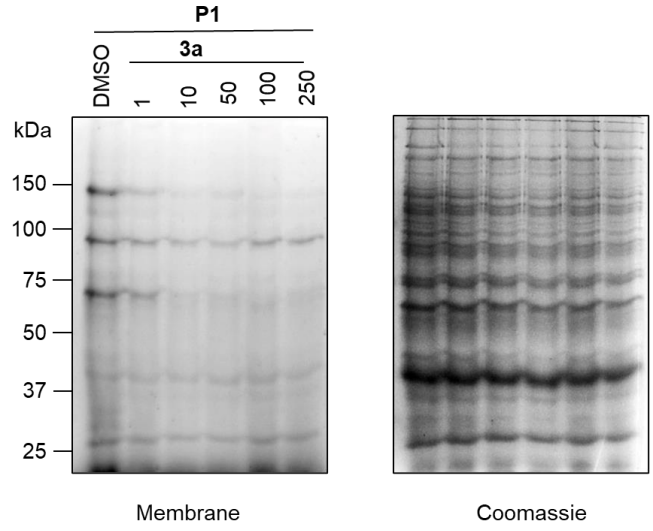

The selectivity of probe **P1** towards cysteine residues in *E. coli* was determined in Chapter **2**. In *A. baumannii*, a similar experiment was conducted, and the soluble proteome of *A. baumannii* was first treated with iodoacetamide (**IAM**, 10 mM, 1 h), then incubated with probe **P1** (100 µM, 1 h). A click reaction was performed with reporter rhodamine azide and visualized after SDS-PAGE. When compared to labelled proteins treated with **P1** alone, a complete

abruption or reduced signal for labelling of proteins was seen in the case of the **IAM**-pretreated sample. This study suggests that probe **P1** modifies the cysteine residue of proteins in *A. baumannii* proteome as well.

Figure 3. 8 Chase experiment - In vitro modification of proteins in soluble fraction of A. baumannii with P1

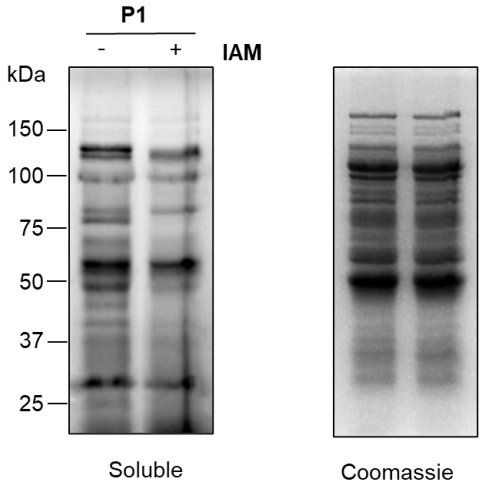

3.2.3. Target Identification of 3a using competitive LC-MS/MS-based ABPP experiment:

Next, a competitive LC-MS/MS based ABPP experiment was carried out to identify the target of **3a** in *A. baumannii* proteome using the similar protocol described in Chapter **2**. Compound **3a** (250 µM) or DMSO pre-treated proteome of *A. baumannii* was labelled with probe **P1** (100 µM), followed by biotin incorporation using click reaction with biotin azide on this alkyne labelled proteins. Next, streptavidin beads enrichment was done to pull down all biotinylated protein from the protein pool. Further, on bead trypsin digestion was performed for 16 h to cleave these proteins into smaller peptides to identify them using LC-MS/MS based analysis.

Table 3. 6 Identified targets of 3a in A. baumannii

Entry	Accession	Name	log_2 FC	- log_{10} (p value)
1	WP_000840835.1	Glutamate synthase subunit β (gltD)	3.38234	2.370173
2	WP_001286300.1	betaine aldehyde dehydrgenase (betB)	2.961814	3.863535
3	WP_136040424.1	FAD-dependent oxidoreductase	2.776662	1.905118
4	WP_171249601.1	alkyl hydroperoxide reductase subunit F (ahpF)	1.477672	2.4707
5	WP_000258957.1	TPM domain-containing protein	1.04138	1.329168

A filter criterion was followed to list out the probable targets of **3a**, where a highly significant (lower p-value) relative ratio [Fold Change (FC) = DMSO/**3a**] of DMSO and **3a** treated proteins was considered to be ≥2. After fulfilling the filtering criteria, five target proteins were listed out for **3a** in the soluble proteome of *A. baumannii* (Table 3.6). The majority of these are redox proteins with NADH as a cofactor, which is similar to our findings for DPIC targets in *E. coli*. Among these identified proteins, the most likely protein targets such as glutamate synthase subunit *β* (gltD) and betaine aldehyde dehydrogenase (betB) are essential for bacterial survival. Enzyme betB, which belongs to the aldehyde dehydrogenase family, is involved in the biosynthesis of glycine betaine.[20,21] This enzyme irreversibly oxidizes the betaine aldehyde to glycine betaine. Glycine betaine is an osmoprotectant, which protects the bacterial cells against environmental stress or drought conditions. Thus, inhibition of betB would also block the oxidation of betaine aldehyde, which itself is toxic to the bacterial cells. On the other hand, gltD is involved in the L-glutamate biosynthesis pathway and the amino acid synthesis pathway.[22,23] Thus, inhibition of this protein would cost the synthesis of essential amino acids

required for protein synthesis. It would eventually increase the susceptibility of *A. baumannii* towards antibiotics.

Also, betB has one catalytic active cysteine residue and glutamate synthase has four cysteine residue which are involved in the coordination of iron sulfur cluster. In Chapter **2**, a possible mechanism of reaction of DPIC with cysteine residue of protein was postulated, where the cystine residue reacts with iodonium centre and form a neutral adduct, which further may undergo a reductive elimination to produce a thiyl radical (R-S$^{\bullet}$) and an aryl radical (Ar$^{\bullet}$); recombination of these radicals (Figure 2.21) produces the covalent adduct. Here, in similar way, compound **3a** may covalently modify these cysteine residues and inactivate the proteins. Hence, the adduct formation is expected to depend on the electrophilic nature of the iodonium functional group, C–I bond strength, as well as radical stability. Orbital calculations show that the LUMO of **1a** was 26.16 meV while the LUMO for **2a** and **3a** were 13.97 meV and 24.85 meV, respectively suggesting the order of reactivity with nucleophile as **1a**>**3a**>**2a** (Figure 3.10). In order to understand the propensity of iodonium salts to undergo reduction, cyclic voltammetry analysis on **1a** was conducted. As expected, an irreversible reduction process and a potential of –0.853 V was obtained (Figure 3.11) while no significant oxidation step was observed. A similar CV profile for **3a** was obtained with a slightly lower reduction potential of –0.711 V, suggesting a higher propensity for this compound to undergo reduction when compared with **dpI**.

Figure. 3.9. Minimized energy structures of (A) dpI (1a), (B) hpI (2a) and (C) dhI (3a) calculated by RB3LYP/STO-3G

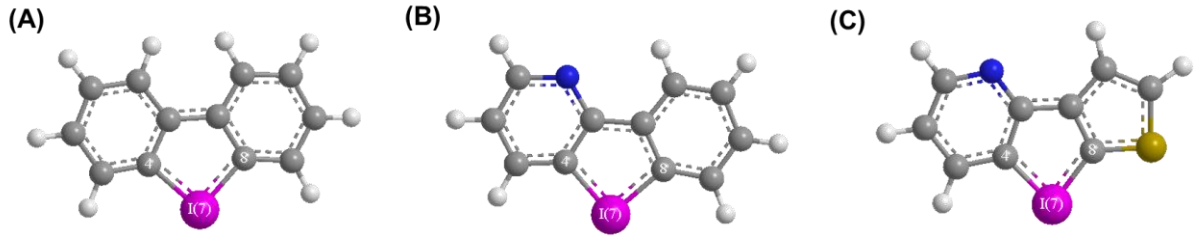

LUMO energy obtained for **dpI**, **hpI** and **dhI** were 26.16 meV, 13.97 meV and 24.85 meV respectively. Although all the molecules exhibited planarity, the C-I bond lengths of **dhI** are slightly shortened compared to corresponding bond lengths of **dpI** and **hpI**. While the theoretically calculated bond lengths of C(4)-I(7) and C(8)-I(7) for **dpI** and **hpI** were 2.00 Å and 2.00 Å respectively, the C(4)-I(7) and C(8)-I(7) bond lengths of 1.99 Å and 1.89 Å were obtained for **dhI**.

Figure 3.10: Cyclic voltammogram of (A) reversible redox reaction of ferrocene; (B) DMSO, (C) 1a and (D) 3a

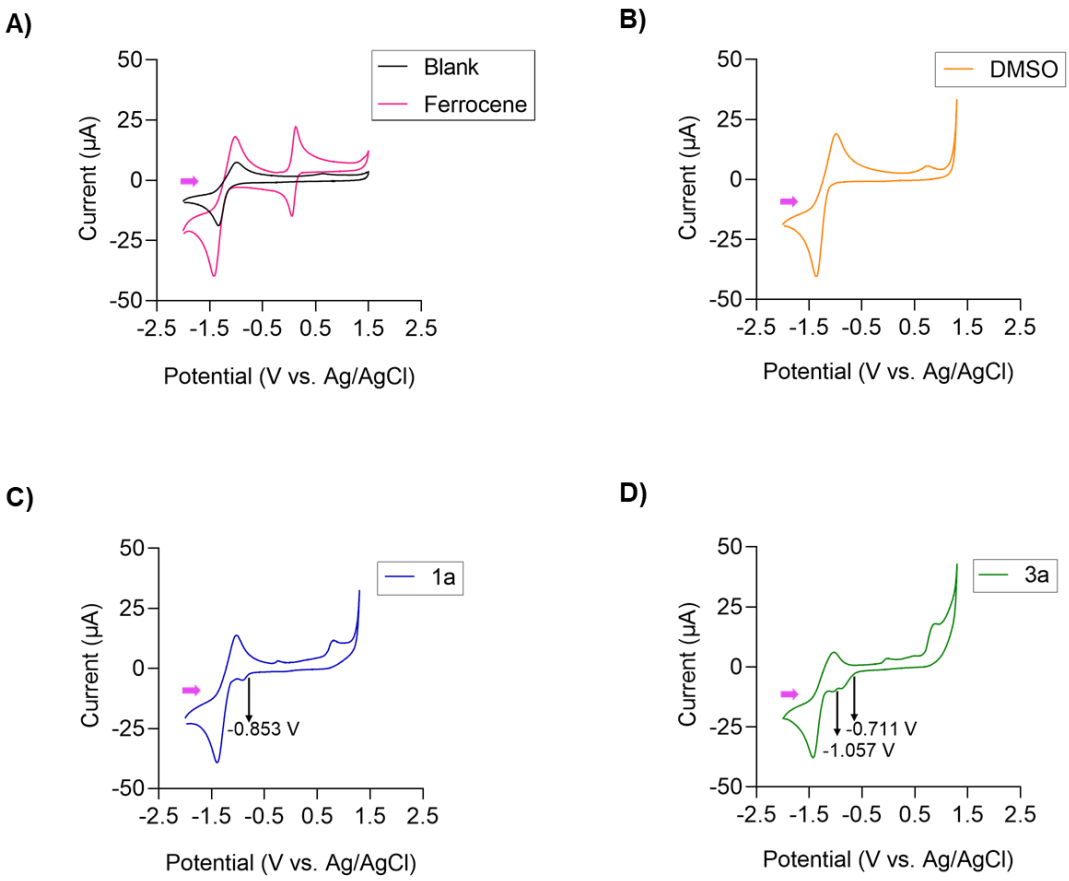

The experiment was conducted following conditions: glassy carbon as working electrode, platinum electrode as counter electrode and Ag/AgCl as reference electrode with an initial positive scan (represented by a pink arrow) at a rate of 100 mV/s; sample interval = 1 mV; quiet time = 2 s; sensitivity = 1e-5 A/V; 0.1 M TBAP as the background electrolyte in dry ACN purged with Argon for 2 min. The final concentration of the analytes was 0.5 mM. The onset reduction potentials are shown with arrows in the voltammogram. Blank indicates 0.1 M TBAP in ACN solution.

These findings suggest that compound **3a** exhibits bactericidal activity by reacting with and modifying essential proteins of *A. baumannii*, indicating it as a promising therapeutic antibacterial candidate.

3.3. Summary:

The SAR study of iodonium compounds with a goal of enhancing activity against *A. baumannii* was carried out. Diphenyleneiodonium loses its potency against ESKAP pathogens when a polar group, such as carboxylic acid, is introduced to it. Next, a series of heterocyclic iodonium

compounds were synthesized using the favourable drug-like properties of pyridine and thiophene to boost the antibacterial activity. Compared to DPIC, the pyridine derivative of DPI showed a significant increase in activity against ESKAP pathogens. The pyridine thiophene derivative was the most potent inhibitor of *A. baumannii*. Compounds **3a** and **3b** were found to have a favorable selectivity index. Compound **3a** was selected for further studies. When tested against patient-derived clinical isolates of MDR *A. baumannii*, compound **3a** showed equipotent action similar to the well-known antibiotic Polymixin B. Time kill kinetic study revealed that compound **3a** displayed bactericidal activity against *A. baumannii*. Next, *in vivo* efficacy of compound **3a** was investigated using a neutropenic thigh infection model. Compound **3a** significantly reduced *A. baumannii*-induced bacterial load in mice. Using chemoproteomics methods, the targets of **3a** in *A. baumannii*, much like in *E. coli*, were found to be redox proteins containing NADH as a cofactor. The two most likely protein targets are glutamate synthase subunit (gltD) and betaine aldehyde dehydrogenase (betB), which are engaged in critical cellular metabolism and inhibition of these proteins is therefore expected to have a major impact on cell survival

3.4. Experimental and characterization Data:

These compounds (**1a**-**1e**) were synthesized according to previously reported work.[24,25]

3.4.1. Procedure for synthesis of 2-(thiophen-3-yl)pyridin-3-amine (15):

To a stirred solution of 2-chloropyridin-3-amine (1g, 1.0 eq.) in EtOH (15 mL) were added arylboronic acid (1.2 eq.), K_3PO_4 (2.5 eq.) and $Pd(PPh_3)_4$ (0.05 eq.). The reaction was refluxed for 16 h under a nitrogen atmosphere. After completion of the reaction as monitored by TLC, the reaction mixture was cooled down to RT and EtOH was removed by rotary evaporation. The residue was dissolved in EtOAc and filtered through celite. The mixture was extracted with EtOAc (3 × 10 mL), and the combined organic layers were washed with H_2O and brine, filtered through anhydrous Na_2SO_4, concentrated by rotary evaporation. The crude product was purified by column chromatography on a silica gel to afford **15** as a yellow liquid.

3.4.2. Procedure for synthesis of 3-iodo-2-(thiophen-3-yl)pyridine (16):

To a stirred solution of **15** (1.0 eq.) in anhydrous MeCN (10 mL) was added *p*-TsOH (3.0 eq.) at 0 ^oC. A solution of $NaNO_2$ (2.0 eq.) and KI (2.5 eq.) (dissolved in a minimum amount of water) was added dropwise to the reaction mixture. Then the reaction mixture was stirred for the next 10 min at 0 ^oC and 12 h at RT. After completion of the reaction as monitored by TLC, H_2O was added to the reaction mixture and quenched with $NaHCO_3$ until pH became 9. Then $Na_2S_2O_3$ was added and the colour of the solution turned to light orange. The organic components were extracted with Et_2O (3 X 15 mL) and collected organic phases were filtered through anhydrous Na_2SO_4, concentrated under vacuum to obtain the crude product as a yellow-coloured residue. The residue was purified by column chromatography on neutral alumina using EtOAc: Hexane (0:100 to 5:95) as the mobile phase to afford **16** as a dark brown liquid.

3.4.3. Procedure for synthesis of thieno[3',2':4,5]iodolo[3,2-b]pyridin-8-ium trifluoromethanesulfonate (3b):

To a stirred solution of **16** (1 eq.) in anhydrous CH_2Cl_2 (5 mL) were added *m*-CPBA (1 eq.) and TfOH (3 eq.). The reaction mixture was stirred for 1 h at 0 ^oC, and DCM was removed by rotary evaporation. To the residue, Et_2O was added, and the mixture was stirred for 20 min and then filtered. The obtained solid was washed with ice-cold H_2O and Et_2O three times, dried in a vacuum to afford **3b** as a grey-white solid

3.4.4. Procedure for synthesis of thieno[2',3':4,5]iodolo[3,2-b]pyridin-4-ium chloride (3a):

To a stirred solution of **16** (1 eq.) in anhydrous CH_2Cl_2 (5 mL) were added *m*-CPBA (1 eq.) and TfOH (3 eq.). The solution was stirred for 1 h at 0 ^oC and DCM was removed by rotary evaporation. The residue was dissolved in HCOOH (0.5 mL).To this mixture was added saturated aq. NaCl (2 mL) and the mixture was stirred for 20 min at 0 ^oC, and then filtered. The collected solid was washed with ice-cold H_2O and Et_2O three times dried in a vacuum to afford **3a** as a grey-white solid.

3.4.5. Procedure for synthesis of 6-iodo-[1,1'-biphenyl]-3,3'-diamine (13):

To a stirred solution of **6** (400 mg, 1 eq.) and HBTU (470 mg, 1 eq.) in dry DMF (10 mL) were added trizma base (151 mg, 1.01 eq.) and DIPEA (1.1 mL, 5 eq.) under nitrogen atmosphere at RT. The reaction was stirred for 24 h. After completion of the reaction as monitored by TLC, dichloromethane was added and the mixture was extracted with DCM (3 × 10 mL). The combined organic layers were washed with H_2O and brine, filtered through anhydrous Na_2SO_4, concentrated by rotary evaporation. The crude product was purified by column chromatography on a silica gel to afford (0- 7% MeOH/$CHCl_3$)**13** as a brown liquid.

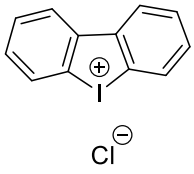

1a

dibenzo[b,d]iodol-5-ium chloride (1a):

^1H NMR (400 MHz, DMSO-d_6): δ 8.60 (d, *J* = 12.0 Hz, 2H), 8.43 (d, *J* = 8.0 Hz, 2H), 7.83 – 7.78 (m, 2H), 7.69 – 7.63 (m, 2H); ^{13}C NMR (100 MHz, DMSO-d6) δ 141.8, 131.1, 130.7, 130.6, 127.0, 121.7; HRMS Calcd for $C_{12}H_8I^+$ $[M]^+$: 278.9665 found $[M]^+$: 278.9675; FT-IR (υ_{max}, cm^{-1}) 3896, 3733, 3639, 2929, 2329, 1702, 645.

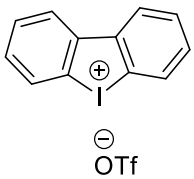

1b

dibenzo[b,d]iodol-5-ium trifluoromethanesulfonate (1b):

^{1}H NMR (400 MHz, DMSO-d_6) δ 8.52 – 8.48 (m, 2H), 8.23 (dd, *J* = 8.0, 0.7 Hz, 2H), 7.90 – 7.81 (m, 2H), 7.75 – 7.69 (m, 2H); ^{13}C NMR (100 MHz, DMSO-d6) δ 141.7, 131.1, 130.7, 130.6, 127.0, 121.7; HRMS Calcd for $C_{12}H_8I^+$ $[M]^+$: 278.9665 found $[M]^+$: 278.9675; ^{19}F NMR (400 MHz, DMSO-d_6) δ -77.75; FT-IR (υ_{max}, cm^{-1}) 3915, 3766, 3037, 2200, 1768, 642.

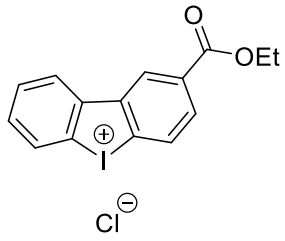

1c

2-(ethoxycarbonyl)dibenzo[b,d]iodol-5-ium chloride (1c): 78% yield; ^{1}H NMR (400 MHz, DMSO-d_6) δ: 9.09 (d, *J* = 1.3 Hz, 1H), 8.6 (d, *J* = 8.2 Hz, 1H), 8.52 (t, *J* = 8.4 Hz, 2H), 8.28 (dd, *J* = 4.1, 1.5 Hz, 1H), 7.85 (t, *J* = 7.5 Hz, 1H), 7.73 (t, *J* = 8.0 Hz, 1H), 4.38 (q, *J* = 7.1 Hz, 2H), 1.36 (t, *J* = 7.1 Hz, 3H); ^{13}C NMR (100 MHz, DMSO-d_6) δ: 164.4, 145.4, 140.3, 131.6, 131.4, 131.0, 130.8, 130.7, 130.6, 127.3, 126.2, 61.5, 14.2; HRMS Calcd for $C_{16}H_{12}IO_2^+$ $[M]^+$: 350.9876 found $[M]^+$: 350.9886.

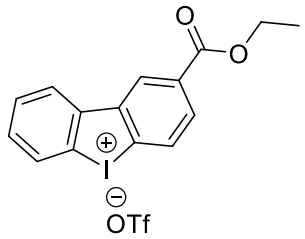

1d

2-(ethoxycarbonyl)dibenzo[b,d]iodol-5 ium trifluoromethanesulfonate (1d): 16 % yield; ^{1}H NMR (400 MHz, DMSO-d_6) δ: 8.81 (d, *J* = 1.5 Hz, 1H), 8.62 (d, *J* = 8.4 Hz, 1H), 8.58 (dd, *J* = 8.0, 1.6 Hz, 1H), 8.35 (dd, *J* = 8.2, 1.6 Hz, 1H), 8.26 (dd, *J* = 8.2, 0.9 Hz, 1H), 7.91 (dt, *J* = 7.6, 1.0 Hz, 1H), 7.79 (dt, *J* = 7.6, 1.4 Hz, 1H), 4.41 (q, *J* = 7.1 Hz, 2H), 1.38 (t, *J* = 7.1 Hz, 3H); ^{13}C NMR (100 MHz, DMSO-d_6) δ: 164.1, 145.8, 140.6, 132.1, 131.4, 131.1, 130.9, 130.7, 127.9, 126.9, 122.8, 121.9, 61.6, 14.1; ^{19}F NMR (400 MHz, DMSO-d_6) δ: -77.76; HRMS Calcd for $C_{16}H_{12}IO_2^+$ $[M]^+$: 350.9876 found $[M]^+$: 350.9886

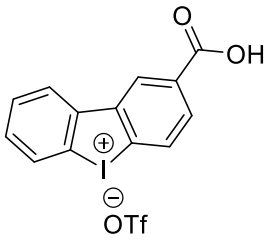

1e

2-carboxydibenzo[b,d]iodol-5-iumtrifluoromethanesulfonate (1e): 46% yield; ^{1}H NMR (400 MHz, DMSO-d_6) δ: 8.771 (d, *J* = 1.5 Hz, 1H), 8.58-8.53 (m, 2H), 8.30 (dd, *J* = 8.2, 1.5 Hz, 1H), 8.24 (dd, *J* = 8.2, 0.9 Hz, 1H), 7.91-7.87 (m, 1H), 7.79-7.75 (m, 1H); ^{13}C NMR (100 MHz, DMSO-d_6) δ: 165.7, 145.5, 140.7, 132.6, 132.0, 131.6, 131.3, 130.9, 130.7, 127.8, 126.8, 122.7, 121.8.

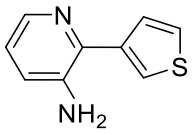

15

2-(thiophen-3-yl)pyridin-3-amine (9): 45% yield; ^{1}H NMR (400 MHz, $CDCl_3$) δ: 8.10 (dd, *J* = 3.7, 2.2 Hz, 1H), 7.70 (dd, *J* = 4.5, 1.2 Hz, 1H), 7.53 (dd, *J* = 4.9, 1.2 Hz, 1H), 7.43 (dd, *J* = 5.0, 2.8 Hz, 1H), 7.07-7.02 (m, 2H), 3.92 (s, 2H); ^{13}C NMR (100 MHz, $CDCl_3$) δ140.9, 140.2, 140.1, 140.0, 128.2, 126.2, 123.9, 123.0, 123.0; HRMS Calcd for $C_9H_8N_2S^+$ $[M+H]^+$: 177.0486 found $[M+H]^+$: 177.0486.

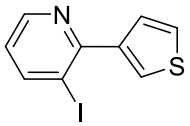

16

3-iodo-2-(thiophen-3-yl)pyridine (10): 53% yield; ^{1}H NMR (400 MHz, $CDCl_3$) δ 8.59 (dd, *J* = 4.6, 1.6 Hz, 1H), 7.81 (dd, *J* = 2.9, 1.2 Hz, 1H), 7.52 (dd, *J* = 5, 1.3 Hz, 1H), 7.37 (dd, *J* = 5.0, 2.9 Hz, 1H), 6.93 (dd, *J* = 7.9, 4.6 Hz 1H); ^{13}C NMR (100 MHz, $CDCl_3$) δ 156.9, 148.7, 148.1, 142.6, 128.9, 126.6, 125.0, 123.2, 93.7; HRMS Calcd for $C_9H_6INS^+$ $[M+H]^+$: 287.9344 found $[M+H]^+$: 287.9348.

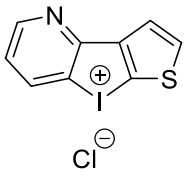

3a

thieno[2',3':4,5]iodolo[3,2-b]pyridin-4-ium chloride (3a): 67% yield: ^{1}H NMR (400 MHz, DMSO-*d6*) δ: 9.09 (dd, *J* = 9.0, 1.4 Hz, 1H), 8.80 (dd, *J* = 4.7, 1.4 Hz, 1H), 8.0 (d, *J* = 5.2 Hz, 1H), 7.74 (d, *J* = 5.3, Hz, 1H), 7.50 (dd, *J* = 8.3, 4.6 Hz 1H); ^{13}C NMR (100 MHz, DMSO-*d6*) δ: 154.1, 150.3, 146.5, 139.1, 135.6, 126.1, 124.0, 123.7, 123.1; HRMS Calcd for $C_9H_6INS^+$ $[M]^+$: 285.9182found $[M]^+$: 285.9193.

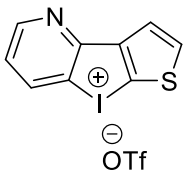

3b

thieno[3',2':4,5]iodolo[3,2-b]pyridin-8-ium trifluoromethanesulfonate (3b): 26% yield: ^{1}H NMR (400 MHz, DMSO-*d6*) δ: 8.91, (dd, *J* = 4.6, 1.2 Hz, 1H), 8.58 (dd, *J* = 8.5, 1.3 Hz, 1H), 8.17 (d, *J* = 5.4 Hz, 1H), 7.83 (d, *J* = 5.4, Hz, 1H), 7.60 (dd, *J* = 8.3, 4.6 Hz 1H); ^{13}C NMR (100 MHz, DMSO-*d6*) δ: 153.7, 151.1, 147.9, 139.1, 137.1, 124.5, 124.0, 122.3, 114.7; ^{19}F NMR (400 MHz, DMSO-*d6*) δ-77.75; HRMS Calcd for $C_9H_6INS^+$ $[M]^+$: 285.9182found $[M]^+$: 285.9197.

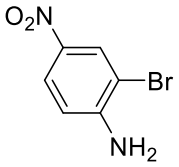

2-bromo-4-nitroaniline (17) 90% yield; ^{1}H NMR (400 MHz, $CDCl_3$) δ: 8.37 (d, *J* = 2.5 Hz, 1H), 8.03 (dd, *J* = 11.5, 2.5 Hz, 1H), 6.74 (d, *J* = 8.9 Hz, 1H), 4.83 (s, 2H); ^{13}C NMR (100 MHz, $CDCl_3$) δ: 149.9, 129.3, 125.0, 113.6, 107.1.

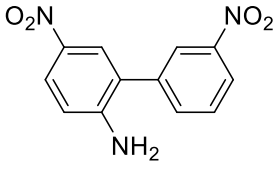

18

3',5-dinitro-[1,1'-biphenyl]-2-amine (18): 95% yiled; ^{1}H NMR (400 MHz, $CDCl_3$) δ: 8.27-8.23 (m, 2H), 8.02 (dd, *J* = 5.9, 2.7 Hz, 1H), 7.91 (d, *J* = 2.7 Hz, 1H), 7.90-7.88 (m, 1H), 7.77 (dt, *J* = 7.8, 0.5 Hz, 1H), 6.83 (d, *J* = 9.1 Hz, 1H), 6.60 (s, 2H); ^{13}C NMR (100 MHz, $CDCl_3$) δ: 152.5, 148.2, 138.7, 136.3, 135.8, 130.7, 127.0, 125.9, 123.8, 122.0, 114.4.

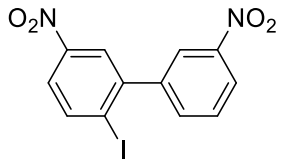

19

2-iodo-3',5-dinitro-1,1'-biphenyl (19): 17% yield; ^{1}H NMR (400 MHz, $CDCl_3$) δ: 8.39-8.33 (m, 2H), 8.27 (t, *J* = 1.9 Hz, 1H), 8.18 (d, *J* = 2.7 Hz, 1H), 7.99 (dd, *J* = 5.7, 3.5 Hz, 1H), 7.92-7.90 (m, 1H), 7.82 (t, *J* = 8.0 Hz, 1H); ^{13}C NMR (100 MHz, $CDCl_3$) δ: 147.7, 147.5, 145.0, 143.1, 141.0, 136.1, 130.1, 124.1, 124.0, 123.4, 108.4.

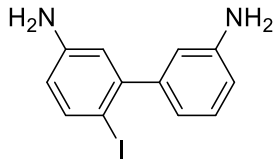

13

6-iodo-[1,1'-biphenyl]-3,3'-diamine (13)[26]**:** 65 %yield; ^{1}H NMR (400 MHz, $CDCl_3$) δ: 7.62 (d, *J* = 8.4 Hz, 1H), 7.18 (d, *J* = 7.7 Hz, 1H), 6.70-6.67 (m, 2H), 6.65 (d, *J* = 2.8 Hz, 1H), 6.62 (t, *J* = 1.8 Hz, 1H), 6.40 (dd, *J* = 5.6, 2.8 Hz, 1H), 3.72 (s, 4H); ^{13}C NMR (100 MHz, $CDCl_3$) δ: 147.5, 146.5, 146.0, 145.5, 139.9, 128.9, 119.7, 117.0, 116.1, 114.4, 83.9.

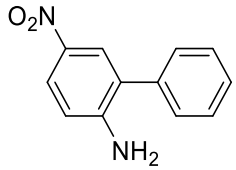

21

5-nitro-[1,1'-biphenyl]-2-amine (21): 60 %yield; ^{1}H NMR (400 MHz, $CDCl_3$) δ: 8.07-8.05 (m, 2H), 7.51-7.47 (m, 2H), 7.43-7.39 (m, 3H), 6.73-6.70 (m, 1Hz, 1H), 4.50 (s, 2H).

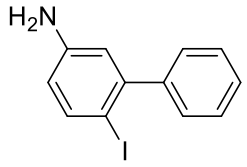

12

6-iodo-[1,1'-biphenyl]-3-amine (12): 53 %yield; ^{1}H NMR (400 MHz, $CDCl_3$) δ: 7.65 (d, *J* = 8.4 Hz, 1H), 7.41-7.36 (m, 3H), 7.33-7.30 (m, 2H), 6.67 (d, *J* = 2.8 Hz, 1H), 6.43 (dd, *J* = 8.5, 1.8 Hz, 1H), 3.06 (s, 2H).

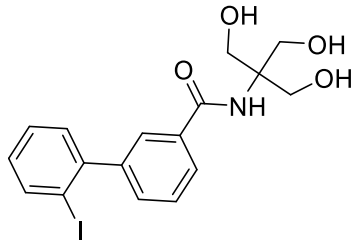

14

6-iodo-[1,1'-biphenyl]-3,3'-diamine (13)[26]**:** 37 %yield; ^{1}H NMR (400 MHz, DMSO-$_{d6}$) δ: 8.0 (dd, *J* = 4.5, 1.0 Hz, 1H), 7.87 (d, *J* = 8.4 Hz, 2H), 7.49 (td, *J* = 7.0, 1.2 Hz, 1H), 7.41 (d, *J* = 8.4, Hz, 2H), 7.38 (s, 1H), 7.34 (dd, *J* = 4.6, 1.6 Hz, 1H), 7.15 (dt, *J* = 7.7, 1.7 Hz, 1H), 4.77 (t, *J* = 5.8 Hz, 3H), 3.71 (t, *J* = 5.6 Hz, 6H); ^{13}C NMR (100 MHz, $CDCl_3$) δ: 166.9, 146.2, 145.2, 139.4, 134.4, 130.1, 129.6, 129.0, 128.6, 127.2, 98.4, 62.8, 60.3.

3.4.5. Protocols for ABPP experiments:

3.4.5.1. Preparation of proteomic fractions:

The Whole cell lysate of *A. baumannii* was received from our collaborator Dr. Sidhharth Chopra, CDRI Lucknow. To separate soluble and membrane protein fractions, it was fractionated using centrifugation at 100,000 g at 4 ºC for 1 hour. Soluble fractions were then separated from the membrane pellets.[27] The membrane pellets were washed, followed by re-suspension in 1X PBS. The protein concentration was measured by conducting either Bradford assay (Biorad) or BCA assay using BSA as a standard, and lysates were finally diluted to 1mg/mL protein concentration with 1X PBS, which was used for all further work.

3.4.5.2. Chase experiment:

100 µL of 1mg/mL protein for membrane and the soluble fraction was taken in a 1.5 mL microcentrifuge tube. 1 µL of a 100X stock solution of compound **3a** in DMSO was added and incubated for 60 min at 37 °C at 700 rpm. To the above solution, IAA or **P1** probe (1 µL of a 100X stock solution of the in DMSO) was added and incubated for 60 min at 37 °C at 700 rpm. A 'click' mixture (11 µL) consisting of a 6 µL TBTA (1.7 mM in 4:1 DMSO-^{t}BuOH), 2 µL $CuSO_4.5H_2O$ (50 mM in water), 2 µL TCEP (50 mM in DPBS - Dulbecco's PBS 1X), 1 µL Rhodamine azide (Alexa Fluor 488, 10 mM in DMSO), was added to every tube and incubated for 60 min at 25 °C at 700 rpm. The loading dye (4x, 40 µL) was added to every tube prior to loading the samples onto the gel.[28]

3.4.5.3. Mass spectrometry-based chemoproteomics:[29,30]

The soluble fraction (1 mL) was incubated with **3a** or vehicle (DMSO) at 250 µM final concentration for 1 hour at 37 °C at 700 rpm. Each group contained three biological replicates. The compound or vehicle treated soluble proteomes were chased with **P1** (100 µM, 1 hour at 37 °C, 700 rpm). The click reaction was done with biotin-azide. Post-biotinylation, the proteomes were denatured and precipitated using methanol: chloroform (4:1) at 4 °C, and re-suspended in urea (0.5 mL 6 M in DPBS) by sonication. Reduction and alkylation were carried out with TCEP (10 mM) for 30 mins at 37 °C with constant shaking, and IAM (50 mM) for 30 mins at room temperature (25°C) in the dark, respectively. The biotinylated proteins were enriched using avidin-agarose beads (100 µL, Sigma-Aldrich) by shaking at room temperature for 1.5 hours in DPBS containing 0.2% (w/v) SDS in a final volume of 6 mL. The beads were pelleted by centrifugation (1000 g, 25 °C, 5 min), and sequentially washed using 10 mL of 0.2% (w/v) SDS in DPBS (3X), 10 mL of DPBS (3X) and 10 mL of deionized water (3X). The beads were transferred to a Protein LoBind 1.5 mL microcentrifuge tube. On-bead protein digestion was performed using sequence grade trypsin (1.5 µg, Promega) in 200 µL of urea (2 M in 100 mM TEAB buffer) at 37 °C for 14 hours at 180 rpm. Reaction was quenched by adding TFA to final concentration of 1% (v/v). Peptides were cleaned on C18 Stage tips and subjected to LC-MS/MS analysis on Agilent 6540 Accurate-Mass Q-ToF mass spectrometer coupled with Agilent HPLC-Chip Cube system. Peptides were separated on Agilent HPLC-Chip consisting of C18 enrichment and analytical column (75 µm, 10 cm) system. The LC run was a 6 hours long linear acetonitrile gradient (5% to 50%). Mass spectrometry data was collected in an information dependent acquisition (IDA) mode over a mass range of 300 – 2000 m/z, and each full MS survey scan was followed by 10 fragment scans. Dynamic exclusion was enabled for all experiments (repeat count 1, exclusion duration 30 s). Protein identification and quantitation

was carried out using Protein Piolet software 5.0.2. Spectral data was searched against *A. baumannii* ATCC 17978 protein databases downloaded from NCBI FTP server. Precursor mass tolerance of 0.01 Da and fragment mass tolerance of 40 p.p.m. was allowed. The peptides and proteins were filtered at 1 % false discovery rate. Label free quantitation was performed using LFQ option in the Protein Piolet software 5.0.2. Protein LFQ intensity value was accepted only when two or more quantifiable peptides were identified in more than 2 replicates per experimental group. Quantitation was performed by taking a ratio of the average intensity with respect to control sample (DMSO treated).

HPLC trace of 3a:

Stock solutions of compound **3a** (10 mM in DMSO) was prepared. From the stock solution, an aliquot of compound **3a** (100 μM, 500 μL) in acetonitrile was prepared and HPLC analysis was conducted. A diode array detector (DAD) operating at 280 nm was used. An aliquot (100 μM in ACN, 25 μL) was injected and a mobile phase of water: acetonitrile (0.1 % HCOOH) was used. A multistep gradient was used with a flow rate of 1 mL/min and a run time of 20 min starting with 60:40 → 0 - 4 min, 60:40 to 20:80→ 4 - 12 min, 20:80 to 40:60 → 12 - 15 min, 40:60 to 60:40 → 15 - 18 min, 40:60 to 60:40 to 60:40→ 18 - 20 min. Retention time for **3a** was obtained at 1.5 min.

Figure 3. 11 HPLC trace of 3a (100 μM) in acetonitrile; The detector wavelength used was 280 nm.

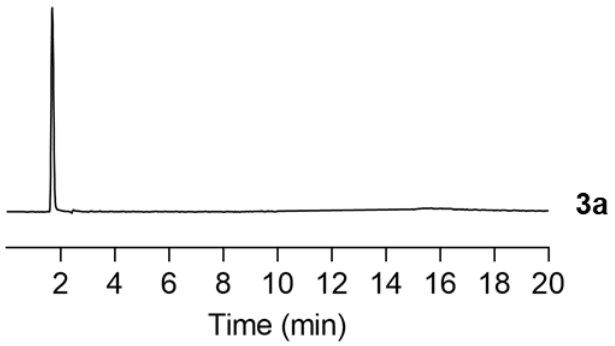

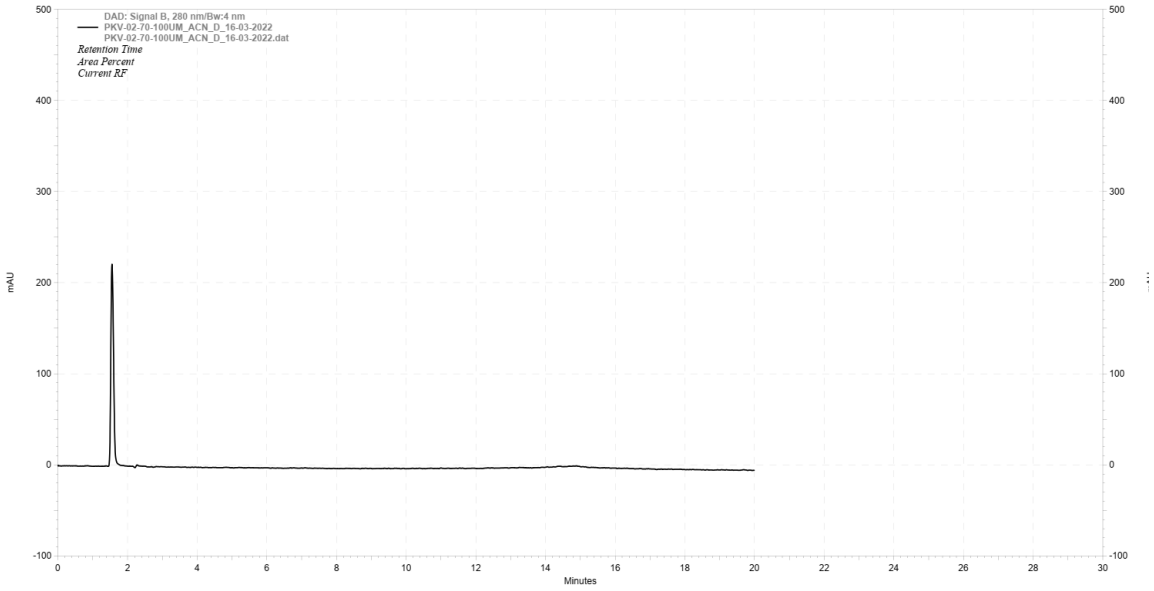

DAD: Signal B,
280 nm/Bw:4 nm
Results

Retention Time	Area	Area %	Height	Height %
1.087	1730	0.07	402	0.09
1.147	1299	0.05	376	0.08
1.267	850	0.03	314	0.07
1.387	4170	0.17	1012	0.21
1.553	2468806	98.66	462998	98.26
18.767	638	0.03	321	0.07
18.940	2547	0.10	668	0.14
19.060	1426	0.06	445	0.09
19.120	758	0.03	418	0.09
19.193	3227	0.13	921	0.20
19.353	1616	0.06	641	0.14
19.440	514	0.02	249	0.05
19.507	450	0.02	208	0.04
19.680	11033	0.44	1467	0.31
19.853	3162	0.13	749	0.16

Totals	2502226	100.00	471189	100.00

3.5. NMR Spectra:

^{1}H NMR of **1a**

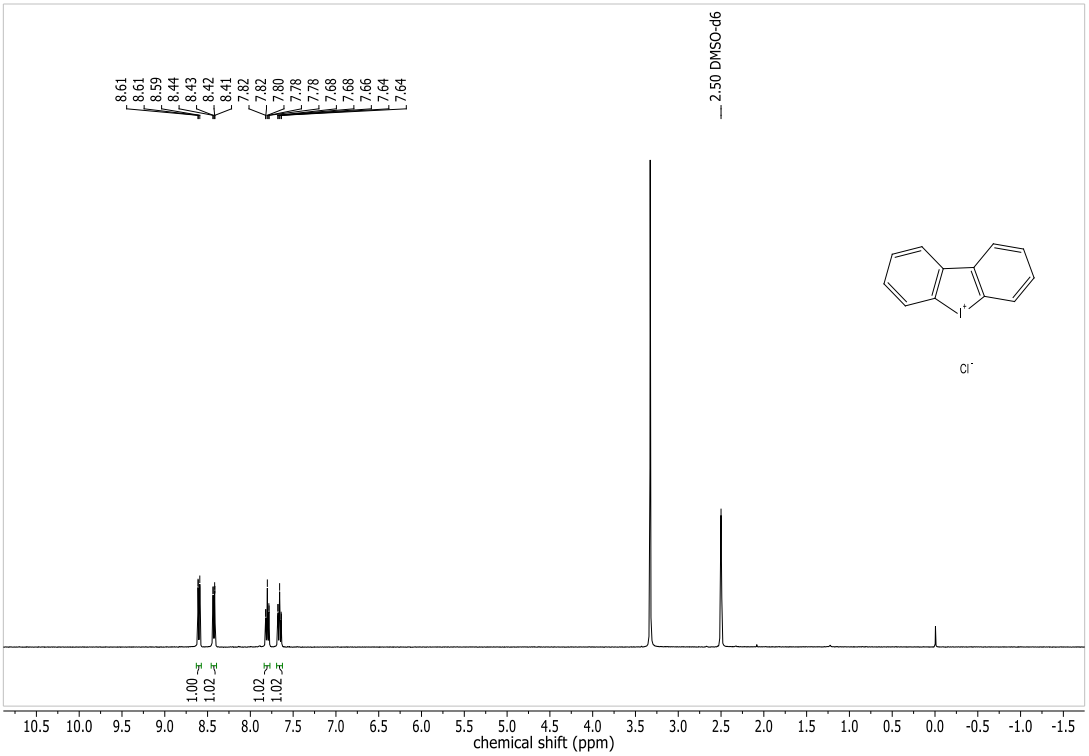

^{1}H NMR of **1b**

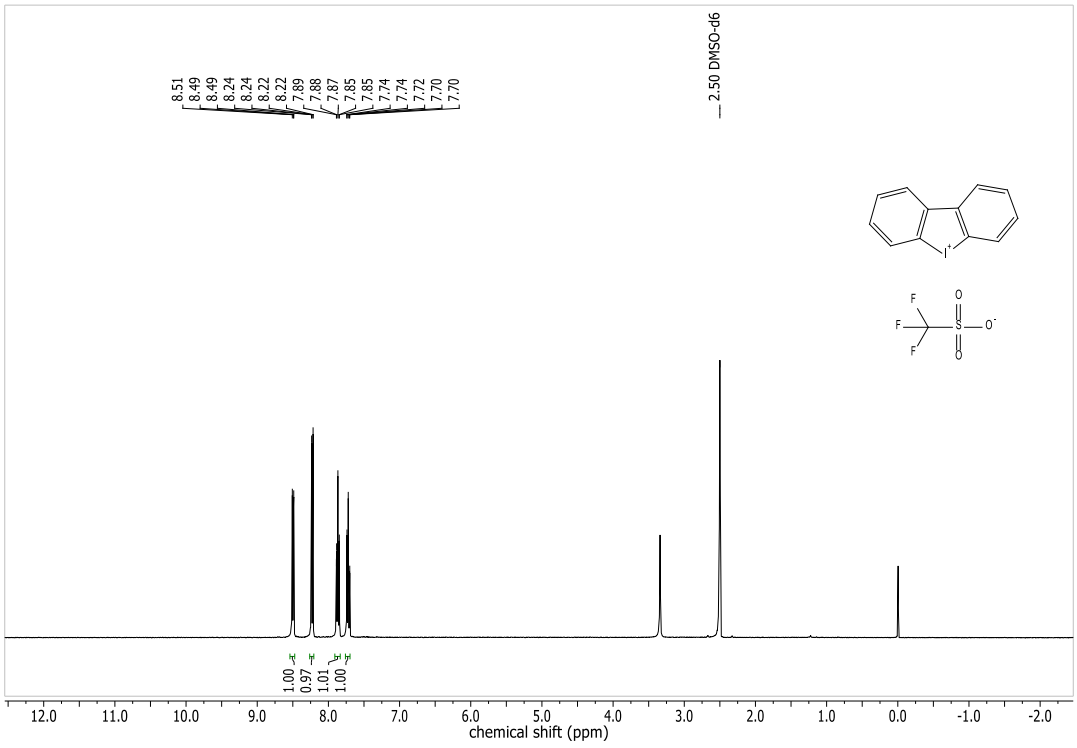

^{1}H NMR of **1c**

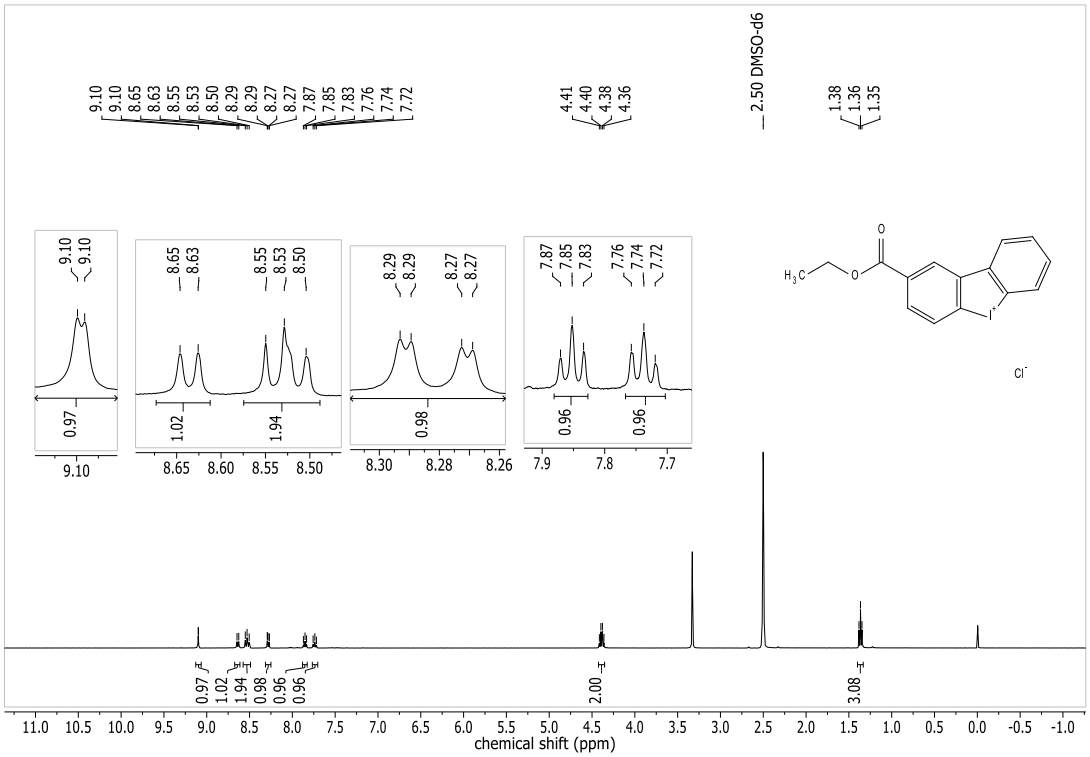

^{13}C NMR of **1c**

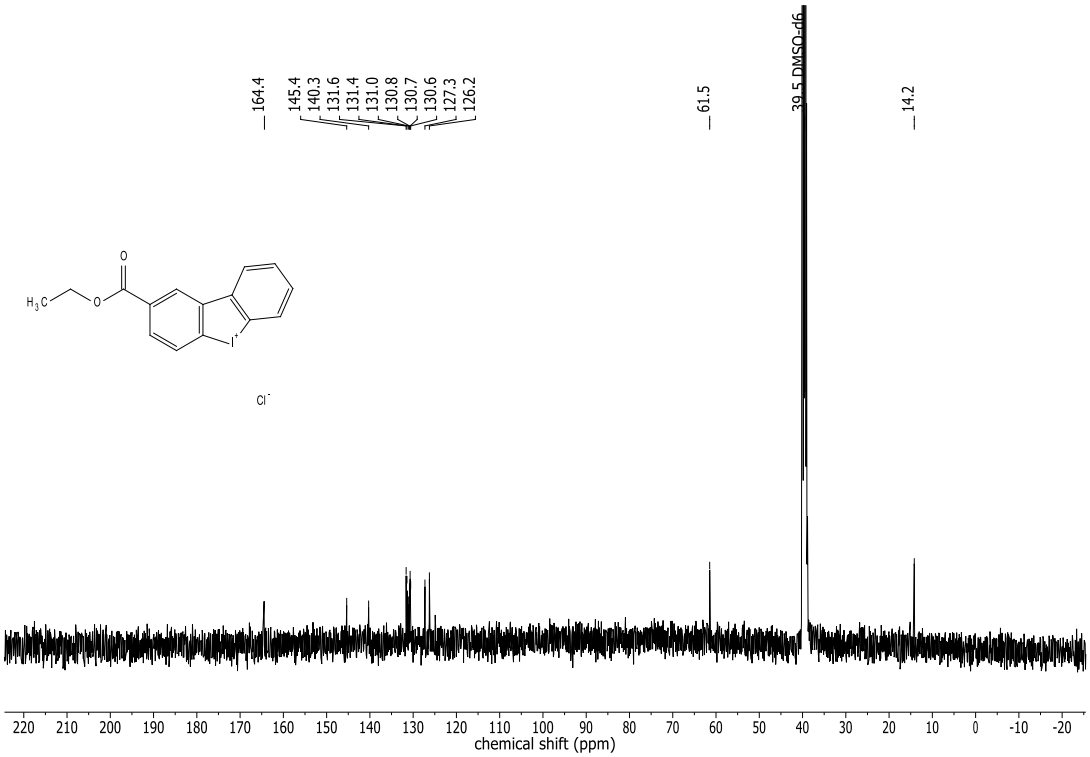

^{1}H NMR of **1d**

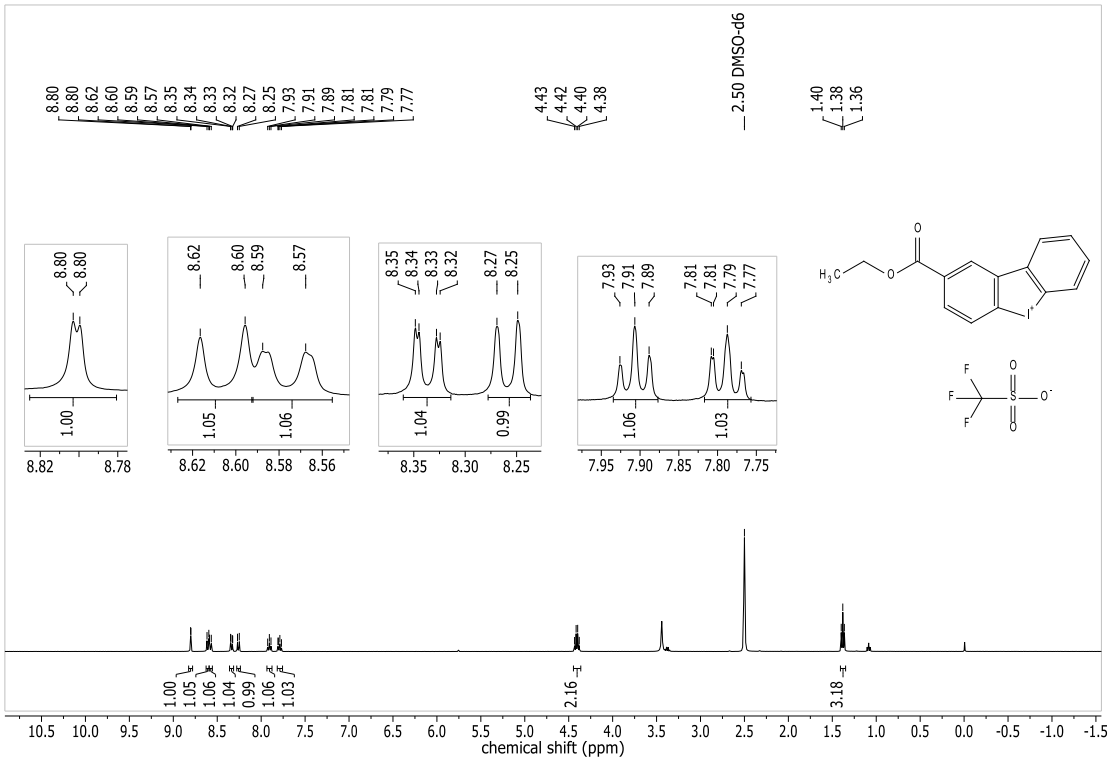

^{13}C NMR of **1d**

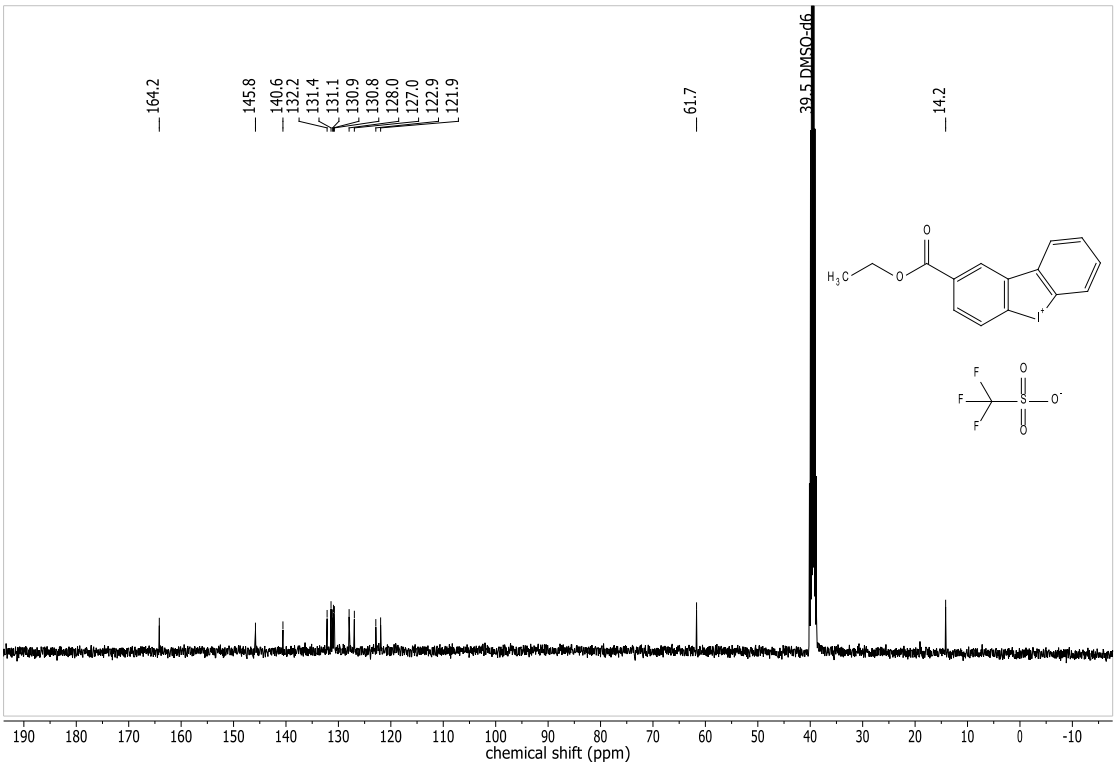

^{19}F NMR of **1d**

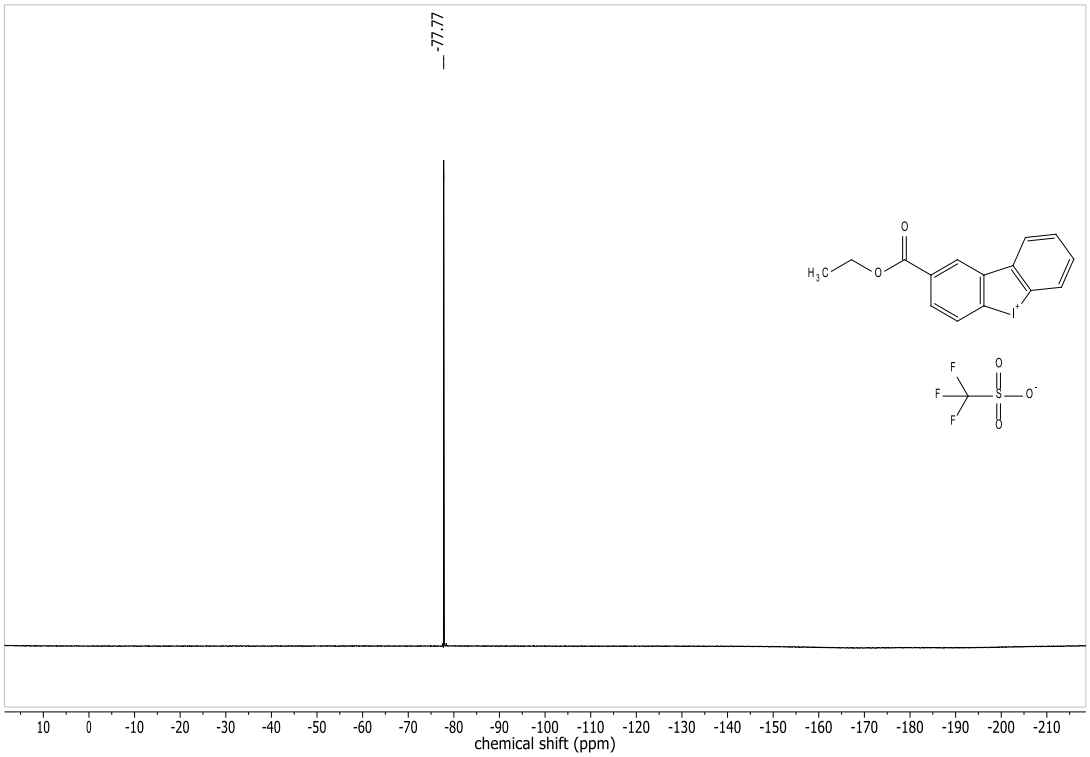

^{1}H NMR of **1e**

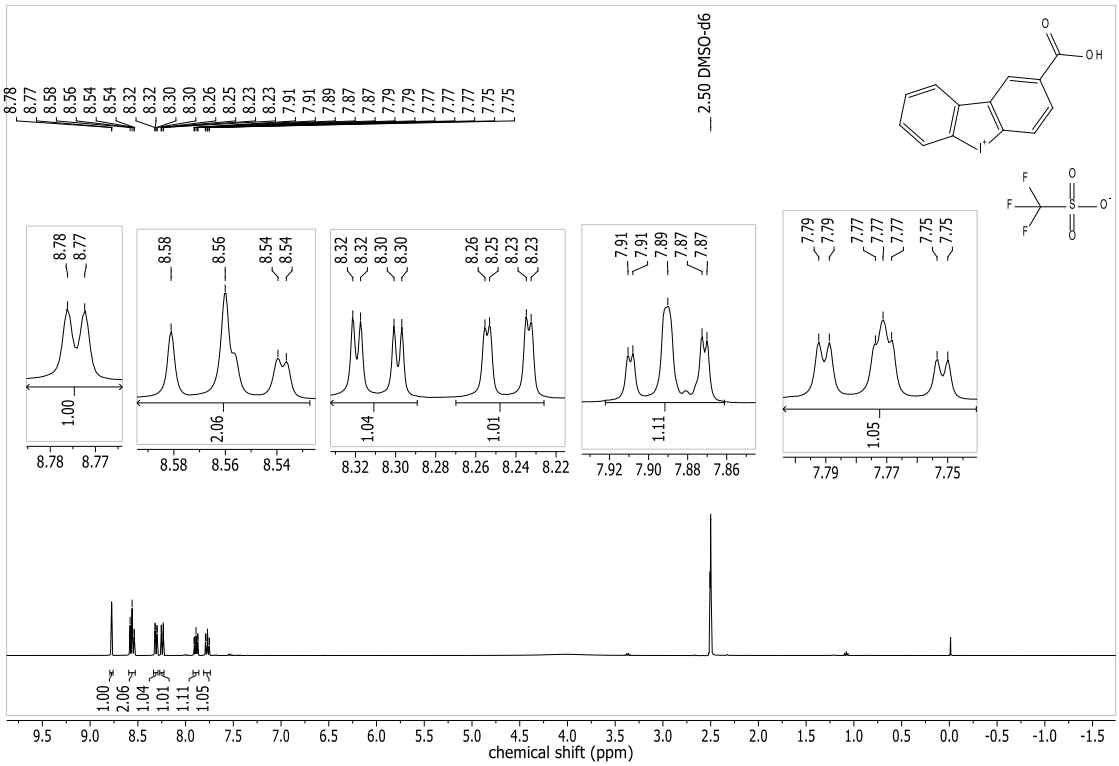

^{13}C NMR of **1e**

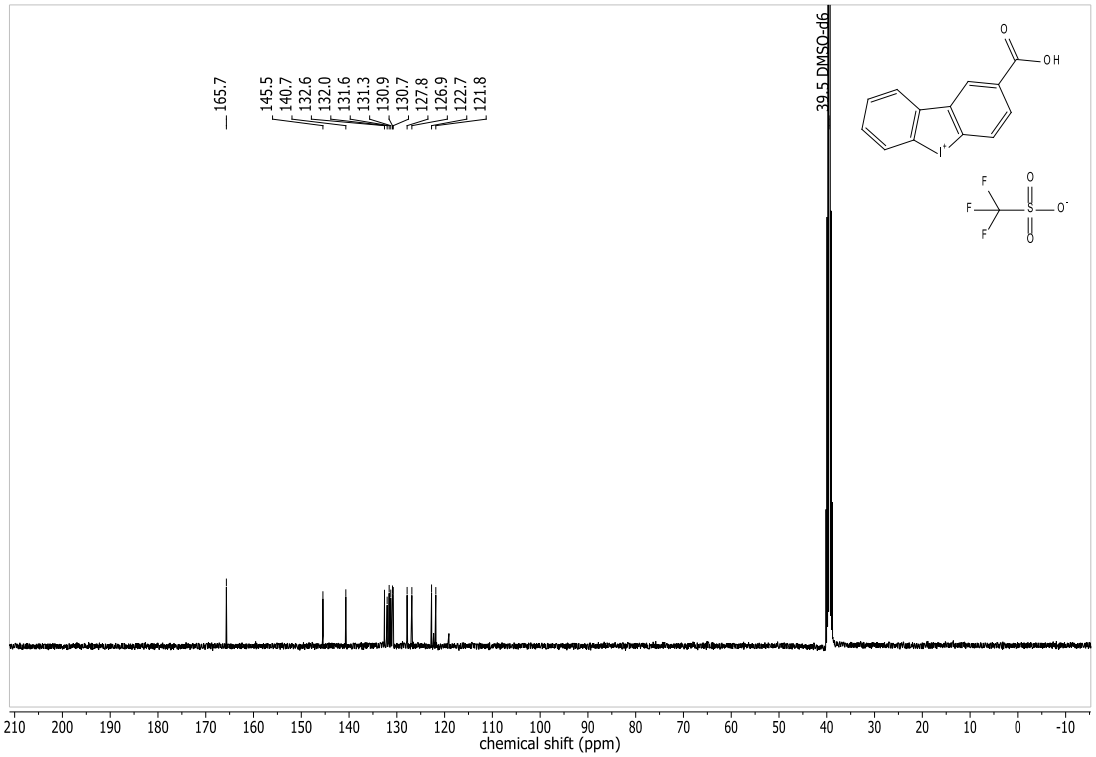

^{19}F NMR of **1e**

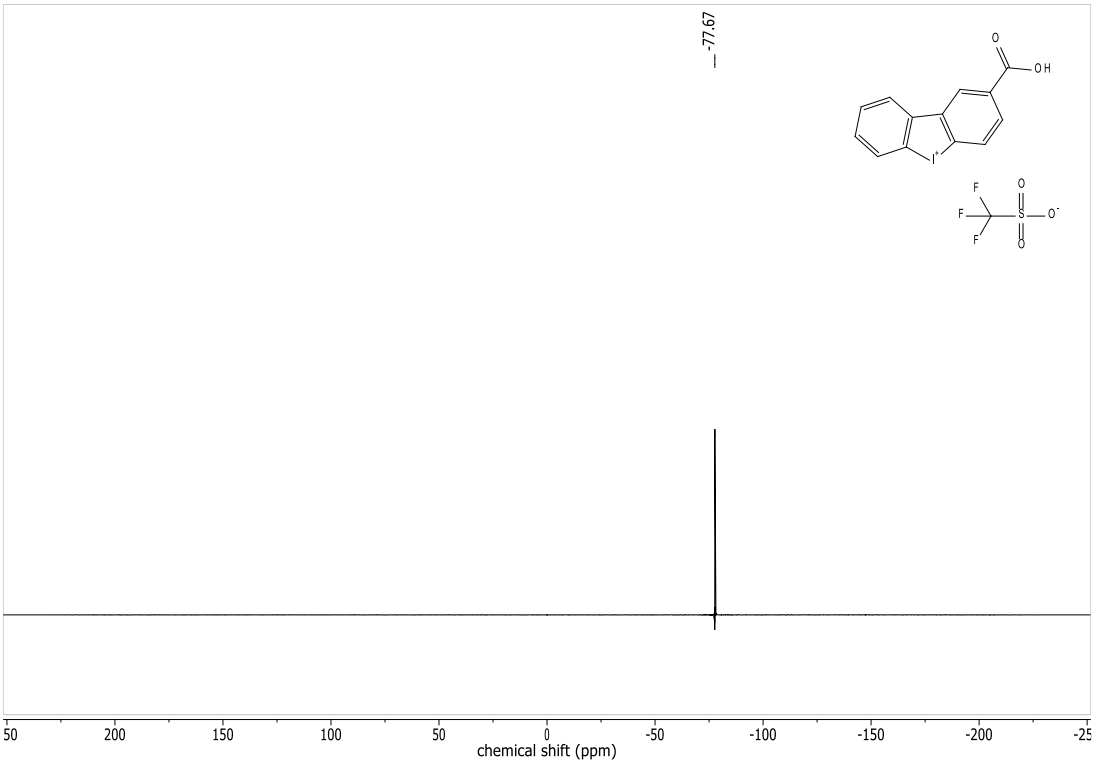

^{1}H NMR of **17**

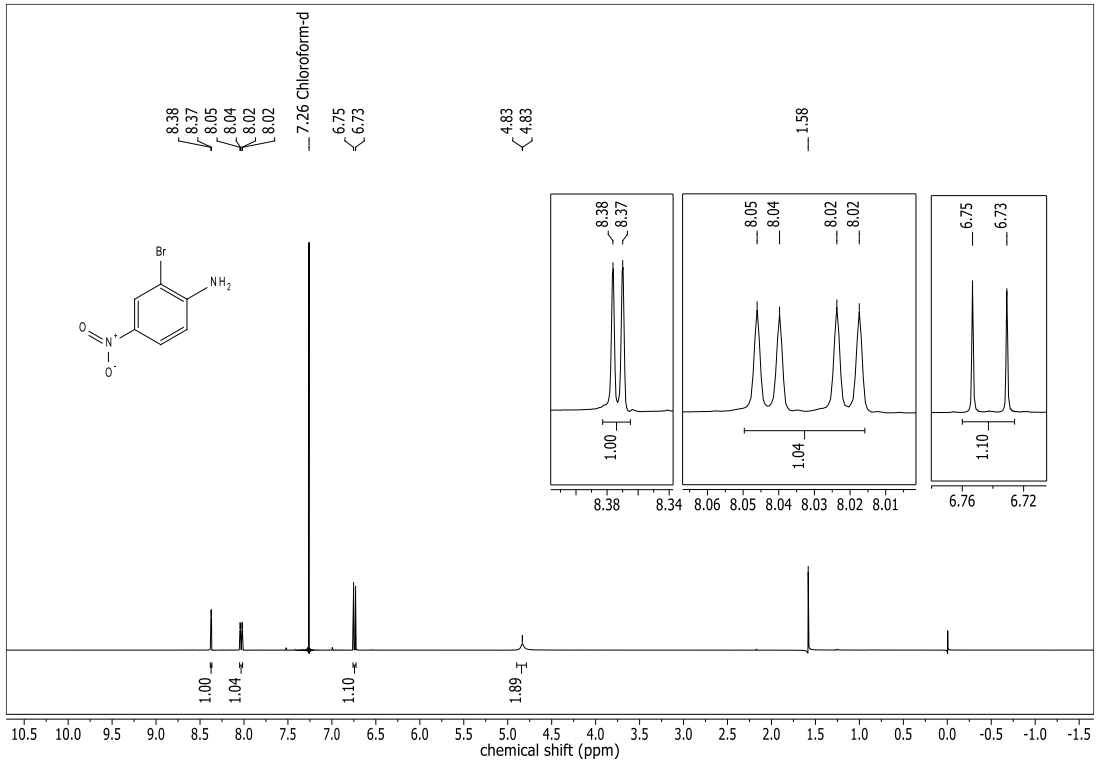

^{13}C NMR of **17**

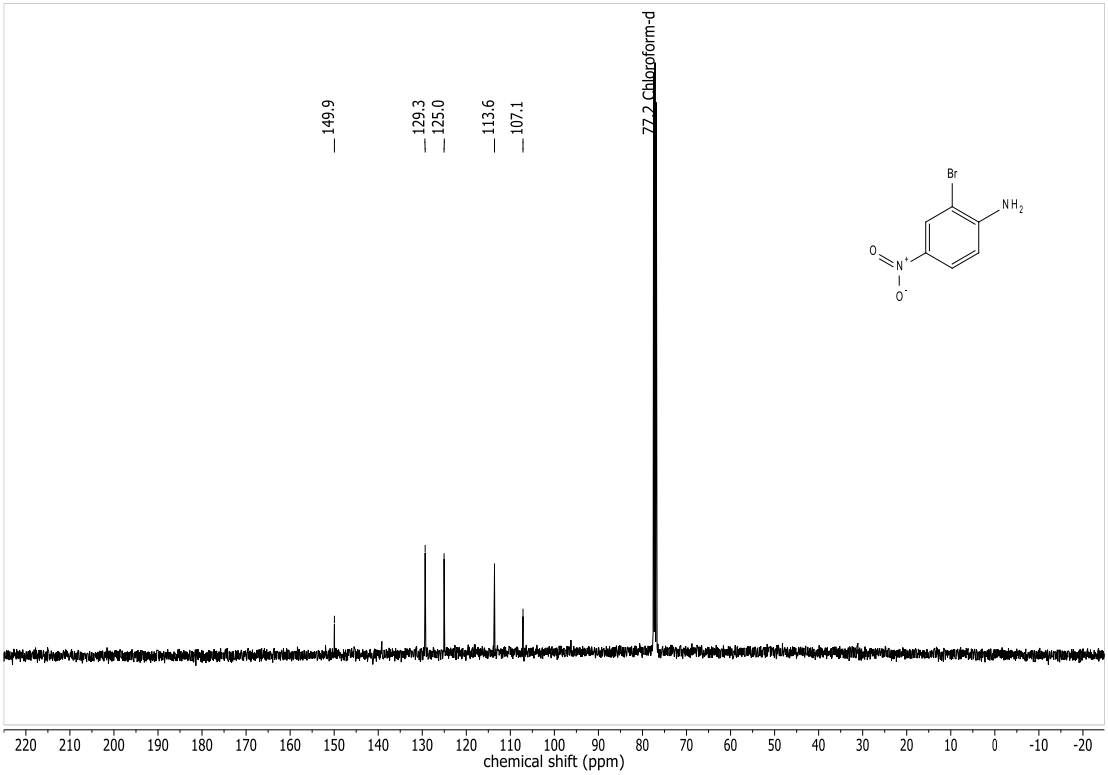

^{1}H NMR of **18**

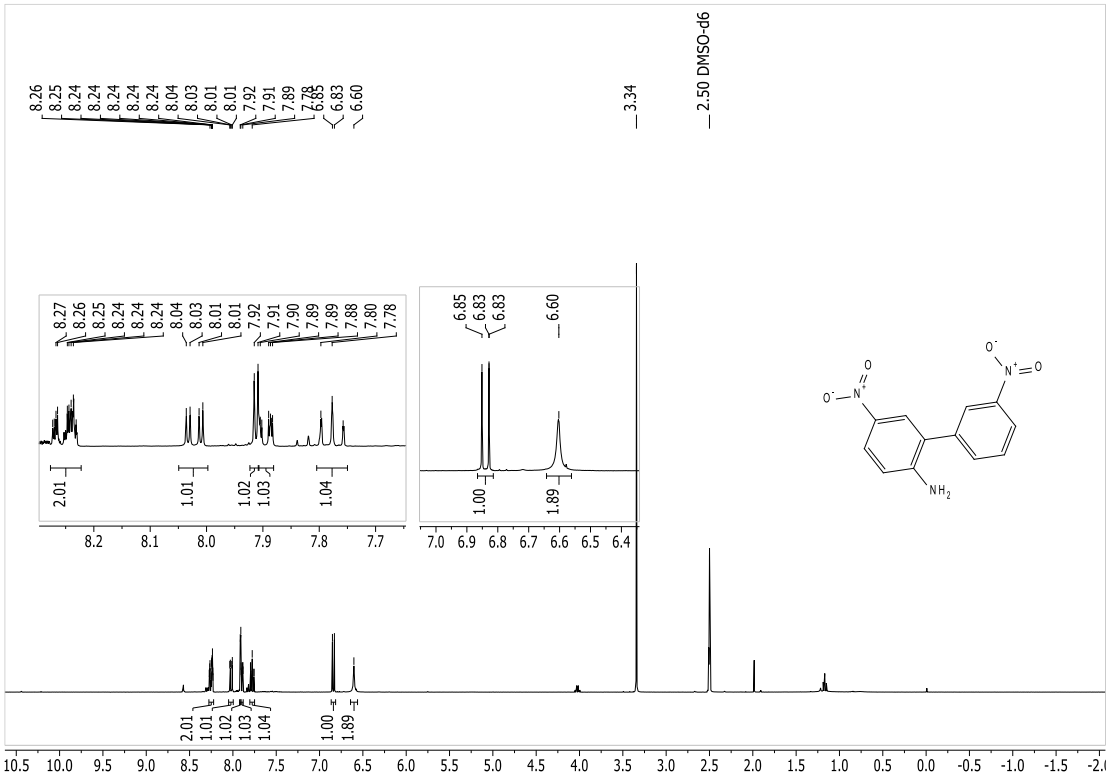

^{13}C NMR of **18**

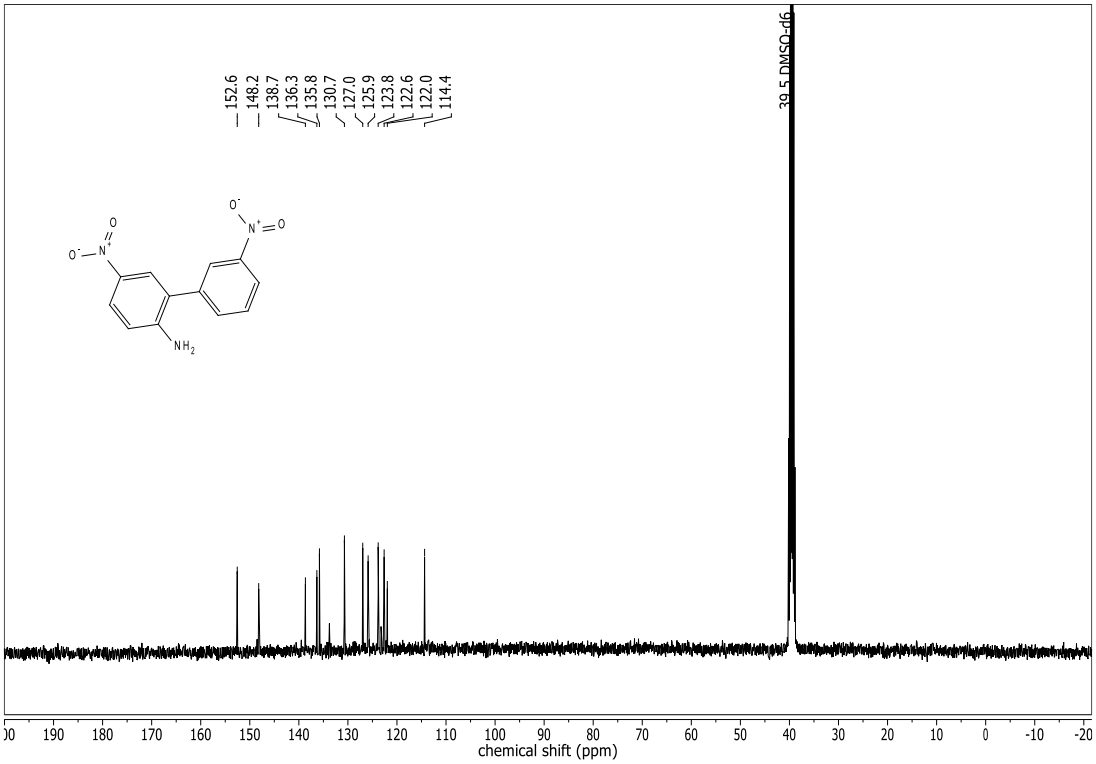

^{1}H NMR of **19**

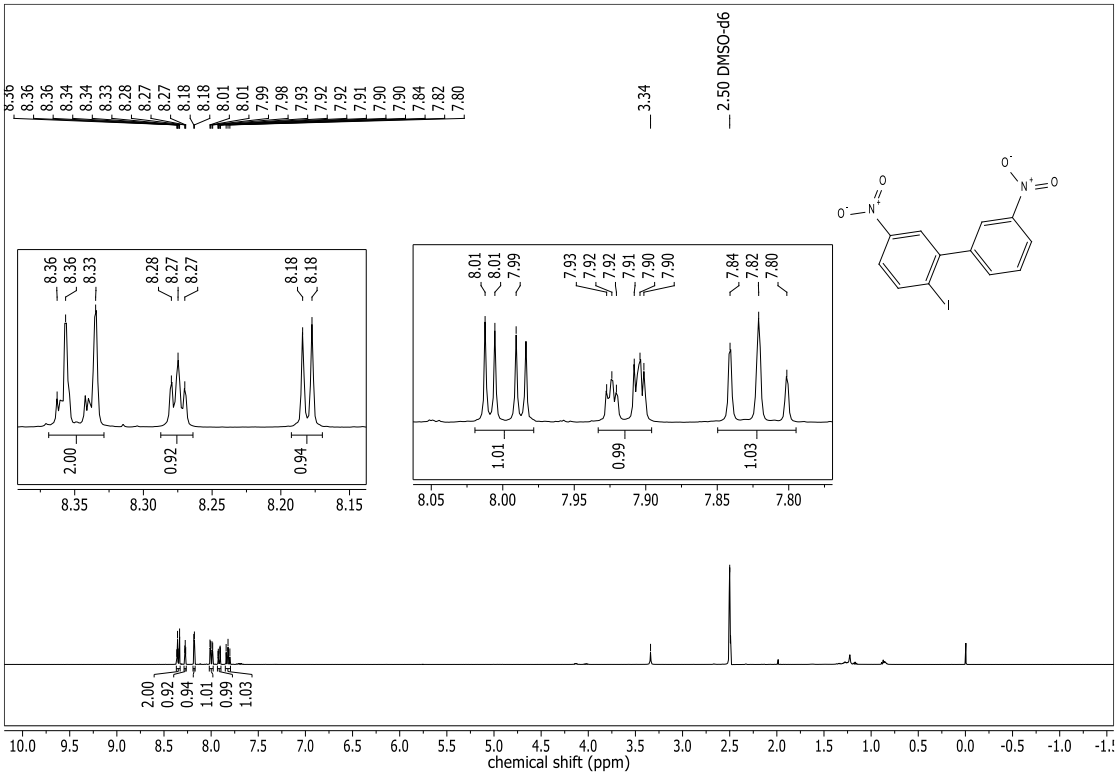

^{13}C NMR of **19**

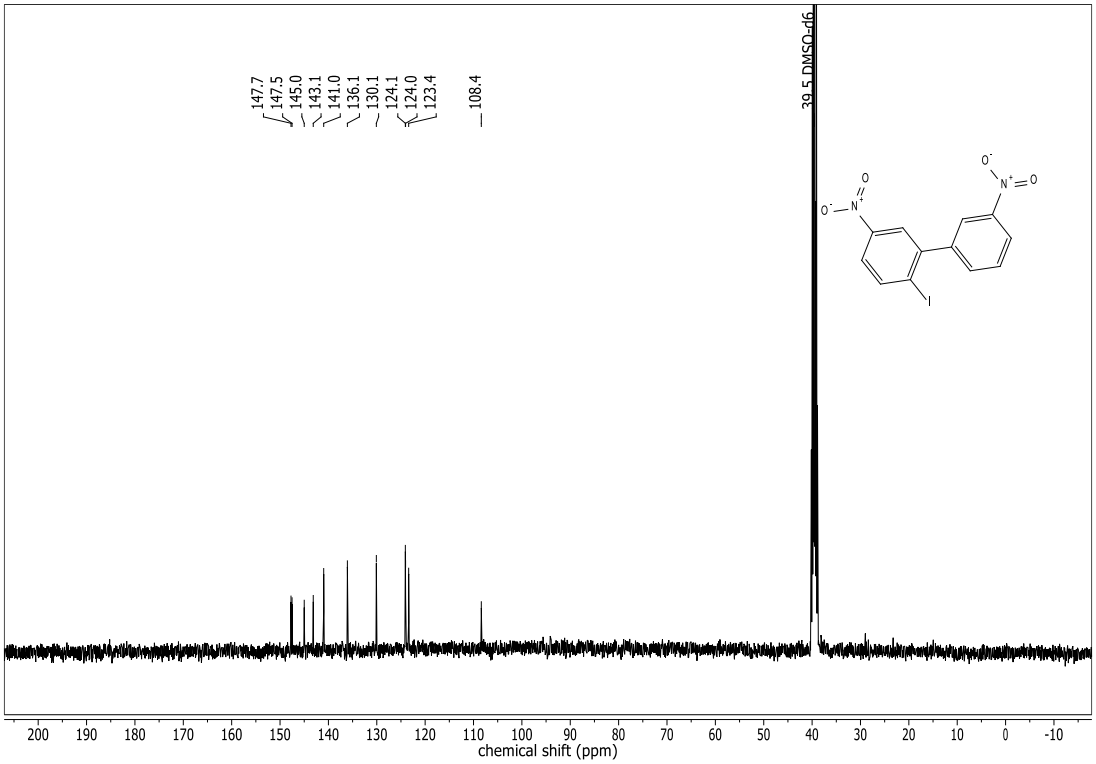

^{1}H NMR of 13

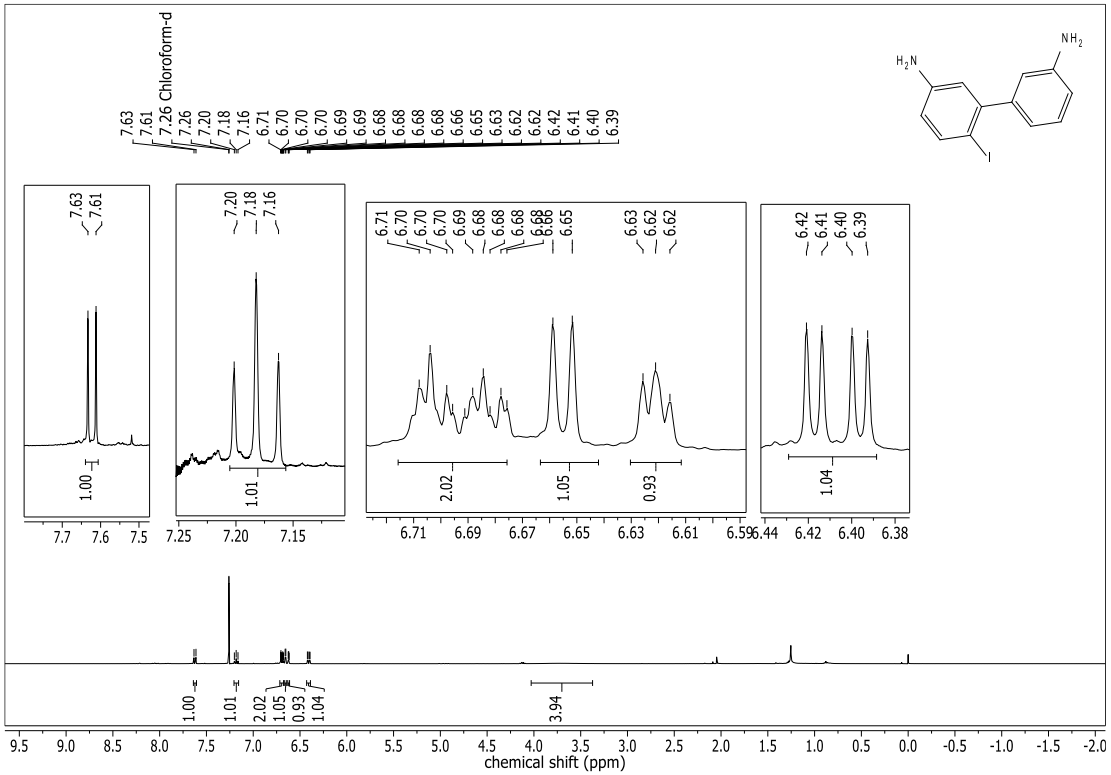

^{13}C NMR of **13**

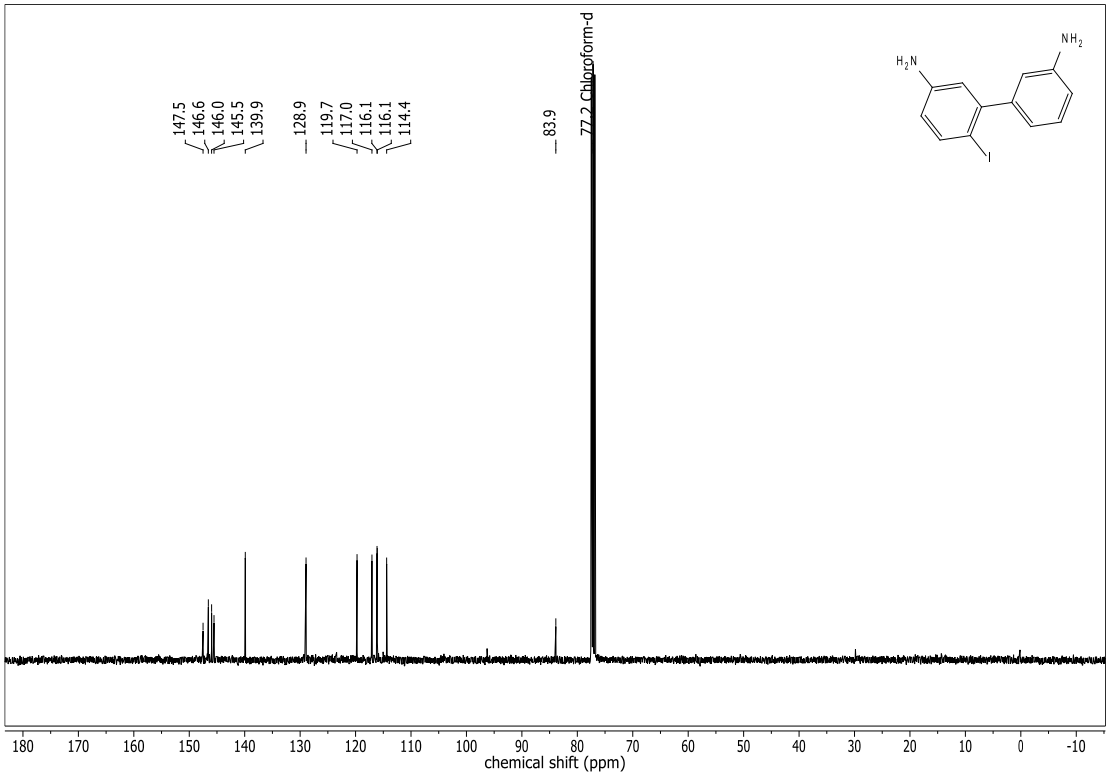

^{1}H NMR of **21**

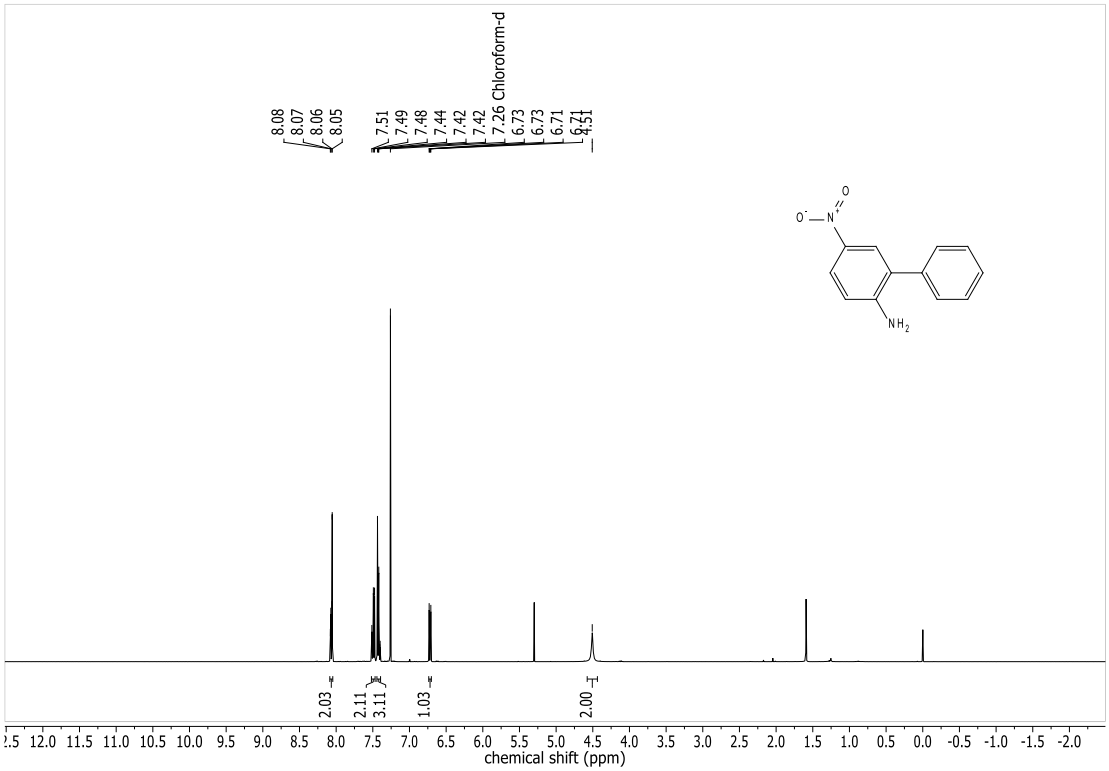

^{1}H NMR of **12**

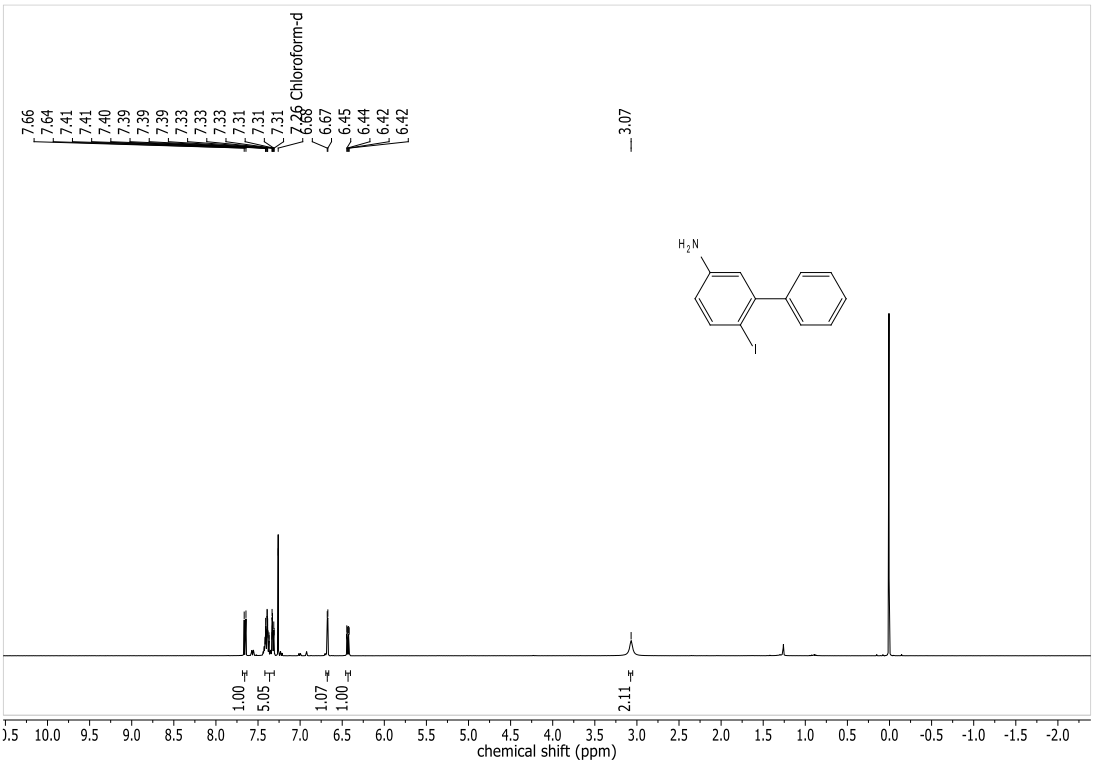

^{1}H NMR of **14**

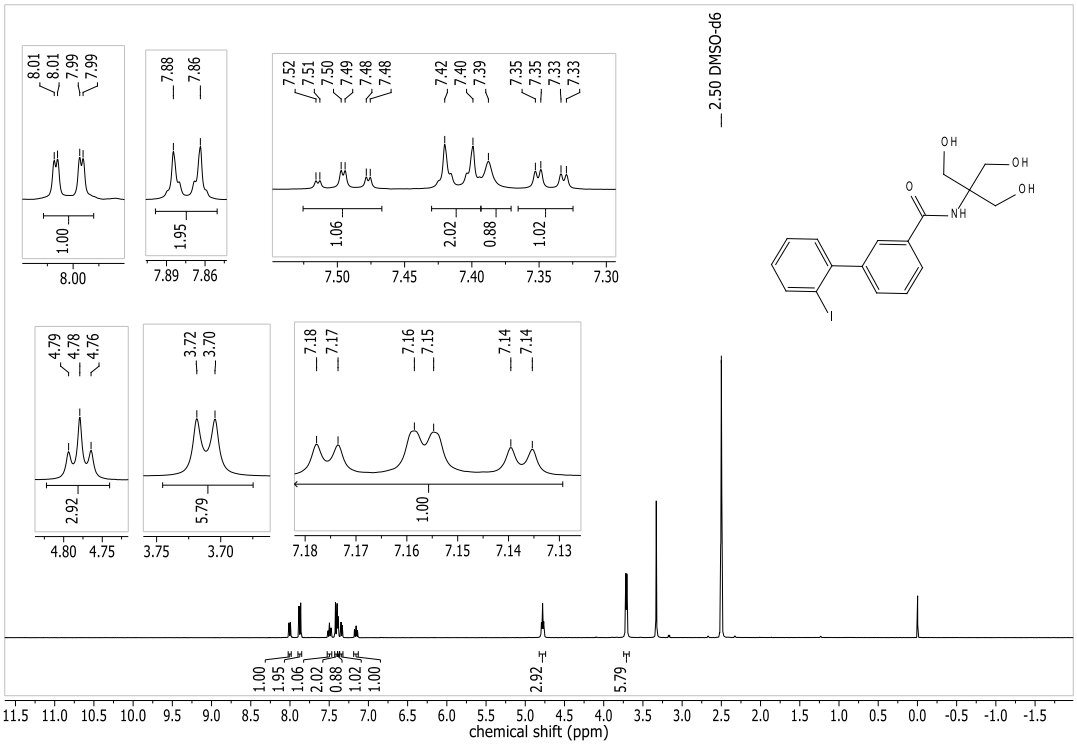

^{13}C NMR of **14**

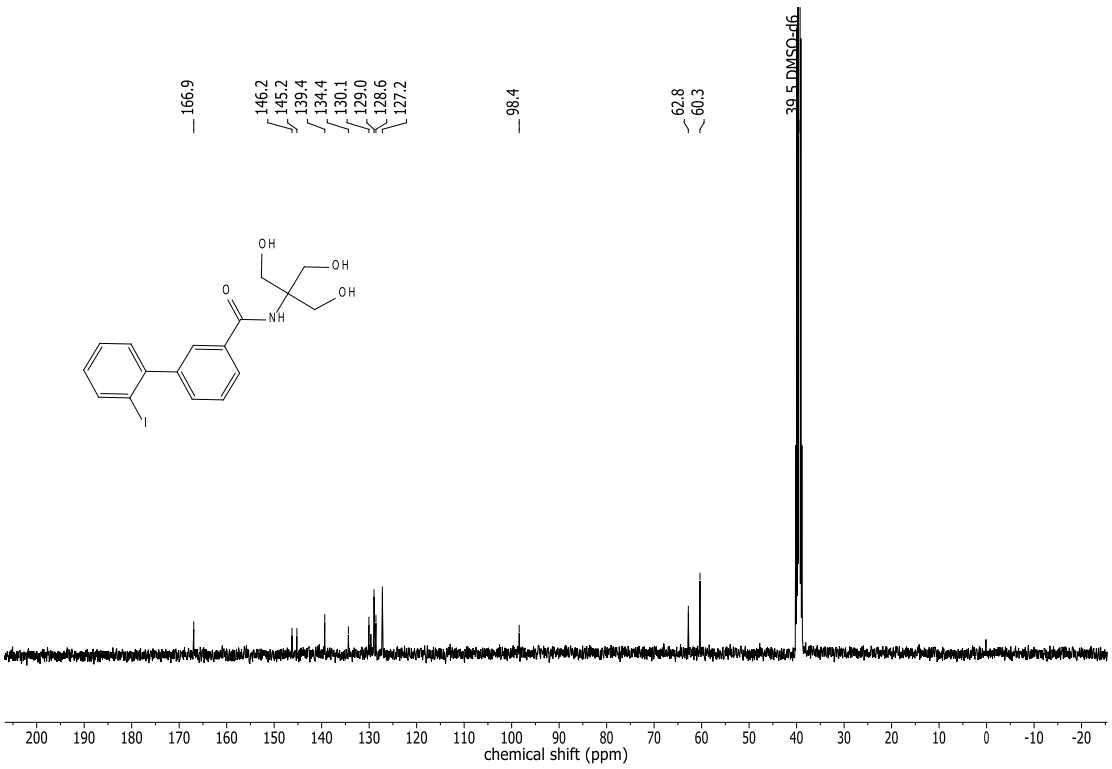

^{1}H NMR of **15**

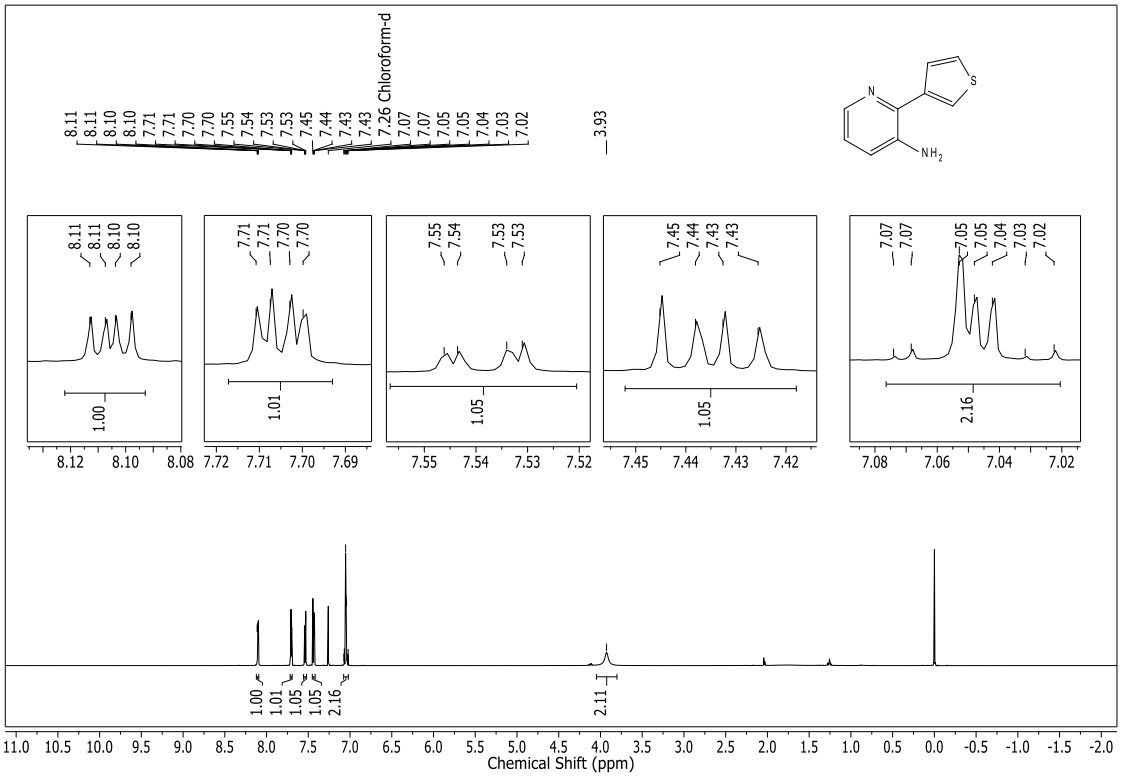

^{13}C NMR of **15**

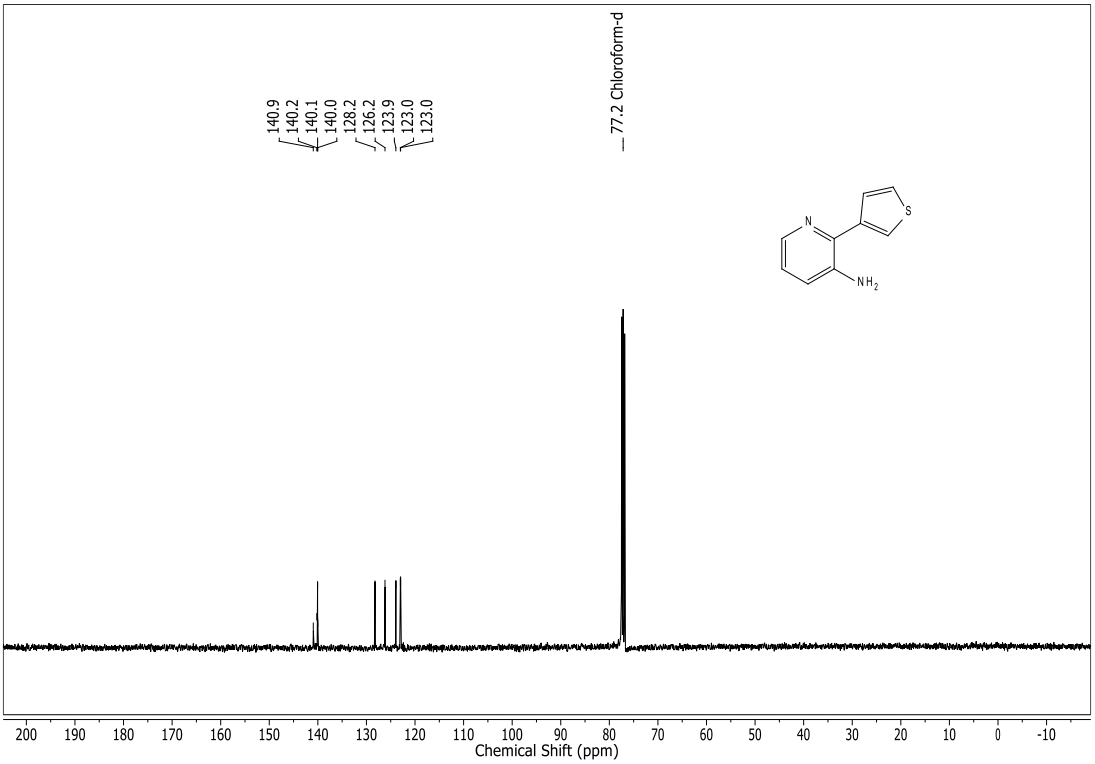

^{1}H NMR of **16**

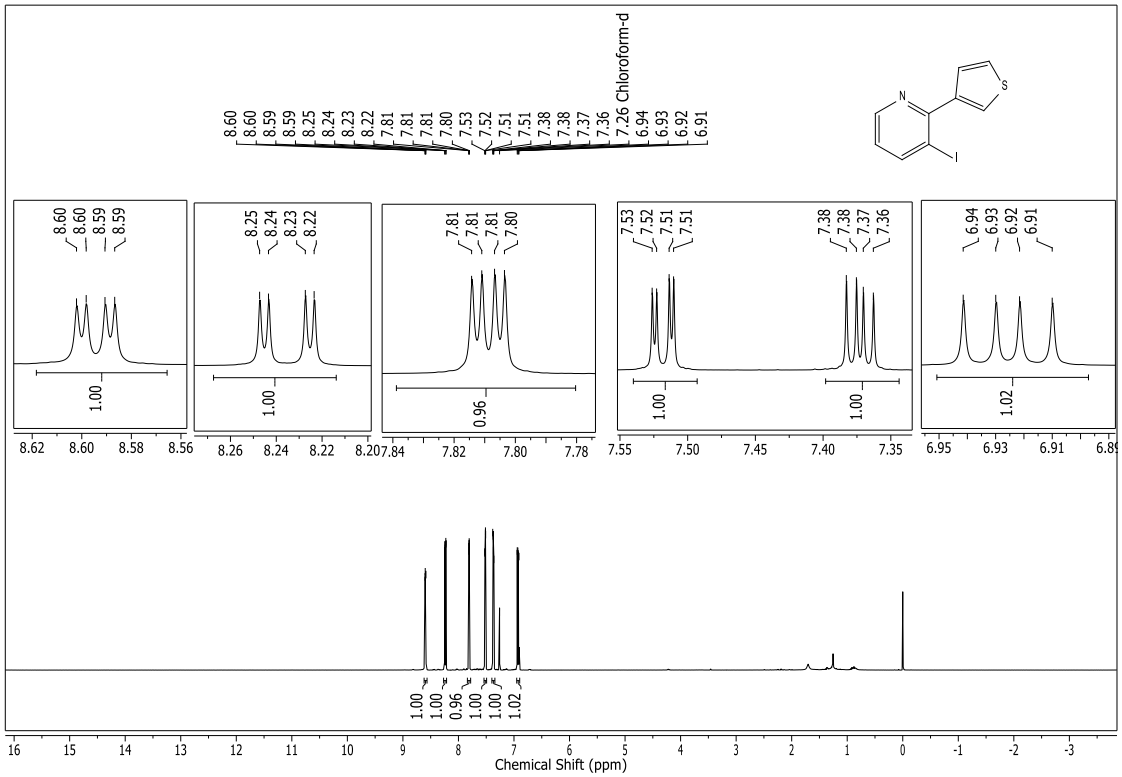

^{13}C NMR of **16**

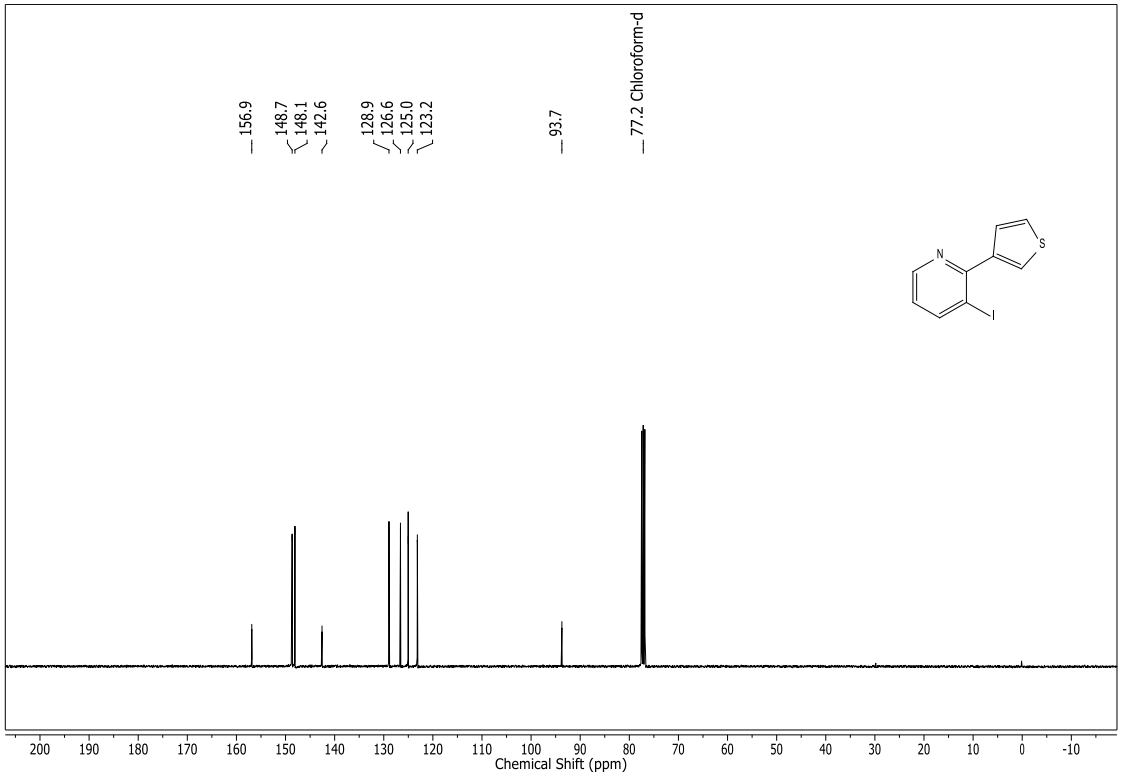

^{1}H NMR of **3a**

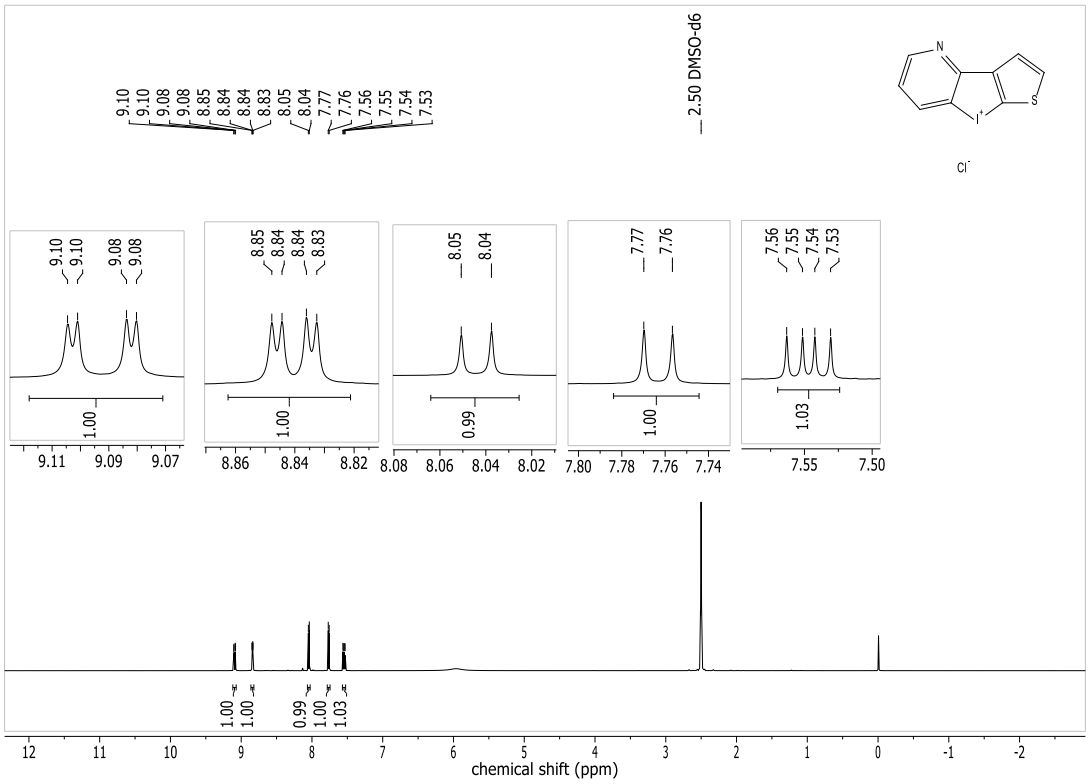

^{13}C NMR of **3a**

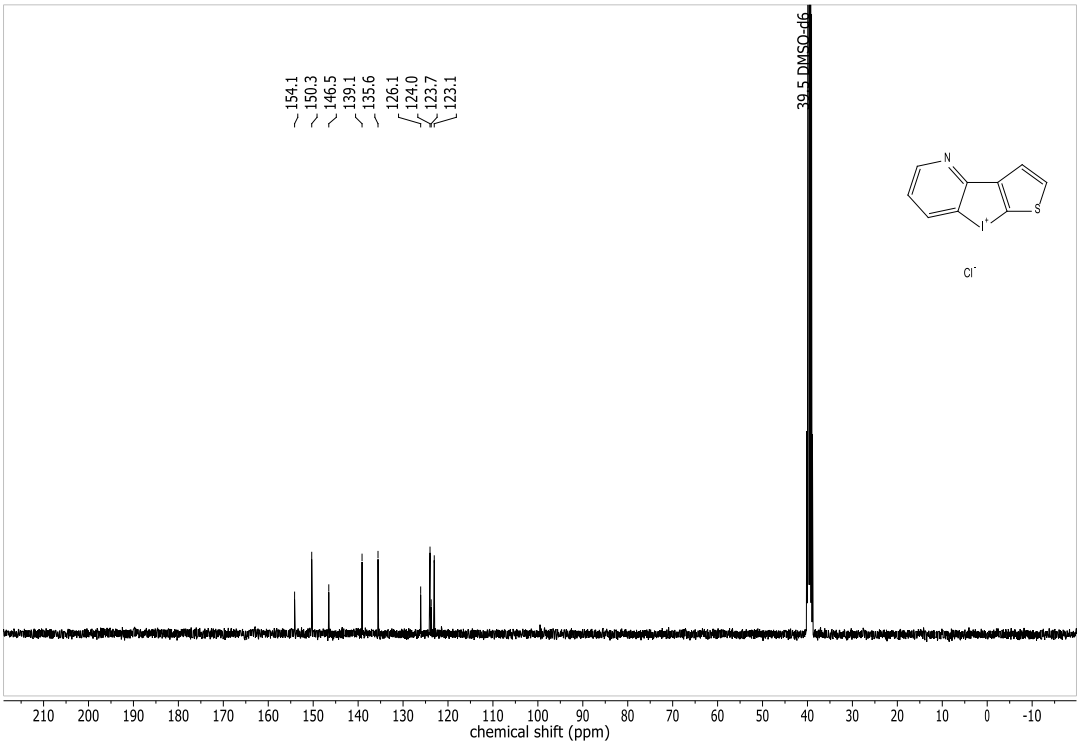

^{1}H NMR of **3b**

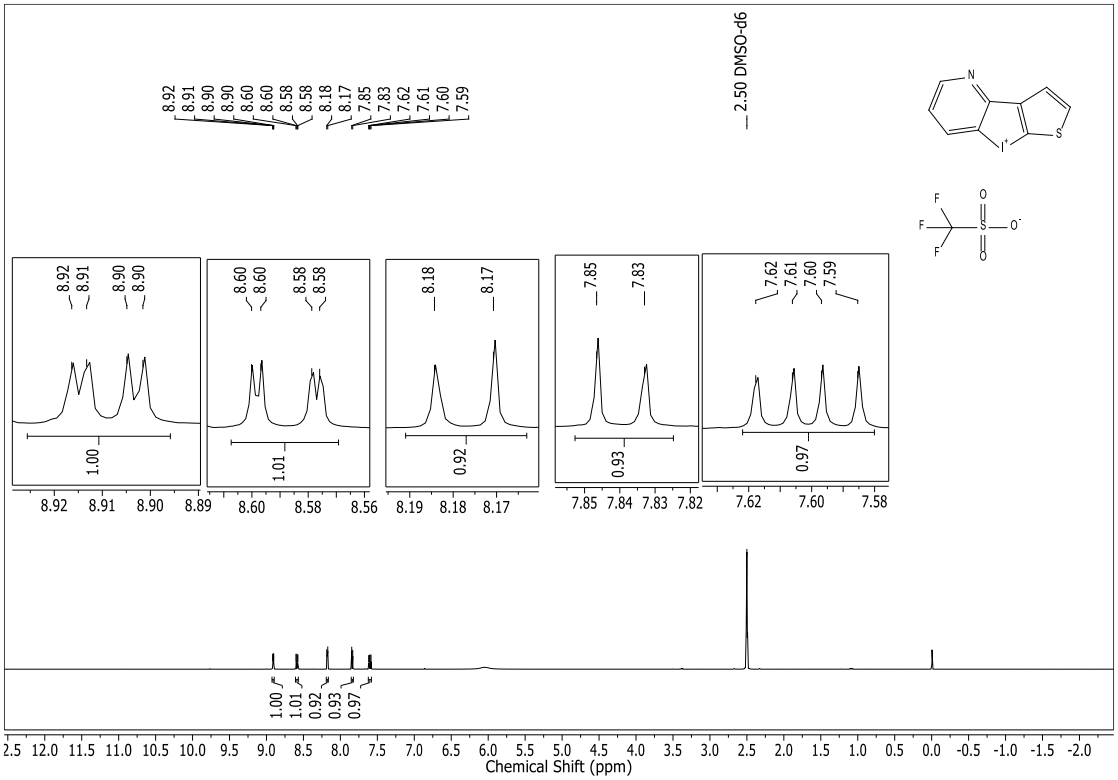

^{13}C NMR of **3b**

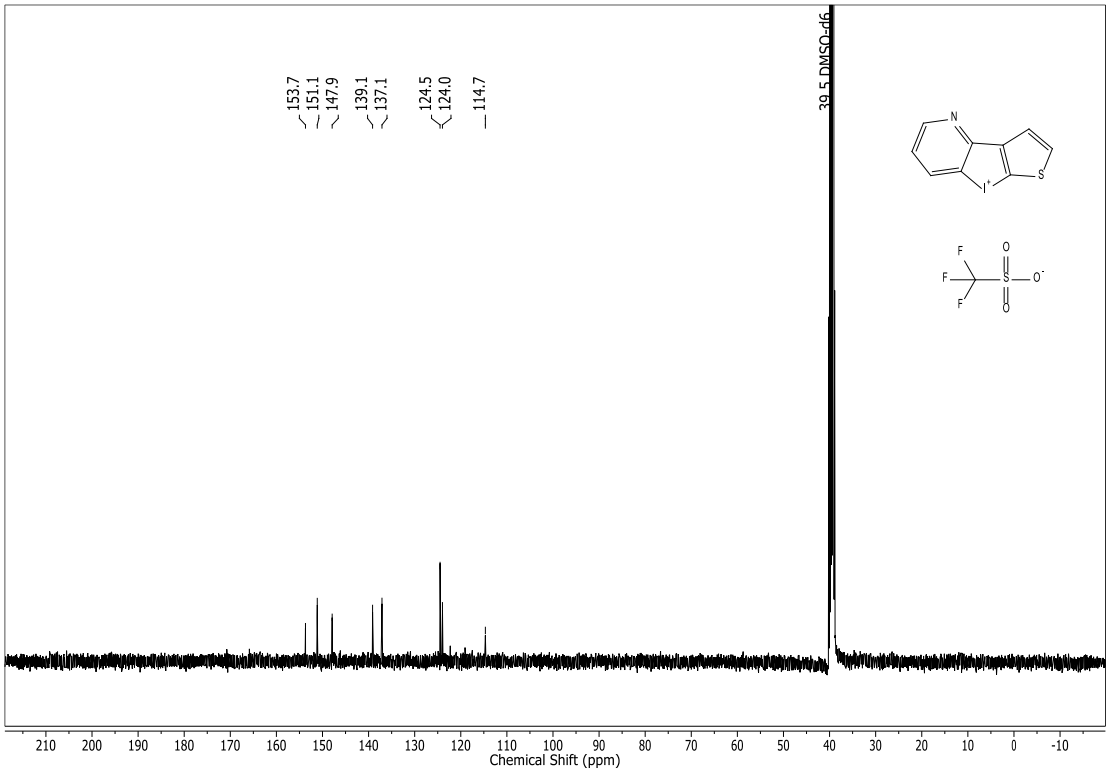

^{19}F NMR of **3b**

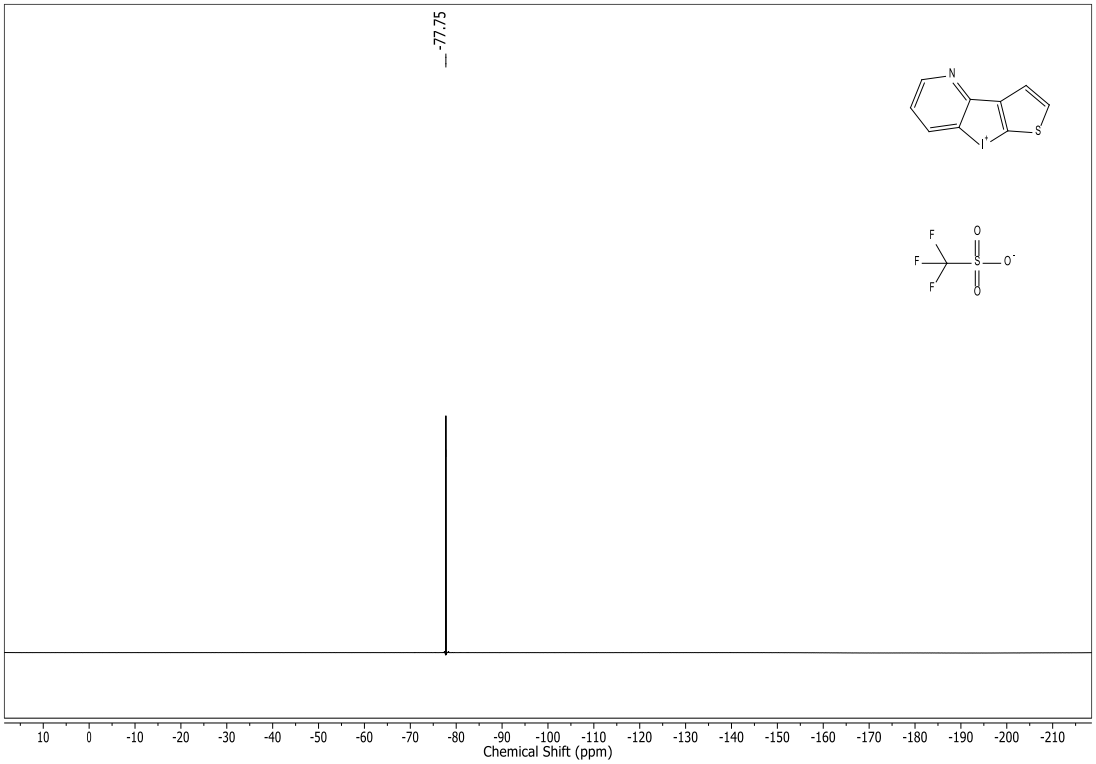
-77.75
N
I+
S
F
F
F
O
S
O
O-
10
0
-10
-20
-30
-40
-50
-60
-70
-80
-90
-100
-110
-120
-130
-140
-150
-160
-170
-180
-190
-200
-210
Chemical Shift (ppm)

3.6. References:

(1) Freedlander, B. L.; French, F. Chemotherapy of Certain Iodonium and Sulfonium Compounds. *Exp. Biol. Med.* **1946**, *63* (2), 319–322. https://doi.org/10.3181/00379727-63-15587.

(2) Engelhard, W. E.; Worton, A. G. Evaluation of an Iodonium Compound as an Antiseptic Agent. *J. Am. Pharm. Assoc. (Scientific ed.)* **1956**, *45* (6), 402–404. https://doi.org/10.1002/jps.3030450616.

(3) Chung, J.-W.; Kim, S. Y.; Park, H. J.; Chung, C. S.; Lee, H. W.; Lee, S. M.; Kim, I.; Pak, J. H.; Lee, G. H.; Jeong, J.-Y. *In Vitro* Activity of Diphenyleneiodonium toward Multidrug-Resistant *Helicobacter Pylori* Strains. *Gut Liver* **2017**, *11* (5), 648–654. https://doi.org/10.5009/gnl16503.

(4) Pandey, M.; Singh, A. K.; Thakare, R.; Talwar, S.; Karaulia, P.; Dasgupta, A.; Chopra, S.; Pandey, A. K. Diphenyleneiodonium Chloride (DPIC) Displays Broad-Spectrum Bactericidal Activity. *Sci. Rep.* **2017**, *7* (1), 11521–11528. https://doi.org/10.1038/s41598-017-11575-5.

(5) Nguyen, N.; Wilson, D. W.; Nagalingam, G.; Triccas, J. A.; Schneider, E. K.; Li, J.; Velkov, T.; Baell, J. Broad Activity of Diphenyleneiodonium Analogues against Mycobacterium Tuberculosis, Malaria Parasites and Bacterial Pathogens. *Eur. J. Med. Chem.* **2018**, *148*, 507–518. https://doi.org/10.1016/j.ejmech.2017.10.010.

(6) Martín-Aspas, A.; Guerrero-Sánchez, F. M.; García-Colchero, F.; Rodríguez-Roca, S.; Girón-González, J.-A. Differential Characteristics of Acinetobacter Baumannii Colonization and Infection: Risk Factors, Clinical Picture, and Mortality. *Infect. Drug Resist.* **2018**, *Volume 11*, 861–872. https://doi.org/10.2147/IDR.S163944.

(7) Dexter, C.; Murray, G. L.; Paulsen, I. T.; Peleg, A. Y. Community-Acquired Acinetobacter Baumannii : Clinical Characteristics, Epidemiology and Pathogenesis. *Expert Rev. Anti. Infect. Ther.* **2015**, *13* (5), 567–573. https://doi.org/10.1586/14787210.2015.1025055.

(8) Peleg, A. Y.; Seifert, H.; Paterson, D. L. Acinetobacter Baumannii : Emergence of a Successful Pathogen. *Clin. Microbiol. Rev.* **2008**, *21* (3), 538–582. https://doi.org/10.1128/CMR.00058-07.

(9) Glew, R. H.; Moellering, R. C.; Kunz, L. J. Infections With Acinetobacter Calcoaceticus (herellea vaginicola). *Medicine (Baltimore).* **1977**, *56* (2), 79–98. https://doi.org/10.1097/00005792-197703000-00001.

(10) McConnell, M. J.; Actis, L.; Pachón, J. Acinetobacter Baumannii : Human Infections, Factors Contributing to Pathogenesis and Animal Models. *FEMS Microbiol. Rev.* **2013**, *37* (2), 130–155. https://doi.org/10.1111/j.1574-6976.2012.00344.x.

(11) Shlaes, D. M.; Bradford, P. A. Antibiotics—From There to Where? *Pathog. Immun.* **2018**, *3* (1), 19. https://doi.org/10.20411/pai.v3i1.231.

(12) Brown, S.; Amyes, S. OXA β-Lactamases in Acinetobacter: The Story so Far. *J. Antimicrob. Chemother.* **2006**, *57* (1), 1–3. https://doi.org/10.1093/jac/dki425.

(13) Mussi, M. A.; Limansky, A. S.; Viale, A. M. Acquisition of Resistance to Carbapenems in Multidrug-Resistant Clinical Strains of Acinetobacter Baumannii : Natural Insertional Inactivation of a Gene Encoding a Member of a Novel Family of β-Barrel Outer Membrane Proteins. *Antimicrob. Agents Chemother.* **2005**, *49* (4), 1432–1440. https://doi.org/10.1128/AAC.49.4.1432-1440.2005.

(14) Li, J.; Nation, R. L.; Milne, R. W.; Turnidge, J. D.; Coulthard, K. Evaluation of Colistin as an Agent against Multi-Resistant Gram-Negative Bacteria. *Int. J. Antimicrob. Agents* **2005**, *25* (1), 11–25. https://doi.org/10.1016/j.ijantimicag.2004.10.001.

(15) Hamada, Y. Role of Pyridines in Medicinal Chemistry and Design of BACE1 Inhibitors Possessing a Pyridine Scaffold. In *Pyridine*; InTech, 2018. https://doi.org/10.5772/intechopen.74719.

(16) Shah, R.; Verma, P. K. Therapeutic Importance of Synthetic Thiophene. *Chem. Cent. J.* **2018**, *12* (1), 137. https://doi.org/10.1186/s13065-018-0511-5.

(17) Parker, E. N.; Drown, B. S.; Geddes, E. J.; Lee, H. Y.; Ismail, N.; Lau, G. W.; Hergenrother, P. J. Implementation of Permeation Rules Leads to a FabI Inhibitor with Activity against Gram-Negative Pathogens. *Nat. Microbiol.* **2020**, *5* (1), 67–75. https://doi.org/10.1038/s41564-019-0604-5.

(18) Firth, N. C.; Brown, N.; Blagg, J. Plane of Best Fit: A Novel Method to Characterize the Three-Dimensionality of Molecules. *J. Chem. Inf. Model.* **2012**, *52* (10), 2516–2525. https://doi.org/10.1021/ci300293f.

(19) Paulekuhn, G. S.; Dressman, J. B.; Saal, C. Trends in Active Pharmaceutical Ingredient Salt Selection Based on Analysis of the Orange Book Database. *J. Med. Chem.* **2007**, *50* (26), 6665–6672. https://doi.org/10.1021/jm701032y.

(20) Halavaty, A. S.; Rich, R. L.; Chen, C.; Joo, J. C.; Minasov, G.; Dubrovska, I.; Winsor, J. R.; Myszka, D. G.; Duban, M.; Shuvalova, L.; Yakunin, A. F.; Anderson, W. F. Structural and Functional Analysis of Betaine Aldehyde Dehydrogenase from Staphylococcus Aureus. *Acta Crystallogr. Sect. D Biol. Crystallogr.* **2015**, *71* (5), 1159–1175. https://doi.org/10.1107/S1399004715004228.

(21) Jackson, B.; Brocker, C.; Thompson, D. C.; Black, W.; Vasiliou, K.; Nebert, D. W.; Vasiliou, V. Update on the Aldehyde Dehydrogenase Gene (ALDH) Superfamily. *Hum. Genomics* **2011**, *5* (4), 283. https://doi.org/10.1186/1479-7364-5-4-283.

(22) Vanoni, M. A.; Curti, B. Structure–Function Studies of Glutamate Synthases: A Class of Self-Regulated Iron-Sulfur Flavoenzymes Essential for Nitrogen Assimilation. *IUBMB Life* **2008**, *60* (5), 287–300. https://doi.org/10.1002/iub.52.

(23) Joo, H. K.; Park, Y. W.; Jang, Y. Y.; Lee, J. Y. Structural Analysis of Glutamine Synthetase from Helicobacter Pylori. *Sci. Rep.* **2018**, *8* (1), 11657. https://doi.org/10.1038/s41598-018-30191-5.

(24) Liu, Z.; Zhu, D.; Luo, B.; Zhang, N.; Liu, Q.; Hu, Y.; Pi, R.; Huang, P.; Wen, S. Mild Cu(I)-Catalyzed Cascade Reaction of Cyclic Diaryliodoniums, Sodium Azide, and Alkynes: Efficient Synthesis of Triazolophenanthridines. *Org. Lett.* **2014**, *16* (21), 5600–5603. https://doi.org/10.1021/ol502654a.

(25) Letessier, J.; Detert, H. First Synthesis of Benzopyridoiodolium Salts and Twofold Buchwald-Hartwig Amination for the Total Synthesis of Quindoline. *Synthesis (Stuttg).* **2012**, *2012* (02), 290–296. https://doi.org/10.1055/s-0031-1289652.

(26) Chandrappa, S.; Vinaya, K.; Ramakrishnappa, T.; Rangappa, K. An Efficient Method for Aryl Nitro Reduction and Cleavage of Azo Compounds Using Iron Powder/Calcium Chloride. *Synlett* **2010**, *2010* (20), 3019–3022. https://doi.org/10.1055/s-0030-1259067.

(27) Kelkar, D. S.; Ravikumar, G.; Mehendale, N.; Singh, S.; Joshi, A.; Sharma, A. K.; Mhetre, A.; Rajendran, A.; Chakrapani, H.; Kamat, S. S. A Chemical–Genetic Screen Identifies ABHD12 as an Oxidized-Phosphatidylserine Lipase. *Nat. Chem. Biol.* **2019**,

15 (2), 169–178. https://doi.org/10.1038/s41589-018-0195-0.

(28) Speers, A. E.; Adam, G. C.; Cravatt, B. F. Activity-Based Protein Profiling in Vivo Using a Copper(I)-Catalyzed Azide-Alkyne [3 + 2] Cycloaddition. *J. Am. Chem. Soc.* **2003**, *125* (16), 4686–4687. https://doi.org/10.1021/ja034490h.

(29) Kulkarni, A.; Soni, I.; Kelkar, D. S.; Dharmaraja, A. T.; Sankar, R. K.; Beniwal, G.; Rajendran, A.; Tamhankar, S.; Chopra, S.; Kamat, S. S.; Chakrapani, H. Chemoproteomics of an Indole-Based Quinone Epoxide Identifies Druggable Vulnerabilities in Vancomycin-Resistant Staphylococcus Aureus. *J. Med. Chem.* **2019**, *62* (14), 6785–6795. https://doi.org/10.1021/acs.jmedchem.9b00774.

(30) Kumar, K.; Mhetre, A.; Ratnaparkhi, G. S.; Kamat, S. S. A Superfamily-Wide Activity Atlas of Serine Hydrolases in Drosophila Melanogaster. *Biochemistry* **2021**, *60* (16), 1312–1324. https://doi.org/10.1021/acs.biochem.1c00171.

Chapter 4: Visible-Light Controlled Release of a Fluoroquinolone Antibiotics

4.1. Introduction:

In chapters **2** and **3**, the drug discovery method was discussed to tackle antibiotic resistance, in which compound **3a**, a member of the iodonium family of compounds, has been discovered as a potential inhibitor of Gram-negative pathogens such as *A. buamannii*. Protein targets of DPIC and **3a** were discovered in *E. coli* and *A. baumannii*, respectively, using chemoproteomic techniques. In order to address antibiotic resistance, methods for spatiotemporal regulated release of an antibacterial molecule will be discussed in this Chapter **4**. In these methods, antibacterial compounds' action is controlled by an external stimulus or a metabolic trigger. For example, Das and co-workers have developed a disulfide-based prodrug with Levofloxacin and demonstrated the glutathione (GSH) induced release of antibiotics in *E. coli* and *S. aureus*.[1] This method can be utilized in *E. coli* caused infections like urinary tract infections, where the concentration of GSH is elevated (in porcine bladder epithelium, 0 .6 mM) than in plasma (~3 μM).[2] In another report, Chakrapani and co-workers have demonstrated nitroreductase (NTR), a bacterial enzyme-activated release of Ciprofloxacin along with a fluorescence reporter in *E. coli*.[3] In a subsequent study, Reynolds and co-workers have shown the NTR enzyme triggered the release of nitric oxide (NO), a potent antibacterial molecule from a polymer-based prodrug upon in *E. coli*.[4] In another study, Bronstrup and co-workers have developed a human antimicrobial peptide- colistin conjugated prodrug[5] and demonstrated the neutrophil elastase (NE) activated liberation of the antimicrobial peptide against gram-negative bacteria *E. coli*, *A. baumannii*, and *P. aeruginosa*. Neutrophil elastase (NE) enzyme is secreted by neutrophil granulocytes at infection sites. However, enzymes are an internal trigger, as they are present inside the cells. As a result, enzyme activity may not be under control, perhaps causing an increase in the concentration of the released antibacterial molecule. It may also interfere with other functional groups in the prodrug.

Photopharmacology, on the other hand, uses "light" as an external regulator to regulate the action of bioactive chemicals. Light as external trigger has several advantages, such as:[6–8]

- It exhibits biorthogonality towards biological system
- It does not cause any contamination to samples and has a negligible or low level of toxicity
- Light delivery can be more precisely controlled by altering intensity and amplitude (wavelength) quantitatively and qualitatively, respectively.

Thus, in the antibacterial photopharmacology domain, light can be employed as a trigger to diminish off-target action and unwanted side effects of antibiotics for specific types of skin infections or wound dressing. In this approach, an antibiotic is appended with either with an optical swich or a photocleavable group, which upon exposing to light will liberate the active antibacterial molecule. For example, Feringa and co-workers have developed Ciprofloxacin appended photoswitch, which upon exposing to UV light undergoes conformational transition to achieve an active molecule conformation and exhibit more potent antibacterial activity than antibiotic alone in *E. coli* (Figure 4.1A)[9].

Figure 4. 1 Reported examples of UV-light triggered release of antibacterial molecules

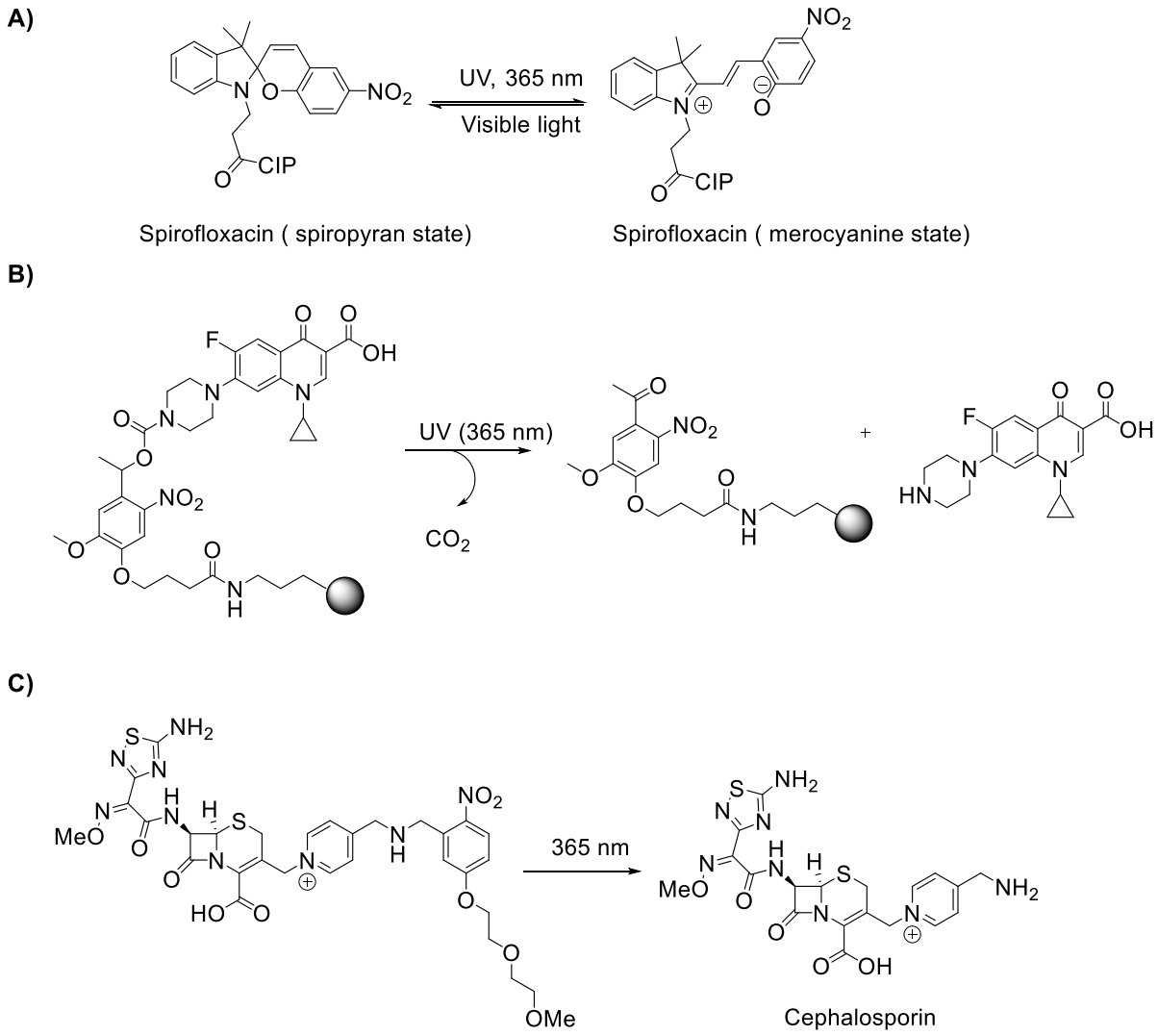

When an antibacterial effect is obtained at the infection site, it can be converted into an inactive molecule, and antibiotic exposure can be modulated by utilizing a different source of light.

Using *o*-nitroaryl photo cleavable group, Forsythe and co-workers have attached Ciprofloxacin on hydrogel and shown the UV light activated release of antibiotic (Figure 4.1B)[10]. The efficacy of antibacterial activity was demonstrated using Muller–Hinton agar plate method against *S. aureus* bacterium. In another study, Gademann and co-workers have linked two different antibiotics to UV light sensitive *o*-nitroaryl photo cleavable group (Figure 4.1C)[11]. and displayed the antibacterial activity against *B. subtilis*, *S. aureus*, MRSA, *E. coli*, and *P. aeruginosa*. However, due to its toxicity and limited tissue penetration, UV light (250–400 nm) is not recommended.[12]. Hence, we set out to design antibiotic release that is initiated by visible light. For instance, Levofloxacin referred as "respiratory fluoroquinolone" was chosen as an antibiotic. It has been in used as a first line treatment against penicillin-resistant *Streptococcus pneumoniae* (PRSP) caused infections[13]. The boron-dipyrromethene (BODIPY)-based photocleavable group was chosen for this investigation from among several previously reported photocleavable groups employed for the triggerable release of bioactive compounds.[14] BODIPY based fluorophores have several distinct advantages, such as[15,16]

- Insensitive to pH and polarity, and stable in physiological conditions
- Have high molar extinction coefficient and photostabilty, making them a good candidate for PDT therapeutic agents and bio-imaging
- Moderately nontoxic and have higher quantum yield
- With certain structural changes, the amplitude of the light source can be adjusted.

Using aryloxy- BODIPY based fluorophore, Urano and co-workers have demonstrated the B-O bond cleavage[17] and release of histamine in HeLa cells[18], with blue-green visible light. In another study, Ambade and co-workers have designed visible light triggered BODIPY-caged polymer scaffold for the destruction of micellar assembly[19] and shown the controlled release of cargo. In a subsequent study, Chakrapani and co-workers have demonstrated the production of a small gaseous specie hydrogen sulfide (H_2S) in presence of carbonic anhydrase enzyme [20], through visible light activated cleavage of B-O bond from BODIPY- based carbamothioate scaffold.

Figure 4. 2 Reported examples of visible-light triggered release of bioactive molecules

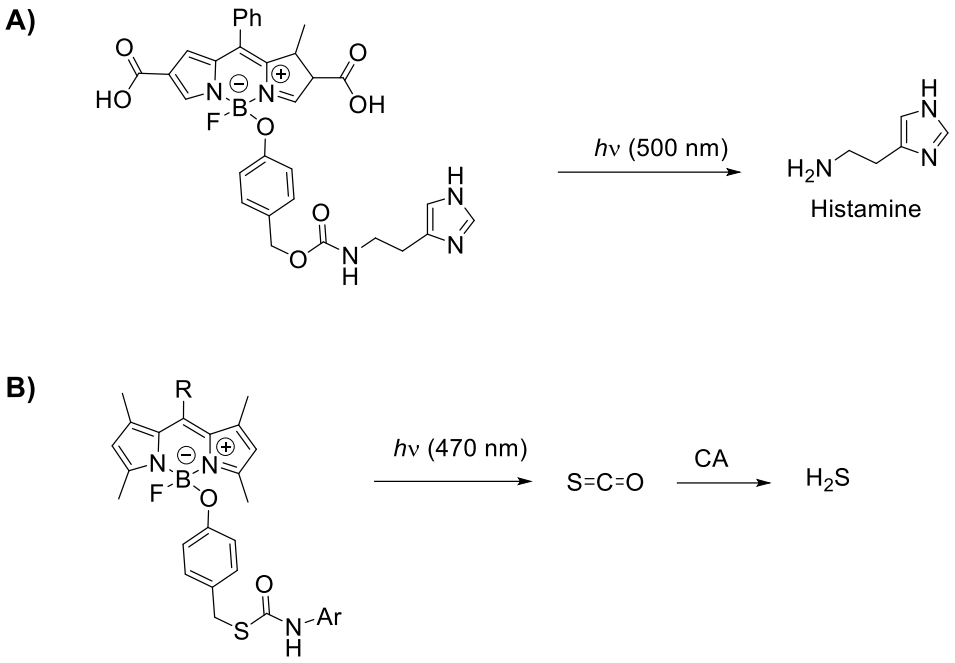

4.2. Design of BODIPY based fluoroquinolone caged scaffold:

With the knowledge of the aforementioned reports, a BODIPY-based scaffold for caging the fluroquinolone antibiotic was designed, which should release the antibiotic by B-O bond cleavage when exposed to visible light.

Figure 4. 3 Design of BODIPY-based fluoroquinolone caged scaffold

(Reproduced with permission from *ACS Omega* https://pubs.acs.org/doi/10.1021/acsomega.7b01906)

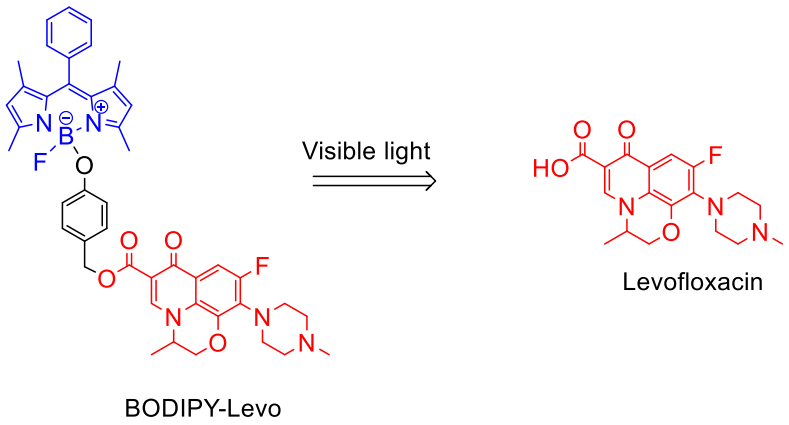

4.3. Results and discussion:

BODIPY-aryloxy derivative **24** was synthesized using reported protocols.[18] Using HBTU-DMAP acid-alcohol coupling reaction[21], compound **24** was reacted with Levofloxacin (Levo), and BODIPY-Levo adduct was obtained with a 69% yield. Following the same scheme compound, **22** was synthesized as a negative control.

Scheme 4. 1 Synthesis of BODIPY-based fluoroquinolone caged scaffold

(Reproduced with permission from *ACS Omega* https://pubs.acs.org/doi/10.1021/acsomega.7b01906)

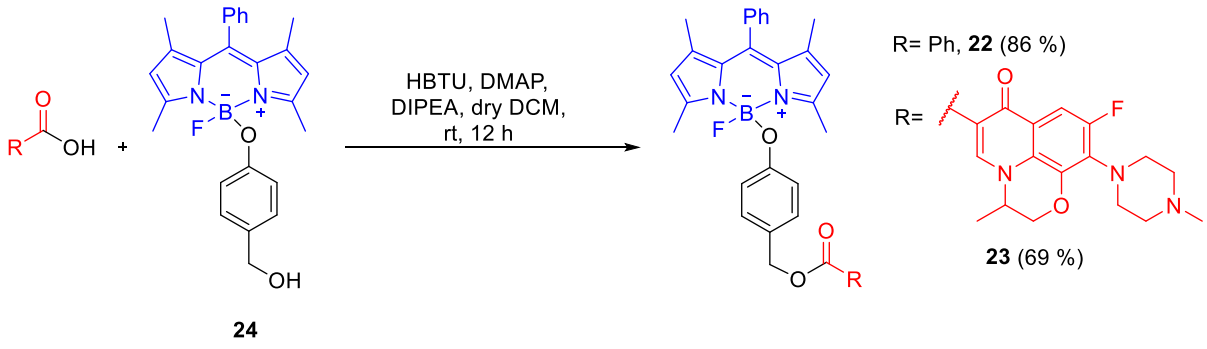

When compound **23** is exposed to light (470 nm, 30 mW/cm^2) for 30 minutes in methanol, it is anticipated that It would break the B-O bond, resulting in intermediate **I** being produced alongside BODIPY-OMe **27** and Levofloxacin being produced *via* electron transfer across the benzene ring of intermediate I in the buffer.

Scheme 4. 2 Proposed mechanism for the generation of Levofloxacin after photo-irradiation of 23

(Reproduced with permission from *ACS Omega* https://pubs.acs.org/doi/10.1021/acsomega.7b01906)

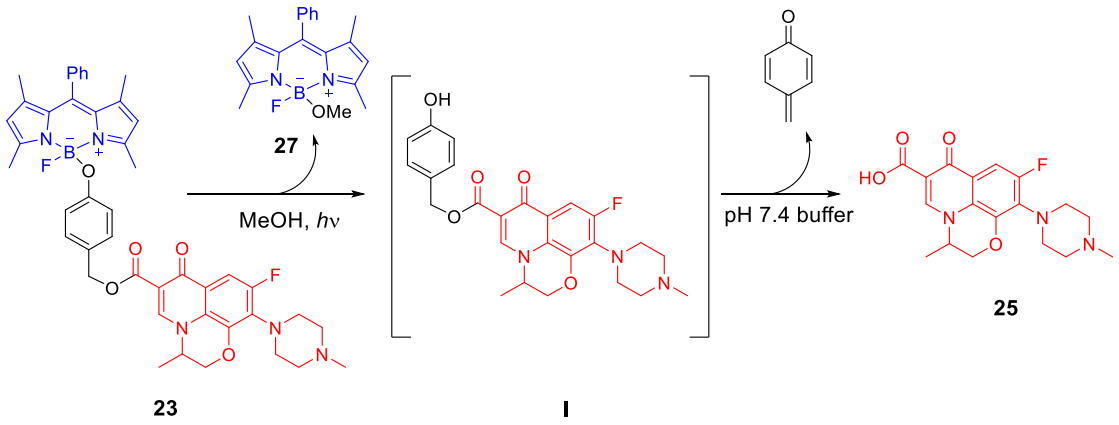

In order to investigate the optical characteristics of these BODIPY derivatives, samples (2.5 μM, MeOH) were irradiated with blue light (470 nm, 30 mW/cm^2) in a tight chamber. The yields after irradiation were similar in each case since the result is BODIPY-OMe.(Table 4.1, Scheme 4.2)

Table 4. 1 Optical properties of BODIPY derivatives

Entry	BODIPY derivatives	λ_{abs} (nm)	λ_{em} (nm)	ϕfl
1	**22**, dark	500	509	0.12
2	**22**, light	500	509	0.62
3	**23**, dark	500	509	0.09
4	**23**, light	500	509	0.64
5	**24**, dark	500	509	0.05
6	**24**, light	500	509	0.64

λ_{abs}: absorption maximum, λ_{em}: emission maximum, ϕ_{fl}: fluorescence quantum efficiency.

4.3.1. TLC-based decomposition:

Following that, a TLC-based experiment was carried out to observe the released Levofloxacin after irradiation. Here, compound **23** (500 μM) was irradiated in methanol with light at 470 nm (30 mW/cm^2) for 30 min. Another batch of an irradiated aliquot of **23** was incubated in pH 7.4 (50 mM) phosphate buffer (250 μM) for 30 min. Using a mobile phase of methanol: chloroform (1:9), TLC analysis of the reaction mixtures (250 μM) was conducted.

Compound **23**, in the dark and in the buffer, was found to be stable. When compound **23** was exposed to light and incubated in buffer, the release of Levofloxacin was observed (Figure 4.4).

Figure 4. 4 Decomposition study by TLC

23, dark indicates **23** is not irradiated with light; **23**, light indicates **23** is irradiated with light for 30 min. UV-lamp (365 nm) was used to visualize TLC.

(Reproduced with permission from *ACS Omega* https://pubs.acs.org/doi/10.1021/acsomega.7b01906)

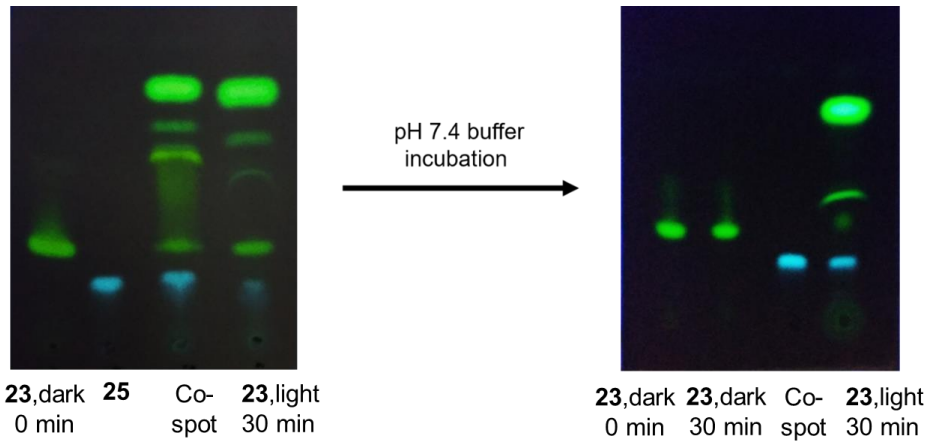

4.3.2. HPLC-based decomposition study:

In addition, investigations using high performance liquid chromatography (HPLC) were carried out to establish the release of Levofloxacin in a qualitative and quantitative manner. For this, Compound **23**(100 μM) was irradiated for 30 minutes in methanol, and HPLC analysis of the aliquot was conducted (Figure 4.5). Compound **23** was stable for 30 minutes in the dark (Retention time at 16.6 min). Following light irradiation, a complete disintegration of compound **23** was observed, as well as the creation of a new peak, which corresponds to the BODIPY-OMe **27** (Retention time at 11.3 min)[18]

Figure 4. 5 Portions of HPLC traces of 23 incubated in methanol

Ctrl, *t* = 0; dark, *t* = 30 min; light, reaction mixture was irradiated for 30 min with 470 nm light. The detector wavelength used is A) 500 nm, B) fluorescence detector wavelength excitation, 470 nm; emission, 540 nm.

(Reproduced with permission from *ACS Omega* https://pubs.acs.org/doi/10.1021/acsomega.7b01906)

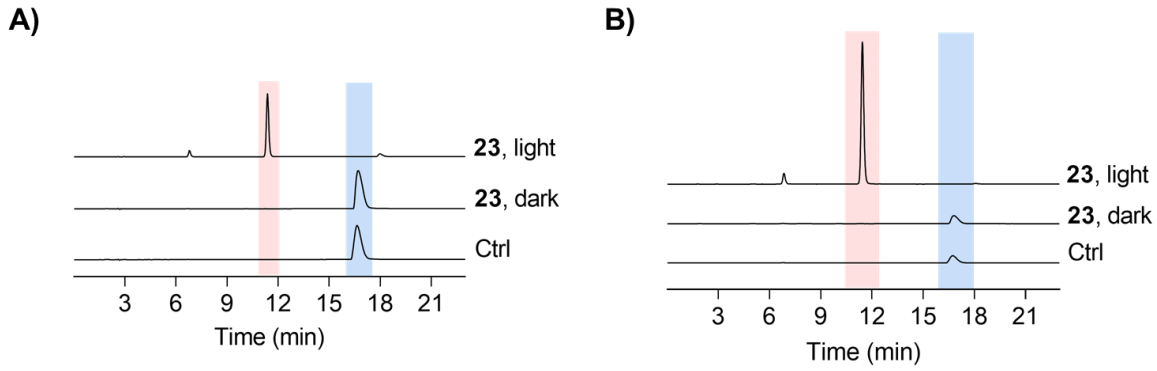

Next, in order to determine the yield of released Levofloxacin 2**5**, another aliquot of **23** (100 µM) was first irradiated in methanol for 30 min. The irradiated sample was then diluted to 25 µM in pH 7.4 phosphate buffer and incubated for 30 minutes at 37 ºC, and HPLC analysis of aliquot was conducted. Formation of a distinct peak was observed (Retention time at 7.3 min), and that corresponds to Levofloxacin **25** (Figure 4.6). The yield of released Levofloxacin was found to be 31%, which was similar to previous results showing histamine release from BODIPY-histamine caged scaffolds.[18]

Figure 4. 6 A portion of HPLC traces of 23 incubated in pH 7.4 buffer after irradiation in methanol

The fluorescence detector was used with excitation, 330 nm; emission, 510 nm.

(Reproduced with permission from *ACS Omega* https://pubs.acs.org/doi/10.1021/acsomega.7b01906)

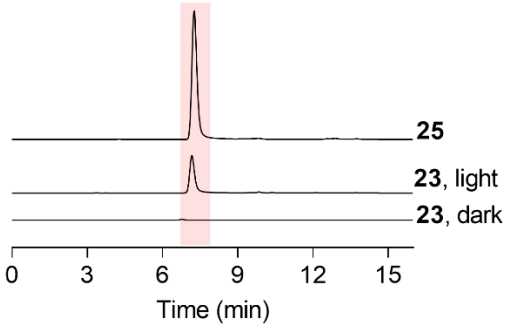

4.3.2. Study of the antibacterial efficacy of released Levofloxacin:

4.3.2.1 Growth curve analysis:

Having established that after exposing compound **23** to light in methanol, Levofloxacin was successfully produced in the buffer. The efficacy of released Levofloxacin's antibacterial activity was next examined utilizing growth curve analysis against Gram-positive and Gram-negative bacteria.

Figure 4. 7 Growth curve analysis of E. coli

Ctrl indicates bacteria in dark; dark indicats not irradiated, light indicates irradiated with light at 470 nm for 5 min, (B) at time point 6 h; **23** indicates **23** (5 μM) in bacteria; **25** indicates 25 (5 μM) in bacteria; **22** indicates **22** (10 μM) in bacteria **** indicates p-Value < 0.001 comparison between **23** dark and **23** light

(Reproduced with permission from *ACS Omega* https://pubs.acs.org/doi/10.1021/acsomega.7b01906)

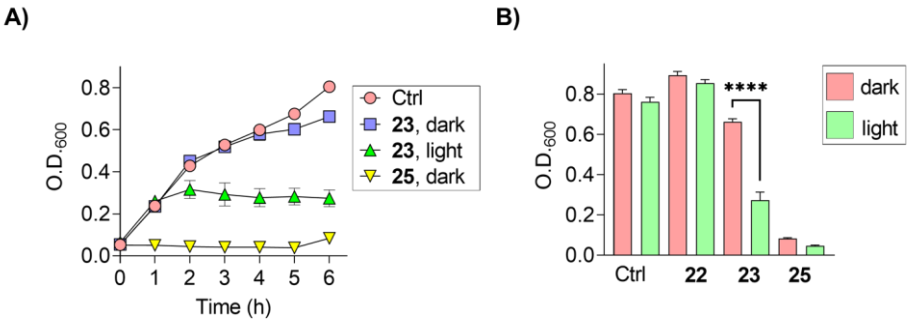

When *E. coli* bacterial cells were exposed to compound **22**, no substantial suppression of bacterial growth was detected in the dark or in the light, showing that compound **22** had no growth inhibitory impact. Levofloxacin **25** showed antibacterial activity in dark and light conditions, implying that its antibacterial potency was unaffected by irradiation. (Figure 4.7). In the dark, compound **23** exhibited no inhibitory impact, but bacterial growth was significantly reduced after irradiation, suggesting that compound 23 only exhibits antibacterial action after being exposed to visible light. Similar results were obtained in *S. aureus* bacterium (Figure 4.8).

Figure 4. 8 Growth curve analysis of S. aureus

Ctrl indicates bacteria in dark; dark indicats not irradiated, light indicates irradiated with light at 470 nm for 5 min, (B) at time point 6 h; **23** indicates **23** (5 μM) in bacteria; **25** indicates 25 (5 μM) in bacteria; **22** indicates **22** (10 μM) in bacteria **** indicates p-Value < 0.001 comparison between **23** dark and **23** light

(Reproduced with permission from *ACS Omega* https://pubs.acs.org/doi/10.1021/acsomega.7b01906)

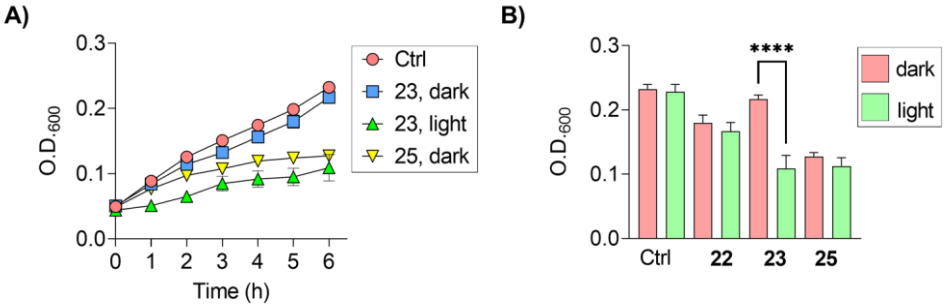

4.3.2.2 Agar growth method:

The efficacy of the released antibiotic induced by visible light was then examined using the agar growth method. *E. coli* bacterial cells on nutrient agar plate were exposed to either dark or light in presence of BODIPY derivative **22** and **23**, and Levofloxacin **25** as reference. Images of these agar plates were recorded periodically to monitor the growth of bacterial cells. When exposed to light, compound 22 had no inhibitory effect, while compound 25's activity was independent of light, confirming the findings from the growth curve. However, when bacterial cells were exposed to light in presence of **23**, no growth was detected for 6 hours. This inhibitory activity was sustained for up to 24 hours and was comparable to that of the antibiotic Levofloxacin (Figure 4.9).

Figure 4. 9 Growth inhibition of E. coli on nutrient agar plate

Ctrl indicates bacteria; **23** indicates **23** (100 μM) in bacteria; **25** indicates **25** (100 μM) in bacteria; **22** indicates **22** (100 μM) in bacteria.

(Reproduced with permission from *ACS Omega* https://pubs.acs.org/doi/10.1021/acsomega.7b01906)

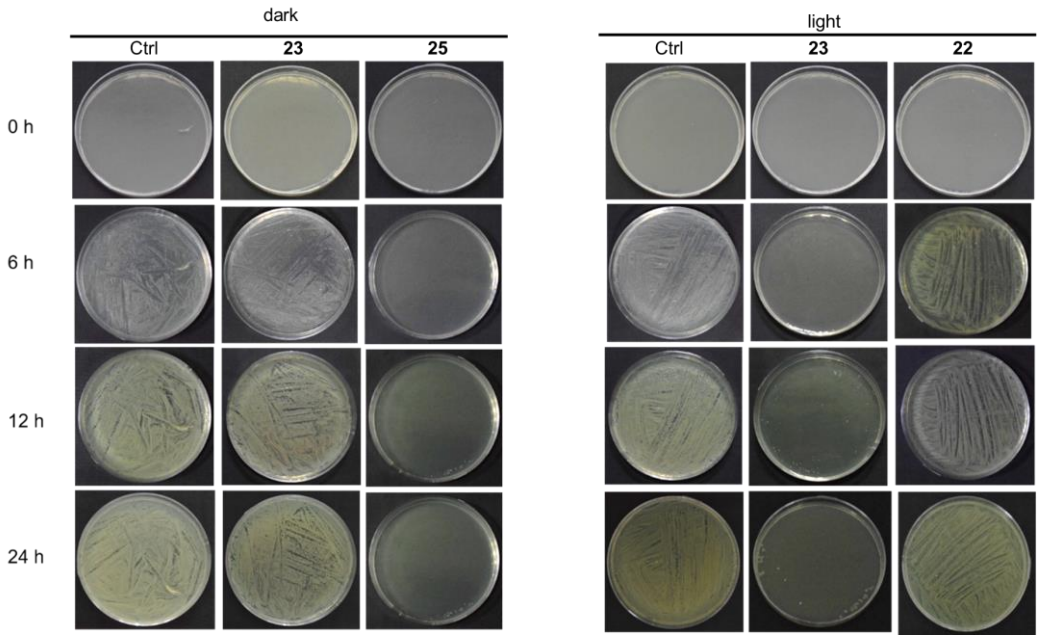

After irradiation of compound **23** with visible light in gram-negative bacteria *E. coli*, the antibacterial activity of the liberated antibiotic was successfully demonstrated using both growth curve and agar growth methods.

4.3.3. Summary:

Antibacterial photopharmacology has been used in Chapter **4** to tackle antibiotic resistance. This approach uses light as an external handle to modulate the antibiotic's activity, allowing for shorter antibiotic exposure times and lower doses. BODIPY-Levofloxacin caged scaffold **23** was devised and synthesized to prevent the toxicity associated with UV light. The optical properties of BODIPY derivatives **22** and **23** were determined. When compound **23** was irradiated with light (470 nm, 30 mW/cm^2) for 30 minutes in methanol, TLC, and HPLC, investigations revealed breaking of the B-O bond and uncaging of the fluorescent molecule BODIPY-OMe. When compound **23** was initially exposed to light for 30 minutes in methanol and then incubated in buffer for 30 minutes, the liberation of antibiotic was detected, and the yield of liberated antibiotic was estimated to be 31%. Next, the efficacy of this released

antibiotic was examined against *E. coli* and *S. aureus*. Compound **23** showed an inhibitory effect after irradiation with visible light. When evaluated against *E. coli* in an agar growth method, the inhibitory activity of **23** was consistent and comparable to Levofloxacin antibiotic.

Using a BODIPY-based scaffold, the visible light-triggered release of a fluoroquinolone antibiotic was successfully demonstrated. It can be used to administer antibiotics directly to the infection site, potentially lowering drug doses and exposure duration. The light source wavelength can be adjusted from blue to a less toxic visible green light by making structural alterations to the BODIPY scaffold.

4.4. Experimental and Characterization Data:

4.4.1. Procedure for synthesis of 4-((5-fluoro-1,3,7,9-tetramethyl-10-phenyl-5H-4λ⁴,5λ⁴-dipyrrolo[1,2-c:2',1'-f][1,3,2]diazaborinin-5-yl)oxy)benzyl benzoate (22):

Following the reported procedure[21] to a stirred solution of benzoic acid (6 mg, 0.123 mmol), HBTU (44 mg, 0.117 mmol) and DMAP (5.7 mg, 0.046 mmol) in anhydrous CH_2Cl_2 (5 mL) were added DIPEA (104 µL, 0.583 mmol) and **24** (50 mg, 0.116 mmol) at rt. The reaction mixture was stirred for 12 hours at rt. After completion of the reaction as monitored by TLC, water (5 mL) and CH_2Cl_2 (15 mL) were added to the reaction mixture. The organic components were extracted with CH_2Cl_2, and collected organic phases were dried over anhydrous Na_2SO_4, concentrated under reduced pressure to obtain the crude product as red colored residue. The residue was purified by column chromatography using neutral alumina as stationary phase andPet Ether: EtOAc (100:0 to 93:7) as mobile phase to afford **22** (56 mg, 86%) as a red-orange solid. FT-IR (ν_{max}, cm^{-1}): 2855, 2736, 1718.15, 1466, 1302; ^1H NMR (400 MHz, $CDCl_3$) δ 8.06 – 8.02 (m, 2H), 7.59 – 7.45 (m, 5H), 7.43-7.41 (m, 2H), 7.34 – 7.31 (m, 1H), 7.19 (d, *J* = 8.0 Hz, 2H), 6.58 (d, *J* = 8.0 Hz, 2H), 5.93 (s, 2H), 5.22 (s, 2H), 2.52 (s, 6H), 1.38 (s, 6H); ^{13}C NMR (100 MHz, $CDCl_3$) δ 166.7, 156.7, 156.0, 143.4, 141.9, 135.1, 133.0, 131.8, 130.5, 130.1, 129.8, 129.3, 129.3, 129.1, 128.4, 128.1, 127.0, 121.8, 118.1, 77.2, 67.0, 15.0, 14.6; HRMS (ESI) for $[C_{33}H_{30}BFN_2O_3+Na]^+$: calcd., 555.2231, found, 555.2239.

4.4.1. Procedure for synthesis of 4-((5-fluoro-1,3,7,9-tetramethyl-10-phenyl-5H-4λ⁴,5λ⁴-dipyrrolo[1,2-c:2',1'-f][1,3,2]diazaborinin-5-yl)oxy)benzyl 9-fluoro-3-methyl-10-(4-methylpiperazin-1-yl)-7-oxo-2,3-dihydro-7H-[1,4]oxazino[2,3,4-ij]quinoline-6-carboxylate (23):

Following the reported procedure,[21] to a stirred solution of Levofloxacin (**25**) (42 mg, 0.116 mmol), HBTU (44 mg, 0.116 mmol) and DMAP (5.7 mg, 0.046 mmol) in anhydrous CH_2Cl_2 (5 mL), were added DIPEA (104 µL, 0.583 mmol) and compound **24** (52 mg, 0.116 mmol) at rt. The reaction mixture was stirred for 12 hours at rt. After completion of the reaction as monitored by TLC, water (5 mL) and CH_2Cl_2 (15 mL) were added to this. The organic components were extracted with CH_2Cl_2, and these collected organic phases were dried over anhydrous Na_2SO_4 and concentrated under reduced pressure to obtain the crude product as a red colored residue. The crude product was purified by column chromatography using neutral alumina as stationary phase and $CHCl_3$: MeOH (100:0 to 93:7) as mobile phase to afford **23**

(62 mg, 69%) as a red-orange solid. FT-IR (ν_{max}, cm^{-1}); 2925, 2849, 2800, 1718, 1617, 1547, 1470, 1300; ^{1}H NMR (400 MHz, $CDCl_3$) δ 8.09 (s, 1H), 7.57 -7.47 (m, 3H), 7.42 (d, *J* = 12.6 Hz, 1H), 7.34 - 7.29 (m, 2H), 7.23 (d, *J* = 8.6 Hz, 2H), 6.58 (d, *J* = 8.6 Hz, 2H), 5.89 (d, *J* = 15.4 Hz, 2H), 5.16 (d, *J* = 1.8 Hz, 2H), 4.35 (dd, *J* = 11.4, 2.3 Hz, 1H), 4.19 (dd, *J* = 11.3, 2.0 Hz, 1H), 4.02 (m, 1H), 3.32 (d, *J* = 4.4 Hz, 4H), 2.53 (s, 4H), 2.48 (d, *J* = 10.9 Hz, 6H), 2.35 (s, 3H), 1.39 (s, 6H), 1.37 (s, 3H); ^{13}C NMR (100 MHz, , $CDCl_3$) δ 172.8, 165.7, 157.0, 156.7, 156.6, 156.0, 155.9, 154.5, 145.3, 143.4, 141.9, 139.6, 135.0, 131.8, 130.4, 129.4, 129.3, 129.2, 128.2, 128.1, 127.1, 123.7, 121.8, 117.9, 109.7, 105.3, 77.2, 68.1, 66.7, 55.8, 54.7, 50.6, 50.6, 46.5, 18.4, 15.0, 14.6; HRMS (ESI) for $[C_{44}H_{44}BF_2N_5O_5+H]^+$: calcd.: 772.3404, found: 772.3498.

4.4.2. General procedure for irradiation:

A quartz cuvette containing **23** in methanol was irradiated at 470 nm (30 mW/cm^2) by blue LED at room temperature in a closed chamber. This solution was used for further analysis as described below.

4.4.3. Decomposition study by TLC after photo-irradiation:

Compound **23**(500 μM, 100 μL) was irradiated for 30 min in methanol. TLC analysis of irradiated aliquot (250 μM, 50μL) in methanol was conducted. Another irradiated aliquot of **1**was incubated in pH 7.4 (50 mM) phosphate buffer (250 μM, 100μL) for 30 min. TLC analysis of aliquot (250 μM, 50μL) in pH 7.4 phosphate buffer was conducted. A mobile phase of methanol: chloroform (1:9) was used to run the TLC.

4.4.4. Decomposition study in methanol by HPLC after photo-irradiation:

Compound **23**(100 μM, 500 μL) was irradiated for 30 min in methanol and HPLC analysis of the aliquot was conducted. A diode array detector (DAD) operating at 500 nm and a fluorescence detector (FLD; λ_{ex} = 470 nm and λ_{em} = 540 nm) were used. 25 μL volume of aliquot (25 μM in ACN) was used for injection. A mobile phase of water: acetonitrile: methanol was used with a run time of 25 min. A multistep gradient was used with a flow rate of 1 mL/min starting with 20:40:40 → 0 - 5 min, 20:40:40 to 5:45:50 → 5 - 15 min, 5:45:50 → 15 - 20 min, 5:45:50 to 20:40:40 → 20 - 22 min, 20:40:40 → 22 - 25 min. Retention time for **23** was obtained at 16.6 min, for **27** was obtained at11.3 min (Scheme 4.2).

4.4.5. Levofloxacin quantification after photo-irradiation:

Compound **23**(100 μM, 500 μL) was irradiated for 30 min in methanol and incubated in pH 7.4 phosphate buffer (25 μM, 500 μL) for 30 minutes at 37 ºC, and HPLC analysis of the aliquot was conducted. A diode array detector (DAD) operating at 500 nm and a fluorescence detector (FLD; λ_{ex} = 330 nm and λ_{em} = 510 nm) were used. 15 μL volume of aliquot (25 μM) was used for injection. A mobile phase of water: acetonitrile (with 0.02% TFA): methanol was used with a run time of 17 min. A multistep gradient was used with a flow rate of 1 mL/min starting with 80:10:10 →0 - 5 min, 80:10:10 to 5:45:50 → 5 - 10 min, 5:45 :50 → 10 - 13 min, 5:45:50 to 80:10:10 → 13 - 15 min, 80:10:10 →15 - 17 min. Retention time for **Levofloxacin** was obtained at 7.3 min. The yield of released Levofloxacin after 30 min incubation in buffer was calculated to be 31%

4.4.6. Bacterial Strains and Growth Conditions.

Both the strains *E. coli* (ATCC 25922) and *S. aureus* (ATCC 29213) were obtained from ATCC. All of the bacterial strains were routinely grown in Luria Bertani (LB) broth, Mueller Hinton broth II (MHB) cation supplemented medium, tryptic soy agar and tryptic soy broth, purchased from Himedia. For every experiment, a starting culture was produced by inoculating a single colony picked from the agar plate into liquid medium and incubated overnight at 37˚C with continuous shaking. Levofloxacin was purchased from TCI in the purified powdered form. *E. coli* ATCC 25922 was grown overnight in Luria Bertani (LB) broth. Bacterial density was adjusted to 10^8 colony forming unit (CFU)/mL corresponding to an optical density (600 nm, OD_{600}) of 0.1. Next, 200 μL of this bacterial suspension was taken in a 96-well microtiter plate. Different lanes were chosen for different conditions such as bacterial control, bacteria with compound **23**, bacteria with compound **22** (negative control), bacteria with Levofloxacin, and so on. Then, 100× stock solutions were used for all of the compounds. One plate without irradiation was incubated at 37 ˚C in the dark by covering with an aluminum foil. Another plate was irradiated at 470 nm (30 mW/cm^2) by blue light-emitting diode (LED) at room temperature in a closed chamber for 5 min and then incubated at 37 ˚C in the dark by covering with an aluminum foil. OD_{600} was measured using a Thermo Scientific Varioskan Flash microwell plate reader for both the plates at an interval of 1 h for 6 h. Values reported are average of six replicates. Errors have been calculated from standard deviation between the values. Methicillin-sensitive *S. aureus* ATCC 29213 was grown overnight in Mueller Hinton broth II (MHB) cation supplemented medium. A similar procedure was followed further as was followed for *E. coli*.

4.4.7. Growth Inhibition of E. coli on Agar Plates.

Agar plates were prepared using soyabean casein digest medium (tryptone soya broth) and agar powder. *E. coli* ATCC 25922 was grown overnight in Luria Bertani (LB) broth. Bacterial density was adjusted to 10^8 colony-forming unit (CFU)/mL corresponding to an optical density (600 nm, OD_{600}) of 0.1. Next, 100 μL of this bacterial suspension was taken for streaking on the agar plate. Then, 100× stock solutions were used for all of the compounds. Bacteria were streaked on the entire surface of the agar plate using a Hi-Flexiloop 4 (Himedia). For samples with irradiation, bacterial suspensions (with or without compound) were taken in a quartz cuvette and irradiated at 470 nm (30 mW/cm^2) by blue LED at room temperature in a closed chamber for 30 min. These irradiated samples were then streaked on the agar plates. All of the plates were then incubated at 37 $^{\circ}C$ in the dark by covering with an aluminium foil. Images were taken from 0 to 24 h using Nikon D3300 DSLR.

4.5. NMR Spectra:

^{1}H NMR of **22**

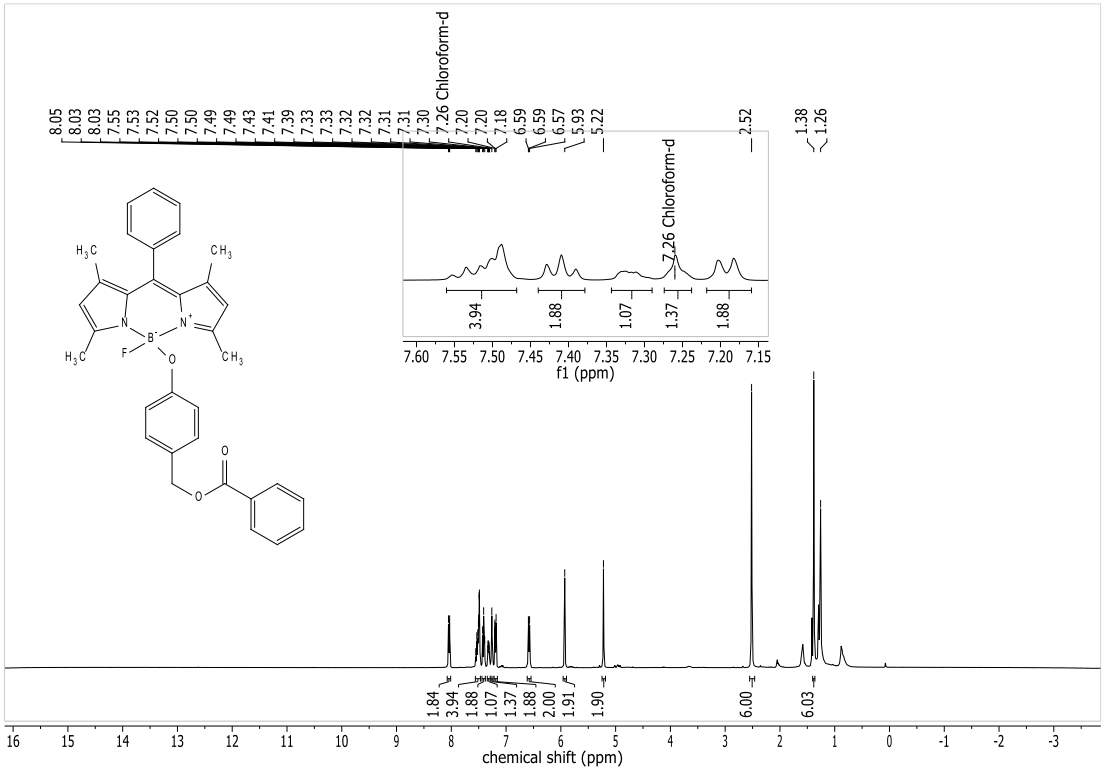

^{13}C NMR of **22**

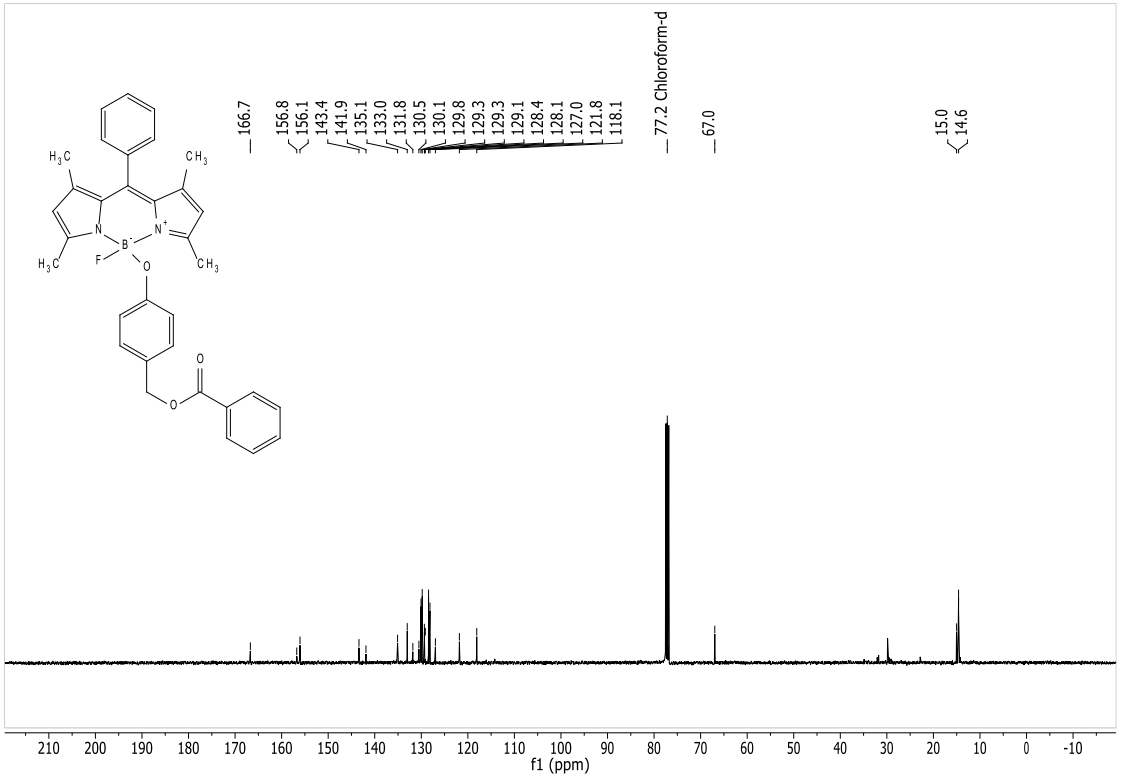

^{1}H NMR of **23**

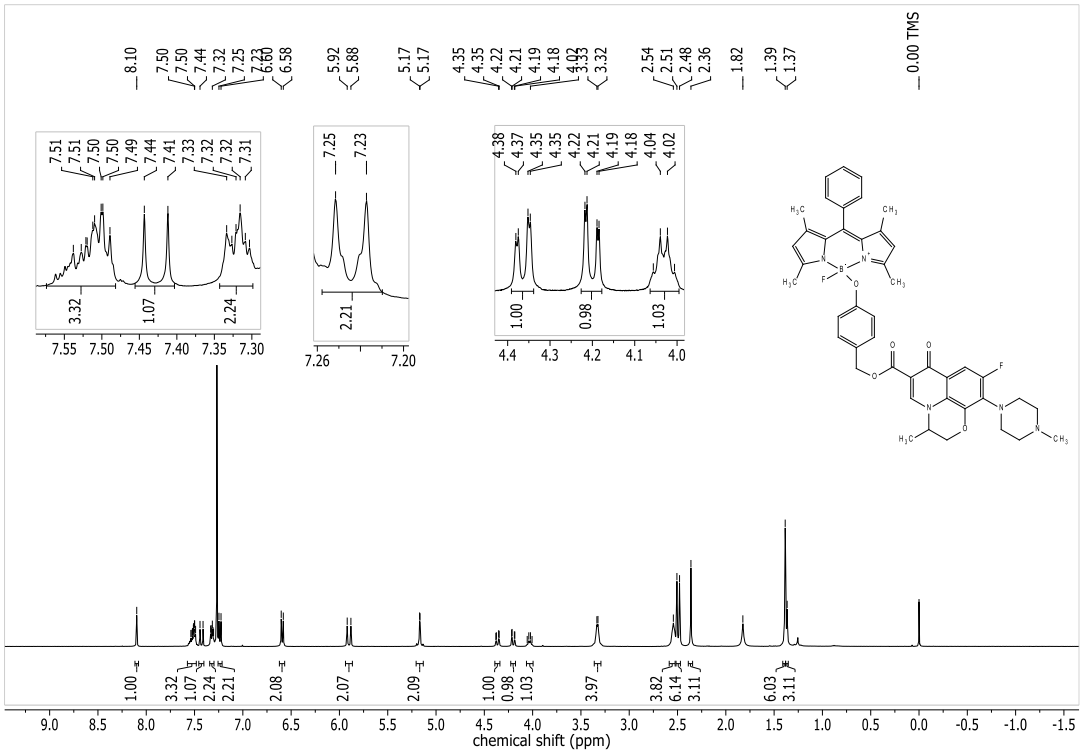

^{13}C NMR of **23**

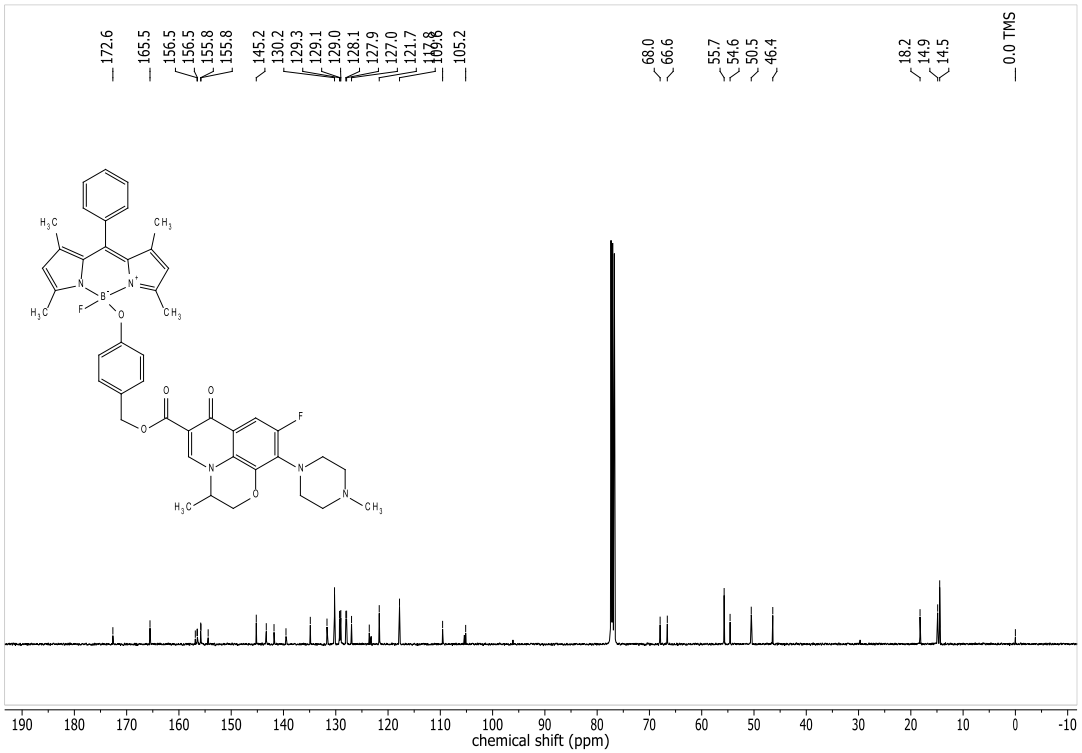

^{1}H NMR of **24**

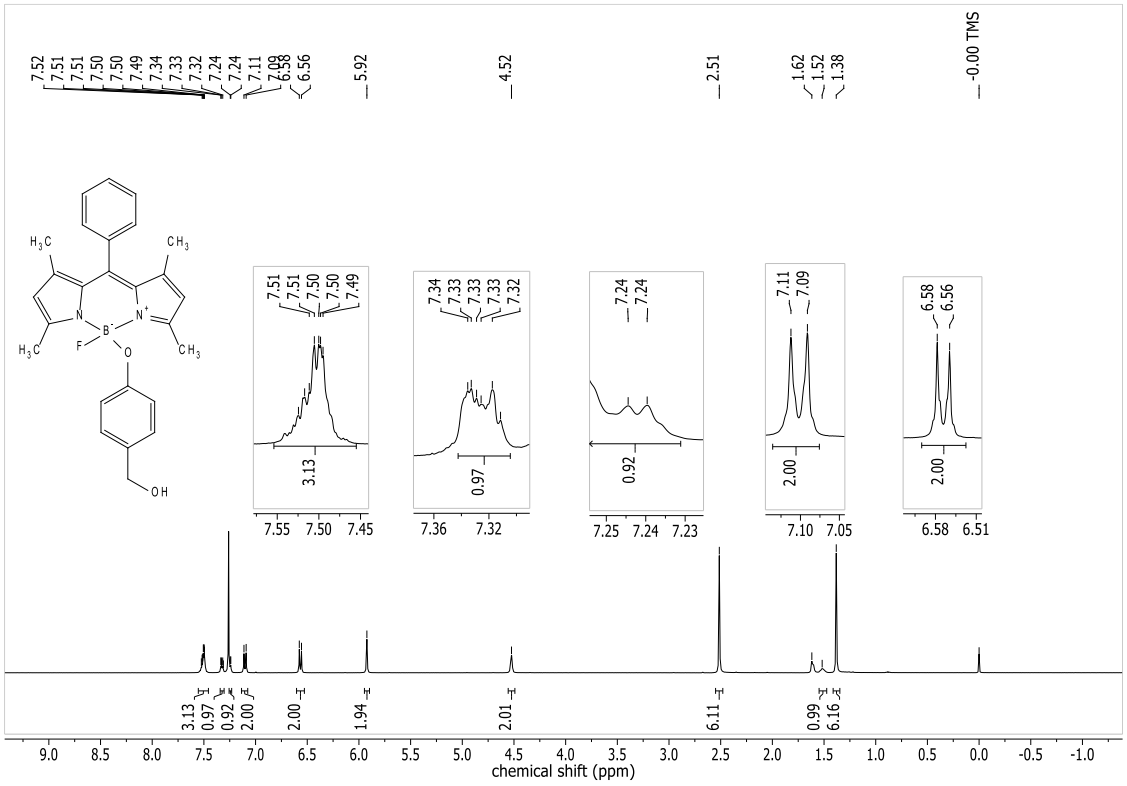
7.52
7.51
7.51
7.50
7.50
7.49
7.34
7.33
7.32
7.24
7.24
7.11
7.09
6.58
6.56
5.92
4.52
2.51
1.62
1.52
1.38
-0.00 TMS
H3C
CH3
N
B
N+
F
O
H3C
CH3
OH
3.13
0.97
0.92
2.00
2.00
1.94
2.01
6.11
0.99
6.16
chemical shift (ppm)

4.6. References:

(1) Pal, S.; Ramu, V.; Taye, N.; Mogare, D. G.; Yeware, A. M.; Sarkar, D.; Reddy, D. S.; Chattopadhyay, S.; Das, A. GSH Induced Controlled Release of Levofloxacin from a Purpose-Built Prodrug: Luminescence Response for Probing the Drug Release in Escherichia Coli and Staphylococcus Aureus. *Bioconjug. Chem.* **2016**, *27* (9), 2062–2070. https://doi.org/10.1021/acs.bioconjchem.6b00324.

(2) Mimata, H.; Tanigawa, T.; Ogata, J.; Takeshita, M. Regulation of Prostaglandin Synthesis by Reduced Glutathione in Urinary Bladder Epithelium. *J. Urol.* **1988**, *139* (3), 616–620. https://doi.org/10.1016/S0022-5347(17)42544-4.

(3) Pardeshi, K. A.; Kumar, T. A.; Ravikumar, G.; Shukla, M.; Kaul, G.; Chopra, S.; Chakrapani, H. Targeted Antibacterial Activity Guided by Bacteria-Specific Nitroreductase Catalytic Activation to Produce Ciprofloxacin. *Bioconjug. Chem.* **2019**, *30* (3), 751–759. https://doi.org/10.1021/acs.bioconjchem.8b00887.

(4) Hibbard, H. A. J.; Reynolds, M. M. Enzyme-Activated Nitric Oxide-Releasing Composite Material for Antibacterial Activity Against Escherichia Coli. *ACS Appl. Bio Mater.* **2020**, *3* (8), 5367–5374. https://doi.org/10.1021/acsabm.0c00670.

(5) Tegge, W.; Guerra, G.; Höltke, A.; Schiller, L.; Beutling, U.; Harmrolfs, K.; Gröbe, L.; Wullenkord, H.; Xu, C.; Weich, H.; Brönstrup, M. Selective Bacterial Targeting and Infection-Triggered Release of Antibiotic Colistin Conjugates. *Angew. Chemie Int. Ed.* **2021**, *60* (33), 17989–17997. https://doi.org/10.1002/anie.202104921.

(6) Young, D. D.; Deiters, A. Photochemical Control of Biological Processes. *Org. Biomol. Chem.* **2007**, *5* (7), 999–1005. https://doi.org/10.1039/B616410M.

(7) Beharry, A. A.; Woolley, G. A. Azobenzene Photoswitches for Biomolecules. *Chem. Soc. Rev.* **2011**, *40* (8), 4422. https://doi.org/10.1039/c1cs15023e.

(8) Szymański, W.; Beierle, J. M.; Kistemaker, H. A. V.; Velema, W. A.; Feringa, B. L. Reversible Photocontrol of Biological Systems by the Incorporation of Molecular Photoswitches. *Chem. Rev.* **2013**, *113* (8), 6114–6178. https://doi.org/10.1021/cr300179f.

(9) Velema, W. A.; Hansen, M. J.; Lerch, M. M.; Driessen, A. J. M.; Szymanski, W.; Feringa, B. L. Ciprofloxacin–Photoswitch Conjugates: A Facile Strategy for

Photopharmacology. *Bioconjug. Chem.* **2015**, *26* (12), 2592–2597. https://doi.org/10.1021/acs.bioconjchem.5b00591.

(10) Shi, Y.; Truong, V. X.; Kulkarni, K.; Qu, Y.; Simon, G. P.; Boyd, R. L.; Perlmutter, P.; Lithgow, T.; Forsythe, J. S. Light-Triggered Release of Ciprofloxacin from an in Situ Forming Click Hydrogel for Antibacterial Wound Dressings. *J. Mater. Chem. B* **2015**, *3* (45), 8771–8774. https://doi.org/10.1039/C5TB01820J.

(11) Shchelik, I. S.; Tomio, A.; Gademann, K. Design, Synthesis, and Biological Evaluation of Light-Activated Antibiotics. *ACS Infect. Dis.* **2021**, *7* (3), 681–692. https://doi.org/10.1021/acsinfecdis.1c00015.

(12) Brieke, C.; Rohrbach, F.; Gottschalk, A.; Mayer, G.; Heckel, A. Light-Controlled Tools. *Angew. Chemie Int. Ed.* **2012**, *51* (34), 8446–8476. https://doi.org/10.1002/anie.201202134.

(13) Bradley, J. S.; Byington, C. L.; Shah, S. S.; Alverson, B.; Carter, E. R.; Harrison, C.; Kaplan, S. L.; Mace, S. E.; McCracken, G. H.; Moore, M. R.; St Peter, S. D.; Stockwell, J. A.; Swanson, J. T. The Management of Community-Acquired Pneumonia in Infants and Children Older Than 3 Months of Age: Clinical Practice Guidelines by the Pediatric Infectious Diseases Society and the Infectious Diseases Society of America. *Clin. Infect. Dis.* **2011**, *53* (7), e25–e76. https://doi.org/10.1093/cid/cir531.

(14) Goswami, P. P.; Syed, A.; Beck, C. L.; Albright, T. R.; Mahoney, K. M.; Unash, R.; Smith, E. A.; Winter, A. H. BODIPY-Derived Photoremovable Protecting Groups Unmasked with Green Light. *J. Am. Chem. Soc.* **2015**, *137* (11), 3783–3786. https://doi.org/10.1021/jacs.5b01297.

(15) Loudet, A.; Burgess, K. BODIPY Dyes and Their Derivatives: Syntheses and Spectroscopic Properties. *Chem. Rev.* **2007**, *107* (11), 4891–4932. https://doi.org/10.1021/cr078381n.

(16) Zou, J.; Yin, Z.; Ding, K.; Tang, Q.; Li, J.; Si, W.; Shao, J.; Zhang, Q.; Huang, W.; Dong, X. BODIPY Derivatives for Photodynamic Therapy: Influence of Configuration versus Heavy Atom Effect. *ACS Appl. Mater. Interfaces* **2017**, *9* (38), 32475–32481. https://doi.org/10.1021/acsami.7b07569.

(17) Kawatani, M.; Kamiya, M.; Takahashi, H.; Urano, Y. Factors Affecting the Uncaging

Efficiency of 500 Nm Light-Activatable BODIPY Caging Group. *Bioorg. Med. Chem. Lett.* **2018**, *28* (1), 1–5. https://doi.org/10.1016/j.bmcl.2017.11.030.

(18) Umeda, N.; Takahashi, H.; Kamiya, M.; Ueno, T.; Komatsu, T.; Terai, T.; Hanaoka, K.; Nagano, T.; Urano, Y. Boron Dipyrromethene As a Fluorescent Caging Group for Single-Photon Uncaging with Long-Wavelength Visible Light. *ACS Chem. Biol.* **2014**, *9* (10), 2242–2246. https://doi.org/10.1021/cb500525p.

(19) Patil, N. G.; Basutkar, N. B.; Ambade, A. V. Visible Light-Triggered Disruption of Micelles of an Amphiphilic Block Copolymer with BODIPY at the Junction. *Chem. Commun.* **2015**, *51* (100), 17708–17711. https://doi.org/10.1039/C5CC06820G.

(20) Sharma, A. K.; Nair, M.; Chauhan, P.; Gupta, K.; Saini, D. K.; Chakrapani, H. Visible-Light-Triggered Uncaging of Carbonyl Sulfide for Hydrogen Sulfide (H 2 S) Release. *Org. Lett.* **2017**, *19* (18), 4822–4825. https://doi.org/10.1021/acs.orglett.7b02259.

(21) Wassvik, C. M.; Holmén, A. G.; Draheim, R.; Artursson, P.; Bergström, C. A. S. Molecular Characteristics for Solid-State Limited Solubility. *J. Med. Chem.* **2008**, *51* (10), 3035–3039. https://doi.org/10.1021/jm701587d.

Synopsis

Development Of Iodonium-Based Gram-Negative Antibacterial Compounds And Target Identification Using A Chemopr oteomics Approach

Chapter 1: Introduction

Bacteria are unicellular living microorganisms that are difficult to visualize without the use of a microscope.[1] Many bacteria are essential for human survival, but pathogenic bacteria cause diseases such as pneumonia, typhoid, and tuberculosis in humans and animals (TB). Bacterial infections are one of the top causes of death around the world. Antibiotics are widely used now to prevent and cure infectious diseases. Depending upon the activity, antibiotics are classified into two categories: bacteriostatic and bactericidal.[2] Bacteriostatic antibiotics only inhibit bacterial growth, whereas bactericidal antibiotics kill the bacterium. Microorganisms can acquire resistance to antibiotics and become immune to them. This phenomenon is referred to as antibiotic resistance. There are many reasons associated with antibiotic resistance[3,4], such as

- Overuse of antibiotics
- Incomplete course of antibiotic treatment by patients
- Use of antibiotics in food farming practices
- Poor hygiene control and longer exposure to infections in hospitals have evoked the emergence of multidrug-resistant bacteria extensively drug-resistant (XDR) bacteria
- Lack of new antibiotics

The term "ESKAPE" refers to a panel of six highly virulent multidrug-resistant bacteria *Enterococcus spp., Staphylococcus aureus, Klebsiella pneumoniae, Acinetobacter baumannii, Pseudomonas aeruginosa,* and *Enterobacter spp.* (ESKAPE) that are responsible for the majority of nosocomial infections.[5] The ESKAPE infections have a high propensity for developing multidrug resistance, which increases mortality and morbidity, therefore limiting the options for therapeutics.[5,6,] The ESKAPE pathogens develop the multidrug resistance (MDR) through several mechanisms as listed out below:[7]

- by inactivating the drug by an enzyme
- by modifying the active site where the antibiotic binds,
- or reduce drug accumulation due to decreased permeability
- by effluxing the drug out

Due to the dwindling treatment options, Gram-negative ESKAPE pathogens (*K. pneumoniae*, *A. baumannii*, *P. aeruginosa*, and *Enterobacter spp.*) require more resources and attention. Also, the paucity of new antibacterial drugs with novel modes of action in the drug development pipeline for multidrug-resistant gram-negative bacteria is concerning.

Figure 1 Timeline of discovery of antibiotic and developed antibiotic resistance

Many therapeutic strategies have been developed to address this concern, such as the use of antibiotics in combination or with adjuvants, photodynamic therapy, spatiotemporal control over the antibiotic generation, antimicrobial peptides, bacteriophage therapy, phytochemicals and nanoparticles as antibacterial agents, antibacterial antibodies, and the discovery of a new class of antibiotics.[7]

In this thesis, two different approaches are discussed to address antibiotic resistance, such as the discovery of a new therapeutic antibacterial agent and the Spatio-temporal release of an antibiotic using antibacterial photopharmacology technique.

An antibacterial photopharmacology technique offers light as an external handle to control the drug's action can reduce off-target activity and avoid the severe side of antibiotics.[8,9] In the antimicrobial photopharmocology field, an antibiotic is appended with either a photocleavable group or an optical switch, which releases the antibiotic upon activation. An exemplary work by, Feringa and co-workers have shown that a model fluoroquinolone is attached with a diazo functional group which acts as an optical switch, and upon activation with UV light, it goes through isomerization and generates the active antibiotic.[10] It was also shown that once the antibiotic action against *E. coli* and *S. aureus* is complete, it can be inactivated by using a

different light source. In another study, Gademann and colleagues integrated vancomycin and cephalosporin antibiotics with an o-nitroaryl cleavable group that can be activated with UV light. The antimicrobial activity of liberated antibiotics was assessed using bacterial growth curve analysis against *B. subtilis*, *S. aureus*, MRSA, *E. coli*, and *P. aeruginosa*.[11] However, the use of UV light is undesirable because of its phototoxicity. Hence, a visible light-triggered photocleavable group with an antibiotic is highly advantageous. This is discussed in Chapter **4**, where visible light-activated release of fluoroquinolone was demonstrated

Given the timeframe and rate of growing antibiotic resistance, new antibacterial discoveries and identification are urgently required. In phenotype-based drug discovery, several molecules are screened using biochemical phenotype assays in cells, tissues, or organisms to identify the lead molecule, which can be utilized to identify the targets.[12] Various target identification technologies have been developed, among them Proteomics and genomic methods, with modern molecular biology, are the most important technologies..[13] Proteomic techniques explore the potential targets for a drug or drug-like chemical by examining a complete pool of proteins known as the proteome. Activity-based protein profiling (ABPP) is used to investigate covalent interactions..[14]

The complex proteomes of various biological systems, such as cancer and bacterial cells, have been intensively studied using activity-based protein profiling (ABPP).[15] ABPP is a chemoproteomic method for determining the functional status of proteins or enzymes in cells or animals using an activity-based chemical probe. A traditional activity-based chemical probe consists of a reactive group that reacts with protein residue and is linked to a reporter tag or analytic handle through a linker. The activity-based probe with alkyne/azide handle can react with fluorescent or azide/alkyne using copper-catalyzed click reaction to obtain the readouts.[16,17] The readouts or identification of target proteins can be obtained using SDS-PAGE analysis or LC-MS/MS.[18–22]

Figure 2 Schematic of Activity-Based Protein Profiling

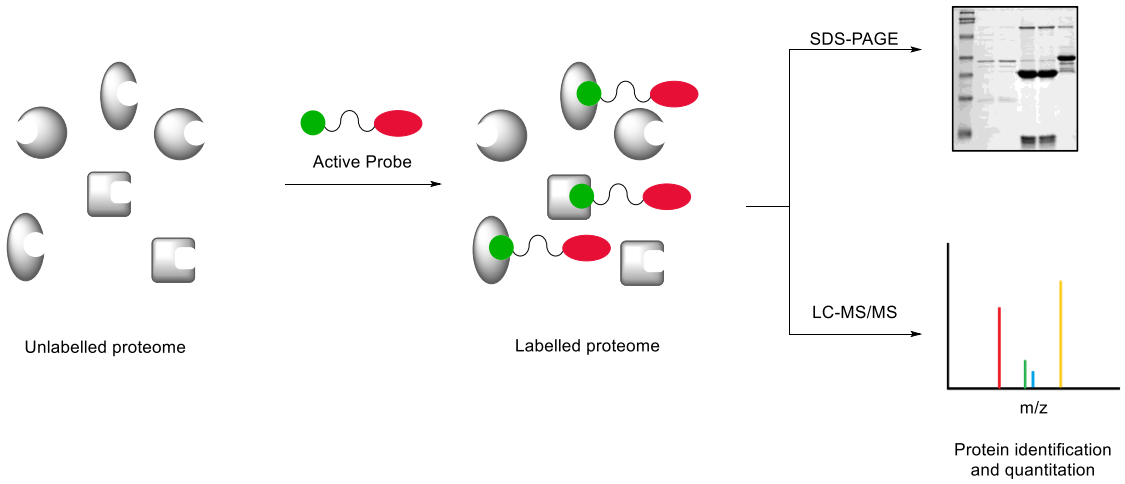

In order to follow the phenotype-based drug discovery approach, screening of antibacterial molecules with a novel mechanism of action is required. Based on the available literature reports, the antibacterial iodonium class of molecules was selected. Jeong and co-workers have demonstrated diphenyleneiodonium chloride (DPIC) as a potent inhibitor of multidrug resistant (MDR) *Helicobacter pylori* strains with <0.03 MIC (µg/mL).[23] Following up on this study, Pandey and co-workers have identified DPIC as a broad-spectrum antibacterial molecule that is significantly potent against multidrug resistant *Staphylococcus aureus* (MIC; 1-2 µg/mL) and *Mycobacterium tuberculosis* (MIC; 0.03 µg/mL).[24], Baell and co-workers have demonstrated the structural activity relationship (SAR) of diphenyleneiodonium triflate series of compounds against multidrug resistant ESKAP pathogens and *Mycobacterium tuberculosis* (*Mtb*) and identified 5-chlorodiphenyleneiodonium as a lead candidate.[25]

Diaryliodonium compounds are therefore promising therapeutic candidates. However, in bacterial cells, the mechanism of action or targets of the iodonium class of chemicals remains to be identified.

Hence, in this study, DPIC was selected as a prototype of the iodonium class of compounds. The targets of DPIC in bacterial cells can be identified using chemoproteomic techniques. Gram-negative bacteria *E. coli* was selected as a model organism for protein profiling. The DPIC alkyne probe **P1** was synthesized. Using ABPP, the proteome of *E. coli* was profiled with probe **P1**, explained in Chapter **2**. The targets of DPIC in *E. coli* were identified using LC-MS/MS-based chemoproteomic methods. The promising target protein was cloned, purified, and validated using ABPP. Further to enhance the antibacterial activity spectrum of

iodonium compounds, heterocyclic iodonium compounds were designed, synthesized, and screened against ESKAPE pathogens. One of these, diheterocyclic iodonium, has been discovered as a lead chemical that is effective against Gram-negative multidrug-resistant bacteria *A. buamannii*. The proteome of *A. baumannii* was also profiled with the identified lead compound using ABPP methods, and targets were identified using an LC-MS/MS-based proteomics methodology, as discussed in Chapter **3**. Furthermore, a visible light-triggered release of a fluoroquinolone antibiotic was demonstrated utilizing one of the photopharmacology methods, as described in Chapter **4**.

Chapter 2: Chemoproteomic Approaches Towards the Probable Target Identification of DPIC in *E. coli*

In the context of antibiotic resistance, diphenylene iodonium chloride (DPIC) is reported to be active against MDR *Helicobacter pylori*, *Staphylococcus aureus*, and *Mycobacterium tuberculosis*.[23,24] However, the mechanism of action or specific targets of the iodonium class of molecules in bacterial cells are not completely characterized. In mammalian model systems, DPIC has been considered as an inhibitor of NADH/ NADPH oxidase.[26,27] However, DPIC is not a specific inhibitor of NADPH oxidase and may interact with other proteins and enzymes. The interaction of DPIC with proteins is yet to be investigated in bacterial cells. However, despite the known inhibitory effects of this compound, the interaction of DPIC with proteins is yet to be investigated in bacterial cells. Considering this, we decided to investigate the possible targets of this potent antibacterial agent utilizing activity-based protein profiling (ABPP) as one of the chemoproteomic approaches. *E. coli* was chosen as a model organism for this study. In order to perform ABPP, It would be necessary to have analytical handle such as an alkyne appended to DPIC. Following Scheme 1 DPIC alkyne probe was synthesised.

Scheme 1 Synthesis scheme for DPIC-alkyne probe

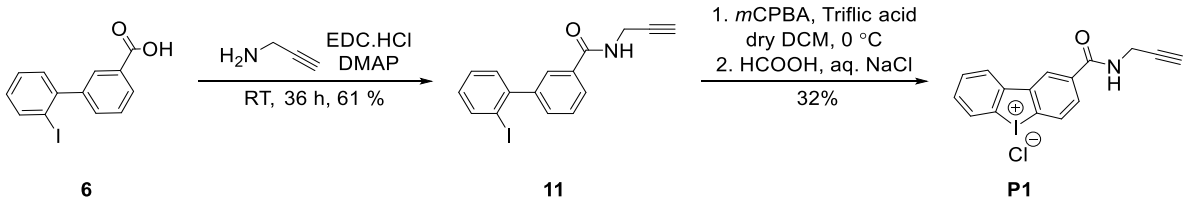

The alkyne probe **P1** was assessed for its antibacterial activity against Gram-negative pathogen *E. coli*. Growth curve analysis showed that **P1** inhibited the growth of bacteria in a dose-dependent manner supporting the use of this compound to elucidate the targets of DPI.

Next, protein profiling by probe **P1** was investigated using ABPP in *E. coli* proteome. A dose-dependent protein labelling by probe **P1** was observed in soluble fraction than membrane fraction.

Figure 3 Dose-dependent profiling in soluble and membrane fractions of E. coli with DPIC alkyne probe P1

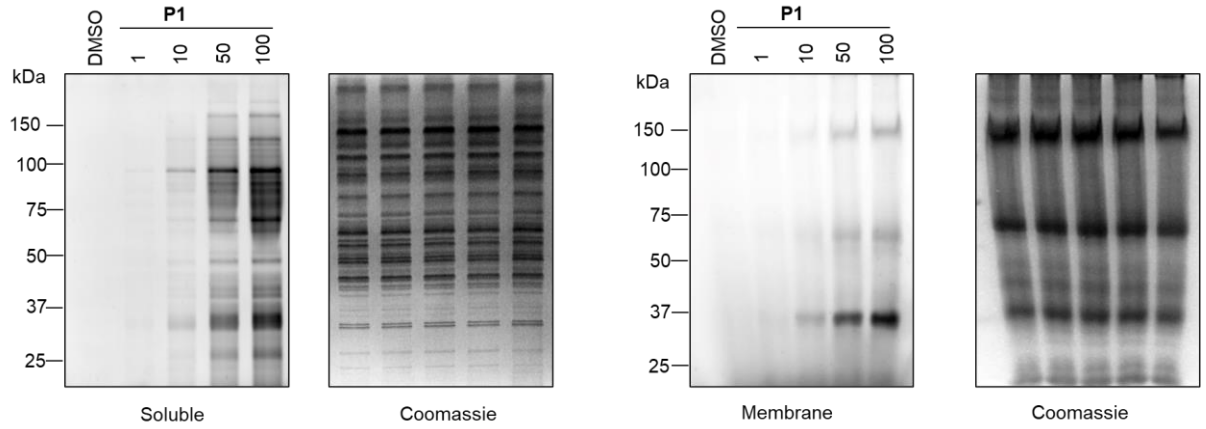

Thus, thiol-based proteins are normally more nucleophilic and are likely to react with electrophiles such as **P1**. In order to investigate the selectivity of the probe **P1** towards thiol, a competitive-ABPP based experiment was conducted with iodoacetamide (**IAM**), a thiol blocking agent[28], if **P1** modified cysteine residues in the proteome, a diminution in signal in the **IAM**-pretreated sample when compared with **P1** alone is expected.

Having established that the probe **P1** preferentially reacts with the cysteine residue of thiol-based proteins, a competitive ABPP based experiment was conducted with DPIC as a competitor. A reduction in intensity of several protein bands (marked as *) with increasing concentration of DPIC was observed indicating that DPIC covalently modifies certain proteins in the soluble proteome.

Figure 4 Chase experiment - In vitro modification of proteins in soluble fraction of E. coli with P1

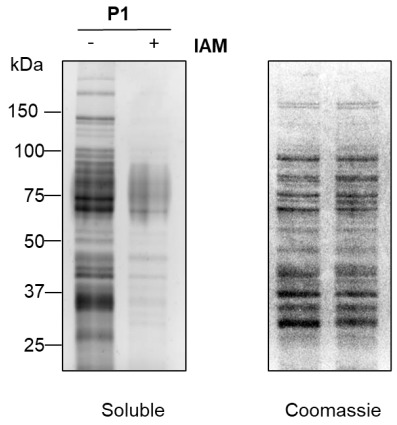

Next, a competitive ABPP based experiment was conducted with DPIC as a competitor. A reduction in intensity of several protein bands (marked as *) with increasing concentration of DPIC was observed, indicating that DPIC covalently modifies certain proteins in the soluble proteome A significant reduction in the intensity of certain protein bands in the DPIC pre-treated proteome (marked as *) when compared with the proteome treated with only **IAA** was observed. This finding is consistent with our earlier result with **IAM** and **P1**, and together these results suggest that DPIC reacted with cysteine residues of the proteins.

Figure 5 Chase experiment - In vitro modification of proteins in soluble fraction of E. coli with A) DPIC 1a chased with P1 and DPIC 1a; B) chased with iodoacetamide alkyne (IAA)

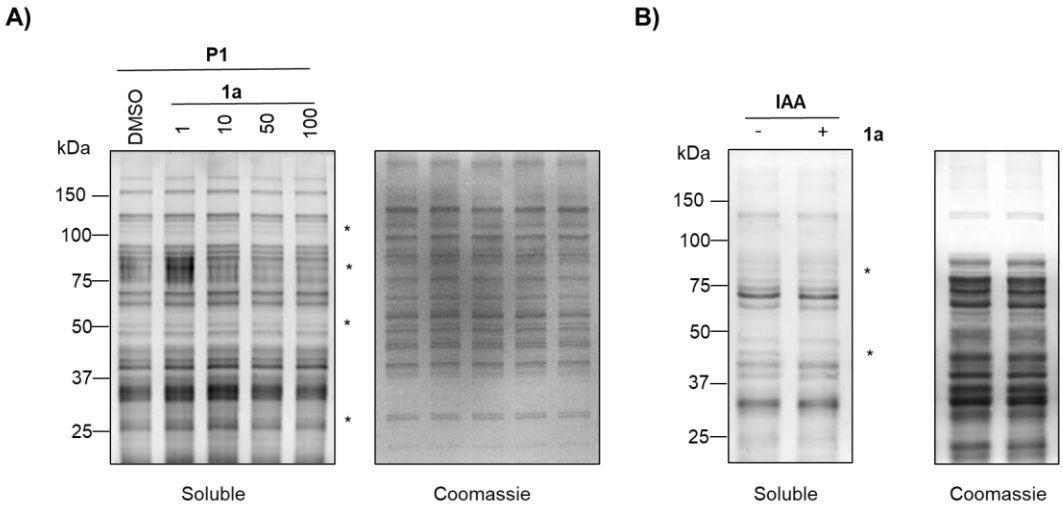

With these preliminary findings, using **P1** as a chemoproteomics probe, a competitive LC-MS/MS-based ABPP experiment was next conducted to identify the targets of DPIC. Based on the filtering criteria, three proteins named NADH-quinone oxidoreductase subunit F (NuOF), succinate dehydrogenase iron-sulfur subunit β (sdhb), and NADH-quinone oxidoreductase subunit G (NuOG) were listed as the probable targets of DPIC out of 125 proteins identified by LC-MS/MS.

All three targets are redox proteins that are involved in the bacterial respiratory system. *E. coli* NuOF has nine cysteine residues, of which a bioinformatics analysis across various bacterial species revealed that five of these are highly conserved.[29] One of the conserved cysteine residues is involved in the FMN binding site, whereas the other four are engaged in iron-sulfur cluster coordination ([4Fe-4S]) (Table 2.2).

Table 1 Bioinformatics assay for NuOF

Entry	Redox protein	Cysteine residues	Conserved cysteine residues
1.	NADH-quinone oxidoreductase subunit F (NuOF)	C89, C180, C215, C223, C351, C354, C357, C388, C398	FMN: C180 N3, 4Fe-4S: C351, C354, C357, C398

Gene cloning, protein expression, and purification were next carried out for NuOF, using *E. coli* as a model organism for validating the target. In order to validate the target protein, NuOF (0-20 µM) was treated with probe **P1** (100 µM) and visualized using in-gel fluorescence as described previously. Labelling by probe **P1** was observed with increasing protein concentration (Figure 6A). In order to understand if P1 modified NuOF through a covalent bond, NuOF (5 µM) was treated with probe **P1** (25 µM). Dialysis was next performed using a dialysis membrane with a molecular weight cut-off (MWCO) of 6-8 kDa in dialysis buffer. The DPIC alkyne probe has a molecular weight of 396 Da, and if the interaction between probe **P1** and protein is non-covalent, the probe will leach out during dialysis. A signal for probe **P1** labelling was observed in both dialyzed and non-dialyzed conditions confirming that probe **P1** covalently modifies NuOF (Figure 6B).

Figure 6 A) Labelling of wild-type NuOF target protein with DPIC probe P1 (100 µM); B) gel filtration experiment with probe P1 (25 µM)

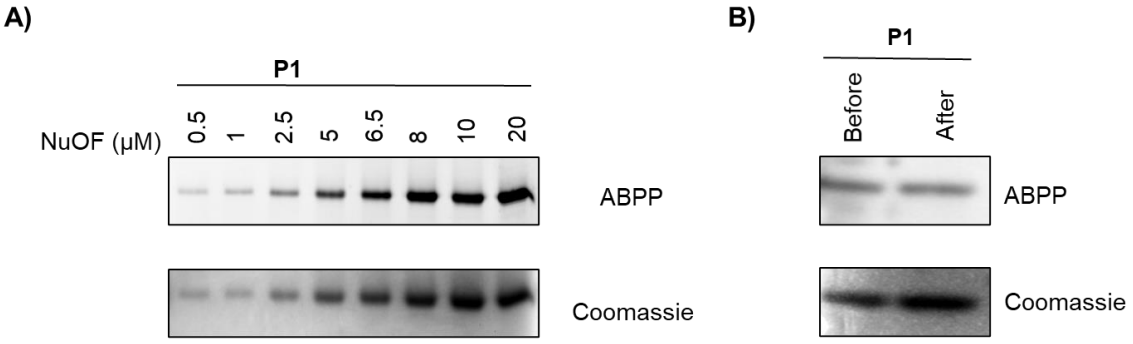

Having established that **P1** covalently modified NuOF, the ability of DPIC to modify NuOF was studied through a competition experiment. A fixed concentration of the protein pre-treated with DPIC (250 µM, 1 h) was treated with the probe **P1** (100 µM, 1 h). Standard ABPP and SDS-PAGE protocols were followed. A reduction in the intensity of the signal was observed for DPIC pre-treated protein when compared with only probe **P1** treated protein, indicating that NuOF certainly is a target of DPIC (Figure 7A). As discussed before, probe **P1** reacts with cysteine residues in proteins. So, a similar competitive ABPP based experiment was conducted with iodoacetamide as a competitor A significant reduction in signal in the iodoacetamide-treated protein when compared with untreated was observed (Figure 7B). This strongly suggested that the probe modifies cysteine residues of the protein. A cysteine to alanine point mutant of this protein to validate the target protein was next carried out to ascertain if any of the conserved cysteine residues were involved in modification by **P1**/DPI.

Figure 7 ABPP chase experiments with NuOF

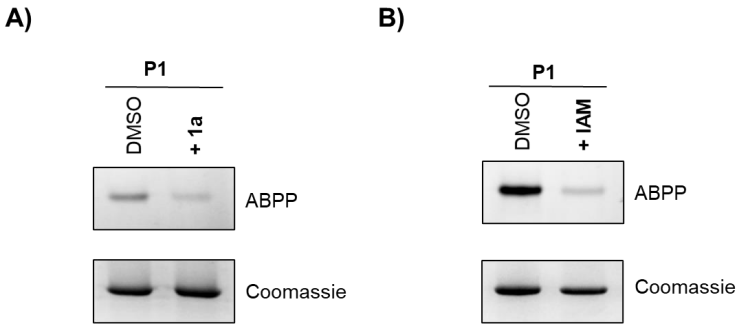

In NuOF, C180 is part of the FMN binding site while C351, C354, C357, and C398 are involved in coordination with Fe^{+2} of [4Fe-4S] iron-sulfur cluster. Cysteine to alanine point

mutations for C180, C351, C354 were considered. If a cysteine to alanine mutant continues to be labelled by **P1**, it is likely that the labelling is happening through other cysteine residues in the protein, suggesting that the cysteine that has been mutated is not an important residue for labelling by **P1**. Labelling with C180A suggested that C180 is not the target site of the probe **P1**(Figure 8. A). A similar labelling profile was observed with C351A and C354A mutant proteins (Figure 8. B, C). Hence, we decided to make a double alanine mutant for Cys351 and Cys354 residues. When tested using standard labelling techniques, a significant reduction in the intensity of the signal for the double mutant C351-354A when compared with WT was observed (Figure 8. D). Taken together, these results show that among the cysteine residues in NuOF, C351 and C354 were targets for modification by **P1**/DPI.

Figure 8 ABPP for validation of wild-type NuOF using cysteine point mutants

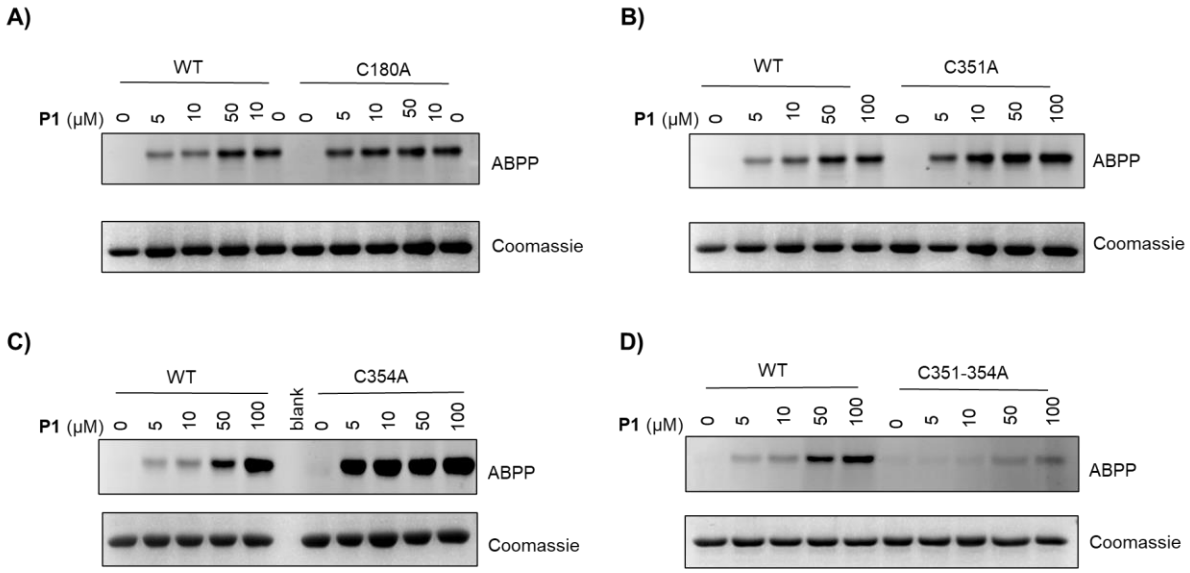

These cysteine residues C351 and C354 of NuOF are coordinated Fe^{+2} of [4Fe-4S] iron-sulfur cluster, which is involved in electron translocation during respiration, and inhibiting this protein is likely to have an effect on cell viability.

Chapter 3: Synthesis of DPIC Analogues and Evaluation of Their Antibacterial Activity against Gram-Negative Bacteria

Although DPIC displayed good antibacterial activity against Gram-negative bacteria[23,24,30,31], but the potency against MDR *A. baumannii*, an opportunistic Gram-negative pathogen, was diminished. *A. baumannii* is a troublesome pathogen responsible for various nosocomial such as skin and soft tissue, bloodstream, urinary tract infections, meningitis, and pneumonia.[32–34]

A. baumannii infections are most common in people who are immunocompromised or who are in hospitals with high-risk underlying illnesses.[35] To boost the effectiveness of iodonium compounds against *A. baumannii*, we aimed to synthesize a focused library of DPI analogs.

The introduction of any polar functional group over the benzene ring was thought to promote aqueous solubility. Hence, carboxylic acid and ester derivatives of DPI were synthesized, and when tested against ESKAP pathogens, these compounds have poor antibacterial efficacy (Table 2).

Figure 9 Structure of synthesized diphenyleneiodonium derivatives

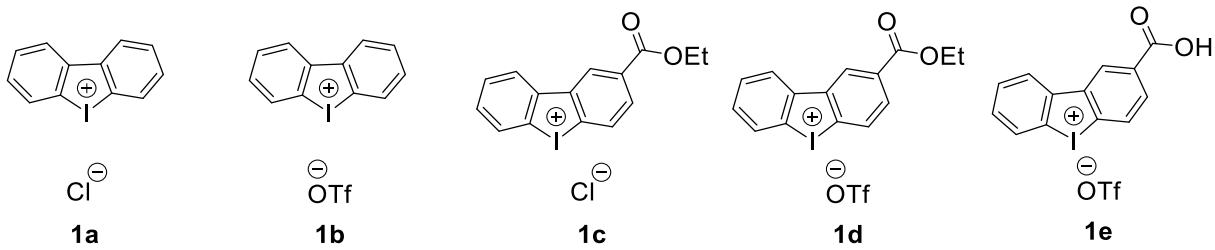

Table 2 Antibacterial activity of the iodonium compounds against ESKAP pathogens

		MIC[a] (µg/mL)				
Entry	Cpd.	*E. coli*	*S. aureus*	*K. pneumoniae*	*A. baumannii*	*P. aeruginosa*
1	**1a**	4	1	16	4	4
2	**1b**	2	2	16	2	2
3	**1c**	8	2	>64	16	16
4	**1d**	4	1	64	8	8
5	**1e**	>64	>64	>64	>64	>64
6	Levofloxacin	0.0156	0.125	64	4	0.5

[a]MIC against ESKAP (*E. coli* ATCC25922, *S. aureus* ATCC 29213, *K. pneumoniae* BAA1705, *A. baumannii* BAA1605, *P. aeruginosa* ATCC 27853) pathogens. (Data provided by: Dr. Sidharth Chopra lab, CSIR-CDRI Lucknow)

Next, the synthesis of heterocyclic iodonium compounds was considered to improve the antibacterial activity. The heterocyclic ring such as pyridine or thiophene was considered instead of benzene. Pyridine is often used in medicinal chemistry due to several unique

properties such as good hydrogen-bond forming ability, small molecular size, and increased water solubility[36]. Another heterocycle that was considered was thiophene, a well-known in medicine and is a constituent of a number of compounds with antibacterial, antihypertensive, and anticancer properties.[37]. The general synthetic approach was revised to synthesize the heterocyclic iodonium compounds, and a series of heterocyclic iodonium compounds were synthesized. (Compound **2a-2g** were synthesized by Mr. Suraj Sharma (BS-MS graduate) under my guidance using Scheme 3.3 with some modifications)

Figure 10 Structure of heterocyclic iodonium derivatives

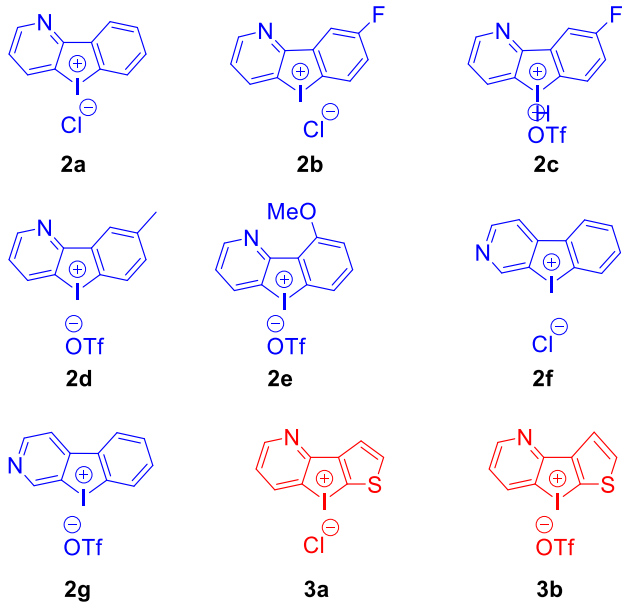

The antibacterial activity of these compounds was investigated against ESKAP pathogens (Table 3). Substitution of one benzene ring to pyridine has substantially improved the activity, notably in Gram-negative bacteria, i.e., *E. coli*, *K. pneumoniae*, *A. baumannii*, *P. aeruginosa.* Interestingly, the substitution of benzene rings with pyridine and thiophene **3a** and **3b** led to a significant increment in the activity against *A. baumannii*.

Table 3 Antibacterial activity of the heterocyclic iodonium compounds against ESKAP pathogens

		MIC[a] (µg/mL)				
Entry	Cpd.	*E. coli*	*S. aureus*	*K. pneumoniae*	*A. baumannii*	*P. aeruginosa*
1	**1a**	4	1	16	4	4
2	**2a**	0.25	0.5	2	0.125	0.25
3	**2b**	0.25	1	1	0.25	1
4	**2c**	0.125	0.25	2	0.125	0.5
5	**2d**	0.25	0.5	8	0.25	1
6	**2e**	0.5	1	2	8	4
7	**2f**	0.5	0.5	4	2	2
8	**2g**	0.5	0.5	2	2	2
9	**3a**	1	1	2	0.0625	1
10	**3b**	0.5	0.5	1	0.0625	0.5
11	Levofloxacin	0.0156	0.125	64	4	0.5

[a]MIC against ESKAP (*E. coli* ATCC25922, *S. aureus* ATCC 29213, *K. pneumoniae* BAA1705, *A. baumannii* BAA1605, *P. aeruginosa* ATCC 27853) pathogens. (Data provided by: Dr. Sidharth Chopra lab, CDRI Lucknow)

The cytotoxicity profile of selected compounds was then examined in Vero cells and compound **3a** was selected for further studies. Subsequently, **3a** was screened against a panel of patient-derived clinical isolates of multidrug resistant (MDR) *A. baumannii* which are only susceptible to Polymyxin B. Remarkably, **3a** was found to be as effective against all of these clinical isolates as as the routinely used Polymyxin B antibiotic against all of these clinical isolates.

Next, a time-kill analysis study revealed that compound **3a** exhibits bactericidal activity against *A. baumannii* at 10x MIC (MIC: 0.0625 µg/mL), clearly suggesting the therapeutic efficacy of compound **3a** (Figure 11A). In addition, the antibacterial potency of compound **3a** (1 mg/kg) and Polymyxin B (5 mg/kg) as a positive control were tested in a murine neutropenic thigh infection model. Compound **3a** was found to have excellent efficacy in this assay and significantly reduced *A. baumannii*-induced bacterial load. Together these results demonstrated that **3a** was bactericidal and worked well against *A. baumannii* in an animal model for infection (Figure 11B).

Figure 11 A) Time-kill curves for A. baumannii BAA 1605 treated with 1X and 10X MIC of 3a and Polymyxin B. B) In vivo efficacy of 3a in murine neutropenic thigh infection model.

A) Ctrl indicates untreated cells; Cell survival was plotted at the 24-h time point as log-change in colony-forming units per mL (log10 CFU/mL), and the curves show mean + SD of three independent experiments; **B)** Mice (24 mice/group) were rendered neutropenic, and the thigh muscle was intramuscularly infected with *A. baumannii* BAA 1605 at 1 x 10^8 CFU. The infected mice were treated with intraperitoneal doses of **3a** (1 mg/kg) and Polymyxin B (5 mg/kg) at 3 h and 6 h post-infection. Polymyxin B was used as a reference antibiotic. Ctrl is untreated mice. Statistical significance is calculated with respect to Ctrl (****p < 0.0001). (Data provided by: Dr. Sidharth Chopra lab, CDRI Lucknow)

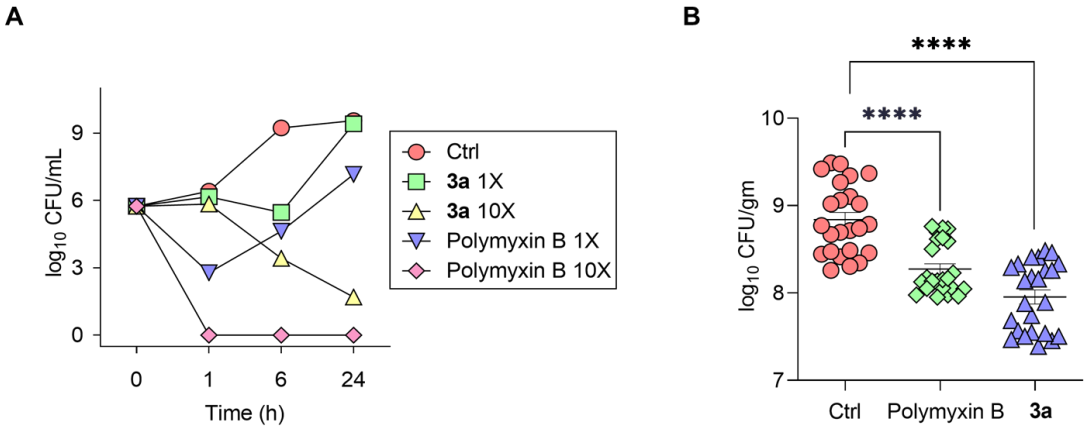

Having identified **3a** as the lead compound against *A. baumannii*, identification of protein targets for **3a** in *A. baumannii* was next carried out.

The *A.* proteomes were profiled with probe **P1** using previously described ABPP protocols. Probe **P1** caused dose-dependent covalent modification of various proteins was observed in both soluble and membrane proteomes (Figure 12).

Figure 12 Dose-dependent profiling of soluble and membrane fraction of A. baumannii with DPIC alkyne probe P1

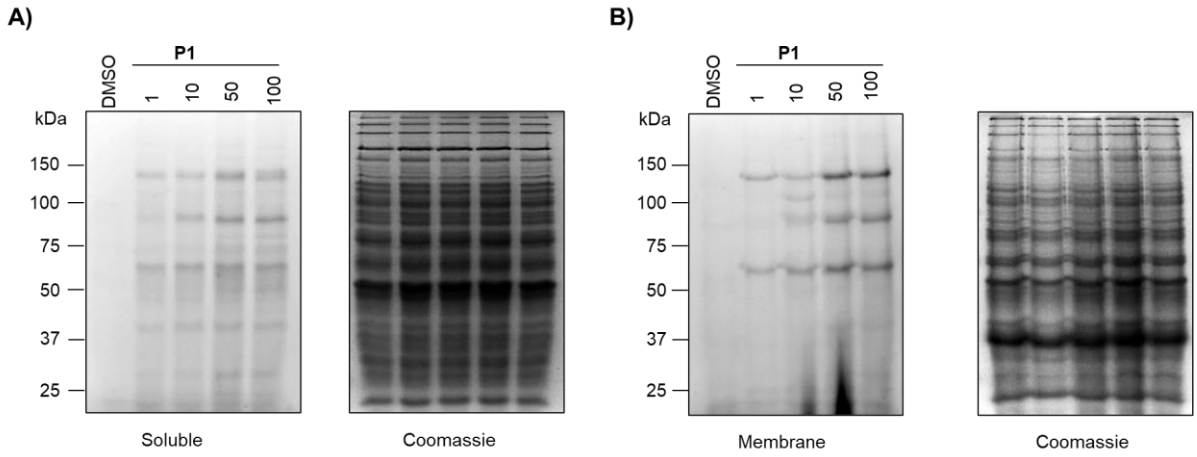

Next, a competitive ABPP based experiment was carried out using **3a** as a competitor. The membrane and soluble proteome were first independently treated with **3a** (1-250 µM, 1 h) followed by the treatment of probe **P1**(100 µM, 1 h). In comparison to the only probe **P1** treated lane, compound **3a** treated lanes showed a significant reduction in the intensity of labeled proteins (Figure 13), suggesting that **3a** covalently modifies certain proteins in the *A. buamannii* proteome.

Figure 13 Dose-dependent profiling in soluble and membrane fraction of A. baumannii with DPIC alkyne probe P1

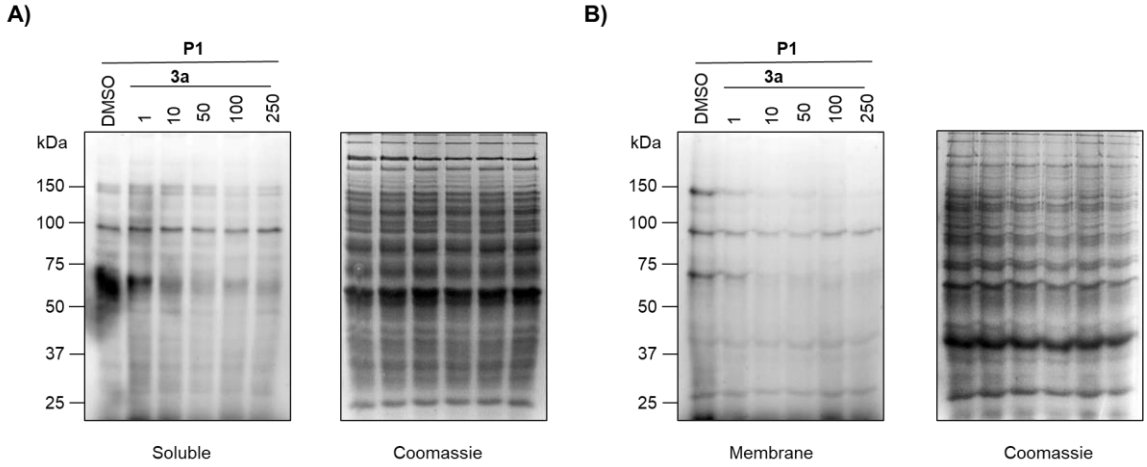

The selectivity of probe **P1** towards cysteine residues in *E. coli* was determined in Chapter **2**. In *A. baumannii*, a similar experiment was conducted. When compared to labelled proteins

treated with **P1** alone, a complete abruption or reduced signal for labelling of proteins was seen in the case of the **IAM**-pretreated sample. This study suggests that probe **P1** modifies the cysteine residue of proteins in *A. baumannii* proteome as well.

Figure 14 Chase experiment - In vitro modification of proteins in soluble fraction of A. baumannii with P1

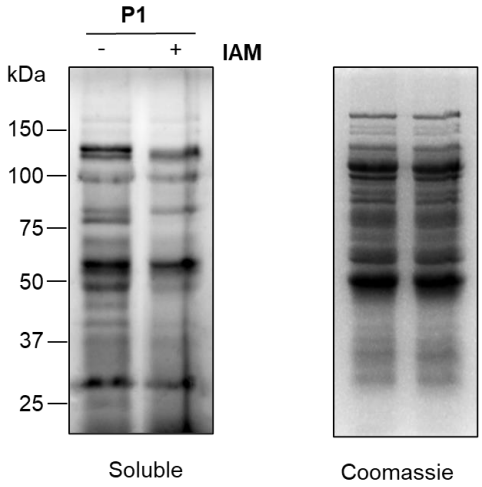

Next, a competitive LC-MS/MS based ABPP experiment was carried out to identify the target of **3a** in *A. baumannii* proteome using the similar protocol described in Chapter **2**. After fulfilling the filtering criteria, five target proteins were listed out for **3a** in the soluble proteome of *A. baumannii* (Table 4).

Table 4 Identified targets of 3a in A. baumannii

Entry	Accession	Name	log_2 FC	- log_{10} (p value)
1	WP_000840835.1	Glutamate synthase subunit β (gltD)	3.38234	2.370173
2	WP_001286300.1	betaine aldehyde dehydrgenase (betB)	2.961814	3.863535
3	WP_136040424.1	FAD-dependent oxidoreductase	2.776662	1.905118
4	WP_171249601.1	alkyl hydroperoxide reductase subunit F (ahpF)	1.477672	2.4707
5	WP_000258957.1	TPM domain-containing protein	1.04138	1.329168

Among these identified proteins, the most likely protein targets such as glutamate synthase subunit *β* (gltD) and betaine aldehyde dehydrogenase (betB) are essential for bacterial survival. Enzyme betB, which belongs to the aldehyde dehydrogenase family, is involved in the biosynthesis of glycine betaine.[38,39] Inhibition of betB would block the oxidation of betaine aldehyde, which itself is toxic to the bacterial cells. On the other hand, gltD is involved in the L-glutamate biosynthesis pathway and the amino acid synthesis pathway.[40,41] Thus, inhibition of this protein would cost the synthesis of essential amino acids required for protein synthesis. It would eventually increase the susceptibility of *A. baumannii* towards antibiotics.

These findings suggest that compound **3a** exhibits bactericidal activity by reacting with and modifying essential proteins of *A. baumannii*, indicating it as a promising therapeutic antibacterial candidate.

Chapter 4: Visible-Light Controlled Release of a Fluoroquinolone Antibiotic

In chapters **2** and **3**, the drug discovery method was discussed to tackle antibiotic resistance. In order to address antibiotic resistance, methods for spatiotemporal regulated release of an antibacterial molecule are in this Chapter **4.** In these methods, antibacterial compounds' action is controlled by an external stimulus or a metabolic trigger. For example, Das and co-workers have developed a disulfide-based prodrug with levofloxacin and demonstrated the glutathione (GSH) induced release of antibiotics in *E. coli* and *S. aureus*.[42] In another report, Chakrapani and co-workers have demonstrated nitroreductase (NTR), a bacterial enzyme-activated release of ciprofloxacin along with a fluorescence reporter in *E. coli*.[43] However, enzymes are an internal trigger and enzyme activity may not be under control, perhaps causing an increase in the concentration of the released antibacterial molecule. It may also interfere with other functional groups in the prodrug.

Photopharmacology, on the other hand, employs "light" as an external regulator to control the action of bioactive chemicals. Light as external trigger has several advantages, such as:[44–46]

- It exhibits biorthogonality towards biological system
- It does not cause any contamination to samples and has a negligible or low level of toxicity
- Light delivery can be more precisely controlled by altering intensity and amplitude (wavelength) quantitatively and qualitatively, respectively.

Thus, light can be used as a trigger in the antibacterial photopharmacology domain to reduce off-target action and unwanted side effects of antibiotics for specific types of skin infections or wound dressing. In this approach, an antibiotic is appended with either with an optical swich or a photocleavable group, which upon exposing to light will liberate the active antibacterial molecule. For example, Feringa and co-workers have developed ciprofloxacin appended photoswitch, which upon exposing to UV light undergoes conformational transition to achieve an active molecule conformation and exhibit more potent antibacterial activity than antibiotic alone in *E. coli*[47]. Using *o*-nitroaryl photo cleavable group, Forsythe and co-workers have attached ciprofloxacin on hydrogel and shown the UV light activated release of antibiotic [48].

The efficacy of antibacterial activity was demonstrated using Muller–Hinton agar plate method against *S. aureus* bacterium. In another study, Gademann and co-workers have linked two different antibiotics to UV light sensitive *o*-nitroaryl photo cleavable group [11]. and displayed the antibacterial activity against *B. subtilis*, *S. aureus*, MRSA, *E. coli*, and *P. aeruginosa*. However, due to its toxicity and limited tissue penetration, UV light (250–400 nm) is not recommended.[49]. Hence, we set out to design antibiotic release that is initiated by visible light. For instance, levofloxacin referred as "respiratory fluoroquinolone" was chosen as an antibiotic.

The boron-dipyrromethene (BODIPY)-based photocleavable group was chosen for this investigation from among several previously reported photocleavable groups employed for the triggerable release of bioactive compounds.[50] BODIPY based fluorophores have several distinct advantages, such as[51,52]

- Insensitive to pH and polarity, and stable in physiological conditions
- Have high molar extinction coefficient and photostabilty, making them a good candidate for PDT therapeutic agents and bio-imaging
- Moderately nontoxic and have higher quantum yield
- With certain structural changes, the amplitude of the light source can be adjusted.

With the knowledge of the aforementioned reports, a BODIPY-based scaffold for caging the fluroquinolone antibiotic was designed, which should release the antibiotic by B-O bond cleavage when exposed to visible light.

Figure 15 Design of BODIPY-based fluoroquinolone caged scaffold

(Reproduced with permission from *ACS Omega* https://pubs.acs.org/doi/10.1021/acsomega.7b01906)

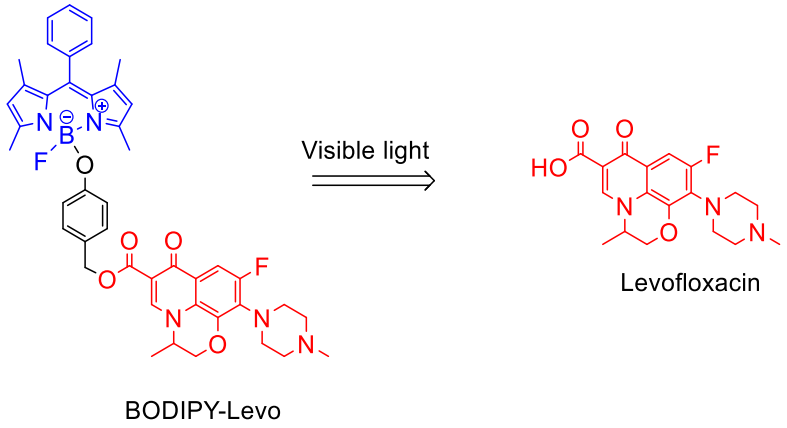

BODIPY-aryloxy derivative **24** was synthesized using reported protocols.[53] Using HBTU-DMAP acid-alcohol coupling reaction[54], compound **24** was reacted with levofloxacin (Levo), and BODIPY-Levo adduct was obtained with a 69% yield (Scheme 2). Following the same scheme compound, **22** was synthesized as a negative control.

Scheme 2 Synthesis of BODIPY-based fluoroquinolone caged scaffold

(Reproduced with permission from *ACS Omega* https://pubs.acs.org/doi/10.1021/acsomega.7b01906)

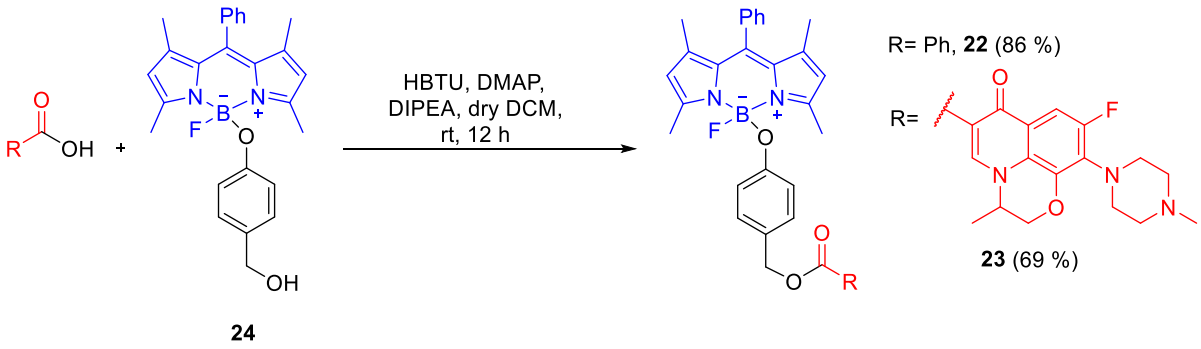

When compound **23** is exposed to light (470 nm, 30 mW/cm^2) for 30 minutes in methanol, it is anticipated that It would break the B-O bond, resulting in intermediate **I** being produced alongside BODIPY-OMe (**27**) and levofloxacin being produced *via* electron transfer across the benzene ring of intermediate I in the buffer (Scheme 3).

Scheme 3 Proposed mechanism for generation of levofloxacin after photo-irradiation of 23

(Reproduced with permission from *ACS Omega* https://pubs.acs.org/doi/10.1021/acsomega.7b01906)

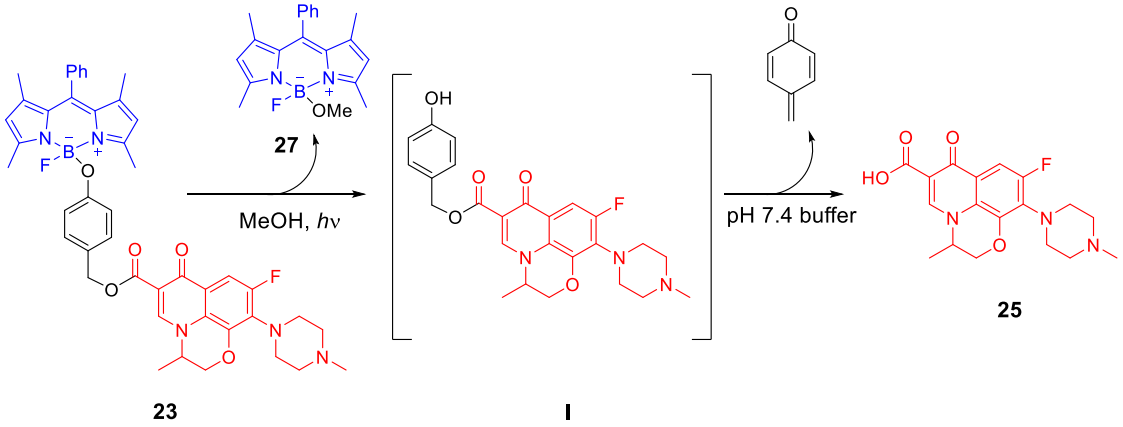

Following that, a TLC-based experiment was carried out to observe the released levofloxacin after irradiation. When compound **23** was exposed to light in methanol and incubated in buffer, the release of levofloxacin was observed. In addition, investigations using high-performance liquid chromatography (HPLC) were carried out to establish the release of levofloxacin in a qualitative and quantitative manner. When compound **23** was exposed to light for 30 minutes in methanol, a complete disintegration of compound **23** was observed, as well as the creation of a new peak, which corresponds to the BODIPY-OMe **27** (Figure 16, Retention time at 11.3 min)[53]

Figure 16 Portions of HPLC traces of 23 incubated in methanol

Ctrl, t = 0; dark, t = 30 min; light, reaction mixture was irradiated for 30 min with 470 nm light. The detector wavelength used is A) 500 nm, B) fluorescence detector wavelength excitation, 470 nm; emission, 540 nm.

(Reproduced with permission from *ACS Omega* https://pubs.acs.org/doi/10.1021/acsomega.7b01906)

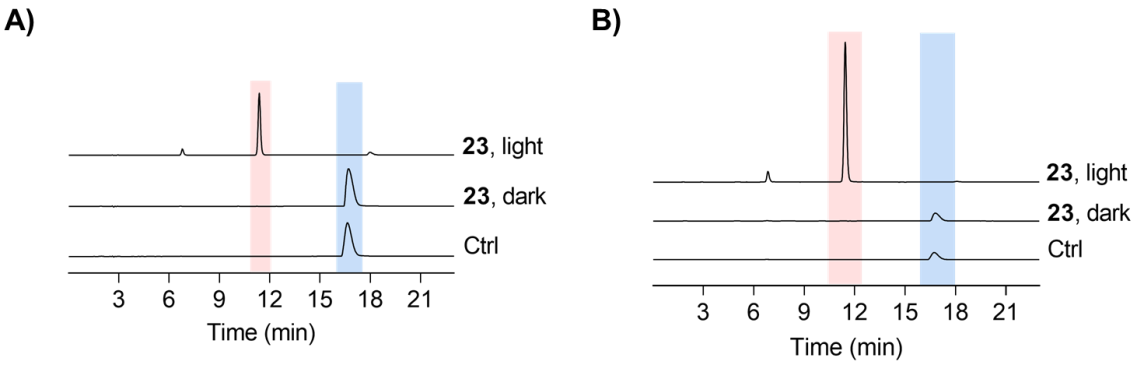

The yield of released levofloxacin was found to be 31%, which was similar to previous results showing histamine release from BODIPY-histamine caged scaffolds.[53]

Figure 17 A portion of HPLC traces of 23 incubated in pH 7.4 buffer after irradiation in methanol

The fluorescence detector was used with excitation, 330 nm; emission, 510 nm.

(Reproduced with permission from *ACS Omega* https://pubs.acs.org/doi/10.1021/acsomega.7b01906)

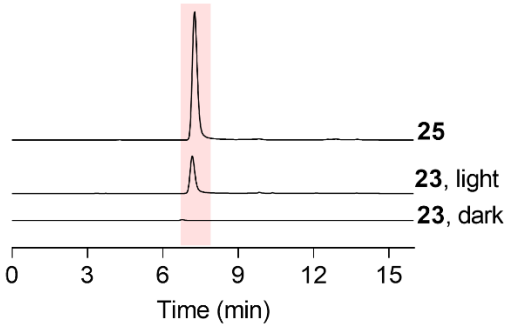

Having established that after exposing compound **23** to light in methanol, levofloxacin was successfully produced in the buffer. The efficacy of released levofloxacin's antibacterial

activity was next examined utilizing growth curve analysis against Gram-positive and Gram-negative bacteria.

Figure 18 Growth curve analysis of E. coli

Ctrl indicates bacteria in dark; dark indicats not irradiated, light indicates irradiated with light at 470 nm for 5 min, (B) at time point 6 h; **23** indicates **23** (5 μM) in bacteria; **25** indicates 25 (5 μM) in bacteria; **22** indicates **22** (10 μM) in bacteria **** indicates p-Value < 0.001 comparison between **23** dark and **23** light

(Reproduced with permission from *ACS Omega* https://pubs.acs.org/doi/10.1021/acsomega.7b01906)

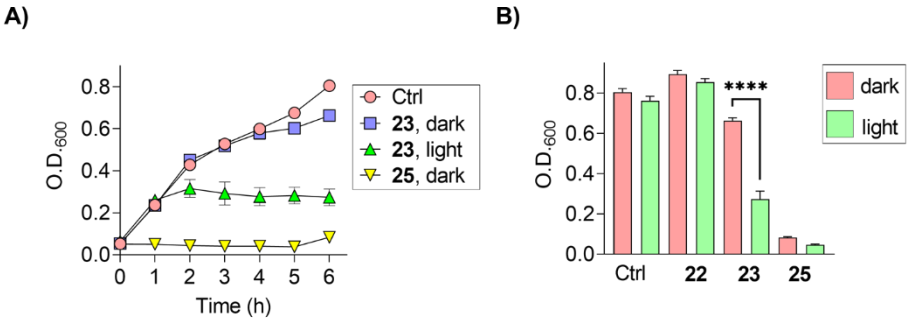

When *E. coli* bacterial cells were exposed to compound **22**, no substantial suppression of bacterial growth was detected in the dark or in the light, showing that compound **22** had no growth inhibitory impact. Levofloxacin (**25**) showed antibacterial activity in dark and light conditions, implying that its antibacterial potency was unaffected by irradiation. (Figure 18). In the dark, compound **23** exhibited no inhibitory impact, but bacterial growth was significantly reduced after irradiation, suggesting that compound 23 only exhibits antibacterial action after being exposed to visible light. Similar results were obtained in *S. aureus* bacterium(Figure 19).

Figure 19 Growth curve analysis of S. aureus

Ctrl indicates bacteria in dark; dark indicats not irradiated, light indicates irradiated with light at 470 nm for 5 min, (B) at time point 6 h; **23** indicates **23** (5 μM) in bacteria; **25** indicates 25 (5 μM) in bacteria; **22** indicates **22** (10 μM) in bacteria **** indicates p-Value < 0.001 comparison between **23** dark and **23** light.

(Reproduced with permission from *ACS Omega* https://pubs.acs.org/doi/10.1021/acsomega.7b01906)

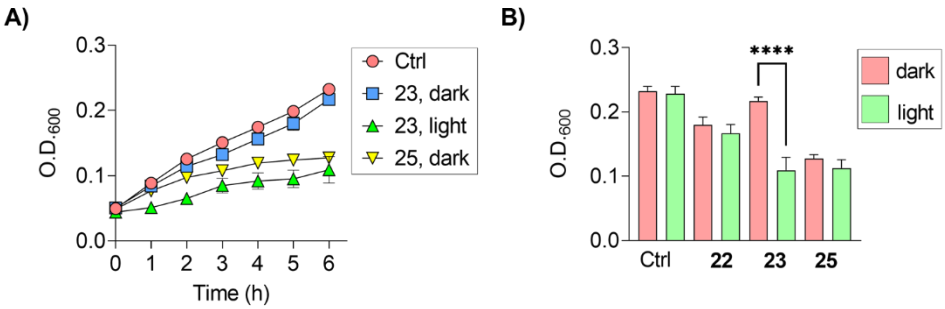

The efficacy of the released antibiotic induced by visible light was then examined using the agar growth method. *E. coli* bacterial cells on nutrient agar plate were exposed to either dark or light in presence of BODIPY derivative **22** and **23**, and levofloxacin (**25**) as reference. Images of these agar plates were recorded periodically to monitor the growth of bacterial cells.

Figure 20 Growth inhibition of E. coli on nutrient agar plate

Ctrl indicates bacteria; **23** indicates **23** (100 μM) in bacteria; **25** indicates **25** (100 μM) in bacteria; **22** indicates **22** (100 μM) in bacteria.

(Reproduced with permission from *ACS Omega* https://pubs.acs.org/doi/10.1021/acsomega.7b01906)

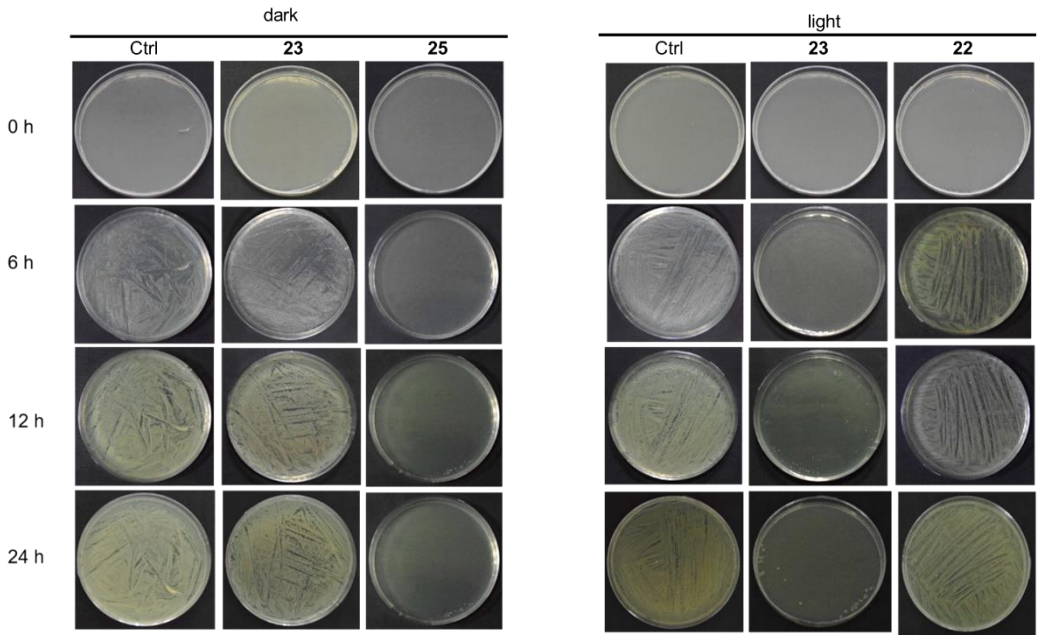

When bacterial cells were exposed to light in the presence of **23**, no growth was detected for 6 hours. This inhibitory activity was sustained for up to 24 hours and was comparable to that of the antibiotic levofloxacin. After irradiation of compound **23** with visible light in gram-negative bacteria *E. coli*, the antibacterial activity of the liberated antibiotic was successfully demonstrated using both growth curve and agar growth methods.

Using a BODIPY-based scaffold, the visible light-triggered release of a fluoroquinolone antibiotic was successfully demonstrated. It can be used to administer antibiotics directly to the infection site, potentially lowering drug doses and exposure duration.

1.7. References:

(1) Bruslind, L. *General Microbiology*, 1st ed.; Oregon State University: Corvallis, 2019.

(2) Lewis, K. Platforms for Antibiotic Discovery. *Nat. Rev. Drug Discov.* **2013**, *12*, 371–387. https://doi.org/10.1038/nrd3975.

(3) Prestinaci, F.; Pezzotti, P.; Pantosti, A. Antimicrobial Resistance: A Global Multifaceted Phenomenon. *Pathog. Glob. Health* **2015**, *109* (7), 309–318. https://doi.org/10.1179/2047773215Y.0000000030.

(4) Murray, C. J.; Ikuta, K. S.; Sharara, F.; Swetschinski, L.; Robles Aguilar, G.; Gray, A.; Han, C.; Bisignano, C.; Rao, P.; Wool, E.; Johnson, S. C.; Browne, A. J.; Chipeta, M. G.; Fell, F.; Hackett, S.; Haines-Woodhouse, G.; Kashef Hamadani, B. H.; Kumaran, E. A. P.; McManigal, B.; Agarwal, R.; Akech, S.; Albertson, S.; Amuasi, J.; Andrews, J.; Aravkin, A.; Ashley, E.; Bailey, F.; Baker, S.; Basnyat, B.; Bekker, A.; Bender, R.; Bethou, A.; Bielicki, J.; Boonkasidecha, S.; Bukosia, J.; Carvalheiro, C.; Castañeda-Orjuela, C.; Chansamouth, V.; Chaurasia, S.; Chiurchiù, S.; Chowdhury, F.; Cook, A. J.; Cooper, B.; Cressey, T. R.; Criollo-Mora, E.; Cunningham, M.; Darboe, S.; Day, N. P. J.; De Luca, M.; Dokova, K.; Dramowski, A.; Dunachie, S. J.; Eckmanns, T.; Eibach, D.; Emami, A.; Feasey, N.; Fisher-Pearson, N.; Forrest, K.; Garrett, D.; Gastmeier, P.; Giref, A. Z.; Greer, R. C.; Gupta, V.; Haller, S.; Haselbeck, A.; Hay, S. I.; Holm, M.; Hopkins, S.; Iregbu, K. C.; Jacobs, J.; Jarovsky, D.; Javanmardi, F.; Khorana, M.; Kissoon, N.; Kobeissi, E.; Kostyanev, T.; Krapp, F.; Krumkamp, R.; Kumar, A.; Kyu, H. H.; Lim, C.; Limmathurotsakul, D.; Loftus, M. J.; Lunn, M.; Ma, J.; Mturi, N.; Munera-Huertas, T.; Musicha, P.; Mussi-Pinhata, M. M.; Nakamura, T.; Nanavati, R.; Nangia, S.; Newton, P.; Ngoun, C.; Novotney, A.; Nwakanma, D.; Obiero, C. W.; Olivas-Martinez, A.; Olliaro, P.; Ooko, E.; Ortiz-Brizuela, E.; Peleg, A. Y.; Perrone, C.; Plakkal, N.; Ponce-de-Leon, A.; Raad, M.; Ramdin, T.; Riddell, A.; Roberts, T.; Robotham, J. V.; Roca, A.; Rudd, K. E.; Russell, N.; Schnall, J.; Scott, J. A. G.; Shivamallappa, M.; Sifuentes-Osornio, J.; Steenkeste, N.; Stewardson, A. J.; Stoeva, T.; Tasak, N.; Thaiprakong, A.; Thwaites, G.; Turner, C.; Turner, P.; van Doorn, H. R.; Velaphi, S.; Vongpradith, A.; Vu, H.; Walsh, T.; Waner, S.; Wangrangsimakul, T.; Wozniak, T.; Zheng, P.; Sartorius, B.; Lopez, A. D.; Stergachis, A.; Moore, C.; Dolecek, C.; Naghavi, M. Global Burden of Bacterial Antimicrobial Resistance in 2019: A

Systematic Analysis. *Lancet* **2022**, *399* (10325), 629–655. https://doi.org/10.1016/S0140-6736(21)02724-0.

(5) Rice, L. B. Federal Funding for the Study of Antimicrobial Resistance in Nosocomial Pathogens: No ESKAPE. *J. Infect. Dis.* **2008**, *197* (8), 1079–1081. https://doi.org/10.1086/533452.

(6) Pogue, J. M.; Kaye, K. S.; Cohen, D. A.; Marchaim, D. Appropriate Antimicrobial Therapy in the Era of Multidrug-Resistant Human Pathogens. *Clin. Microbiol. Infect.* **2015**, *21* (4), 302–312. https://doi.org/10.1016/j.cmi.2014.12.025.

(7) Santajit, S.; Indrawattana, N. Mechanisms of Antimicrobial Resistance in ESKAPE Pathogens. *Biomed Res. Int.* **2016**, *2016*, 1–8. https://doi.org/10.1155/2016/2475067.

(8) Velema, W. A.; Szymanski, W.; Feringa, B. L. Photopharmacology: Beyond Proof of Principle. *J. Am. Chem. Soc.* **2014**, *136* (6), 2178–2191. https://doi.org/10.1021/ja413063e.

(9) Broichhagen, J.; Frank, J. A.; Trauner, D. A Roadmap to Success in Photopharmacology. *Acc. Chem. Res.* **2015**, *48* (7), 1947–1960. https://doi.org/10.1021/acs.accounts.5b00129.

(10) Velema, W. A.; van der Berg, J. P.; Szymanski, W.; Driessen, A. J. M.; Feringa, B. L. Orthogonal Control of Antibacterial Activity with Light. *ACS Chem. Biol.* **2014**, *9* (9), 1969–1974. https://doi.org/10.1021/cb500313f.

(11) Shchelik, I. S.; Tomio, A.; Gademann, K. Design, Synthesis, and Biological Evaluation of Light-Activated Antibiotics. *ACS Infect. Dis.* **2021**, *7* (3), 681–692. https://doi.org/10.1021/acsinfecdis.1c00015.

(12) Szabo, M.; Svensson Akusjärvi, S.; Saxena, A.; Liu, J.; Chandrasekar Janebjer, G.; Kitambi, S. S. Cell and Small Animal Models for Phenotypic Drug Discovery. *Drug Des. Devel. Ther.* **2017**, *Volume 11*, 1957–1967. https://doi.org/10.2147/DDDT.S129447.

(13) Yue, R.; Shan, L.; Yang, X.; Zhang, W. Approaches to Target Profiling of Natural

Products. *Curr. Med. Chem.* **2012**, *19* (22), 3841–3855. https://doi.org/10.2174/092986712801661068.

(14) Backus, K. M.; Correia, B. E.; Lum, K. M.; Forli, S.; Horning, B. D.; González-Páez, G. E.; Chatterjee, S.; Lanning, B. R.; Teijaro, J. R.; Olson, A. J.; Wolan, D. W.; Cravatt, B. F. Proteome-Wide Covalent Ligand Discovery in Native Biological Systems. *Nature* **2016**, *534* (7608), 570–574. https://doi.org/10.1038/nature18002.

(15) Cravatt, B. F.; Wright, A. T.; Kozarich, J. W. Activity-Based Protein Profiling: From Enzyme Chemistry to Proteomic Chemistry. *Annu. Rev. Biochem.* **2008**, *77* (1), 383–414. https://doi.org/10.1146/annurev.biochem.75.101304.124125.

(16) Speers, A. E.; Adam, G. C.; Cravatt, B. F. Activity-Based Protein Profiling in Vivo Using a Copper(I)-Catalyzed Azide-Alkyne [3 + 2] Cycloaddition. *J. Am. Chem. Soc.* **2003**, *125* (16), 4686–4687. https://doi.org/10.1021/ja034490h.

(17) Speers, A. E.; Cravatt, B. F. Profiling Enzyme Activities In Vivo Using Click Chemistry Methods. *Chem. Biol.* **2004**, *11* (4), 535–546. https://doi.org/10.1016/j.chembiol.2004.03.012.

(18) Liu, Y.; Patricelli, M. P.; Cravatt, B. F. Activity-Based Protein Profiling: The Serine Hydrolases. *Proc. Natl. Acad. Sci.* **1999**, *96* (26), 14694–14699. https://doi.org/10.1073/pnas.96.26.14694.

(19) Kidd, D.; Liu, Y.; Cravatt, B. F. Profiling Serine Hydrolase Activities in Complex Proteomes. *Biochemistry* **2001**, *40* (13), 4005–4015. https://doi.org/10.1021/bi002579j.

(20) Patricelli, M. P.; Giang, D. K.; Stamp, L. M.; Burbaum, J. J. Direct Visualization of Serine Hydrolase Activities in Complex Proteomes Using Fluorescent Active Site-Directed Probes. *Proteomics* **2001**, *1* (8), 1067–1071. https://doi.org/10.1002/1615-9861(200109)1:9<1067::AID-PROT1067>3.0.CO;2-4.

(21) Greenbaum, D.; Baruch, A.; Hayrapetian, L.; Darula, Z.; Burlingame, A.; Medzihradszky, K. F.; Bogyo, M. Chemical Approaches for Functionally Probing the Proteome. *Mol. Cell. Proteomics* **2002**, *1* (1), 60–68. https://doi.org/10.1074/mcp.T100003-MCP200.

(22) Jessani, N.; Niessen, S.; Wei, B. Q.; Nicolau, M.; Humphrey, M.; Ji, Y.; Han, W.; Noh, D.-Y.; Yates, J. R.; Jeffrey, S. S.; Cravatt, B. F. A Streamlined Platform for High-Content Functional Proteomics of Primary Human Specimens. *Nat. Methods* **2005**, *2* (9), 691–697. https://doi.org/10.1038/nmeth778.

(23) Chung, J.-W.; Kim, S. Y.; Park, H. J.; Chung, C. S.; Lee, H. W.; Lee, S. M.; Kim, I.; Pak, J. H.; Lee, G. H.; Jeong, J.-Y. *In Vitro* Activity of Diphenyleneiodonium toward Multidrug-Resistant *Helicobacter Pylori* Strains. *Gut Liver* **2017**, *11* (5), 648–654. https://doi.org/10.5009/gnl16503.

(24) Pandey, M.; Singh, A. K.; Thakare, R.; Talwar, S.; Karaulia, P.; Dasgupta, A.; Chopra, S.; Pandey, A. K. Diphenyleneiodonium Chloride (DPIC) Displays Broad-Spectrum Bactericidal Activity. *Sci. Rep.* **2017**, *7* (1), 11521–11528. https://doi.org/10.1038/s41598-017-11575-5.

(25) Nguyen, N.; Wilson, D. W.; Nagalingam, G.; Triccas, J. A.; Schneider, E. K.; Li, J.; Velkov, T.; Baell, J. Broad Activity of Diphenyleneiodonium Analogues against Mycobacterium Tuberculosis, Malaria Parasites and Bacterial Pathogens. *Eur. J. Med. Chem.* **2018**, *148*, 507–518. https://doi.org/10.1016/j.ejmech.2017.10.010.

(26) Cross, A. R.; Jones, O. T. G. The Effect of the Inhibitor Diphenylene Iodonium on the Superoxide-Generating System of Neutrophils. Specific Labelling of a Component Polypeptide of the Oxidase. *Biochem. J.* **1986**, *237* (1), 111–116. https://doi.org/10.1042/bj2370111.

(27) O'Donnell, V. B.; Tew, D. G.; Jones, O. T. G.; England, P. J. Studies on the Inhibitory Mechanism of Iodonium Compounds with Special Reference to Neutrophil NADPH Oxidase. *Biochem. J.* **1993**, *290* (1), 41–49. https://doi.org/10.1042/bj2900041.

(28) Weerapana, E.; Wang, C.; Simon, G. M.; Richter, F.; Khare, S.; Dillon, M. B. D.; Bachovchin, D. A.; Mowen, K.; Baker, D.; Cravatt, B. F. Quantitative Reactivity Profiling Predicts Functional Cysteines in Proteomes. *Nature* **2010**, *468* (7325), 790–795. https://doi.org/10.1038/nature09472.

(29) Velazquez, I.; Nakamaru-Ogiso, E.; Yano, T.; Ohnishi, T.; Yagi, T. Amino Acid Residues Associated with Cluster N3 in the NuoF Subunit of the Proton-Translocating

NADH-Quinone Oxidoreductase from Escherichia Coli. *FEBS Lett.* **2005**, *579* (14), 3164–3168. https://doi.org/10.1016/j.febslet.2005.05.005.

(30) Freedlander, B. L.; French, F. Chemotherapy of Certain Iodonium and Sulfonium Compounds. *Exp. Biol. Med.* **1946**, *63* (2), 319–322. https://doi.org/10.3181/00379727-63-15587.

(31) Engelhard, W. E.; Worton, A. G. Evaluation of an Iodonium Compound as an Antiseptic Agent. *J. Am. Pharm. Assoc. (Scientific ed.)* **1956**, *45* (6), 402–404. https://doi.org/10.1002/jps.3030450616.

(32) Martín-Aspas, A.; Guerrero-Sánchez, F. M.; García-Colchero, F.; Rodríguez-Roca, S.; Girón-González, J.-A. Differential Characteristics of Acinetobacter Baumannii Colonization and Infection: Risk Factors, Clinical Picture, and Mortality. *Infect. Drug Resist.* **2018**, *Volume 11*, 861–872. https://doi.org/10.2147/IDR.S163944.

(33) Dexter, C.; Murray, G. L.; Paulsen, I. T.; Peleg, A. Y. Community-Acquired Acinetobacter Baumannii : Clinical Characteristics, Epidemiology and Pathogenesis. *Expert Rev. Anti. Infect. Ther.* **2015**, *13* (5), 567–573. https://doi.org/10.1586/14787210.2015.1025055.

(34) Peleg, A. Y.; Seifert, H.; Paterson, D. L. Acinetobacter Baumannii : Emergence of a Successful Pathogen. *Clin. Microbiol. Rev.* **2008**, *21* (3), 538–582. https://doi.org/10.1128/CMR.00058-07.

(35) Glew, R. H.; MOELLERING, R. C.; KUNZ, L. J. INFECTIONS WITH ACINETOBACTER CALCOACETICUS (HERELLEA VAGINICOLA). *Medicine (Baltimore).* **1977**, *56* (2), 79–98. https://doi.org/10.1097/00005792-197703000-00001.

(36) Hamada, Y. Role of Pyridines in Medicinal Chemistry and Design of BACE1 Inhibitors Possessing a Pyridine Scaffold. In *Pyridine*; InTech, 2018. https://doi.org/10.5772/intechopen.74719.

(37) Shah, R.; Verma, P. K. Therapeutic Importance of Synthetic Thiophene. *Chem. Cent. J.* **2018**, *12* (1), 137. https://doi.org/10.1186/s13065-018-0511-5.

(38) Halavaty, A. S.; Rich, R. L.; Chen, C.; Joo, J. C.; Minasov, G.; Dubrovska, I.; Winsor, J. R.; Myszka, D. G.; Duban, M.; Shuvalova, L.; Yakunin, A. F.; Anderson, W. F. Structural and Functional Analysis of Betaine Aldehyde Dehydrogenase from Staphylococcus Aureus. *Acta Crystallogr. Sect. D Biol. Crystallogr.* **2015**, *71* (5), 1159–1175. https://doi.org/10.1107/S1399004715004228.

(39) Jackson, B.; Brocker, C.; Thompson, D. C.; Black, W.; Vasiliou, K.; Nebert, D. W.; Vasiliou, V. Update on the Aldehyde Dehydrogenase Gene (ALDH) Superfamily. *Hum. Genomics* **2011**, *5* (4), 283. https://doi.org/10.1186/1479-7364-5-4-283.

(40) Vanoni, M. A.; Curti, B. Structure–Function Studies of Glutamate Synthases: A Class of Self-Regulated Iron-Sulfur Flavoenzymes Essential for Nitrogen Assimilation. *IUBMB Life* **2008**, *60* (5), 287–300. https://doi.org/10.1002/iub.52.

(41) Joo, H. K.; Park, Y. W.; Jang, Y. Y.; Lee, J. Y. Structural Analysis of Glutamine Synthetase from Helicobacter Pylori. *Sci. Rep.* **2018**, *8* (1), 11657. https://doi.org/10.1038/s41598-018-30191-5.

(42) Pal, S.; Ramu, V.; Taye, N.; Mogare, D. G.; Yeware, A. M.; Sarkar, D.; Reddy, D. S.; Chattopadhyay, S.; Das, A. GSH Induced Controlled Release of Levofloxacin from a Purpose-Built Prodrug: Luminescence Response for Probing the Drug Release in Escherichia Coli and Staphylococcus Aureus. *Bioconjug. Chem.* **2016**, *27* (9), 2062–2070. https://doi.org/10.1021/acs.bioconjchem.6b00324.

(43) Pardeshi, K. A.; Kumar, T. A.; Ravikumar, G.; Shukla, M.; Kaul, G.; Chopra, S.; Chakrapani, H. Targeted Antibacterial Activity Guided by Bacteria-Specific Nitroreductase Catalytic Activation to Produce Ciprofloxacin. *Bioconjug. Chem.* **2019**, *30* (3), 751–759. https://doi.org/10.1021/acs.bioconjchem.8b00887.

(44) Young, D. D.; Deiters, A. Photochemical Control of Biological Processes. *Org. Biomol. Chem.* **2007**, *5* (7), 999–1005. https://doi.org/10.1039/B616410M.

(45) Beharry, A. A.; Woolley, G. A. Azobenzene Photoswitches for Biomolecules. *Chem. Soc. Rev.* **2011**, *40* (8), 4422. https://doi.org/10.1039/c1cs15023e.

(46) Szymański, W.; Beierle, J. M.; Kistemaker, H. A. V.; Velema, W. A.; Feringa, B. L.

Reversible Photocontrol of Biological Systems by the Incorporation of Molecular Photoswitches. *Chem. Rev.* **2013**, *113* (8), 6114–6178. https://doi.org/10.1021/cr300179f.

(47) Velema, W. A.; Hansen, M. J.; Lerch, M. M.; Driessen, A. J. M.; Szymanski, W.; Feringa, B. L. Ciprofloxacin–Photoswitch Conjugates: A Facile Strategy for Photopharmacology. *Bioconjug. Chem.* **2015**, *26* (12), 2592–2597. https://doi.org/10.1021/acs.bioconjchem.5b00591.

(48) Shi, Y.; Truong, V. X.; Kulkarni, K.; Qu, Y.; Simon, G. P.; Boyd, R. L.; Perlmutter, P.; Lithgow, T.; Forsythe, J. S. Light-Triggered Release of Ciprofloxacin from an in Situ Forming Click Hydrogel for Antibacterial Wound Dressings. *J. Mater. Chem. B* **2015**, *3* (45), 8771–8774. https://doi.org/10.1039/C5TB01820J.

(49) Brieke, C.; Rohrbach, F.; Gottschalk, A.; Mayer, G.; Heckel, A. Light-Controlled Tools. *Angew. Chemie Int. Ed.* **2012**, *51* (34), 8446–8476. https://doi.org/10.1002/anie.201202134.

(50) Goswami, P. P.; Syed, A.; Beck, C. L.; Albright, T. R.; Mahoney, K. M.; Unash, R.; Smith, E. A.; Winter, A. H. BODIPY-Derived Photoremovable Protecting Groups Unmasked with Green Light. *J. Am. Chem. Soc.* **2015**, *137* (11), 3783–3786. https://doi.org/10.1021/jacs.5b01297.

(51) Loudet, A.; Burgess, K. BODIPY Dyes and Their Derivatives: Syntheses and Spectroscopic Properties. *Chem. Rev.* **2007**, *107* (11), 4891–4932. https://doi.org/10.1021/cr078381n.

(52) Zou, J.; Yin, Z.; Ding, K.; Tang, Q.; Li, J.; Si, W.; Shao, J.; Zhang, Q.; Huang, W.; Dong, X. BODIPY Derivatives for Photodynamic Therapy: Influence of Configuration versus Heavy Atom Effect. *ACS Appl. Mater. Interfaces* **2017**, *9* (38), 32475–32481. https://doi.org/10.1021/acsami.7b07569.

(53) Umeda, N.; Takahashi, H.; Kamiya, M.; Ueno, T.; Komatsu, T.; Terai, T.; Hanaoka, K.; Nagano, T.; Urano, Y. Boron Dipyrromethene As a Fluorescent Caging Group for Single-Photon Uncaging with Long-Wavelength Visible Light. *ACS Chem. Biol.* **2014**, *9* (10), 2242–2246. https://doi.org/10.1021/cb500525p.

(54) Wassvik, C. M.; Holmén, A. G.; Draheim, R.; Artursson, P.; Bergström, C. A. S. Molecular Characteristics for Solid-State Limited Solubility. *J. Med. Chem.* **2008**, *51* (10), 3035–3039. https://doi.org/10.1021/jm701587d.

List of Figures

List of Schemes

List of Tables

IISER PUNE

Pooja Kumari <pooja.kumari@students.iiserpune.ac.in>

Request for permission to reuse some data in my Ph.D thesis from my publication

1 message

ACS Publications <support@services.acs.org> Mon, Feb 28, 2022 at 3:58 PM
Reply-To: support@services.acs.org
To: pooja.kumari@students.iiserpune.ac.in

Dear Dr. Kumari,

Thank you for contacting us.

Your permission requested is granted and there is no fee for this reuse. In your planned reuse, you must cite the ACS article as the source, add this direct link https://pubs.acs.org/doi/10.1021/acsomega.7b01906 and include a notice to readers that further permissions related to the material excerpted should be directed to the ACS.

Kind regards,

Nikola Markovic
ACS Publications Support
Customer Services & Information
Website: https://acs.service-now.com/acs
Email: support@services.acs.org
Phone: 800-227-9919 | 202-872-(HELP) 4357

Case Info:

Case Number : CSCSI0054848

Created On: 02-28-2022 04:54:22 AM EST

Short Description: Request for permission to reuse some data in my Ph.D thesis from my publication

Description: Dear Sir/Ma'am,
I, Pooja Kumari, a Ph.D. student at the Indian Institute of Science Education and Research (IISER) Pune, am writing my Ph.D. thesis. We have published a paper in ACS OMEGA in February 2018 and I am the first author of this publication. I wish to use some figures and data for my thesis.
I request you to kindly provide copyright permission for the same.
Details are as follows
1) Publication: "ACS Omega" 2018, 3, 2, 2155–2160. (DOI: 10.1021/acsomega.7b01906 <https://doi.org/10.1021/acsomega.7b01906>)
2) Portion of content to be reused: Figures only (2, 3,4, and 5 from the Main manuscript and others from SI)
3) where the content will be reused: Ph.D. Thesis

Thanks and Regards
Pooja Kumari
Research Scholar
IISER Pune

Ref:MSG0382994_2c26fzB7T8ha5ZHecNsJ

List of Publications

(1) **Kumari, P**.; Kulkarni, A.; Sharma, A. K.; Chakrapani, H. Visible-Light Controlled Release of a Fluoroquinolone Antibiotic for Antimicrobial Photopharmacology. *ACS Omega* **2018**, *3* (2), 2155–2160. https://doi.org/10.1021/acsomega.7b01906.

(2) **Kumari, P**.; Kaul, G.; Kumar, T. A.; Akhir, A.; Shukla, M.; Sharma, S.; Kamat, S.; Chopra, S.; Chakrapani, H. *Chemoproteomics with a Diaryliodonium Probe Reveals New Vulnerabilities in Multidrug-resistant Gram-Negative Pathogens* manuscript under review.

ACS OMEGA

Article

Cite This: *ACS Omega* 2018, 3, 2155−2160

Visible-Light Controlled Release of a Fluoroquinolone Antibiotic for Antimicrobial Photopharmacology

Pooja Kumari, Amogh Kulkarni, Ajay Kumar Sharma, and Harinath Chakrapani*

Department of Chemistry, Indian Institute of Science Education and Research Pune, Dr. Homi Bhabha Road, Pune 411008, Maharashtra, India

Supporting Information

ABSTRACT: Owing to the dwindling arsenal of antibiotics, new methodologies for their effective and localized delivery are necessary. The use of optical control over delivery of drugs, also known as photopharmacology, has emerged as an important option for the spatiotemporally controlled generation of drugs and bioactive molecules. In the field of antimicrobial photopharmacology, most strategies utilize ultraviolet light for triggering release of the antibiotic. The use of such short wavelength light may have limitations such as phototoxicity. Here, a small molecule that is activated by visible light to release a fluoroquinolone, a broad-spectrum antibiotic, is reported. A boron-dipyrromethene, which is sensitive to cleavage at 470 nm, was used, and levofloxacin was used as a model fluoroquinolone. BDP-Levo was found to undergo cleavage in the presence of visible light to release the active antibiotic. Using growth inhibitory studies in Gram-positive as well as Gram-negative bacteria, the efficacy of BDP-Levo is demonstrated. Together, our study demonstrates that visible light can be used for optical control over antibiotic release and lays the foundation for visible-light-mediated antimicrobial photopharmacology.

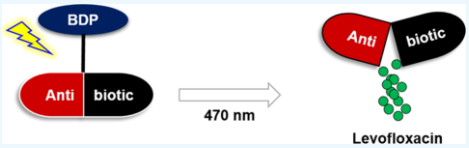

INTRODUCTION

The modern antibiotic era has exacerbated the morbidity and mortality associated with bacterial infections. The overuse and misuse of antibiotics have, in part, contributed to the emergence of drug resistance.[1] Antimicrobial drug resistance, compounded with a limited pipeline of new antibiotics, has now become a major global public health threat.[2,3] The number of antibiotics that continue to remain effective is dwindling at an alarming rate, and the existing classes of antibiotics need to be better used to increase longevity.[4] Because antibiotics are used systemically, a large buildup of the bioactive molecule is invariably unavoidable. This affects not only the pathogen of interest but also gut microbiota that are crucial for our health and well-being. Furthermore, environmental exposure to antibiotics leads to the possible buildup of drug-resistant pathogens. For certain types of infection, if spatiotemporal control over antibiotic generation can be achieved, side effects can be reduced and perhaps patient compliance can be improved. The past several decades have seen the emergence of photopharmacology, which aims to minimize the problem of off-target activity and decrease deleterious side effects by offering an external control over the action of the drug.[5,6] In the field of antimicrobial photopharmacology, an antibiotic is attached to an optical switch or a photocleavable group;[7] upon irradiation, the active form of the antibiotic is produced (Figure 1a). For example, Feringa and co-workers have reported a diazo functional group linked to a model fluoroquinolone (Figure 1b).[7−9] This functional group serves as an optical switch. Upon exposure to UV light, isomerization occurs, which results in the active antibiotic being formed. It is proposed that after the antibiotic action is completed, another source of light could be used to inactivate the antibiotic. Fuchter and co-workers have developed a methodology for aminohydrolase-based antibiotics.[10] Using a 2-nitroaryl cleavable group, Forsythe and co-workers have reported a hydrogel that is triggered by UV light (Figure 1c).[11] Although this liberates ciprofloxacin, the use of UV light is not highly desirable and may have problems associated with phototoxicity. The use of visible light, on the contrary, has considerably lower toxicity and is therefore highly desirable. Here, we report a methodology that is suitable for visible-light-triggered release of a fluoroquinolone.

Among the various fluorophores that have been previously used as triggerable scaffolds to deliver bioactive molecules,[12] boron-dipyrromethene (BODIPY)-based fluorophores have distinct advantages. They are stable in buffer, have high quantum yields, are relatively nontoxic, and their wavelengths of absorption can be tuned by systematic structural modifications.[13] Recently, Urano and co-workers have reported the cleavage of a B−O bond in aryloxy-BODIPY derivatives.[14,15] In addition, there are two other reports of a polymeric scaffold for drug delivery[16] as well as a small molecule for delivery of the pharmacologically active gaseous species, hydrogen sulfide.[17] We thus designed BDP-Levo, **1**, to deliver a fluoroquinolone using visible light as a trigger (Figure 2). This compound is expected to undergo cleavage by visible light to

Received: December 1, 2017
Accepted: February 8, 2018
Published: February 21, 2018

DOI: 10.1021/acsomega.7b01906
ACS Omega 2018, 3, 2155−2160

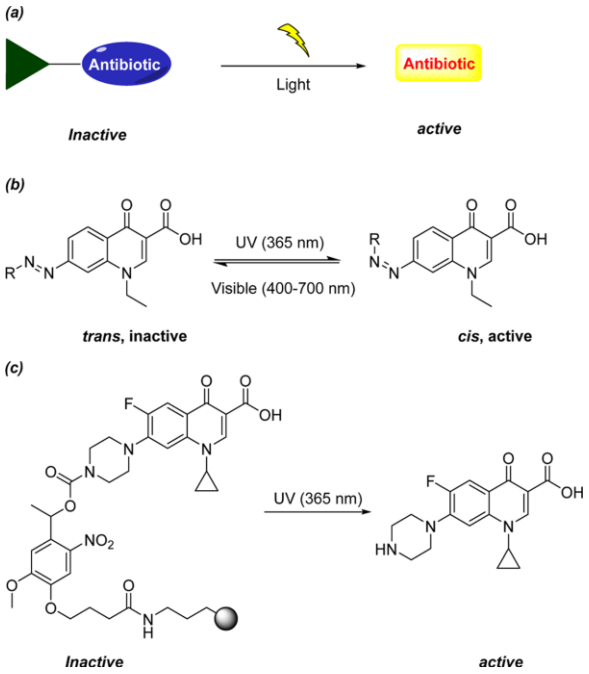

Figure 1. (a) Generic design of a visible-light-triggered antibiotic. (b) Example of an optically controlled antibiotic: UV light is used to convert an inactive trans isomer to the active cis isomer. (c) UV-triggered release of ciprofloxacin, a clinically used antibiotic. The sphere represents a tether for cross-linking.

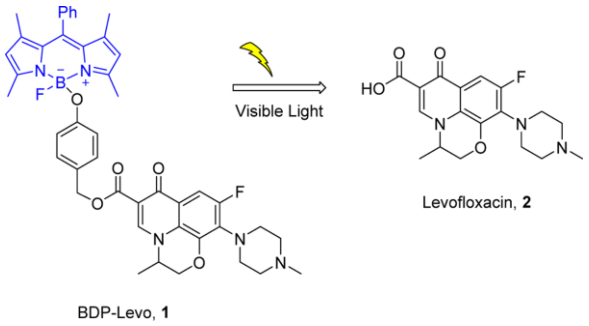

Figure 2. Design of a BODIPY-based scaffold for visible-light-triggered release of a fluoroquinolone antibiotic.

produce a self-immolative phenolate that rearranges to generate the active antibiotic (Scheme S1, Supporting Information (SI)).

RESULTS AND DISCUSSION

First, the BODIPY derivative, **3**, was synthesized using a reported procedure, and this compound was reacted with levofloxacin (Levo) to produce the desired BDP-Levo, **1**, with good yield (Scheme 1).[18] Because the release of carboxylic acids has hitherto not been studied using this BODIPY protective group, benzoate ester **5** was synthesized (Scheme 1). The photophysical properties of these BODIPY derivatives were studied. Fluorescence measurements (excitation 470 nm, emission 509 nm) were conducted (see Figure S1, Supporting Information), and quantum yields were determined using standard protocols. Consistent with previous reports, the esters were weakly fluorescent and diminished quantum yields were recorded (see Table S1, Supporting Information). Next, using the irradiation conditions that were previously reported, **1** was

DOI: 10.1021/acsomega.7b01906
ACS Omega 2018, 3, 2155−2160

Scheme 1. Syntheses of 1 and 5 from 3

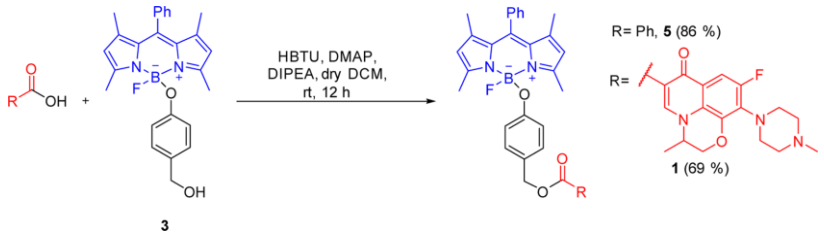

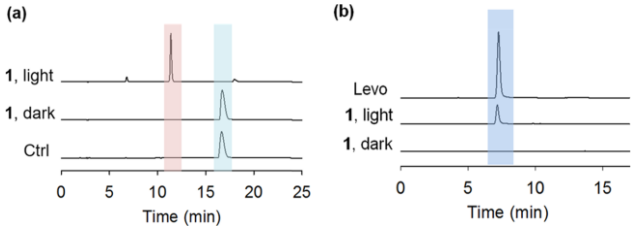

Figure 3. (a) Portions of HPLC traces of **1** incubated in methanol: Ctrl, t = 0; dark, t = 30 min; light, reaction mixture was irradiated for 30 min with 470 nm light (30 mW/cm^2), decomposition of **1** produces the methoxy derivative, BDP-OMe (**4**, Scheme S1; see SI). Here, the detector wavelength is 500 nm. (b) Irradiation for 30 min with 470 nm light was followed by incubation of **1** in pH 7.4 phosphate buffer. A fluorescence detector was used with excitation 330 nm and emission 510 nm. Yield was estimated as 31% using authentic Levo.

incubated in methanol and exposed to 470 nm light.[14] High performance liquid chromatography (HPLC) analysis of the reaction mixture showed complete decomposition of **1** to produce the methoxy derivative, BDP-OMe (**4**, Scheme S1; see SI). In the absence of light, we found no evidence for the decomposition of **1** (Figure 3a). Quantum yield measurements of the irradiated samples showed a significant increase compared to those of the unirradiated samples (see Table S1, SI). Because the product in each case is the BDP-OMe, the quantum yields were identical (see Table S1, SI).

The BDP-Levo derivative, **1**, was next incubated in pH 7.4 phosphate buffer and was found to be stable for 30 min. After irradiation, the reaction mixture was diluted in pH 7.4 buffer, and thin-layer chromatography (TLC) analysis showed nearly complete decomposition of **1** when exposed to light and the formation of levofloxacin **2**. The experiment in dark, as expected, did not generate **2**, suggesting the stability of **1** in pH 7.4 buffer (Figure S2; see SI). Next, the formation of Levo was assessed by HPLC analysis of **1** in pH 7.4 buffer that was irradiated for 30 min. A distinct peak that corresponded to the formation of **2** was observed (Figure 3b). The yield of **2** under these conditions was estimated as 31%. This yield is similar to the yield of histamine that was generated by a previous report of a BODIPY-histamine scaffold.[14,17]

To study the bactericidal effects of the BODIPY scaffold, bacteria were exposed to the BODIPY derivative **3** (Figure S6; see SI). No significant inhibition of growth was observed in dark as well as in light, suggesting that the scaffold does not contribute to the growth inhibitory effects. Under similar conditions, levofloxacin **2** was a potent inhibitor of growth of *Escherichia coli* (*E. coli*) in dark as well as in light, suggesting that the efficacy of levofloxacin was not dependent on irradiation (Figure 4b). A similar result was obtained when

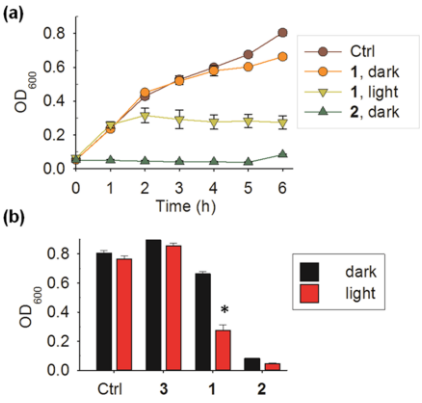

Figure 4. Growth curve analysis of *E. coli* in broth: (a) Ctrl indicates bacteria in dark; **1**, dark indicates bacteria treated with **1** (5 μM) but not irradiated with light; **1**, light indicates bacteria treated with **1** (5 μM) and irradiated with light for 5 min at 470 nm; **2**, dark indicates bacteria treated with **2** (5 μM) but not irradiated with light; (b) at time point 6 h: Ctrl indicates bacterial growth control in dark as well as in light. *p-Value < 0.001 for comparison of bacteria treated with **1** in dark versus irradiated with 470 nm light.

this experiment was conducted using the Gram-positive pathogen *Staphylococcus aureus* (*S. aureus*) (Figure 5). Together, these data support the use of **1** to effectively inhibit the growth of bacteria only when exposed to visible light.

The OD_{600} of compound **1** under irradiation conditions was negligible during the assay, suggesting no interference in the

DOI: 10.1021/acsomega.7b01906
ACS Omega 2018, 3, 2155−2160

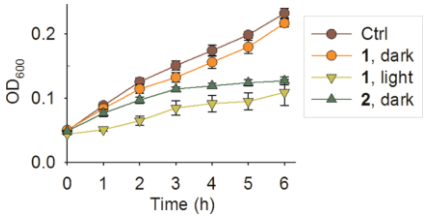

Figure 5. Growth curve analysis of *S. aureus* in broth. Ctrl indicates bacteria in dark; **1**, dark indicates bacteria treated with **1** (5 μM) but not irradiated with light; **1**, light indicates bacteria treated with **1** (5 μM) and irradiated with light for 5 min; **2**, dark indicates bacteria treated with **2** (5 μM) but not irradiated with light.

broth dilution assay by the compound (see SI). In addition, an agar-growth method was used to evaluate the efficacy of **1** (Figure 6). Here, bacteria after exposure to **1** (either light or dark) were grown on an agar plate. Images of these plates were recorded periodically (Figure S8; see SI).

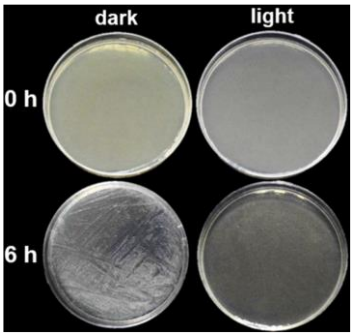

Figure 6. Growth inhibition of *E. coli* on agar plates: *E. coli* grown on an agar medium for 6 h after exposure to **1**. Dark indicates agar plates with **1** (100 μM) were not exposed to light; light indicates agar plates with **1** (100 μM) were exposed to light for 30 min at 470 nm.

After 6 h, a clear inhibition of growth of bacteria was recorded with respect to the control (Figure 6). This data was consistent during 24 h incubation as well. No significant inhibition of growth of bacteria incubated with **1** in dark was observed. Similarly, the negative control, **3**, showed no inhibition of bacterial growth. In the presence of light, the inhibitory potency of **1** was comparable with the clinically used antibiotic, **2** (Figure S8; see SI).

Taken together, we report for the first time a small-molecule-based methodology for visible-light-triggered release of levofloxacin, a clinically used antibiotic in its pharmacologically active form. This third-generation antibiotic has superior antibacterial properties compared with those of ciprofloxacin that has been previously used.[19,20] Feringa and co-workers have proposed that inactivation of the antibiotic after use is important, and this is not possible in the present methodology and may be a shortcoming that will need to be addressed.[21] A number of dendrimer-/polymer-based scaffolds for photo-triggered release of an antibiotic are known.[22,23] A cell-wall-targeted dendrimer nanoconjugate containing ciprofloxacin was recently reported. Using this method, phototriggered release of ciprofloxacin was achieved. Our approach can be adapted to incorporate such targeting ligands in future. Recently, hollow microspheres that can rapidly produce localized heat activated by near-infrared light and control the release of an antibiotic via a "molecular switch" in their polymer shells have been reported.[22,23] This photothermally responsive drug delivery system has distinct advantages and presents an attractive methodology for combination therapy.[23] Because the scaffold reported herein is triggered at 470 nm, further modification is necessary to enhance the wavelength of cleavage as well as for incorporation into polymeric scaffolds. These studies are presently under way in our laboratory.

Although there is an urgent need to develop antibiotics with novel targets and new mechanisms of action,[24−28] adjuvants that can enhance the activity of antibiotics,[29−31] preserving the existing classes of antibiotics, is a major public health priority. Improving patient compliance and monitoring inappropriate use are among the long-term solutions. Directed delivery of antibiotics to the site of infection,[32] perhaps, will result in minimizing the systemic exposure to the antibiotic[6] and may minimize certain unwanted side effects of fluoroquinolones.[33,34] Although this strategy is in its infancy, our small molecule lays the foundation for visible-light-activated antibiotic delivery. Lastly, the mechanism of antibiotic action is being investigated and the role of redox mechanisms in lethality is under scrutiny.[35] Development of new tools, such as the compound reported herein that can facilitate a better understanding of antibiotic mechanisms, will be useful. These experiments are presently under way in our lab, and results will be reported in due course.

METHODS

Synthesis of 4-((5-Fluoro-1,3,7,9-tetramethyl-10-phenyl-5*H*-4λ^4,5λ^4-dipyrrolo[1,2-*c*:2′,1′-*f*][1,3,2]-diazaborinin-5-yl)oxy)benzyl 9-fluoro-3-methyl-10-(4-methylpiperazin-1-yl)-7-oxo-2,3-dihydro-7*H*-[1,4]-oxazino[2,3,4-*ij*]quinoline-6-carboxylate (1). Following the reported procedure,[18] to a stirred solution of **2** (42 mg, 0.116 mmol), 2-(1*H*-benzotriazol-1-yl)-1,1,3,3-tetramethyluronium hexafluorophosphate (44 mg, 0.116 mmol), and 4-dimethylaminopyridine (5.7 mg, 0.046 mmol) in anhydrous CH_2Cl_2 (5 mL) were added *N*,*N*-diisopropylethylamine (104 μL, 0.583 mmol) and **3** (52 mg, 0.116 mmol) at room temperature (rt). The reaction[20] mixture was stirred for 12 h at rt. After completion of the reaction as monitored by TLC, water (5 mL) and CH_2Cl_2 (15 mL) were added to the reaction mixture. The organic components were extracted with CH_2Cl_2, and collected organic phases were dried over anhydrous Na_2SO_4, concentrated under reduced pressure to obtain the crude product as red residue. The residue was purified by column chromatography using neutral alumina as stationary phase and $CHCl_3$: MeOH (100:0 to 93:7) as mobile phase to afford **1** (62 mg, 69%) as a red-orange solid. FT-IR (ν_{max}, cm^{-1}); 2925, 2849, 2800, 1718, 1617, 1547, 1470, 1300; ^{1}H NMR (400 MHz, $CDCl_3$), δ 8.09 (s, 1H), 7.57−7.47 (m, 3H), 7.42 (d, J = 12.6 Hz, 1H), 7.34−7.29 (m, 2H), 7.23 (d, J = 8.6 Hz, 2H), 6.58 (d, J = 8.6 Hz, 2H), 5.89 (d, J = 15.4 Hz, 2H), 5.16 (d, J = 1.8 Hz, 2H), 4.35 (dd, J = 11.4, 2.3 Hz, 1H), 4.19 (dd, J = 11.3, 2.0 Hz, 1H), 4.06−4.02 (m, 1H), 3.32 (d, J = 4.4 Hz, 4H), 2.53 (s, 4H), 2.48 (d, J = 10.9 Hz, 6H), 2.35 (s, 3H), 1.39 (s, 6H), 1.37 (s, 3H); ^{13}C NMR (100 MHz, $CDCl_3$), δ

DOI: 10.1021/acsomega.7b01906
ACS Omega 2018, 3, 2155−2160

172.6, 165.5, 156.8, 156.5, 156.4, 155.8, 154.4, 145.2, 143.3, 141.8, 139.5, 134.8, 131.7, 130.2, 129.3, 129.1, 129.0, 128.1, 127.9, 127.0, 123.6, 121.7, 117.8, 109.6, 105.1, 68.0, 66.6, 55.7, 54.6, 50.5, 46.4, 18.2, 14.9, 14.5; HRMS (ESI) for $[C_{44}H_{44}BF_2N_5O_5 + H]^+$: calcd, 772.3482; found, 772.3498.

Bacterial Strains and Growth Conditions. Both the strains *E. coli* (ATCC 25922) and *S. aureus* (ATCC 29213) were obtained from ATCC. All of the bacterial strains were routinely grown in Luria Bertani (LB) broth, Mueller Hinton broth II (MHB) cation supplemented medium, tryptic soy agar and tryptic soy broth, purchased from Himedia. For every experiment, a starting culture was produced by inoculating a single colony picked from the agar plate into liquid medium and incubated overnight at 37 °C with continuous shaking. Levofloxacin was purchased from TCI in the purified powdered form.

E. coli ATCC 25922 was grown overnight in Luria Bertani (LB) broth. Bacterial density was adjusted to 10^8 colony-forming unit (CFU)/mL corresponding to an optical density (600 nm, OD_{600}) of 0.1. Next, 200 μL of this bacterial suspension was taken in a 96-well microtiter plate. Different lanes were chosen for different conditions such as bacterial control, bacteria with compound **1**, bacteria with compound **3** (negative control), bacteria with levofloxacin, and so on. Then, 100× stock solutions were used for all of the compounds. One plate without irradiation was incubated at 37 °C in the dark by covering with an aluminum foil. Another plate was irradiated at 470 nm (30 mW/cm^2) by blue light-emitting diode (LED) at room temperature in a closed chamber for 5 min and then incubated at 37 °C in the dark by covering with an aluminum foil. OD_{600} was measured using a Thermo Scientific Varioskan Flash microwell plate reader for both the plates at an interval of 1 h for 6 h. Values reported are average of six replicates. Errors have been calculated from standard deviation between the values.

Methicillin-sensitive *S. aureus* ATCC 29213 was grown overnight in Mueller Hinton broth II (MHB) cation supplemented medium. A similar procedure was followed further as was followed for *E. coli*.

Growth Inhibition of *E. coli* on Agar Plates. Agar plates were prepared using soyabean casein digest medium (tryptone soya broth) and agar powder. *E. coli* ATCC 25922 was grown overnight in Luria Bertani (LB) broth. Bacterial density was adjusted to 10^8 colony-forming unit (CFU)/mL corresponding to an optical density (600 nm, OD_{600}) of 0.1. Next, 100 μL of this bacterial suspension was taken for streaking on the agar plate. Then, 100× stock solutions were used for all of the compounds. Bacteria were streaked on the entire surface of the agar plate using a Hi-Flexiloop 4 (Himedia). For samples with irradiation, bacterial suspensions (with or without compound) were taken in a quartz cuvette and irradiated at 470 nm (30 mW/cm^2) by blue LED at room temperature in a closed chamber for 30 min. These irradiated samples were then streaked on the agar plates. All of the plates were then incubated at 37 °C in the dark by covering with an aluminum foil. Images were taken from 0 to 24 h using Nikon D3300 DSLR.

■ ASSOCIATED CONTENT

Supporting Information

The Supporting Information is available free of charge on the ACS Publications website at DOI: 10.1021/acsomega.7b01906.

Compound characterization data, spectra, and assay protocols (PDF)

■ AUTHOR INFORMATION

Corresponding Author

*E-mail: harinath@iiserpune.ac.in.

ORCID

Harinath Chakrapani: 0000-0002-7267-0906

Notes

The authors declare no competing financial interest.

■ ACKNOWLEDGMENTS

P.K. and A.K.S. acknowledge the Council of Scientific and Industrial Research (CSIR), New Delhi, for their fellowship. A.K. thanks the University Grants Commission (UGC) for his fellowship. The authors are grateful to the Department of Science and Technology (DST, Grant number EMR/2015/000668) for financial support and the Central Instrument Facility (CIF) of IISER Pune.

■ REFERENCES

(1) Walsh, C.; Wright, G. Introduction: Antibiotic Resistance. *Chem. Rev.* **2005**, *105*, 391−394.

(2) Butler, M. S.; Blaskovich, M. A. T.; Cooper, M. A. Antibiotics in the clinical pipeline at the end of 2015. *J. Antibiot.* **2017**, *70*, 3.

(3) Taubes, G. The Bacteria Fight Back. *Science* **2008**, *321*, 356−361.

(4) Carlet, J.; Collignon, P.; Goldmann, D.; Goossens, H.; Gyssens, I. C.; Harbarth, S.; Jarlier, V.; Levy, S. B.; N'Doye, B.; Pittet, D.; Richtmann, R.; Seto, W. H.; van der Meer, J. W. M.; Voss, A. Society's failure to protect a precious resource: antibiotics. *Lancet* **2011**, *378*, 369−371.

(5) Velema, W. A.; Szymanski, W.; Feringa, B. L. Photopharmacology: Beyond Proof of Principle. *J. Am. Chem. Soc.* **2014**, *136*, 2178−2191.

(6) Hamblin, M. R.; Hasan, T. Photodynamic therapy: a new antimicrobial approach to infectious disease? *Photochem. Photobiol. Sci.* **2004**, *3*, 436−450.

(7) Velema, W. A.; van der Berg, J. P.; Szymanski, W.; Driessen, A. J. M.; Feringa, B. L. Orthogonal Control of Antibacterial Activity with Light. *ACS Chem. Biol.* **2014**, *9*, 1969−1974.

(8) Velema, W. A.; van der Berg, J. P.; Hansen, M. J.; Szymanski, W.; Driessen, A. J. M.; Feringa, B. L. Optical control of antibacterial activity. *Nat. Chem.* **2013**, *5*, 924−928.

(9) Velema, W. A.; Hansen, M. J.; Lerch, M. M.; Driessen, A. J. M.; Szymanski, W.; Feringa, B. L. Ciprofloxacin−Photoswitch Conjugates: A Facile Strategy for Photopharmacology. *Bioconjugate Chem.* **2015**, *26*, 2592−2597.

(10) Weston, C. E.; Krämer, A.; Colin, F.; Yildiz, Ö.; Baud, M. G. J.; Meyer-Almes, F.-J.; Fuchter, M. J. Toward Photopharmacological Antimicrobial Chemotherapy Using Photoswitchable Amidohydrolase Inhibitors. *ACS Infect. Dis.* **2017**, *3*, 152−161.

(11) Shi, Y.; Truong, V. X.; Kulkarni, K.; Qu, Y.; Simon, G. P.; Boyd, R. L.; Perlmutter, P.; Lithgow, T.; Forsythe, J. S. Light-triggered release of ciprofloxacin from an in situ forming click hydrogel for antibacterial wound dressings. *J. Mater. Chem. B* **2015**, *3*, 8771−8774.

(12) Goswami, P. P.; Syed, A.; Beck, C. L.; Albright, T. R.; Mahoney, K. M.; Unash, R.; Smith, E. A.; Winter, A. H. BODIPY-Derived Photoremovable Protecting Groups Unmasked with Green Light. *J. Am. Chem. Soc.* **2015**, *137*, 3783−3786.

(13) Loudet, A.; Burgess, K. BODIPY Dyes and Their Derivatives: Syntheses and Spectroscopic Properties. *Chem. Rev.* **2007**, *107*, 4891−4932.

(14) Umeda, N.; Takahashi, H.; Kamiya, M.; Ueno, T.; Komatsu, T.; Terai, T.; Hanaoka, K.; Nagano, T.; Urano, Y. Boron Dipyrromethene As a Fluorescent Caging Group for Single-Photon Uncaging with Long-Wavelength Visible Light. *ACS Chem. Biol.* **2014**, *9*, 2242−2246.

DOI: 10.1021/acsomega.7b01906
ACS Omega 2018, 3, 2155−2160

(15) Kawatani, M.; Kamiya, M.; Takahashi, H.; Urano, Y. Factors affecting the uncaging efficiency of 500 nm light-activatable BODIPY caging group. *Bioorg. Med. Chem. Lett.* **2018**, *28*, 1−5.
(16) Patil, N. G.; Basutkar, N. B.; Ambade, A. V. Visible light-triggered disruption of micelles of an amphiphilic block copolymer with BODIPY at the junction. *Chem. Commun.* **2015**, *51*, 17708−17711.
(17) Sharma, A. K.; Nair, M.; Chauhan, P.; Gupta, K.; Saini, D. K.; Chakrapani, H. Visible-Light-Triggered Uncaging of Carbonyl Sulfide for Hydrogen Sulfide (H2S) Release. *Org. Lett.* **2017**, *19*, 4822−4825.
(18) Tehler, U.; Fagerberg, J. H.; Svensson, R.; Larhed, M.; Artursson, P.; Bergström, C. A. S. Optimizing Solubility and Permeability of a Biopharmaceutics Classification System (BCS) Class 4 Antibiotic Drug Using Lipophilic Fragments Disturbing the Crystal Lattice. *J. Med. Chem.* **2013**, *56*, 2690−2694.
(19) King, D. E.; Malone, R.; Lilley, S. H. New Classification and Update on the Quinolone Antibiotics. *Am. Fam. Physician* **2000**, *61*, 2741−2748.
(20) Doorslaer, X. V.; Dewulf, J.; Langenhove, H. V.; Demeestere, K. Fluoroquinolone antibiotics: An emerging class of environmental micropollutants. *Sci. Total Environ.* **2014**, *500*−*501*, 250−269.
(21) Wegener, M.; Hansen, M. J.; Driessen, A. J. M.; Szymanski, W.; Feringa, B. L. Photocontrol of Antibacterial Activity: Shifting from UV to Red Light Activation. *J. Am. Chem. Soc.* **2017**, *139*, 17979−17986.
(22) Wong, P. T.; Tang, S.; Mukherjee, J.; Tang, K.; Gam, K.; Isham, D.; Murat, C.; Sun, R.; Baker, J. R.; Choi, S. K. Light-controlled active release of photocaged ciprofloxacin for lipopolysaccharide-targeted drug delivery using dendrimer conjugates. *Chem. Commun.* **2016**, *52*, 10357−10360.
(23) Meeker, D. G.; Jenkins, S. V.; Miller, E. K.; Beenken, K. E.; Loughran, A. J.; Powless, A.; Muldoon, T. J.; Galanzha, E. I.; Zharov, V. P.; Smeltzer, M. S.; Chen, J. Synergistic Photothermal and Antibiotic Killing of Biofilm-Associated *Staphylococcus aureus* Using Targeted Antibiotic-Loaded Gold Nanoconstructs. *ACS Infect. Dis.* **2016**, *2*, 241−250.
(24) Malwal, S. R.; Sriram, D.; Yogeeswari, P.; Chakrapani, H. Synthesis and antimycobacterial activity of prodrugs of sulfur dioxide (SO_2). *Bioorg. Med. Chem. Lett.* **2012**, *22*, 3603−3606.
(25) Pardeshi, K. A.; Malwal, S. R.; Banerjee, A.; Lahiri, S.; Rangarajan, R.; Chakrapani, H. Thiol activated prodrugs of sulfur dioxide (SO2) as MRSA inhibitors. *Bioorg. Med. Chem. Lett.* **2015**, *25*, 2694−2697.
(26) Tyagi, P.; Dharmaraja, A. T.; Bhaskar, A.; Chakrapani, H.; Singh, A. *Mycobacterium tuberculosis* has diminished capacity to counteract redox stress induced by elevated levels of endogenous superoxide. *Free Radical Biol. Med.* **2015**, *84*, 344−354.
(27) Malwal, S. R.; Sriram, D.; Yogeeswari, P.; Konkimalla, V. B.; Chakrapani, H. Design, Synthesis, and Evaluation of Thiol-Activated Sources of Sulfur Dioxide (SO_2) as Antimycobacterial Agents. *J. Med. Chem.* **2012**, *55*, 553−557.
(28) Baym, M.; Stone, L. K.; Kishony, R. Multidrug evolutionary strategies to reverse antibiotic resistance. *Science* **2016**, *351*, No. aad3292.
(29) Shukla, P.; Khodade, V. S.; Sharath Chandra, M.; Chauhan, P.; Mishra, S.; Siddaramappa, S.; Pradeep, B. E.; Singh, A.; Chakrapani, H. "On demand" redox buffering by H2S contributes to antibiotic resistance revealed by a bacteria-specific H2S donor. *Chem. Sci.* **2017**, *8*, 4967−4972.
(30) Meylan, S.; Porter, C. B. M.; Yang, J. H.; Belenky, P.; Gutierrez, A.; Lobritz, M. A.; Park, J.; Kim, S. H.; Moskowitz, S. M.; Collins, J. J. Carbon Sources Tune Antibiotic Susceptibility in *Pseudomonas aeruginosa* via Tricarboxylic Acid Cycle Control. *Cell Chem. Biol.* **2017**, *24*, 195−206.
(31) Brynildsen, M. P.; Winkler, J. A.; Spina, C. S.; MacDonald, I. C.; Collins, J. J. Potentiating antibacterial activity by predictably enhancing endogenous microbial ROS production. *Nat. Biotechnol.* **2013**, *31*, 160.
(32) Pal, S.; Ramu, V.; Taye, N.; Mogare, D. G.; Yeware, A. M.; Sarkar, D.; Reddy, D. S.; Chattopadhyay, S.; Das, A. GSH Induced Controlled Release of Levofloxacin from a Purpose-Built Prodrug: Luminescence Response for Probing the Drug Release in *Escherichia coli* and *Staphylococcus aureus*. *Bioconjugate Chem.* **2016**, *27*, 2062−2070.
(33) Christ, W. Central nervous system toxicity of quinolones: human and animal findings. *J. Antimicrob. Chemother.* **1990**, *26*, 219−225.
(34) Norrby, S. R. Side-effects of quinolones: comparisons between quinolones and other antibiotics. *Eur. J. Clin. Microbiol. Infect. Dis.* **1991**, *10*, 378−383.
(35) Dwyer, D. J.; Collins, J. J.; Walker, G. C. Unraveling the Physiological Complexities of Antibiotic Lethality. *Annu. Rev. Pharmacol. Toxicol.* **2015**, *55*, 313−332.

DOI: 10.1021/acsomega.7b01906
ACS Omega 2018, 3, 2155−2160